
Unbiased Angular Overlap Model parameters from *ab initio* calculations

Zur Erlangung des Grades eines Doktors der Naturwissenschaften (Dr. rer. nat.)
Genehmigte Dissertation von Moritz Buchhorn aus Groß-Gerau
Tag der Einreichung: 04. Dezember 2023, Tag der Prüfung: 19. Januar 2024

1. Gutachten: Prof. Dr. Vera Krewald
2. Gutachten: Prof. Dr. Herbert Plenio
Darmstadt, Technische Universität Darmstadt



TECHNISCHE
UNIVERSITÄT
DARMSTADT

Chemistry Department
Theoretical Chemistry
AK Krewald

Unbiased Angular Overlap Model parameters from
ab initio calculations

Accepted doctoral thesis by Moritz Buchhorn

Date of submission: 04. Dezember 2023

Date of thesis defense: 19. Januar 2024

Darmstadt, Technische Universität Darmstadt

Bitte zitieren Sie dieses Dokument als:

URN: urn:nbn:de:tuda-tuprints-267127

URL: <http://tuprints.ulb.tu-darmstadt.de/26712>

Jahr der Veröffentlichung auf TUpriints: 2024

Dieses Dokument wird bereitgestellt von tuprints,

E-Publishing-Service der TU Darmstadt

<http://tuprints.ulb.tu-darmstadt.de>

tuprints@ulb.tu-darmstadt.de

Die Veröffentlichung steht unter folgender Creative Commons Lizenz:

Namensnennung – Nicht kommerziell 4.0 International

<https://creativecommons.org/licenses/by-nc/4.0/>

This work is licensed under a Creative Commons License:

Attribution–NonCommercial 4.0 International

<https://creativecommons.org/licenses/by-nc/4.0/>

Erklärungen laut Promotionsordnung

§ 8 Abs. 1 lit. c PromO

Ich versichere hiermit, dass die elektronische Version meiner Dissertation mit der schriftlichen Version übereinstimmt.

§ 8 Abs. 1 lit. d PromO

Ich versichere hiermit, dass zu einem vorherigen Zeitpunkt noch keine Promotion versucht wurde. In diesem Fall sind nähere Angaben über Zeitpunkt, Hochschule, Dissertationsthema und Ergebnis dieses Versuchs mitzuteilen.

§ 9 Abs. 1 PromO

Ich versichere hiermit, dass die vorliegende Dissertation selbstständig und nur unter Verwendung der angegebenen Quellen verfasst wurde.

§ 9 Abs. 2 PromO

Die Arbeit hat bisher noch nicht zu Prüfungszwecken gedient.

Darmstadt, 04. Dezember 2023

M. Buchhorn



Erklärung zum Eigenanteil an den Veröffentlichungen der kumulativen Dissertation

Im Folgenden ist aufgelistet, mit welchem Anteil ich an den Veröffentlichungen beteiligt war.

Mein Anteil an der folgenden Veröffentlichung beträgt 70%

1] M. Buchhorn, R. J. Deeth, V. Krewald, Chemistry - A European Journal **2022**, *28*, e202103775.

Mein Anteil an der folgenden Veröffentlichung beträgt 75%

2] M. Buchhorn, V. Krewald, Dalton Transactions **2023**, *52*, 6685.

Mein Anteil an der folgenden Veröffentlichung beträgt 80%

3] M. Buchhorn, V. Krewald, Journal of Computational Chemistry **2024**, *45*, 122.

Die folgende Veröffentlichung ist im Rahmen der Promotion entstanden, aber kein Teil der Dissertation und daher ohne genaue Angabe eines Anteils.

4] A. Brinkmeier, R. A. Schulz, M. Buchhorn, C.-J. Spyra, S. Dechert, S. Demeshko, V. Krewald, F. Meyer, Journal of the American Chemical Society **2021**, *143*, 10361.

30.11.2023

Moritz Buchhorn

(Name und Unterschrift)



Erklärung zur Begutachtung der Veröffentlichung

Vera Krewald

Referent*in

Herbert Plenio

Co-Referent*in

30.11.23

Datum

Weder Referent*in (Prof. Dr. Vera Krewald) noch Co-Referent*in (Prof. Dr. Herbert Plenio) der vorliegenden kumulativen Doktorarbeit waren an der Begutachtung nachstehender Veröffentlichungen beteiligt:

- 1] M. Buchhorn, R. J. Deeth, V. Krewald, Chemistry - A European Journal **2022**, 28, e202103775.
- 2] M. Buchhorn, V. Krewald, Dalton Transactions **2023**, 52, 6685.
- 3] M. Buchhorn, V. Krewald, Journal of Computational Chemistry **2024**, 45, 122.
- 4] A. Brinkmeier, R. A. Schulz, M. Buchhorn, C.-J. Spyra, S. Dechert, S. Demeshko, V. Krewald, F. Meyer, Journal of the American Chemical Society **2021**, 143, 10361.

30.11.23

V. Krewald

Referent*in
(Prof. Dr. Vera Krewald)

30.11.2023

HP

Co-Referent*in
(Prof. Dr. Herbert Plenio)

Zusammenfassung

In der vorliegenden Arbeit werden molekulare Übergangsmetallkomplexe mit einer quantenchemischen Multikonfigurationsmethode in Verbindung mit Ligandenfeldtheorie (LFT) untersucht. Die Ligandenfeldtheorie ist ein bewährtes Modell zur Parametrisierung der elektronischen und magnetischen Eigenschaften von Übergangsmetallkomplexen. Die in dieser Arbeit verwendete Parametrisierung ist das *Angular Overlap Model* (AOM), das das Ligandenfeld lokal parametrisiert, d.h. jeder Parametersatz bezieht sich auf ein bestimmtes Metall-Liganden-Paar. Der Vorteil des AOM im Vergleich zu anderen Ligandenfeldparametrisierungen ist somit die Möglichkeit, den Einfluss bestimmter Liganden in einem Komplex zu beurteilen. Im Gegensatz dazu können globale Parameter nur ganze Komplexe beschreiben. Der Nachteil dieses Ansatzes ist die hohe Anzahl von Parametern, die oft zu unterbestimmten Problemen führt, die eine AOM-Parametrisierung erschweren. Übliche Ansätze zur Lösung dieses Problems sind Annahmen und künstliche Beziehungen zwischen Parametern, die zu voreingenommenen Ergebnissen führen können.

In dieser Arbeit werden mithilfe von *complete active space* (CAS)-Rechnungen und dem in der Quantenchemie-Software ORCA implementierten Ligandenfeldtheorie-Modul Energien der elektronischen Zustände berechnet, die für die Bestimmung der AOM-Parameter erforderlich sind. Die berechneten Daten sind äquivalent zu den Informationen, die mit spektroskopischen Methoden gewonnen werden, die die Energiedifferenz angeregter Zustände liefern, z. B. UV/Vis-Spektroskopie. Der Einsatz von Berechnungsmethoden bringt eine Reihe von Vorteilen gegenüber spektroskopischen Messungen mit sich, vor allem die eindeutige Zuordnung von Zuständen und die Möglichkeit, strukturelle Momentaufnahmen anstelle von thermisch gemittelten Strukturen zu untersuchen. Diese Eigenschaften können genutzt werden, um Strukturen mit geringer Symmetrie zu erzeugen, die weniger entartete elektronische Zustände aufweisen und daher AOM-Parametrisierungen erlauben, die auf der Basis experimenteller Daten unmöglich wären. Auf diese Weise ist es nicht mehr notwendig, eine Unterbestimmung des AOM durch die Festlegung von Parametern oder die Einführung von Beziehungen zu vermeiden. Es handelt sich also um einen Ansatz, der die Wichtigkeit solcher Annahmen mindert und daher objektivere Parametrisierungen ermöglicht.

Es wird gezeigt, dass der Ansatz der asymmetrischen Strukturprobe bekannte Trends zuverlässig reproduziert, sodass damit Lücken in experimentellen Serien gefüllt werden können, wenn weitere experimentelle Daten schwer zu erhalten oder zu interpretieren sind. Weiterhin wird gezeigt, dass die unvoreingenommene Parametrisierung von Ammoniak-Liganden eine signifikante π -Wechselwirkung ergibt, was im Widerspruch zu bisher üblichen Näherungen bei der AOM-Parametrisierung steht. Die Arbeiten zur Bestätigung des Ansatzes werden durch eine Software unterstützt, die das asymmetri-

sche Struktursampling und die AOM-Parametrisierung durchführt. Diese Software wird ebenfalls in dieser Arbeit vorgestellt und ihre Entwicklungsversionen wurden für alle hier durchgeführten theoretischen Untersuchungen verwendet.

Abstract

In this work, molecular transition metal complexes are investigated with a quantum chemical multiconfigurational method in conjunction with ligand field theory (LFT). Ligand field theory is an established tool to parameterize electronic and magnetic properties of transition metal complexes. The parameterization used is the angular overlap model (AOM), which parameterizes the ligand field locally, i.e. each parameter set refers to a specific metal-ligand pair. The advantage of the AOM compared with other ligand field schemes is thus the possibility to assess the effect of particular ligands in a complex instead of relying on global parameters that can only describe whole complexes. The downside of this approach is the high number of parameters, often leading to underdetermined problems that make an AOM fit difficult. Common approaches to solve this issue are artificial relationships and assumptions that introduce biased parameters.

In this work, complete active space (CAS) calculations and the *ab initio* ligand field theory routine implemented in the ORCA quantum chemistry software are used to calculate electronic state energies that are necessary to fit AOM parameters. The calculated data is equivalent to the information obtained by spectroscopic methods that yield the energy difference of excited states, e.g. UV-Vis spectroscopy. The use of computational methods comes with an array of advantages compared to spectroscopic measurements, most importantly the unambiguous assignment of states and the possibility to investigate structural snapshots instead of thermally averaged structures. These properties can be used to create structural samples of low symmetry, which have fewer degenerate electronic states and therefore permit AOM parameterizations that are impossible when only considering experimental data. By this, it is not necessary anymore to avoid AOM underdetermination by fixing parameters or introducing relational rules. It is thus an approach to remove bias and obtain more objective parameter sets.

The asymmetric structure sample approach is shown to reproduce known trends reliably, so it can be used to fill data gaps in series, for which experimental data is difficult to obtain or interpret. It is also shown that the unbiased parameterization of ammonia ligands yields a significant π interaction, which is in contrast to common approximations in the AOM parameterization. The proof of concept works are supported by a software that performs the asymmetric structure sampling and the AOM parameterization. This software is also presented in this work and its development versions were used for all computational investigations performed here.

Contents

1	Introduction	1
2	Multiconfiguration methods	5
2.1	Basics	5
2.1.1	Wave functions	6
2.1.2	Spatial orbitals	7
2.2	Variational principle	8
2.2.1	Linear variational problems	9
2.2.2	The matrix equivalence	11
2.2.3	The electronic Hamiltonian	11
2.2.4	Approximations and Hartree–Fock	12
2.3	Configuration Interaction	13
2.3.1	Constructing excited determinants	14
2.3.2	The CI matrix elements	15
2.4	Cherry-picking determinants	17
2.4.1	Active space example	18
2.4.2	Multiconfiguration self-consistent field methods	19
3	Ligand Field Theory and the Angular Overlap Model	21
3.1	Ligand Field Theory	21
3.1.1	The d orbital basis	22
3.1.2	Configurations and the CI matrix	24
3.1.3	Two-electron integrals	27
3.1.4	One-electron integrals	28
3.2	Angular Overlap Model	29
3.2.1	The local frame	29
3.2.2	The global frame	32
3.3	Common adjustments to the AOM	34
3.3.1	d–s mixing	34
3.3.2	δ interactions	36
3.3.3	The basis energy E	37
3.3.4	AOM master equation	37
3.4	Interpretation	38
3.4.1	The ligand field operator	38
3.4.2	AOM parameters	39
3.4.3	The two-electron operator	39

3.4.4	CASSCF vs. Experiment	40
4	History of the Angular Overlap Model	43
4.1	Origins	43
4.2	AOM for f-shell elements	44
4.3	The divide	44
4.4	Phase-coupled ligation	46
4.5	LFT from a computational perspective	46
4.6	AOM and molecular mechanics	47
4.7	Concluding remarks	48
5	Results and Discussion	49
5.1	Revisiting the Fundamental Nature of Metal-Ligand Bonding: An Impartial and Automated Fitting Procedure for Angular Overlap Model Parameters .	49
5.2	The π -interactions of ammonia ligands evaluated by <i>ab initio</i> ligand field theory	90
5.3	AOMadillo: A program for fitting angular overlap model parameters	120
6	Conclusion and Perspective	153
6.1	Perspective	153
6.1.1	Phase-coupling in non-coupled ligators	153
6.1.2	The divide	153
6.1.3	Differential covalency	154
6.1.4	Solids and highly charged complexes	156
6.1.5	AOM-enhanced force fields	157
6.2	Conclusion	159

1 Introduction

Transition metal complexes are a class of compounds that consist of a transition metal (TM), and a coordination sphere around this metal. The molecules making up the coordination sphere are called ligands, and the vast amount of possible metal-ligand combinations represent a rich and diverse field of chemistry. There are molecular complexes as well as coordination subunits in solids, and while their phase is different, they share some characteristics. The chemical (e.g. reactivities, redox properties) and physical (e.g. electronic spectra, magnetism) properties of TM complexes are dominated by their valence electrons in the d or f shell, respectively. Their electronic structure makes TM complexes have a variety of properties, occurrences and applications. A famous example is haemoglobin, which includes a haem group consisting of an iron ion coordinated by a porphyrin structure and one or two axial ligands. Transition metals are generally very common active centres in proteins.^[1] Just as they are catalytically active in biological systems, TM complexes are used as homogeneous^[2] and heterogeneous^[3,4] catalysts in various applications. Metal-organic frameworks, which enjoy a lot of attention in current research, also contain coordination subunits, similar to regular crystals.^[5]

The colourful appearance of many TM complexes fascinated chemists early on, and these colours are often caused by d-d transitions, enabled by a partly filled valence shell. These complexes have a d^1 to d^9 (lanthanoids and actinoids f^1 to f^{13}) electron configuration.^[6] Bethe was the first to provide a theoretical framework for the description of the corresponding electron transitions in 1929.^[7] Derived from subunits in crystals, he assumed the transition metal to be surrounded by negatively charged ligands, the electrostatic potential of which would cause the d orbitals to split in energy. The basis set for this quantum chemical treatment are the metal d orbitals only, so this approach is a considerable simplification compared to more complete quantum chemical models. Due to its origin, the model was termed “crystal field theory” (CFT), and it enabled some explanations on the colour and also magnetism^[8,9] of TM complexes. It provided chemists and physicists with a tool to describe the electron configuration of transition metals and the impact that a coordination sphere has on them. Conceptually, it was very successful, but over the years it became apparent that it is not well suited to predict the energies of electron transitions and lacked some consideration for neutral ligands that exert almost no electrostatic field but still cause a significant d orbital energy splitting. Since the underlying concept of treating the metal d orbitals only was proven to be qualitatively correct, the model was not abandoned, but developed further. Researchers started to fit the crystal field parameters to experimental data instead of calculating them from the molecular geometry. This empirically fitted parameterization was called *ligand field theory* (LFT), and remains in use today. The transition from the *ab initio* crystal field calculation

of properties to empirical parameterization happened successively and no sharp distinction was made by researchers at that time. Due to this, CFT and LFT are often conflated until today, but chapter 3 explains how they differ.

Regarding its empirical nature, LFT is not meant to *predict* these properties, but rather to rationalize experimental observations. We will see in chapter 3 why a prediction of these properties is not possible with LFT, and in fact this was never its purpose.^[10,11] Its parameters are empirically fitted to experimental or calculated data and generally, the parameters obtained for one complex cannot be transferred to another. The true strength of LFT is that the parameters used can be interpreted and yield a much simpler picture than for example a complete quantum chemical treatment of the electronic structure. Common for all schemes is the usage of Racah parameters A, B, C that represent electron-electron interactions, with B being the one that is most often interpreted as an electronic repulsion parameter. The effect of the ligands on the metal d electrons can be covered in various parameterizations and there is no universal scheme that suits every complex.

Generally, an arbitrary set of parameters can be chosen to cover vaguely defined effects, a practice that has been criticized due to the lacking relevance of such a parameterization.^[12] In this regard, it is important to emphasize that a parameterization that *works* is not necessarily one that is *useful*. Probably the most popular parameterization is the use of Δ in octahedral complexes, where a single parameter suffices to capture all one-electron metal-ligand interactions. It represents the ligand field strength in a single parameter and is the origin of the spectrochemical series. It is a very useful parameter for octahedral, homoleptic complexes. However, it is also an example of the ambiguity that is carried with the parameterization flexibility. The single parameter Δ often defines the energy difference between e_g and t_{2g} orbitals, but is sometimes also taken to be the first electronic transition energy. These quantities can be equal by coincidence, but are usually different.^[13]

Other parameter sets like Ds, Dt, Dq are able to cover more asymmetric complexes, so a different approach might be chosen for each complex.^[13] The focus of this work lies on the angular overlap model (AOM), which is a parameterization scheme that seeks to partition metal-ligand interactions in arbitrary complexes.^[14] It uses parameters that are local to each metal-ligand-pair in a complex, and represents this local interaction in terms of σ and π parameters. The AOM is a very general LFT parameterization scheme, since any metal-ligand interaction and thus any complex, independent of its symmetry, can in principle be parameterized. Its main problem is the fact that this approach leads to large sets of parameters, making it notoriously underdetermined. This problem together with the fact that electronic spectra tend to have broad bands with rather low intensities for d-d transitions means that a complete parameterization in terms of the AOM is often hard to achieve and subject to many assumptions and simplifications.^[13]

Quantum chemical calculations are an established tool for the prediction and interpretation of chemical properties in molecules and solids.^[15] There is a wide array of methods that can be used to calculate structural, electronic and thermodynamic properties with different levels of accuracy. From a ligand field perspective, the most important properties are the energies of electronic states, which is of course the same information that is experimentally obtained from electronic spectra. As we will show in chapter 2 and

3, there is a clear theoretical connection between quantum chemical complete active space (CAS) calculations and the quantities that are parameterized by LFT. CAS calculations are commonly used to investigate electronic transitions that are specified by a set of orbitals. If this set is chosen to be the metal d orbitals, the energy of electronic d states can be calculated to a satisfactory accuracy and enables a direct connection of the quantum chemical approach and LFT.^[16]

Just as LFT can be used to parameterize experimental results, it is possible to apply it on calculated data, too. Quantum chemical calculations permit investigations that are almost impossible to perform experimentally, such as bond length scans, the investigation of structural snapshots in contrast to averaged spectra, ligand exchange or the investigation of non-existing molecules. The combination of computational methods with LFT thus allows to express obtained results with chemically intuitive parameters that can be interpreted much more easily than the overwhelming amount of detailed data that is generated by an average electronic structure calculation.

We will see in chapter 5 that the quantum chemical approach can also be used to lift the underdetermination problem of the AOM, enabling the investigation of complexes that were so far not parametrizable. The possible inaccuracies that are always part of calculated data are unproblematic due to the interpretative nature of LFT. In chapter 5, it is shown that trends are reproduced correctly and that calculated data is reliable enough to interpret calculated data that is not backed up by experimental results. With the confirmation that the data obtained by this approach is qualitatively correct, several trends along the periodic table are investigated. The exchange of metals and ligands is assessed in section 5.1, as well as bond length dependencies and correlations of ligand field strength and chemical hardness. Since the quantum chemical approach allows for an exact assignment of electronic states, experimental results with ambiguous interpretations can be reassessed. Doing this, it was possible to assign spectral transitions in two copper ammine complexes, and it is shown in section 5.2 that this is also experimental evidence on ammonia π interactions. Along with the applications in 5.1 and 5.2, a software was developed specifically for fitting AOM parameters to calculated data. A detailed presentation of further applications, limitations and technical details of this software can be found in section 5.3.

2 Multiconfiguration methods

In this first theory chapter, quantum chemical basics are presented which are necessary to understand the foundations of ligand field theory (LFT). Please note that we will not discuss how well the methods perform and how successful certain models have been applied, as this is covered in general inorganic chemistry textbooks and reviews. LFT is concerned with the description of d–d electronic transitions and the d electron configuration of the ground state. Both topics can be covered when employing multiconfiguration wave functions, so we will focus on the discussion of these. The introduction of standard quantum chemical approaches will be short and, most notably, will skip most of the Hartree–Fock (HF) approach. We will then see how multiconfiguration wave functions are set up systematically and how the complete active space approach works, which is crucial for the understanding of *ab initio* LFT. This chapter is mainly based on refs. [17–19]. Additional sources are refs. [20–23]. For more information on fundamental quantum chemistry, recommended literature is ref. [18] and for a detailed description of the ground state electronic structure methods (especially HF), ref. [17].

2.1 Basics

Quantum chemistry is interested in the prediction of measurable quantities, also termed physical observables. Key to this prediction is the usage of operators and wave functions, where the application of the operator \hat{O} on the wave function f yields the quantity of interest as the eigenvalue o .

$$\hat{O}f = o \cdot f \quad (2.1)$$

Due to the probabilistic interpretation of the wave function, we can obtain the average or expectation value of an operator \hat{O} for a system described by the wave function f by multiplying with the complex conjugate of f and integrating over all space (indicated by $d\tau$).

$$\int f^* \hat{O} f d\tau = o \int f^* f d\tau \quad (2.2)$$

In the more compact Dirac notation, the integrands are placed in bras ($\langle f|$) and kets ($|f\rangle$), and the above equation is then written as

$$\langle f|\hat{O}|f\rangle = o\langle f|f\rangle \quad (2.3)$$

where the complex conjugation is implicit. In the following definitions, both notations are given, but from subsection 2.1.1 on we will stick to the Dirac notation.

The wave function specifies the state of the system of interest and the operator corresponds to the observable that we want to predict. A few restrictions are in place for operators and wave functions. The wave function must be an eigenfunction to the operator, otherwise it would not yield an eigenvalue. Operators and wave functions can be complex (i.e. have imaginary parts), but the observables must be real. This is fulfilled when the operator is hermitian, i.e. it satisfies the relation

$$\int f_i^* \hat{O} f_j d\tau = \int f_j \hat{O}^* f_i^* d\tau \quad (2.4)$$
$$\langle f_i | \hat{O} | f_j \rangle = [\langle f_j | \hat{O} | f_i \rangle]^*$$

Eigenfunctions of hermitian operators are always orthogonal, which means that the integral $\langle f_i | f_j \rangle$ equals zero for $i \neq j$. If they are also normalized (which is optional), they are called orthonormal and we can write

$$\langle f_i | f_j \rangle = \int f_i f_j^* d\tau = \delta_{ij} = \begin{cases} 1 & \text{if } i = j \\ 0 & \text{if } i \neq j \end{cases} \quad (2.5)$$

where δ_{ij} is called the Kronecker delta. Normalization is generally not required, but can be handy under several circumstances. There are more properties and restrictions to the operators, but for understanding LFT, only the ones mentioned above are needed. The most important point to keep in mind is that there is an operator to every observable and a wave function that describes the state of a system.

As chemists are most often interested in molecules and their electronic structures, a natural focus on the electronic energy operator and the corresponding wave functions arises. The electronic energy operator is so important that it has its own name, Hamiltonian, and its eigenvalue equation is called Schrödinger equation.

$$\hat{H}\Psi = E\Psi \quad (2.6)$$

Electronic structure investigations generally revolve around the solution of the Schrödinger equation for a given system, and a colossal amount of research effort has been put into the approximation of its solution. We will not define the Hamiltonian until later in this chapter, and instead focus on the wave functions first. Until then, we simply take \hat{H} as a known term.

2.1.1 Wave functions

Since the wave function specifies the state of a system, it must take the coordinates of the investigated particles as parameters. An N -electron wave function Ψ is thus a function of the positions of the electrons, and $\Psi = \Psi(x_1, x_2, \dots, x_N)$. Since electrons are fermions, a

wave function of two or more of them must be antisymmetric, that means it must change its sign upon the exchange of two electrons. This property is a formulation of the Pauli exclusion principle.

$$\Psi(x_1, x_2, \dots, x_N) = -\Psi(x_2, x_1, \dots, x_N) \quad (2.7)$$

To ensure the wave functions antisymmetry, it can be constructed as a Slater determinant. They are antisymmetrized sums of products of one-electron wave functions called *orbitals*. The general property of determinants to change their sign when two rows or columns are exchanged guarantees that the exclusion principle is fulfilled.

$$|\Psi\rangle = \frac{1}{\sqrt{2}} \begin{vmatrix} \chi_1(x_1) & \chi_1(x_2) & \dots & \chi_1(x_N) \\ \chi_2(x_1) & \chi_2(x_2) & \dots & \chi_2(x_N) \\ \vdots & & \ddots & \vdots \\ \chi_N(x_1) & \chi_N(x_2) & \dots & \chi_N(x_N) \end{vmatrix} = |\chi_1\chi_2\dots\chi_N\rangle \quad (2.8)$$

As indicated in the above equation, we can write a determinant in the shorter Dirac notation, where only its diagonal elements are listed. The Schrödinger equation then becomes

$$\hat{H}|\Psi\rangle = E|\Psi\rangle \quad (2.9)$$

In practice, the orbitals χ in the determinant are linear combinations themselves. They are defined as a sum of K basis functions ϕ .

$$\chi_i = \sum_{j=1}^K c_{ij}\phi_j \quad (2.10)$$

Accordingly, there are up to K orbitals available for the construction of the determinant $|\Psi_0\rangle$. The number of basis functions almost always exceeds the number of electrons in the system and due to this, not all orbitals enter the ground state determinant. The orbitals that are not part of the determinant are called *virtual* or *unoccupied* orbitals, the other ones are *occupied* orbitals. The selection of occupied orbitals is called a *configuration*. Section 2.2 deals with the variational principle which provides a criterion for how wave functions should be composed in order to accurately approximate a true state.

2.1.2 Spatial orbitals

In the next sections, we use spin orbitals χ to define most expressions. They implicitly contain the spin coordinate and are thus useful for indexing and constructing the matrices we will encounter. Nonetheless, quantum chemical calculations are commonly based on spatial orbitals that are defined as a product of a spatial and a spin function:

$$\chi(\vec{x}) = \gamma(\vec{r})\sigma(\omega) \quad (2.11)$$

Here, γ is the spatial function, depending on the spatial coordinates \vec{r} and the spin function σ that depends on the spin coordinate ω . Only two spin functions are allowed, namely $\alpha(\omega)$ and $\beta(\omega)$, and they are orthonormal such that $\langle\alpha(\omega)|\alpha(\omega)\rangle = 1$ and $\langle\alpha(\omega)|\beta(\omega)\rangle = \langle\beta(\omega)|\alpha(\omega)\rangle = 0$. For the sake of brevity, the spin function is often included into the spatial orbital symbol in form of a bar. The spatial orbital ψ without bar includes the spin function $\alpha(\omega)$, and $\bar{\psi}(\omega)$ with bar.

$$\begin{aligned}\psi(\vec{x}) &= \gamma(\vec{r})\alpha(\omega) \\ \bar{\psi}(\vec{x}) &= \gamma(\vec{r})\beta(\omega)\end{aligned}\tag{2.12}$$

In a closed-shell system, each spatial orbital corresponds to two spin orbitals:

$$\psi_1 = \chi_1, \quad \bar{\psi}_1 = \chi_2\tag{2.13}$$

Most chemists intuitively use spatial orbitals as their basis of expressing electron configurations and concepts like occupation numbers, HOMO, LUMO and SOMO. We will use spatial orbitals in the ligand field theory part of this work.

2.2 Variational principle

We stated that the application of a hermitian operator on an eigenfunction of this operator yields a real eigenvalue. We also saw in the last section that the respective function is constructed in a way that it adheres to the antisymmetry principle and that it consists of linear combinations of one-electron functions. Any many-electron wave function is defined in the given basis by the choice of the coefficients c in Equation 2.10. The question that arises naturally is: what is a “good” wave function and consequently, how to choose the coefficients if we use linear combinations as in Equation 2.10?

The *variational principle* states that in a given basis, the smallest possible electronic energy is still larger than the “true” one. That means that the wave function that yields this smallest energy is also the best approximation to the “true” wave function. In the given form of the many-electron wave function, the coefficients c can be tweaked such that a minimal eigenvalue is achieved. That makes them the variational parameters in this approach, and most quantum chemical methods aim for the variational minimization of the electronic energy.

Different methods for minimization can be employed, but it is a common (although not necessary) restriction to keep the variational parameters linear. It is in principle possible to have, say, an exponent as variational parameter, but its optimization is much more complicated and thus not practical in common quantum chemical calculations.

Each additional basis function increases the parameter space in which the wave function can be optimized and thus improves the electronic energy, but it also increases the computational effort that is necessary to find an optimal solution.¹ Thus, the choice of basis functions is crucial for the description of any electronic structure. Most often for

¹Although additional basis functions do not always improve the electronic energy significantly.

molecular investigations, *atomic orbitals* are employed: functions that are centred on the atoms in the investigated molecule. Their linear combinations are called *molecular orbitals*, and the corresponding approach *linear combination of atomic orbitals* (LCAO). Let us recall the symbols in Equation 2.10: χ_i are molecular orbitals, to which we will only refer as orbitals in the rest of the text. The coefficients c_{ij} are the variational parameters, and ϕ_j are the basis functions, commonly atomic orbitals.

2.2.1 Linear variational problems

The variational principle tells us that we must minimize the electronic energy with respect to the variational parameters. Let us assume a wave function f that is a linear combination of basis functions (not a Slater determinant!), similar to Equation 2.10. The energy associated with this function, derived from Equation 2.9, is

$$E = \frac{\langle f | \hat{H} | f \rangle}{\langle f | f \rangle} \quad (2.14)$$

with $|f\rangle = \sum_i c_i |x_i\rangle$. The numerator can be expanded as

$$\begin{aligned} \langle f | \hat{H} | f \rangle &= \sum_i^K \sum_j^K c_i c_j \langle x_i | \hat{H} | x_j \rangle \\ &= \sum_i^K \sum_j^K c_i c_j H_{ij} \\ &= c_1^2 H_{11} + c_1 c_2 H_{12} + c_2 c_1 H_{21} + c_1 c_3 H_{13} + \cdots + c_K^2 H_{KK} \end{aligned} \quad (2.15)$$

The Hamiltonian is hermitian, so $H_{ij} = H_{ji}$ and the above sum can be compacted slightly.

$$\langle f | \hat{H} | f \rangle = c_1^2 H_{11} + 2c_1 c_2 H_{12} + 2c_1 c_3 H_{13} + \cdots + c_K^2 H_{KK} \quad (2.16)$$

Proceeding similarly, we obtain for the denominator

$$\begin{aligned} \langle f | f \rangle &= \sum_i^K \sum_j^K c_i c_j \langle x_i | x_j \rangle \\ &= \sum_i^K \sum_j^K c_i c_j S_{ij} \\ &= c_1^2 S_{11} + 2c_1 c_2 S_{12} + 2c_1 c_3 S_{13} + \cdots + c_K^2 S_{KK} \end{aligned} \quad (2.17)$$

To find the minimum energy associated with the given Hamiltonian and function, we need to take the partial derivatives of the energy and equal them to 0. Before taking the derivative, it is beneficial to restructure Equation 2.14 such that there is no fraction.

$$\langle f | f \rangle E = \langle f | \hat{H} | f \rangle \quad (2.18)$$

We now take the derivative and apply the product rule on the left term.

$$E \cdot \frac{\partial}{\partial c_k} \langle f|f \rangle + \langle f|f \rangle \frac{\partial E}{\partial c_k} = \frac{\partial}{\partial c_k} \langle f|\hat{H}|f \rangle \quad (2.19)$$

Since $\partial E/\partial c_k = 0$, the equation simplifies further and we can expand it.

$$E \cdot \frac{\partial}{\partial c_k} \left(\sum_i^K \sum_j^K c_i c_j S_{ij} \right) = \frac{\partial}{\partial c_k} \left(\sum_i^K \sum_j^K c_i c_j H_{ij} \right) \quad (2.20)$$

After taking the derivatives, we get

$$E \cdot \left(\sum_i^K 2c_i S_{ik} \right) = \sum_i^K 2c_i H_{ik} \quad (2.21)$$

The overlap integrals are shifted to the right, the equation is divided by 2 and c_i is factored out.

$$0 = \sum_i^K c_i (H_{ik} - E S_{ik}) \quad (2.22)$$

Since the partial derivative needs to be taken for all c_k , we obtain K such equations, making up a linear equation system that can be solved for E . This equation system can be expressed in a determinantal form, the equation is then called *secular equation* and the determinant accordingly *secular determinant*.

$$0 = \begin{vmatrix} H_{11} - ES_{11} & H_{12} - ES_{12} & \dots & H_{1K} - ES_{1K} \\ H_{21} - ES_{21} & H_{22} - ES_{22} & \dots & H_{2K} - ES_{2K} \\ \vdots & & & \vdots \\ H_{K1} - ES_{K1} & H_{K2} - ES_{K2} & \dots & H_{KK} - ES_{KK} \end{vmatrix} \quad (2.23)$$

There are two very important points arising from the above result. First: We saw that any function that is a linear combination of basis function leads to a secular equation when minimized for the energy with respect to the linear variational parameters. Second and maybe not as obvious: The resulting equation is a polynomial of K^{th} degree (if the determinant is expanded), so solving it for E will yield K values, each with a separate set of coefficients. The lowest E_k is by definition the ground state energy, and the corresponding set of coefficients defines the ground state wave function. It is common to label ground state symbols with an index 0. The larger energies and sets of coefficients represent excited states, and we will use this property of the linear variational problem as basis for the next sections.

2.2.2 The matrix equivalence

Let us go a step back to Equation 2.21 and collect the set of equations in matrix form. We can order it in terms of a hamiltonian matrix, an overlap matrix and a set of coefficients and obtain

$$E \begin{pmatrix} S_{11} & S_{12} & \dots & S_{1K} \\ S_{21} & S_{22} & \dots & S_{2K} \\ \vdots & & & \vdots \\ S_{K1} & S_{K2} & \dots & S_{KK} \end{pmatrix} \begin{pmatrix} c_1 \\ c_2 \\ \vdots \\ c_K \end{pmatrix} = \begin{pmatrix} H_{11} & H_{12} & \dots & H_{1K} \\ H_{21} & H_{22} & \dots & H_{2K} \\ \vdots & & & \vdots \\ H_{K1} & H_{K2} & \dots & H_{KK} \end{pmatrix} \begin{pmatrix} c_1 \\ c_2 \\ \vdots \\ c_K \end{pmatrix} \quad (2.24)$$

or

$$E\mathbf{S}\mathbf{c} = \mathbf{H}\mathbf{c} \quad (2.25)$$

We assume that the functions we use are orthonormal. In this case, $S_{ij} = \delta_{ij}$ and the overlap matrix becomes unity.

$$E\mathbf{c} = \mathbf{H}\mathbf{c} \quad (2.26)$$

as stated above, there are K solutions for E , and we can express this by introducing a matrix \mathbf{C} that collects the sets of coefficients \mathbf{c} and an matrix \mathbf{E} which is diagonal with the corresponding energies E_k as elements. The resulting expression

$$\mathbf{E}\mathbf{C} = \mathbf{H}\mathbf{C} \quad (2.27)$$

is a well-known problem and corresponds to the diagonalization of \mathbf{H} , with the matrices \mathbf{E} and \mathbf{C} containing the eigenvalues and eigenvectors, respectively.

In the rest of this text, all electronic problems are expressed in the matrix form, even when we refer to the secular equation. It is important to keep in mind that the expression “diagonalizing the hamiltonian matrix” means the same as “solving the linear variational problem for the given Hamiltonian and wave function”.

2.2.3 The electronic Hamiltonian

For the connection of the quantum chemical approach and LFT, we need to further specify the elements of the matrix \mathbf{H} . They are integrals of the type $\langle x_i | \hat{H} | x_j \rangle$, representing the electronic energy contributions, so we are concerned with the mathematical form of the Hamiltonian \hat{H} . We will operate in the Born–Oppenheimer picture, which takes the positions of the nuclei as fixed, while the positions of the electrons are flexible and thus the parameters of the wave function. This assumption is very common and justified by the fact that electrons are at least 1000 times lighter than nuclei and thus move much faster. Please notice that we are using atomic units for the definition of the Hamiltonian.

$$\hat{H} = -\frac{1}{2} \sum_i \nabla_i^2 - \sum_i \sum_A \frac{q_A}{r_{iA}} + \sum_{i>j} \frac{1}{r_{ij}} \quad (2.28)$$

The first term is the kinetic energy of the electrons, the second is the electrostatic attraction of the electrons to all nuclei with charge q , indexed with A . The last part is the electrostatic repulsion between the electrons i and j . All sums presented here always include all electrons or all nuclei, respectively. It can be very convenient to group the terms of the electronic Hamiltonian into a one-electron part \hat{h} , only depending on individual electron coordinates and a two-electron part \hat{g} that includes electron-electron interactions.

$$\hat{H} = \sum_i \hat{h}_i(x_i) + \sum_{i>j} \hat{g}_{ij}(x_i, x_j) \quad (2.29)$$

This grouping is a common way to reduce the complexity of the integral notation occurring when applying the Hamiltonian on a wave function.

2.2.4 Approximations and Hartree–Fock

Before we turn to multi-configurational methods, let us make a short digression to the single-configuration approach. Since the orbitals that make up a Slater determinant are composed of basis functions with variational coefficients (see Equation 2.10), the variational principle can be applied and there must be a set of coefficients for which the electronic energy is minimal. There are two problems that hinder a straightforward solution, and they will become apparent when expanding the Hamiltonian in the Schrödinger equation.

If we use a single, normalized Slater determinant as wave function, the associated energy is

$$E_0 = \langle \Psi_0 | \hat{H} | \Psi_0 \rangle \quad (2.30)$$

$$(2.31)$$

and the expansion of the Hamiltonian leads to

$$E_0 = \sum_i \langle \chi_i | \hat{h} | \chi_i \rangle + \sum_i \sum_{j<i} \langle \chi_i \chi_j | \hat{g} | \chi_i \chi_j \rangle - \langle \chi_i \chi_j | \hat{g} | \chi_j \chi_i \rangle \quad (2.32)$$

The two-electron operator gives rise to two terms, the first one is called *Coulomb integral*, the second one *exchange integral*. The problem with these terms is that the interaction of a molecular orbital χ_i with another molecular orbital χ_j depends on the exact functional form of χ_j . Vice versa, the interaction of χ_j with χ_i depends on the exact form of χ_i . The next catch is that we cannot apply the rules for linear variational problems here; Slater determinants are antisymmetrized and thus we do not deal with a matrix diagonalization problem.

As it is not the actual focus of this work, I want to give a short summary on how the Hartree–Fock procedure approximates a solution to these problems. The linear variational problem can be restored by introducing independent one-electron operators, the eigenvalues of which are the orbital energies in

$$\hat{F} \chi_i = \varepsilon_i \chi_i \quad (2.33)$$

This *Fock operator* still contains the dependency on the other orbitals, so the solution is found in multiple iterative steps. A set of starting orbitals is guessed, with which the Fock eigenvalue equation is solved. The obtained set of eigenvectors (the variational coefficients) will differ from the starting set, so in a next step this new set is used to solve the Fock equation again. This procedure is repeated until the obtained coefficients are sufficiently close to the ones from the last iteration, i.e. considered converged.

With this scheme, we obtain a wave function that is the best solution to the Fock eigenvalue equation in a given basis set, but it can be shown that it is also the best wave function for the complete electronic energy expression in Equation 2.32.

The Hartree–Fock wave function as a single determinant is the origin of many concepts of electronic structures in chemistry. The HF method constructs molecular orbitals from basis functions, and we can interpret the particular compositions found. We can see whether atomic orbitals mix, what the highest occupied and the lowest unoccupied orbitals look like or if an electron is delocalized or not. Most importantly, the determinant can be directly associated with a *configuration*, i.e. which orbitals are occupied and which are not. In the single-determinant picture, a configuration represents an electronic state, and heuristically the exchange of an occupied with an unoccupied orbital is then an excited state. This is where the somewhat sloppy idea comes from that upon excitation, an electron is moved from an occupied into an unoccupied orbital.² The predictive power of HF calculations is extremely limited for several reasons, and cannot be used to obtain quantitative results. Due to HF missing a large part of electron correlation effects, energies and derived properties that are predicted by it are not reliable. Reaction enthalpies for example are usually of the same magnitude as the error of HF energies. So-called post-Hartree–Fock methods aim to improve on this, and we will deal with the most straightforward way of improving the results obtained by quantum chemical calculations in the next section.

Another method that is used in parallel with HF is density functional theory (DFT), which is generally more successful than HF. DFT is formally exact and does only depend on the electron density as variable, but in practice, the electron density must be approximated. Kohn-Sham (KS)-DFT uses a wave function to approximate the electron density, and this wave function is a Slater determinant composed of basis functions, just as in the HF method. However, the operators employed in KS-DFT are defined differently compared to HF and therefore the optimized determinants of KS-DFT and HF calculations are not the same.

2.3 Configuration Interaction

The HF approach deals with a single determinant and is designed to approximate the ground state energy of the system. If we want to include excited states or perhaps need to take a degenerate ground state into account, we can expand a wave function $|\Phi\rangle$ in terms

²And the wrong notion that the energy difference of electronic states is the energy difference of two orbitals.

of determinants $|\Psi\rangle$ as basis functions.

$$|\Phi\rangle = \sum_{i=0}^{D-1} C_i |\Psi_i\rangle \quad (2.34)$$

where D is the total number of determinants. We assume them to be orthonormal, such that $\langle\Psi_i|\Psi_j\rangle = \delta_{ij}$, but how they are constructed is discussed in the next subsection.

We saw that solving the Schrödinger equation for any wave function that depends linearly on its variational parameters (here C_i) will lead to a secular equation, which is equivalent to the diagonalization of the matrix

$$\begin{pmatrix} \langle\Psi_0|\hat{H}|\Psi_0\rangle & \langle\Psi_0|\hat{H}|\Psi_1\rangle & \langle\Psi_0|\hat{H}|\Psi_2\rangle & \dots & \langle\Psi_0|\hat{H}|\Psi_D\rangle \\ \langle\Psi_1|\hat{H}|\Psi_0\rangle & \langle\Psi_1|\hat{H}|\Psi_1\rangle & \langle\Psi_1|\hat{H}|\Psi_2\rangle & \dots & \langle\Psi_1|\hat{H}|\Psi_D\rangle \\ \langle\Psi_2|\hat{H}|\Psi_0\rangle & \langle\Psi_2|\hat{H}|\Psi_1\rangle & \langle\Psi_2|\hat{H}|\Psi_2\rangle & \dots & \langle\Psi_2|\hat{H}|\Psi_D\rangle \\ \vdots & & & \ddots & \vdots \\ \langle\Psi_D|\hat{H}|\Psi_0\rangle & \langle\Psi_D|\hat{H}|\Psi_1\rangle & \langle\Psi_D|\hat{H}|\Psi_2\rangle & \dots & \langle\Psi_D|\hat{H}|\Psi_D\rangle \end{pmatrix} \quad (2.35)$$

which will yield D energy eigenvalues and eigenvectors, with the lowest eigenvalue being the ground state energy while the others are excited state energies. Each state is thus composed of several determinants and the coefficients we obtain in the diagonalization procedure can tell us how “important” certain determinants are for a given state. An interpretation is only possible if we know how the excited determinants are defined.

2.3.1 Constructing excited determinants

The decision of how the excited determinants are constructed is limited by the basis that we chose to compose the orbitals χ . If we restrict ourselves to the given basis, the only possibility to compose excited determinants is by exchanging occupied and virtual orbitals. In the ground state determinant, let χ_a and χ_b be any two occupied orbitals.

$$|\Psi_0\rangle = |\chi_1\chi_2\dots\chi_a\chi_b\dots\chi_N\rangle \quad (2.36)$$

Let χ_r and χ_s be any two virtual orbitals. If we exchange, say χ_a and χ_r , we are describing an excited state, where the electron that occupied χ_a is excited into χ_r . The determinant that corresponds to this excited configuration can be written as:

$$|\Psi_a^r\rangle = |\chi_1\chi_2\dots\chi_r\chi_b\dots\chi_N\rangle \quad (2.37)$$

Since there are several occupied and virtual orbitals, many configurations can be formed. In the same manner, doubly excited determinants can be constructed, where two occupied orbitals are exchanged with two virtual ones. We write these as

$$|\Psi_{ab}^{rs}\rangle = |\chi_1\chi_2\dots\chi_r\chi_s\dots\chi_N\rangle \quad (2.38)$$

Any number of excitations is possible as long as the basis set size permits. These additional determinants can be used to systematically improve the total wave function, by forming a

linear combination of determinants that takes increasing advantage of the basis set size with every added term:

$$|\Phi\rangle = c_0|\Psi_0\rangle + \sum_{ar} c_a^r|\Psi_a^r\rangle + \sum_{abrs} c_{ab}^{rs}|\Psi_{ab}^{rs}\rangle + \dots \quad (2.39)$$

The sum over ar includes every single excitation, the one over $abrs$ every double excitation, and so on.

This is a systematic way of constructing the wave function in Equation 2.34. Since we enhance the total wave function with additional configurations, this approach is called *configuration interaction* (CI).³ If every possible excitation is regarded, it is called full CI and its solution does not depend on whether we use the basis functions as orbitals or linear combinations of them. By applying this scheme, we use the basis set size to its full capacity; each possible determinant that can be constructed in the given set is then present in the solution and the total wave function is the best approximation to the true wave function in the given basis. If the wave function shall be further improved, it is necessary to include more basis functions, which in turn allows more determinants to be constructed. The determinantal approach thus leads to two axes of improvement: the basis set size and the number of excited determinants. It is intuitive that this scheme leads to numerous determinants to deal with. The total number of determinants D that can be formed with N electrons and K basis functions is

$$D = \binom{K}{N} \quad (2.40)$$

which is unmanageably large for every system that is of chemical interest. Even for small basis sets, the number of possible excitations leads to a computational load that is too big to justify. In general, full CI is more of a concept than a method, but there are good approximations that can be derived from this approach.

Because the additional determinants resemble electron configurations, we can carefully interpret the resulting eigenvalues and eigenvectors. In the single-determinantal approach, a state corresponds directly with an electron configuration, which is an approximation. In reality, a state is not defined by a single configuration, instead the complete solution would include all possible determinants with an infinite basis set. An interpretation in terms of single configurations may still be permitted in some cases, when a particular determinant's coefficient is close to one and this state can be seen as composed of essentially a single configuration. On the other hand, states with significant contributions from multiple configurations point to near-degeneracies and show that a single-determinantal approach will not yield a reliable result for the given system.

2.3.2 The CI matrix elements

In order to see how any ligand field parameterization is derived, we need to understand how the elements of the CI matrix are expressed in terms of one and two-electron integrals.

³Although *configuration mixing* might be a more descriptive term, since the resulting wave functions are admixtures of configurations.

We saw in the last section that we can separate the electronic Hamiltonian into one-electron and two-electron parts. Let us now take a look at the CI matrix in Equation 2.35, and define the additional determinants as the ones corresponding to excited configurations.

$$\begin{pmatrix} \langle \Psi_0 | \hat{H} | \Psi_0 \rangle & \langle \Psi_0 | \hat{H} | \Psi_a^r \rangle & \langle \Psi_0 | \hat{H} | \Psi_{ab}^{rs} \rangle & \dots \\ \langle \Psi_a^r | \hat{H} | \Psi_0 \rangle & \langle \Psi_a^r | \hat{H} | \Psi_a^r \rangle & \langle \Psi_a^r | \hat{H} | \Psi_{ab}^{rs} \rangle & \dots \\ \langle \Psi_{ab}^{rs} | \hat{H} | \Psi_0 \rangle & \langle \Psi_{ab}^{rs} | \hat{H} | \Psi_a^r \rangle & \langle \Psi_{ab}^{rs} | \hat{H} | \Psi_{ab}^{rs} \rangle & \dots \\ \vdots & \vdots & \vdots & \ddots \end{pmatrix} \quad (2.41)$$

In the above matrix,⁴ the excited configurations are subsumed into one matrix element, so for example the element $\langle \Psi_0 | \hat{H} | \Psi_a^r \rangle$ is itself a matrix and represents multiple elements:

$$\langle \Psi_0 | \hat{H} | \Psi_a^r \rangle = \left(\langle \Psi_0 | \hat{H} | \Psi_i^t \rangle \quad \langle \Psi_0 | \hat{H} | \Psi_j^t \rangle \quad \langle \Psi_0 | \hat{H} | \Psi_k^t \rangle \quad \dots \right) \quad (2.42)$$

The matrix elements depicted here are thus matrices themselves, which is important to keep in mind. If we separate the Hamiltonian in this matrix, we can also separate the matrix into a one-electron and a two-electron matrix while their structure each remains the same.⁵ This leads to the following hamiltonian matrix:

$$\mathbf{H} = \begin{pmatrix} \langle \Psi_0 | \hat{h} | \Psi_0 \rangle & \langle \Psi_0 | \hat{h} | \Psi_a^r \rangle & \langle \Psi_0 | \hat{h} | \Psi_{ab}^{rs} \rangle & \dots \\ \langle \Psi_a^r | \hat{h} | \Psi_0 \rangle & \langle \Psi_a^r | \hat{h} | \Psi_a^r \rangle & \langle \Psi_a^r | \hat{h} | \Psi_{ab}^{rs} \rangle & \dots \\ \langle \Psi_{ab}^{rs} | \hat{h} | \Psi_0 \rangle & \langle \Psi_{ab}^{rs} | \hat{h} | \Psi_a^r \rangle & \langle \Psi_{ab}^{rs} | \hat{h} | \Psi_{ab}^{rs} \rangle & \dots \\ \vdots & \vdots & \vdots & \ddots \end{pmatrix} \quad (2.43)$$

$$+ \begin{pmatrix} \langle \Psi_0 | \hat{g} | \Psi_0 \rangle & \langle \Psi_0 | \hat{g} | \Psi_a^r \rangle & \langle \Psi_0 | \hat{g} | \Psi_{ab}^{rs} \rangle & \dots \\ \langle \Psi_a^r | \hat{g} | \Psi_0 \rangle & \langle \Psi_a^r | \hat{g} | \Psi_a^r \rangle & \langle \Psi_a^r | \hat{g} | \Psi_{ab}^{rs} \rangle & \dots \\ \langle \Psi_{ab}^{rs} | \hat{g} | \Psi_0 \rangle & \langle \Psi_{ab}^{rs} | \hat{g} | \Psi_a^r \rangle & \langle \Psi_{ab}^{rs} | \hat{g} | \Psi_{ab}^{rs} \rangle & \dots \\ \vdots & \vdots & \vdots & \ddots \end{pmatrix}$$

If the basis set used in the determinants is orthonormal, the elements can be further simplified by a set of rules, called Slater's rules. By comparison of how many orbitals of the two determinants in $\langle \Psi_i | \hat{h} | \Psi_j \rangle$ or $\langle \Psi_i | \hat{g} | \Psi_j \rangle$ are different, the elements can be expressed in defined integrals over these orbitals. The rules differ for one-electron and two-electron operators and are listed below. The list entries below begin with the number of different orbitals.

⁴According to Brillouin's theorem, the elements $\langle \Psi_0 | \hat{H} | \Psi_a^r \rangle$ and $\langle \Psi_a^r | \hat{H} | \Psi_0 \rangle$ are 0, but this is a rather distracting detail here.

⁵This is a separation that only serves to partition the expressions into manageable pieces for the reader. Diagonalizing a sum of matrices is generally *not* the same as summing up diagonalized matrices.

One-electron operator

$$\begin{aligned} 0: \langle \dots \chi_a \chi_b \dots | \hat{h} | \dots \chi_a \chi_b \dots \rangle &= \sum_j \langle \chi_j | \hat{h} | \chi_j \rangle \\ 1: \langle \dots \chi_a \chi_b \dots | \hat{h} | \dots \chi_r \chi_b \dots \rangle &= \langle \chi_a | \hat{h} | \chi_r \rangle \\ 2+: \langle \dots \chi_a \chi_b \dots | \hat{h} | \dots \chi_r \chi_s \dots \rangle &= 0 \end{aligned} \quad (2.44)$$

Two-electron operator

$$\begin{aligned} 0: \langle \dots \chi_a \chi_b \chi_c \dots | \hat{g} | \dots \chi_a \chi_b \chi_c \dots \rangle &= \frac{1}{2} \sum_i \sum_j \langle \chi_i \chi_j | | \chi_i \chi_j \rangle \\ 1: \langle \dots \chi_a \chi_b \chi_c \dots | \hat{g} | \dots \chi_r \chi_b \chi_c \dots \rangle &= \sum_j \langle \chi_a \chi_j | | \chi_r \chi_j \rangle \\ 2: \langle \dots \chi_a \chi_b \chi_c \dots | \hat{g} | \dots \chi_r \chi_s \chi_c \dots \rangle &= \langle \chi_a \chi_b | | \chi_r \chi_s \rangle \\ 3+: \langle \dots \chi_a \chi_b \chi_c \dots | \hat{g} | \dots \chi_r \chi_s \chi_t \dots \rangle &= 0 \end{aligned} \quad (2.45)$$

with $\langle \chi_a \chi_b | | \chi_r \chi_s \rangle = \langle \chi_a \chi_b | \hat{g} | \chi_r \chi_s \rangle - \langle \chi_a \chi_b | \hat{g} | \chi_s \chi_r \rangle$.

In an actual CI calculation, these integrals are solved and the resulting eigenvalues are *ab initio* approximations to the ground state and the excited states, limited by the basis set size and how well the chosen basis functions cover the molecular structure in general.

2.4 Cherry-picking determinants

As we have seen above, CI is clearly not a viable approach to solve an electronic structure problem, but there are possibilities to reduce the computational complexity. Many determinants do not contribute significantly to the energies one might be interested in (most prominently the ground state energy), although they increase the computational load just as much as more important determinants do. The obvious solution to that problem is the omission of determinants that are considered “unimportant”, and the subsequent question is how to tell the important and the unimportant ones apart.

Before presenting possible simplification approaches we have to be aware that every scheme that includes more determinants without reaching the full CI limit is dependent on the chosen orbitals. While in full CI we could just take the basis functions as orbitals and obtain the same results, reduced CI schemes profit from optimizing the orbitals first. It is common to choose an optimized (HF) ground state determinant as reference for the generation of excited determinants.

Common are so-called truncated CI schemes, for example CI singles (CIS), CI singles and doubles (CISD). The idea is to restrict the excitation level to singly or doubly excited states, so Equation 2.39 is cut after the second or third summand. It is chemically intuitive in the sense that multiply excited states are much rarer and their determinants should be less relevant. Although they do work and are certainly more popular than full CI,

truncated CI schemes are superseded by coupled cluster approaches and have low practical relevance.⁶

The most interesting approach with regard to LFT are active space schemes. Instead of choosing a certain general excitation level as a chemically reasonable limit, the excitations are selected depending on a specific set of active orbitals. For example, a researcher might be interested in a specific transition in photochemistry, say the π electrons in a dyeing agent or the d excitations in a transition metal complex. The chosen orbitals would then include the bonding and antibonding π orbitals or the five antibonding d orbitals respectively. These orbitals make up the *active space*, and we do not restrict the level of excitation in the determinants constructed from that active space. Notice that we must choose a set of occupied orbitals as well as a set of virtual ones, otherwise no excitations are possible at all. In the chosen set, all possible excitations of the active orbitals are constructed, which means that the CI calculation is performed on a smaller sized configurational space. This method is called *complete active space* (CAS). Commonly, three spaces are distinguished in a CAS calculation: the *occupied* orbitals are doubly occupied and not subject to any excitation. Still, they are part of the total wave function and thus contribute to the electronic state energies. The *active* orbitals make up the CI space, all excitations are performed within that space. The *virtual* orbitals do not contribute to the excited states.⁷ It is common to use a (n, m) notation for active spaces, indicating that n electrons are distributed over m spatial orbitals.

2.4.1 Active space example

In a spin orbital basis, let us assume a ground state determinant for eight electrons, $|\Psi_0\rangle = |\chi_1\chi_2 \dots \chi_7\chi_8\rangle$ and 12 additional virtual orbitals with the indices 9 to 20. Say we further choose the orbitals 7 to 10 to be in the active space, making the orbitals χ_1 to χ_6 occupied and the orbitals χ_{11} to χ_{20} virtual. To keep the example easy to overview, we write the occupied orbitals as dots and focus on the active space. The full CI wave function within the active space is then written:

$$\begin{aligned} |\Phi\rangle = & c_{7,8} |\dots \chi_7\chi_8\rangle \\ & + c_{7,9} |\dots \chi_7\chi_9\rangle + c_{8,9} |\dots \chi_8\chi_9\rangle \\ & + c_{7,10} |\dots \chi_7\chi_{10}\rangle + c_{8,10} |\dots \chi_8\chi_{10}\rangle \\ & + c_{9,10} |\dots \chi_9\chi_{10}\rangle \end{aligned} \quad (2.46)$$

As illustrated, the occupied orbitals remain fixed, the ones in the active space are exchanged in the excited determinants and the virtual ones do not enter the function at all.

Let us repeat the above example with spatial orbitals, to clarify the shorthand notation for active spaces and ease the coming transition to ligand field theory. In a closed-shell system, the eight electrons would occupy four spatial orbitals, and the ground state

⁶Mainly because coupled cluster approaches are more accurate and do not suffer from the truncated CI state consistency problem.

⁷Another flavour of active space schemes is *restricted active space* (RAS), where more restrictions are employed on the excitations that are allowed in the active space.^[24]

determinant would be $|\Psi_0\rangle = |\psi_1\bar{\psi}_1\psi_2\bar{\psi}_2\psi_3\bar{\psi}_3\psi_4\bar{\psi}_4\rangle$. Since the spatial orbitals 1, 2 and 3 are inactive, this would be abbreviated $|\Psi_0\rangle = |\dots\psi_4\bar{\psi}_4\rangle$. The unoccupied orbitals that enter the active space are ψ_5 and $\bar{\psi}_5$, and all the higher ones do not enter the wave function at all. As the active space consists of two spatial orbitals and two electrons, its shorthand notation is (2, 2). The CI wave function is then:

$$\begin{aligned}
 |\Phi\rangle = & c_{4,\bar{4}}|\dots\psi_4\bar{\psi}_4\rangle \\
 & + c_{4,5}|\dots\psi_4\psi_5\rangle + c_{\bar{5},\bar{4}}|\dots\bar{\psi}_5\bar{\psi}_4\rangle \\
 & + c_{4,\bar{5}}|\dots\psi_4\bar{\psi}_5\rangle + c_{\bar{5},4}|\dots\bar{\psi}_5\psi_4\rangle \\
 & + c_{\bar{5},\bar{5}}|\dots\bar{\psi}_5\bar{\psi}_5\rangle
 \end{aligned}
 \tag{2.47}$$

In the open shell case with a triplet ground state, the ground state determinant would be $|\Psi_0\rangle = |\dots\psi_4\psi_5\rangle$, but the CI wave function would be exactly the same as for the singlet ground state. This is an important detail: the multiplicity of the ground state plays no role for the construction of the CAS wave function, only the selection of orbitals and the number of electrons. On the other hand, it is of course possible to choose a set of active orbitals from which the true ground state cannot be constructed. For this reason, it is common to start with a determinant that was optimized by a ground state electronic structure method like HF, ensuring a reasonable selection of molecular orbitals.

In the next chapter, we will see how ligand field theory and the CAS approach are very similar in many regards and that LFT is in fact just a highly compact parameterization of the CI matrix. The rules for the matrix elements in the above sets of equations will help to understand how ligand field parameters are derived.

2.4.2 Multiconfiguration self-consistent field methods

Since the accuracy of truncated CI and active space methods depends on the orbitals that make up the determinants, it is useful to optimize these, too. In a simple case, we could perform an HF calculation to obtain orbital coefficients c_{ij} and use the resulting wave function as a reference. When performing an active space calculation afterwards in order to optimize the determinant coefficients C_i , we will likely get a very good approximation to the ground state energy, but the excited states might be less accurate due to the focus of the reference determinant.

In multiconfiguration self-consistent field (MCSCF) methods, both sets of coefficients are optimized in an alternating process. For each diagonalization performed on the CI matrix of the CAS, another SCF optimization of the orbital coefficients is conducted such that the orbital coefficients c_{ij} are not only optimized with regard to the ground state, but possibly to excited states, too.

While the diagonalization of the CAS-CI matrix always yields all eigenvalues and vectors, the underlying reference determinant has a large impact on the accuracy of the states. If the orbital coefficients c_{ij} are optimized such that the energy of one particular state is minimal, it is a *state-specific* CASSCF calculation. If they are optimized that two to all states are minimal (on average), it is called *state-average* CASSCF. Of course, the state-specific

method could be separately performed for each particular state, which would yield the best approximation for the state energies. In consequence however, the orbitals of the different states would not be orthonormal any more and for example the prediction of transition moments (i.e. intensities) is not possible. All active space calculations presented in the main text are state-average CASSCF calculations.

3 Ligand Field Theory and the Angular Overlap Model

Ligand field theory is an approach to explain and understand the optical and magnetic properties of transition metal complexes. It is constructed from perturbation theory or effective Hamiltonian theory, respectively, and assumes the metal valence d orbitals¹ to be the basis functions. All LFT schemes have in common that they parameterize the electronic energies obtained in the given basis, and the flavours of LFT are distinguished by the chosen sets of parameters.

Historically, LFT is a generalization of crystal field theory and the underlying concept is the same. Due to its little practical relevance and the fact that it can be viewed as special case of LFT, we will not treat crystal field theory here. Before we dive into the ligand field parameterization schemes, we will specify a few terms that were introduced more generally in the last chapter, such as the Hamiltonian, the employed basis functions and the possible configurations resulting from the basis. We will construct a CI matrix for the given basis and then show how the elements of this matrix can be parameterized.

After the presentation of the general ligand field parameterizations we narrow the scope further by focusing on the angular overlap model. Its derivation and common adjustments are laid out, providing the theoretical foundation to understand the main discussions in the publications that make up the main body of this work.

The content of this chapter is mainly based on refs. [6, 13, 22, 25], where ref. [22] is especially detailed on the connection of ligand field theory and the quantum chemical treatment of electronic structure problems. The derivation of the AOM is presented in large detail in ref. [26] and the d-s mixing extension in ref. [27]

3.1 Ligand Field Theory

Ligand field theory is a perturbation or effective Hamiltonian approach, where a perturbation operator is used to describe the electronic energies in a d orbital basis. As usual in perturbation theory, we approximate effects that are considered a perturbation as addition \hat{H}_1 to an unperturbed Hamiltonian \hat{H}_0 and expansions of the wave function Ψ .

$$\hat{H} = \hat{H}_0 + \hat{H}_1 \quad (3.1)$$

In the case of ligand field theory, the unperturbed Hamiltonian contains the kinetic energy of the electrons and their electrostatic interactions with the (fixed) nuclei. What is left to

¹Or f orbitals, but these are not subject of this work.

be a perturbation is the electron-electron repulsion G and the ligand field V_{LF} , a vaguely specified effect that the ligands have on the electrons.

$$\hat{H}_1 = \hat{H}_{LF} = \sum_i^N \hat{V}_{LF}(r_i) + \sum_{i<j}^N \hat{G}_{ij}(r_i, r_j) \quad (3.2)$$

This is abbreviated further to include the sums into the operator symbols.

$$\hat{H}_{LF} = \hat{V}_{LF} + \hat{G} \quad (3.3)$$

The one-electron ligand field operator is \hat{V}_{LF} , the two-electron operator is \hat{G} . Since \hat{V}_{LF} and \hat{H}_{LF} are both termed ligand field operator, some confusion can arise here. Generally, the symbol is given to avoid this, or we refer to either the *total* or *one-electron* ligand field operator.

The unperturbed Hamiltonian \hat{H}_0 is of little interest to us in the context of LFT. The solutions to its eigenvalue equation are the degenerate, unperturbed electronic states which only serve as an energy basis in the ligand field picture. Since spectroscopic methods can only capture energy differences, this basis energy cancels in experiment and has no practical relevance. We will encounter it again at the very end of the AOM section, where it is incorporated in a single parameter.

3.1.1 The d orbital basis

Central to CFT and LFT is that they work on a d orbital basis. Consequently, they can only describe electronic transitions between states that differ (mainly) in their d electron configuration. As another consequence, LFT loses validity as soon as the actual bonding situation in a complex requires strong mixing of the transition metal d orbitals with ligand orbitals.

Most approaches to quantum chemical wave functions of electrons in molecules use atomic orbitals that are linearly combined to form molecular orbitals. This scheme is called linear combination of atomic orbitals (LCAO) and manifests such that the basis functions in Equation 2.10 are atomic orbitals, consisting of a radial part and an angular part.

$$\phi = R(r)Y_l^{m_l}(\theta, \varphi) \quad (3.4)$$

They are located at an atom, hence the name, so the used spherical coordinates r, θ, φ are related to the position of the atom. The radial part is commonly a Slater-type function or a Gaussian, but its exact shape does not matter to us. The angular dependent part $Y_l^{m_l}$ is a complex spherical harmonic which defines the type of the orbital via the quantum numbers l and m_l . The d orbitals have $l = 2$, for which the spherical harmonics are listed in the appendix. Very often, chemists do not use the complex spherical harmonics themselves, but linear combinations that do not have an imaginary part. There is no fundamental reason for this, but the real spherical harmonics are somewhat easier to visualize and

have clearer directional properties. The real d orbitals are based on the following linear combinations:

$$\begin{aligned}
Y_{2,-2} &= -\frac{i}{\sqrt{2}}(Y_2^2 - Y_2^{-2}) = \sqrt{\frac{15}{16\pi}} \sin^2(\theta) \sin(2\varphi) \\
Y_{2,-1} &= \frac{i}{\sqrt{2}}(Y_2^1 + Y_2^{-1}) = \sqrt{\frac{15}{4\pi}} \sin(\theta) \cos(\theta) \sin(\varphi) \\
Y_{2,0} &= Y_2^0 = \sqrt{\frac{5}{16\pi}} (3 \cos^2(\theta) - 1) \\
Y_{2,1} &= -\frac{1}{\sqrt{2}}(Y_2^1 - Y_2^{-1}) = \sqrt{\frac{15}{4\pi}} \sin(\theta) \cos(\theta) \cos(\varphi) \\
Y_{2,2} &= \frac{1}{\sqrt{2}}(Y_2^2 + Y_2^{-2}) = \sqrt{\frac{15}{16\pi}} \sin^2(\theta) \cos(2\varphi)
\end{aligned} \tag{3.5}$$

Accordingly, the basis functions that are employed in LFT are linear combinations of the complex spherical harmonics and the basis is defined in terms of d orbitals. The spherical harmonics are orthonormal and thus, all simplification rules from the last chapter can be used.

$$d_{m_l} = R(r)Y_{2,m_l}(\theta, \varphi) \tag{3.6}$$

In the context of the real spherical harmonics, m_l is substituted by the geometrical descriptors $xy, yz, z^2, xz, x^2 - y^2$. According to the above definition of the basis functions, the orbitals that are employed are linear combinations of these which are also orthonormal:

$$\begin{aligned}
d'_i &= \sum_{m_l} c_{m_l,i} d_{m_l} \\
&= \sum_{m_l} c_{m_l,i} R(r)Y_{2,m_l}(\theta, \varphi)
\end{aligned} \tag{3.7}$$

It might be helpful to note that in most publications, the coefficients $c_{m_l,i}$ are implicitly chosen such that the orbitals d'_i coincide with the basis functions d_{m_l} . This is the case if in each linear combination, one of the coefficients is 1 while the others are 0. For a free ion, the orbitals are degenerate, and the results for any chosen set of coefficients are equal. Only when ligands are present that lift the degeneracy of the d orbitals, it might be necessary to adapt the coefficients such that the state energies are minimal. Similarly, we choose the orbitals d'_i such that they coincide with d_{m_l} in the next sections.

On another note, the term d orbital can mean three slightly different functions depending on the context. Quite generally, d orbital means any orbital which has $l = 2$ and accordingly, d_{m_l} and d'_i are often used interchangeably. In most mathematical operations, they also behave equally, so their exact specification does not matter. A slightly closer look can be necessary when the symbol d means the spherical harmonics without the radial part. Again, this might not matter since e.g. under rotations, the radial part remains unaltered.

Table 3.1: Determinants of all possible d^1 configurations, ordered by $M_S = \sum m_s$ and $M_L = \sum m_l$.

$M_L \backslash M_S$	$\frac{1}{2}$	$-\frac{1}{2}$
2	$ d_{xy}\rangle$	$ \bar{d}_{xy}\rangle$
1	$ d_{yz}\rangle$	$ \bar{d}_{yz}\rangle$
0	$ d_{z^2}\rangle$	$ \bar{d}_{z^2}\rangle$
-1	$ d_{xz}\rangle$	$ \bar{d}_{xz}\rangle$
-2	$ d_{x^2-y^2}\rangle$	$ \bar{d}_{x^2-y^2}\rangle$

3.1.2 Configurations and the CI matrix

In the previous chapter, we discussed the structure of the CAS wave functions, which are constructed by linearly adding the determinants of each excited state to the ground state determinant. Phrased slightly differently, the CAS wave function must contain all possible electron configurations.

The construction of excited states is possible by using a scheme following the second quantization approach of using excitation operators. Starting from a state where the electrons are distributed over a selection of orbitals, the application of an excitation operator replaces a selected occupied orbital with a selected virtual one. Doing this for all combinations of occupied and virtual orbitals will yield each singly excited state determinant. To obtain double and higher excitations, an appropriate number of distinct excitation operators needs to be applied to the original determinant, up to a maximum excitation level equal to the number of electrons.

The basis that we use in LFT always consists of the five d orbitals, which makes ten basis functions in total when regarding spin.² In the simplest case of one electron, single excitations are the maximum making ten different configurations. To get an overview, it is convenient to arrange them in a table where one axis is the total spin of the configuration and the other is the total angular momentum. The d^1 case is presented in Table 3.1. Obviously, the determinants are just single functions and in the resulting 10×10 CI matrix, there would be no two-electron integral. This is the simplest case for an open d shell, but according to Equation 2.40, the number of possible configurations increases strongly if more electrons are included. The number of configurations for each possible number of d electrons is shown in Table 3.2.

An acceptable balance between example completeness and simplicity is provided by the d^2 case, where all possible one and two electron integrals appear. There are 45 configurations as shown in Table 3.3. Although these are too many to present or discuss the whole CI matrix, it is at least possible to keep the overall structure in mind and to collect all configurations in a single table. In the next section, the d^2 case serves as example system for the more detailed discussion of LFT.

As we have seen in the last chapter, a configuration interaction approach can be used to

²For actinoides and lanthanoides, the basis consists of the seven f orbitals, leading to fourteen basis functions.

Table 3.2: Number of possible configurations for 10 basis functions and n electrons. Note that due to the electron–hole analogy, partly filled and partly empty orbitals behave equal in the construction of excited state configurations.

Electron configuration	d^0, d^{10}	d^1, d^9	d^2, d^8	d^3, d^7	d^4, d^6	d^5
Number of configurations	1	10	45	120	210	252

Table 3.3: Determinants of all possible d^2 configurations, ordered by $M_S = \sum m_s$ and $M_L = \sum m_l$.

$M_L \backslash M_S$	-1	0	1
-4		$ \bar{d}_{xy}d_{xy}\rangle$	
-3	$ \bar{d}_{xy}\bar{d}_{yz}\rangle$	$ d_{xy}\bar{d}_{yz}\rangle, \bar{d}_{xy}d_{yz}\rangle$	$ d_{xy}d_{yz}\rangle$
-2	$ \bar{d}_{xy}\bar{d}_{z^2}\rangle$	$ d_{xy}\bar{d}_{z^2}\rangle, \bar{d}_{xy}d_{z^2}\rangle,$ $ \bar{d}_{yz}d_{yz}\rangle$	$ d_{xy}d_{z^2}\rangle$
-1	$ \bar{d}_{xy}\bar{d}_{xz}\rangle, \bar{d}_{yz}\bar{d}_{z^2}\rangle$	$ d_{xy}\bar{d}_{xz}\rangle, \bar{d}_{xy}d_{xz}\rangle,$ $ \bar{d}_{yz}d_{z^2}\rangle, \bar{d}_{yz}\bar{d}_{z^2}\rangle$	$ d_{xy}d_{xz}\rangle, d_{yz}d_{z^2}\rangle$
0	$ \bar{d}_{xy}\bar{d}_{x^2-y^2}\rangle, \bar{d}_{yz}\bar{d}_{xz}\rangle$	$ d_{xy}\bar{d}_{x^2-y^2}\rangle,$ $ \bar{d}_{xy}d_{x^2-y^2}\rangle, \bar{d}_{yz}d_{xz}\rangle,$ $ d_{yz}\bar{d}_{xz}\rangle, \bar{d}_{z^2}d_{z^2}\rangle$	$ d_{xy}d_{x^2-y^2}\rangle, d_{yz}d_{xz}\rangle$
1	$ \bar{d}_{yz}\bar{d}_{x^2-y^2}\rangle, \bar{d}_{z^2}\bar{d}_{xz}\rangle$	$ \bar{d}_{yz}d_{x^2-y^2}\rangle,$ $ d_{yz}\bar{d}_{x^2-y^2}\rangle, \bar{d}_{z^2}d_{xz}\rangle,$ $ d_{z^2}\bar{d}_{xz}\rangle$	$ d_{yz}d_{x^2-y^2}\rangle, d_{z^2}d_{xz}\rangle$
2	$ \bar{d}_{z^2}\bar{d}_{x^2-y^2}\rangle$	$ \bar{d}_{z^2}d_{x^2-y^2}\rangle,$ $ d_{z^2}\bar{d}_{x^2-y^2}\rangle, \bar{d}_{xz}d_{xz}\rangle$	$ d_{z^2}d_{x^2-y^2}\rangle$
3	$ \bar{d}_{xz}\bar{d}_{x^2-y^2}\rangle$	$ \bar{d}_{xz}d_{x^2-y^2}\rangle,$ $ d_{xz}\bar{d}_{x^2-y^2}\rangle$	$ d_{xz}d_{x^2-y^2}\rangle$
4		$ \bar{d}_{x^2-y^2}d_{x^2-y^2}\rangle$	

obtain the electronic state energies. This requires setting up the CI matrix in the chosen basis and its diagonalization. It is futile to present a whole CI matrix here, so instead we discuss just a section of it. The matrix below is a section of the 45×45 CI matrix constructed from the d^2 configuration.

$$\mathbf{H}_{\text{section}} = \begin{pmatrix} \langle d_{xy}d_{yz} | \hat{H} | d_{xy}d_{x^2-y^2} \rangle & \langle d_{xy}d_{yz} | \hat{H} | \bar{d}_{xy}\bar{d}_{yz} \rangle & \langle d_{xy}d_{yz} | \hat{H} | \bar{d}_{xy}d_{yz} \rangle \\ \langle d_{xy}\bar{d}_{z^2} | \hat{H} | d_{xy}d_{x^2-y^2} \rangle & \langle d_{xy}\bar{d}_{z^2} | \hat{H} | \bar{d}_{xy}\bar{d}_{yz} \rangle & \langle d_{xy}\bar{d}_{z^2} | \hat{H} | \bar{d}_{xy}d_{yz} \rangle \\ \langle d_{xy}d_{z^2} | \hat{H} | d_{xy}d_{x^2-y^2} \rangle & \langle d_{xy}d_{z^2} | \hat{H} | \bar{d}_{xy}\bar{d}_{yz} \rangle & \langle d_{xy}d_{z^2} | \hat{H} | \bar{d}_{xy}d_{yz} \rangle \end{pmatrix} \quad (3.8)$$

The Hamiltonian is a sum of one and two-electron operators, and thus the matrix can be written as sum, too:

$$\mathbf{H}_{\text{section}} \quad (3.9)$$

$$= \mathbf{V}_{\text{section}} + \mathbf{G}_{\text{section}} \quad (3.10)$$

$$= \begin{pmatrix} \langle d_{xy}d_{yz} | \hat{V}_{LF} | d_{xy}d_{x^2-y^2} \rangle & \langle d_{xy}d_{yz} | \hat{V}_{LF} | \bar{d}_{xy}\bar{d}_{yz} \rangle & \langle d_{xy}d_{yz} | \hat{V}_{LF} | \bar{d}_{xy}d_{yz} \rangle \\ \langle d_{xy}\bar{d}_{z^2} | \hat{V}_{LF} | d_{xy}d_{x^2-y^2} \rangle & \langle d_{xy}\bar{d}_{z^2} | \hat{V}_{LF} | \bar{d}_{xy}\bar{d}_{yz} \rangle & \langle d_{xy}\bar{d}_{z^2} | \hat{V}_{LF} | \bar{d}_{xy}d_{yz} \rangle \\ \langle d_{xy}d_{z^2} | \hat{V}_{LF} | d_{xy}d_{x^2-y^2} \rangle & \langle d_{xy}d_{z^2} | \hat{V}_{LF} | \bar{d}_{xy}\bar{d}_{yz} \rangle & \langle d_{xy}d_{z^2} | \hat{V}_{LF} | \bar{d}_{xy}d_{yz} \rangle \end{pmatrix} \quad (3.11)$$

$$+ \begin{pmatrix} \langle d_{xy}d_{yz} | \hat{G} | d_{xy}d_{x^2-y^2} \rangle & \langle d_{xy}d_{yz} | \hat{G} | \bar{d}_{xy}\bar{d}_{yz} \rangle & \langle d_{xy}d_{yz} | \hat{G} | \bar{d}_{xy}d_{yz} \rangle \\ \langle d_{xy}\bar{d}_{z^2} | \hat{G} | d_{xy}d_{x^2-y^2} \rangle & \langle d_{xy}\bar{d}_{z^2} | \hat{G} | \bar{d}_{xy}\bar{d}_{yz} \rangle & \langle d_{xy}\bar{d}_{z^2} | \hat{G} | \bar{d}_{xy}d_{yz} \rangle \\ \langle d_{xy}d_{z^2} | \hat{G} | d_{xy}d_{x^2-y^2} \rangle & \langle d_{xy}d_{z^2} | \hat{G} | \bar{d}_{xy}\bar{d}_{yz} \rangle & \langle d_{xy}d_{z^2} | \hat{G} | \bar{d}_{xy}d_{yz} \rangle \end{pmatrix} \quad (3.12)$$

The integrals we encounter in these matrices can be simplified with the rules presented in Equation 2.44 and Equation 2.45. We do not have a case in this matrix section where the configurations on the bra and ket are identical, so only the rules for differences ≥ 1 apply.

$$\mathbf{V}_{\text{section}} + \mathbf{G}_{\text{section}} \quad (3.13)$$

$$= \begin{pmatrix} \langle d_{yz} | \hat{V}_{LF} | d_{x^2-y^2} \rangle & 0 & \langle d_{xy} | \hat{V}_{LF} | \bar{d}_{xy} \rangle \\ \langle \bar{d}_{z^2} | \hat{V}_{LF} | d_{x^2-y^2} \rangle & 0 & 0 \\ \langle d_{z^2} | \hat{V}_{LF} | d_{x^2-y^2} \rangle & 0 & 0 \end{pmatrix} \quad (3.14)$$

$$+ \begin{pmatrix} \sum_j \langle d_j d_{yz} | | d_j d_{x^2-y^2} \rangle & \langle d_{xy} d_{yz} | | \bar{d}_{xy} \bar{d}_{yz} \rangle & \sum_j \langle d_{xy} d_j | | \bar{d}_{xy} d_j \rangle \\ \sum_j \langle d_j \bar{d}_{z^2} | | d_j d_{x^2-y^2} \rangle & \langle d_{xy} \bar{d}_{z^2} | | \bar{d}_{xy} \bar{d}_{yz} \rangle & \langle d_{xy} \bar{d}_{z^2} | | \bar{d}_{xy} d_{yz} \rangle \\ \sum_j \langle d_j d_{z^2} | | d_j d_{x^2-y^2} \rangle & \langle d_{xy} d_{z^2} | | \bar{d}_{xy} \bar{d}_{yz} \rangle & \langle d_{xy} d_{z^2} | | \bar{d}_{xy} d_{yz} \rangle \end{pmatrix} \quad (3.15)$$

Additional properties of the terms found can be used to further simplify the problem. In a last step, we use the hermiticity of the Hamiltonian, which says that $\langle a | \hat{H} | b \rangle = \langle b | \hat{H} | a \rangle^*$. Since we deal with real basis functions in LFT, the complex conjugation can be omitted.

After applying these simplifications, it is apparent that the one-electron integrals have very limited variety. They can be collected in a symmetric 5×5 matrix:

$$(\mathbf{V}_{LF})_{ij} = \langle d_i | \hat{V}_{LF} | d_j \rangle \quad (3.16)$$

such that only 15 unique elements remain. In the context of LFT, no attempt to solve these integrals is made. Instead, they are subject to parameterization, and it is this parameterization that is the very essence of ligand field theory.

Although their expression seems to be more complicated, we start with the treatment of the two-electron integrals. The next section deals with the further simplification and subsequent parameterization of these terms.

3.1.3 Two-electron integrals

The parameterization of the two-electron integrals is derived from the free ion, with the assumption that the electron-electron interaction is independent of the involved d orbital.

The exact derivation for the expression of the two-electron part is lengthy and can be found for example in section 6.8 of ref. [25]. It bases on the expansion of the Coulomb operator $1/r_{ij}$ in terms of spherical harmonics, which makes it possible to integrate over the angular coordinates. The definition of the two-electron integrals $\langle \chi_i \chi_j | \hat{g} | \chi_r \chi_s \rangle$ then becomes:

$$\begin{aligned} \langle \chi_i \chi_j | \hat{g} | \chi_r \chi_s \rangle &= \delta_{m_s^i, m_s^r} \cdot \delta_{m_s^j, m_s^s} \cdot \delta_{(m_l^i + m_l^j), (m_l^r + m_l^s)} \\ &\cdot \sum_{k=0}^{\infty} c^k(l^i m_l^i, l^r m_l^r) c^k(l^s m_l^s, l^j m_l^j) R^k(n^i l^i n^j l^j, n^r l^r n^s l^s) \end{aligned} \quad (3.17)$$

The coefficients in the above equation depend on the principal quantum number n , the orbital quantum number l , the magnetic quantum number m_l and the spin quantum number m_s . The Kronecker deltas emerge from the integration over the angular coordinate φ , the coefficients c^k , called Gaunt integrals, represent the integration over the other angular coordinate θ . The Gaunt integrals are zero unless k meets certain conditions, which only leaves the remaining values for $k = 0, 2, 4$. The values for these c^k are tabulated for example in ref. [25], p.178f. The integral R^k represents the integration over the electron-nucleus distance r and are not integrated explicitly. Our restriction to a single central atom and its d orbitals requires all n^i to be equal and $l = 2$, which means that the values of R^k are independent of the orbitals that enter the integral. Hence, we shorten it and define $R^k = F^k$ under the given restrictions.

With the known quantities in Equation 3.17, every two-electron integral occurring in the CI matrix can be expressed in terms of F^k . By convention, they are either given in a weighted form, called Condon-Shortley parameters,

$$\begin{aligned} F_0 &= F^0 \\ F_2 &= \frac{1}{49} F^2 \\ F_4 &= \frac{1}{441} F^4 \end{aligned} \quad (3.18)$$

or in terms of Racah parameters, which are linear combinations of F_k .

$$\begin{aligned} A &= F_0 - 49F_4 \\ B &= F_2 - 5F_4 \\ C &= 35F_4 \end{aligned} \quad (3.19)$$

As mentioned at the beginning of the section, this derivation was originally done for free ion terms, where the one-electron term is neglected and all d orbitals have the same energy. The presence of a ligand field does not necessarily decrease the validity of the above derivation, but allows a physical interpretation of the Racah parameters. They are thus suitable for the description of free ions and complexes alike.

The value of the parameters is always positive, the coefficient of A is constant for a given electron number. More relevant is the parameter B (and C), which depicts the electronic repulsion and as such it decreases when the d orbitals spatially increase. This is due to the increased average distance of the electrons that occupy said orbitals. In most complexes, B is decreased compared to the free ion, leading to the interpretation that the presence of ligands expands the valence d orbitals. This spatial expansion is called *nephelauxetic effect*. In order to understand an important part of the critique of ligand field theory, we need to pay attention the fact that the derivation assumes the radial parts of the d orbitals to depend only on the quantum numbers n and l . For a set of d orbitals, they are equal, although the spatial expansion is known to be dependent on the complex geometry and affects the d orbitals differently.

3.1.4 One-electron integrals

Now, *what is ligand field theory?* LFT is an approximation to the d electron part of an electronic spectrum. It parameterizes the integrals that occur if we approach the electronic problem in an active space picture. The parameterization scheme of the two-electron integrals is the same among different flavours of LFT, while the parameterization of the one-electron integrals distinguishes them. Each of its sub-models is thus only described in how it parameterizes the one-electron integrals which are commonly subsumed and referred to in matrix form with the elements:

$$(\mathbf{V}_{LF})_{ij} = \langle d_i | \hat{V}_{LF} | d_j \rangle \quad (3.20)$$

This matrix is called *one electron ligand field matrix*, but often abbreviated to just ligand field matrix. Its elements are real and it is symmetric, so only up to 15 of its 25 elements are unique. In practice, the number of unique elements is usually smaller.

An important fact is that the eigenvalues of \mathbf{V}_{LF} are the d orbital energies. As chemists tend to rationalize trends and observation in terms of orbitals and orbital energies, this is an important basis for discussion. Although they are no observables, they help understand the effects of ligands on transition metals.

With the given derivations of the ligand field operator and matrix elements, we can make a clear distinction between CFT and LFT. In CFT, the elements of \mathbf{V}_{LF} are predicted by defining the ligand field operator as electrostatic interaction operator. The only experimental data that is used for the computation of electronic states is the geometry of the complex. It is thus an *ab initio* theory, because all parts of the calculation of any property are derived from first principles. On the contrary, LFT is an *empirical* theory, since the expressions obtained by the *ab initio* treatment are parameterized with the help of experimental data. As with all empirical theories, LFT is in constant danger of producing

meaningless parameters, and because of this their interpretation is usually carried out carefully.

The simplest way to parameterize the one-electron integrals is to treat them as parameters themselves. This approach is somewhat straightforward, but suffers from the fact that the obtained parameters have no physical meaning. A simple reproduction of experimental data is not an end in itself. Due to this, the matrix elements are usually parameterized with specified parameter sets that take the molecule's geometry into account. Widespread parameterization schemes make use of the symmetry of the investigated complex, which relates the elements of \mathbf{V}_{LF} to each other, and in doing so reduces the number of parameters needed. The parameterization of the ligand field splitting in octahedral complexes is an example of such a reduction by symmetry, where only a single parameter Δ is sufficient. In the next section, we will derive and discuss the angular overlap model (AOM), which parameterizes \mathbf{V}_{LF} in terms of additive ligand contributions.

3.2 Angular Overlap Model

In deriving the angular overlap model, we largely follow the approach of Schäffer and Jørgensen,^[14,28] in the notation presented by Deeth and Foulis in the SI of ref. [27]. Further useful sources for understanding the derivation are refs. [29, 30] for a general overview on the AOM and refs. [31, 32] for specific information about rotations of spherical harmonics. As all ligand field theory schemes, the AOM is concerned with the parameterization of the one-electron integrals $\langle d_i | \hat{V}_{LF} | d_j \rangle$. We will go through the assumptions and steps that are necessary to derive the AOM in this section. First and most importantly, the ligands' perturbations on the metal d orbitals are assumed to be additive. The ligand field effect of each ligand L can be expressed in a separate ligand field matrix and the total one is then expressed as

$$\mathbf{V}_{LF} = \sum_L \mathbf{V}_{LF,L} \quad (3.21)$$

Accordingly, we need to derive the individual ligand field matrices next.

3.2.1 The local frame

To express the ligands' perturbation on the metal d orbitals, we apply a mathematical scheme that significantly simplifies the complexity of the problem. Each ligand is treated in a local coordinate frame, where we find the expressions for the local ligand field matrix. This matrix has a simple shape, as we will see. To move the ligand field matrix into the global frame, a rotation of the d orbitals is applied. This rotation accounts for the actual position of the ligand in the global frame and is treated in the next subsection.

The local coordinate frame in which the ligand field matrix is constructed is chosen such that the metal lies in its origin, while the ligand resides on the z-axis at an arbitrary distance. The AOM assumes that the ligand field contribution from this ligand emerges from the overlap of the ligand's orbitals with the valence metal d orbitals. We will specify

the ligand orbitals later on, but for now we just take them as $|\phi_{L,k}\rangle$. In order to express the one electron ligand field operator \hat{V}_{LF} in terms of orbital overlap, we use the ligand orbitals as operators.

$$\hat{V}_{LF} = \sum_k |\phi_{L,k}\rangle \langle \phi_{L,k}| \quad (3.22)$$

The sum includes all k ligand orbitals, so we capture the overlap of all ligand orbitals with each metal orbital. When inserting the ligand field operator into the one-electron integral expressions, we obtain a sum of metal-ligand orbital integrals.

$$(\mathbf{V}_{LF,L,loc})_{ij} = \langle d_{loc,i} | \hat{V}_{LF} | d_{loc,j} \rangle = \sum_k \langle d_{loc,i} | \phi_{L,k} \rangle \langle \phi_{L,k} | d_{loc,j} \rangle \quad (3.23)$$

The two bra-ket expressions are the overlap integrals of the metal and ligand orbitals S_{iL} with i being the m_l of the respective metal d orbital. We can now integrate the overlap integrals to obtain the matrix elements, but there is a faster way: non-zero integrals are only found if the symmetry of the metal orbitals differs from the symmetry of the ligand orbital. In Figure 3.1, atomic orbitals are plotted and ordered by symmetry to illustrate the overlap possibilities. The σ -type d_{z^2} orbital for example will overlap only with another orbital of σ -type symmetry, like an s or p_z orbital. This argument also applies to the other integrals, so the d_{xz} and d_{yz} orbitals can only overlap with orbitals of π symmetry in the same orientation, and lastly there is an overlap for the d_{xy} and $d_{x^2-y^2}$ orbitals with δ symmetry ligand orbitals. *All other integrals are zero.* When aligning e.g. a σ -type orbital and a π -type orbital along the z-axis, it is apparent that the positive overlap is as large as the negative overlap, such that the total overlap is zero.

Speaking in mathematical terms, the integral over antisymmetric functions is zero, and the product of a symmetric and an antisymmetric function is again antisymmetric. Only products of the same symmetry will be symmetric and thus have non-vanishing integrals.

Since the elements in $\mathbf{V}_{LF,L,loc}$ are products of the overlap integrals, the only remaining elements are on the diagonal, where we find S_{iL}^2 . These overlap integrals are the parameters of the AOM, and we label them according to their symmetry, i.e.:

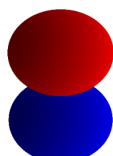
$$\begin{aligned} S_{z^2,L}^2 &= e_\sigma \\ S_{xz,L}^2 &= e_{\pi_x} \\ S_{yz,L}^2 &= e_{\pi_y} \\ S_{xy,L}^2 &= e_{\delta_1} \\ S_{x^2-y^2,L}^2 &= e_{\delta_2} \end{aligned} \quad (3.24)$$

Writing the complete single-ligand local ligand field matrix, we get:

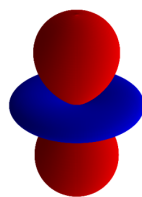
σ symmetry



s

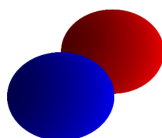


p_z



d_{z^2}

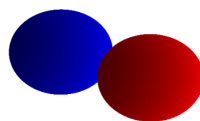
π symmetry



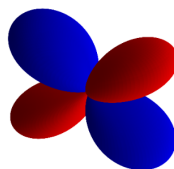
p_x



d_{xz}

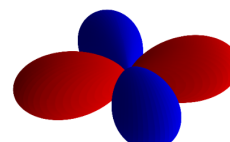


p_y

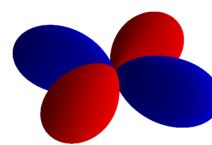


d_{yz}

δ symmetry



d_{xy}



$d_{x^2-y^2}$

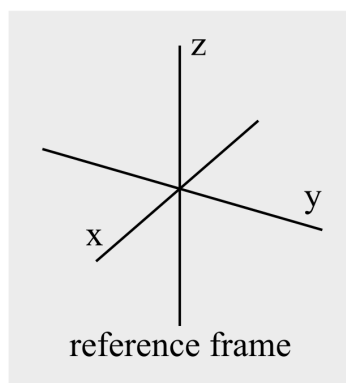


Figure 3.1: Spherical harmonics for $l = 1, 2, 3$ labelled by the usual atomic orbital labels and ordered by their rotational symmetry with respect to the z-axis as given in the reference frame. Red lobes are positive values, blue ones negative.

$$\mathbf{V}_{LF,L,loc} = \begin{matrix} z^2 & xz & yz & x^2 - y^2 & xy \\ z^2 & e_\sigma & & & \\ xz & & e_{\pi_x} & & 0 \\ yz & & & e_{\pi_y} & \\ x^2 - y^2 & & & & e_{\delta_1} \\ xy & & 0 & & & e_{\delta_2} \end{matrix} \quad (3.25)$$

Of course, we do not expect the parameters e_λ to be equal in size, since the orbital overlap decreases in the sequence $e_\sigma > e_\pi > e_\delta$.

3.2.2 The global frame

Given the local ligand field matrix, the next task is its translation into the global coordinate frame. To clarify the necessary operations, let us first recall Equation 3.5 and write the linear combinations in a matrix notation:

$$\mathbf{d} = \begin{pmatrix} d_{z^2} \\ d_{xz} \\ d_{yz} \\ d_{x^2-y^2} \\ d_{xy} \end{pmatrix} = \begin{pmatrix} 0 & 0 & 1 & 0 & 0 \\ 0 & -1/\sqrt{2} & 0 & 1/\sqrt{2} & 0 \\ 0 & i/\sqrt{2} & 0 & i/\sqrt{2} & 0 \\ 1/\sqrt{2} & 0 & 0 & 0 & 1/\sqrt{2} \\ -i/\sqrt{2} & 0 & 0 & 0 & i/\sqrt{2} \end{pmatrix} \cdot \begin{pmatrix} Y_2^2 \\ Y_2^1 \\ Y_2^0 \\ Y_2^{-1} \\ Y_2^{-2} \end{pmatrix} = \mathbf{C}\mathbf{y} \quad (3.26)$$

Here, \mathbf{d} and \mathbf{y} are the real and complex spherical harmonics, respectively, aligned in column matrices. The matrix \mathbf{C} that defines the linear combination coefficients is the matrix for the transformation of the complex into the spherical harmonics.

If we take the above basis to be the global one, there exists a local basis with a similar definition:

$$\mathbf{d}_{loc} = \mathbf{C}\mathbf{y}_{loc} \quad (3.27)$$

Multiplying with \mathbf{C}^{-1} from the left, we obtain $\mathbf{C}^{-1}\mathbf{d}_{loc} = \mathbf{y}_{loc}$ and $\mathbf{C}^{-1}\mathbf{d} = \mathbf{y}$. We are looking for a matrix \mathbf{F} that transforms the local \mathbf{d} orbital basis into the global one, i.e.³

$$\begin{aligned} \mathbf{F}\mathbf{d}_{loc} &= \mathbf{d} \\ \mathbf{d}_{loc}^\dagger \mathbf{F}^\dagger &= \mathbf{d}^\dagger \end{aligned} \quad (3.28)$$

It is known that for complex spherical harmonics, such a rotation is performed with the Wigner \mathbf{D} matrices, which are applied to the conjugate transposed vector from the right.

$$\mathbf{y}_{loc}^\dagger \mathbf{D} = \mathbf{y}^\dagger \quad (3.29)$$

This can be brought into the same form as Equation 3.28 by taking its conjugate transpose.

$$\mathbf{D}^\dagger \mathbf{y}_{loc} = \mathbf{y} \quad (3.30)$$

³Since the d orbitals are real, we could substitute the conjugate transpose (\dagger) with the transpose (T).

Taking Equation 3.28 and subsequently substituting \mathbf{d} with Equation 3.26, 3.30 and the variant of Equation 3.27, we find the sought after expression for \mathbf{F} :

$$\mathbf{C}\mathbf{D}^\dagger\mathbf{C}^{-1}\mathbf{d}_{loc} = \mathbf{F}\mathbf{d}_{loc} \quad (3.31)$$

$$\Rightarrow \mathbf{C}\mathbf{D}^\dagger\mathbf{C}^{-1} = \mathbf{F} \quad (3.32)$$

At this point it is noteworthy that \mathbf{C} is unitary, so $\mathbf{C}^{-1} = \mathbf{C}^\dagger$.

The searched rotation \mathbf{F} is a translation of the complex Wigner \mathbf{D} matrix into the space of the real spherical harmonics. The \mathbf{D} matrix is defined as a rotation along the Euler angles α, β, γ . Since our goal is to rotate the local basis into the global frame, we must perform a backwards rotation from the global position of the local axis. The position of the local axis corresponds to the position of the ligand and is commonly given in spherical coordinates θ, ϕ . Another coordinate ψ defines the orientation of the ligand on the axis, or the orientation of the x and y axes in the local frame, respectively. To perform the backwards rotation, we define $\alpha = -\psi, \beta = -\theta, \gamma = -\phi$ and define the parameters of \mathbf{D} and \mathbf{F} :⁴

$$\mathbf{F}(\theta, \phi, \psi) = \mathbf{C}\mathbf{D}^\dagger(-\psi, -\theta, -\phi)\mathbf{C}^{-1} \quad (3.33)$$

Now that we have defined the rotation matrix \mathbf{F} that we were looking for, we can translate the local ligand field matrix $\mathbf{V}_{LF,L,loc}$ into the global frame.

We write the global ligand field matrix in terms of a vector product

$$\mathbf{V}_{LF,L} = \mathbf{d}\hat{V}_{LF}\mathbf{d}^\mathbf{T} \quad (3.34)$$

and subsequently substitute the \mathbf{d} basis vectors with the expressions from Equation 3.28 and get:

$$\mathbf{V}_{LF,L} = \mathbf{F}\mathbf{d}_{loc}\hat{V}_{LF}\mathbf{d}_{loc}^\mathbf{T}\mathbf{F}^\mathbf{T} \quad (3.35)$$

where the conjugate transposed is replaced with the transposed, because all occurring vectors and matrices are real. The central part of the right-hand side is the diagonal, local ligand field matrix from Equation 3.25, so this reduces to

$$\mathbf{V}_{LF,L} = \mathbf{F}\mathbf{V}_{LF,L,loc}\mathbf{F}^\mathbf{T} \quad (3.36)$$

The elements of the local matrix are, according to matrix multiplication rules:

$$(V_{LF,L})_{ij} = \sum_{\lambda} (\mathbf{F})_{i\lambda} e_{L,\lambda} (\mathbf{F}^\mathbf{T})_{\lambda j} \quad (3.37)$$

We can further transpose $\mathbf{F}^\mathbf{T}$ again by exchanging its indices, leaving two instances of \mathbf{F} .

$$(V_{LF,L})_{ij} = \sum_{\lambda} (\mathbf{F})_{i\lambda} e_{L,\lambda} (\mathbf{F})_{j\lambda} \quad (3.38)$$

⁴There are different conventions for the angles in \mathbf{D} and whether an active or passive rotation is carried out. The reader is referred to refs. [31] and [32] for further details.

The elements e of $\mathbf{V}_{LF,L,loc}$ are each affected by one column of \mathbf{F} , so these columns can be identified as belonging to a specific interaction type. Consequently, we replace the column indices with labels for these interactions, such that $\lambda = \sigma, \pi_x, \pi_y, \delta_1, \delta_2$. The elements of \mathbf{F} are called *angular overlap factors* and its columns are generally tabulated as $F_\sigma(\theta, \phi), F_{\pi_x}(\theta, \phi, \psi), F_{\pi_y}(\theta, \phi, \psi), \dots$. Expanding Equation 3.21 with the expressions derived above, we obtain the following equation for the matrix elements v_{ij} of the total, global ligand field matrix \mathbf{V}_{LF} :

$$(\mathbf{V}_{LF})_{ij} = v_{ij} = \sum_L \sum_\lambda F_{L,\lambda,i} F_{L,\lambda,j} e_{L,\lambda} \quad (3.39)$$

As we can see, the metal-ligand orbital overlap $e_{L,\lambda}$ is scaled by the position of the ligand in the global frame. When defining the parameters e , we implicitly assumed this scaling factor to be one; reasonably so since in the local frame, overlap is maximized. In a rotated frame, this overlap must be smaller than or equal the reference and indeed we find $F_{\lambda,i}$ to fulfil this expectation. $F_{\lambda,i}$ can thus be interpreted to be the angular part of the metal-ligand overlap integral, hence the name of the model.

3.3 Common adjustments to the AOM

The final equation of the last section, Equation 3.39, is the expression for the ligand field matrix elements as originally derived by Schäffer and Jørgensen.^[14] Since then, several adjustments have been made, of which we will focus on the ones that are important for chapter 5.

3.3.1 d-s mixing

In chapter 2, we saw that the determinants in a CI matrix are constructed from molecular orbitals χ . A central point to LFT is that the molecular orbital basis regarded for constructing excited configurations consists of the valence d orbitals, i.e. the basis functions ϕ in Equation 2.10 are d functions. When treating complexes of certain symmetries, some encountered states have energies that are not parametrizable with the parameters employed in Equation 3.39. Square planar complexes are well known for such orbital energy sequences, where the d_{z^2} orbital has a lower energy than expected. It was assumed that this orbital mixes with the unoccupied s orbital of the metal, lowering its energy. This effect is called *d-s mixing*, its formalization is presented in refs. [27, 33–35] and we will generally stick to the derivation presented in ref. [27].

Any two metal orbitals that overlap with one or more ligand orbitals can mix. From a symmetry perspective, this can be rationalized by the irreducible representation of the d orbital: any d orbital that is found in the totally symmetric representation of the given point group *can* mix with the s orbital and *might* have a lower energy than it would be expected from a pure d orbital basis.

The conceptual problem of this idea is that the basis of the problem needs an expansion, since we would need to add the s orbital, obtain a 6×6 ligand field matrix and compute

the state energies from there. To avoid this, the d-s interaction contribution is treated as second order correction and the ligand field matrix collapsed back to its 5×5 shape, adding a correction term to the ligand field matrix.

The 6×6 ligand field matrix can be written as composition of a 1×1 matrix and the known 5×5 ligand field matrix:

$$\mathbf{V}_{ds} = \begin{pmatrix} \Delta + \xi & \mathbf{c}^T \\ \mathbf{c} & \mathbf{V}_{LF} \end{pmatrix} \quad (3.40)$$

Where Δ is the energy difference between the unperturbed d and s orbital energies, ξ is the effect of the ligand field operator on the s orbital, $\langle s | \hat{V}_{LF} | s \rangle$, and the vectors \mathbf{c} and \mathbf{c}^T are the d-s interaction terms $\langle s | \hat{V}_{LF} | d_i \rangle$. The corresponding eigenvalue equation (equivalent to Equation 2.26), yields the energy including by d-s mixing E_{ds} .

$$\mathbf{V}_{ds} \begin{pmatrix} \mu \\ \mathbf{m} \end{pmatrix} = E_{ds} \begin{pmatrix} \mu \\ \mathbf{m} \end{pmatrix} \quad (3.41)$$

Here, μ is the extension of the eigenvector to include the s orbital and required to be non-zero, otherwise there would be no d-s mixing. Due to this, it can be eliminated and the dimension of the problem is reduced again to 5×5 :

$$\mathbf{V} \mathbf{m} - \left(\frac{\mathbf{c} \mathbf{c}^T}{\Delta + \xi - E_{ds}} \right) \mathbf{m} = E_{ds} \mathbf{m} \quad (3.42)$$

This can be simplified further under the assumption that the d-s mixing is after all very small and the energy gap between d and s orbitals Δ is large compared to $\xi - E_{ds}$.

$$\left(\mathbf{V} - \frac{\mathbf{c} \mathbf{c}^T}{\Delta} \right) \mathbf{m} = E_{ds} \mathbf{m} \quad (3.43)$$

We now need to define the elements in \mathbf{c} . Like the rest of the ligand field contributions, it is first defined in a local frame:

$$c_{i,L,loc} = \langle d_i | \hat{V}_{LF,L,loc} | s \rangle \quad (3.44)$$

Just like the vectors in Equation 3.28, this expression can be transformed into the global frame using the rotation matrix \mathbf{F} :

$$c_{i,L} = \sum_j F_{L,ij} \langle d_j | \hat{V}_{LF,L,loc} | s \rangle \quad (3.45)$$

Like the other parameters, most interactions cancel due to symmetry. We can use Figure 3.1 for illustration, the only non-zero integral is $\langle d_{z^2} | \hat{V}_{LF} | s \rangle$. The sum over j thus simplifies to $j = 1$, which means the used $F_{L,ij}$ are effectively the same as for the σ interaction.

$$c_{i,L} = F_{L,\sigma,i} \langle d_{z^2} | \hat{V}_{LF,L,loc} | s \rangle \quad (3.46)$$

In order to parameterize the effect of d–s mixing, e_{ds} is introduced,

$$e_{L,ds} = \frac{\langle d_{z^2} | \hat{V}_{LF,L,loc} | s \rangle^2}{\Delta} \quad (3.47)$$

and we set:

$$b_{i,L} = F_{L,\sigma,i} \sqrt{e_{L,ds}} \quad (3.48)$$

The obtained vector \mathbf{b} is additive if multiple ligands are considered, so

$$\begin{aligned} \mathbf{b} &= \sum_L \mathbf{b}_L \\ b_i &= \sum_L F_{L,\sigma,i} \sqrt{e_{L,ds}} \end{aligned} \quad (3.49)$$

Note that this sum defines a vector element, and the total d–s mixing correction is expressed by

$$\mathbf{V}_{LF} = \mathbf{V} - \mathbf{b}\mathbf{b}^T \quad (3.50)$$

This means that the sum over the ligands is taken before the vector product is calculated. An element in the matrix of $\mathbf{b}\mathbf{b}^T$ is then:

$$(\mathbf{b}\mathbf{b}^T)_{ij} = \left(\sum_L F_{L,\sigma,i} \sqrt{e_{L,ds}} \right) \left(\sum_L F_{L,\sigma,j} \sqrt{e_{L,ds}} \right) \quad (3.51)$$

Including d–s mixing accounts for the corresponding energy changes, but causes some complications. The main conceptual problem is that the parameter e_{ds} is global, although apparently linked to a particular ligand by the sum over L . This contradicts the very essence of the AOM: the introduction of ligand specific parameters that are independent of the global symmetry. Of course, global symmetry always plays a role and AOM parameters are never truly local due to ligand-ligand interactions. Still, the notion of a set of parameters per ligand is somewhat lost, and it is hard to tell the physical meaning of the parameters e_{ds} .

The other complication affects the structure of the AOM equation system, although it can be considered a technical detail that is solved. Without d–s mixing, it is linear and therefore rather easy to solve. The d–s mixing term is nonlinear, which excludes many well established algorithms from working and can also prevent fast heuristic calculations with pencil and paper.

3.3.2 δ interactions

The most straightforward change that is common to almost all applications of the AOM is the disregard of any metal-ligand δ interaction. These interactions are assumed to be very weak, and thus employing e_{δ_1} and e_{δ_2} would not improve the understanding of the metal-ligand interaction but increase the number of total parameters. Consequently, $\lambda = \sigma, \pi_x, \pi_y$.

3.3.3 The basis energy E

When considering the ligand field, the most important property is the splitting of the d orbital energies and the subsequent splitting of electronic terms according to the one-electron operator. It is intuitive and often pointed out in textbooks that the ligand field has a spherical part which shifts all d orbitals by the same energy. It also subsumes the energy obtained from the zeroth order perturbation energy, which is a constant for a given element. From the investigation of d-d transitions, this field contribution can of course never be obtained, since all states are equally affected. In consequence, most ligand field schemes omit its explicit calculation.

Obtaining the electronic state energies from CASSCF calculations permits the parameterization of this spherical contribution. Since it affects all d orbitals equally, it can be written as a product of a parameter and the identity matrix:

$$E \cdot \mathbf{I} \quad (3.52)$$

In hindsight the selection of the symbol E for the spherical contribution is a bit unfortunate, since it is used for too many other relevant quantities. It nonetheless needs to be introduced as such, since chapter 5 uses this notation.

On a side note: when the metal-ligand bonds in a complex are increased until the ligands are effectively removed, E does not become the unperturbed energy E_0 . The electron-electron interaction that is present in the perturbative term still applies, so somewhat counterintuitive the total ligand field Hamiltonian \hat{H}_{LF} includes an effect that does not strictly arise from the ligands.

3.3.4 AOM master equation

The above-mentioned adjustments are the ones that are used in chapter 5, so we are ready to write the AOM equation for the ligand field matrix, as it will be used for the parameterization of all following problems.

$$\mathbf{V}_{LF} = E \cdot \mathbf{I} + \sum_L \mathbf{F}_L \mathbf{V}_{LF,L,loc} \mathbf{F}_L^{-1} - \mathbf{b}\mathbf{b}^T \quad (3.53)$$

In order to parameterize the ligand field matrix, its elements are written as follows:

$$v_{ij} = \delta_{ij}E + \sum_L \sum_{\lambda} F_{L,\lambda,i} F_{L,\lambda,j} e_{L,\lambda} - \sum_L F_{ds,i} \sqrt{e_{L,ds}} \cdot \sum_L F_{ds,j} \sqrt{e_{L,ds}} \quad (3.54)$$

This set of equations has to be solved when using the AOM for a parameterization of d electronic states, no matter whether they are determined experimentally or by *ab initio* methods. In chapter 5, more details are provided about how this resulting equation system is solved and which problems may arise.

With the AOM master equation 3.54 and the two-electron parameterization in subsection 3.1.3, it is now possible to express each element in the CI matrix in terms of AOM and Racah parameters. We can plug in numbers for the parameters and diagonalize the CI matrix to obtain the energies of the electronic states as eigenvalues. In an optimization process (without specification), the chosen parameters are adapted such that the found electronic states reproduce a set of reference states as well as possible. This approach would be the direct one. The indirect approach is a two-step parameterization, where only the two-electron integrals are parameterized and the one-electron integrals in \mathbf{V}_{LF} are just parameters themselves, optimized to reproduce a given set of states. In the second step, each v_{ij} with $i \geq j$ is expressed with Equation 3.54, again in an optimization process such that the AOM parameters reproduce the matrix elements v_{ij} as well as possible. We employ the second, indirect approach in chapter 5.

3.4 Interpretation

In the last two chapters, the necessary equations to describe an electronic structure problem in a d orbital basis are presented. After all, a parameterization is only worth consideration when its parameters can be interpreted in some way and when the scope of applicability is clear. We will only scratch the surface of the LFT interpretation here, since extensive discussions are provided for the cases in chapter 5.

3.4.1 The ligand field operator

Lacking some clearness, the meaning of the ligand field operator could be described as “containing the effects of the ligands on the metal d electrons”. Since the operator is never actually specified physically, it has no rigorous meaning. Still we can think of physical laws that would be incorporated in such a one-electron operator. The most prominent effect is the electrostatic interaction with negatively charged ligands. If we take this as the only source of the ligand field, we could define \hat{V}_{LF} as an electrostatic repulsion operator, leading to crystal field theory. With ligands like water and ammonia, it is however clear that this cannot be the only source of interaction between d electrons and ligands, and in fact crystal field theory has been shown to have poor predictive power.

From the perspective of molecular orbital theory, we can consider the ligand field to be the mixing of ligand and d orbitals, similar to the overlap considerations in the derivation of the AOM. The mixing must be weak (otherwise, the assumption of a pure d orbital basis would be flawed), and the part we consider to be d orbitals are in fact the antibonding MOs. From this perspective, the ligand field operator would simulate the orbital mixing effect by changing the d orbital energies without needing to include ligand orbitals into the basis set.

The notion of the antibonding character of the considered orbitals is useful to keep in mind; confusion can arise about why ligands even bond with the metal when they apparently increase the overall energy of the system. Would a separation not end in a more favourable situation? Since the bonding MOs that consist mainly of ligand AOs

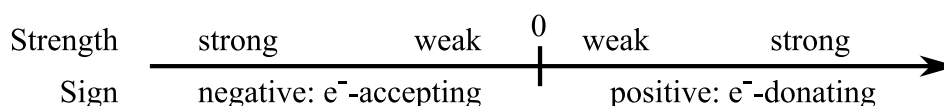


Figure 3.2: Interpretation of AOM parameters depending on the sign and magnitude.

are doubly occupied, their bonding contribution is usually larger than the antibonding character of the partly filled (mainly) d orbitals. Furthermore, other metal orbitals also participate in bonding, which is not regarded in LFT. This leads to the next important part of our interpretation: the strength of a ligand field, represented by the increase in energy of the d orbitals, does not hold any information about the thermodynamic stability of a complex.

3.4.2 AOM parameters

The parameters defined by the angular overlap model are defined such that each ligand has its own set of parameters, which represent the σ and π interactions of the ligand with the metal d electrons. Generally speaking, positive parameters can be viewed as electron donating; they increase the energy of the d orbitals. The MO interpretation of positive parameters is an orbital mixing where the ligands orbitals are lower in energy, and the d orbital is shifted due to being the antibonding linear combination. Most “classical” ligands like halides, water, ammonia, cyanates, etc. have positive parameters. In general, the σ interaction is stronger than the π interaction, which can be rationalized by the larger overlap of possible metal-ligand MOs.

Negative parameters are associated with an electron-accepting interaction. No known ligand is expected to have a negative e_{σ} , but ligands that show π backbonding like CO, CN^- and phosphines are thought to have negative e_{π} parameters. We could not always confirm this view from *ab initio* calculations and as reasoned in the next section, LFT could be generally unreliable for those ligands. In the molecular orbital perspective, negative AOM parameters mean that there are ligand orbitals that are higher in energy than the metal d orbitals, so the d orbital would in fact be the bonding linear combination.

3.4.3 The two-electron operator

The parameterization of the two-electron operator is based on free metal ions without a ligand sphere. Nonetheless, the obtained parameters are successfully used in any standard ligand field parameterization, where especially the Racah parameter B can be interpreted to represent ligand field dependent electron-electron repulsion.

An important assumption in the derivation of this parameterization is that the electron-electron interaction is equal in all d orbitals, e.g. it does not make a difference whether we find a pair of electrons in the d_{xy} or the d_{z^2} orbital. This assumption is perfectly fine for free atoms and ions, since all orbitals of the same l are equivalent. However, in an MO picture of LFT, the d orbitals mix differently: due to the different energies of ligand orbitals and the varying overlap with the metal d orbitals, the resulting MOs do not have the same

d orbital contribution. If this covalency in a set of d orbitals is much more pronounced than in another, the assumption of equal electron-electron interactions is not fulfilled anymore and thus the Racah parameters cannot capture them adequately. This case is sometimes termed a strong *differential covalency*, and extensively discussed for example in chapter 7 of ref. [36].

When expressing the electronic states of the d electrons in terms of a diagonalized CI matrix with parameterized integrals, the two-electron parameters cannot capture any asymmetry of the complex. The stronger the actual mixing of metal and ligand orbitals, the more important this problem becomes. Consequently, a reproduction of experimentally or calculated electronic state energies may fail. Although it is not possible to predict exactly what any fitting routine would yield in this case, it is to be expected that the one-electron parameters v_{ij} are adjusted accordingly to account for the energies of electronic states that cannot be accounted for with the Racah parameters. In other words, the insufficiency of the Racah parameterization for the two-electron integrals would leak into the one-electron parameterization and thus spoil the AOM parameterization.

When considering ligands with π backbonding such as CO, metal d orbitals that exert a π interaction with the ligand are lowered in energy. This is only possible when the occupied ligand orbitals are slightly higher in energy than the metal d orbitals. This leads to strong mixing compared to the orbitals affected by an antibonding σ interaction, corresponding to a more covalent bond. Thus, these ligands can be expected to *always* break the assumption of equal electron-electron interaction in all d orbitals. No good fit can be obtained in such a situation, and we should refrain from applying LFT to these complexes.

3.4.4 CASSCF vs. Experiment

In the method developed in this work (see chapter 5), we do not use experimental data⁵ to fit AOM parameters. In fact, the whole routine that was developed for the presented research can only work with calculated state energies. It is important to mention that these calculated energies are not meant to accurately reproduce experimental data. It has been shown that CASSCF calculations are sufficient to reproduce trends and qualitative results. The results can be improved for example by the use of perturbation theory or inclusion of solvent models. Since LFT is a model that helps to understand the electronic structure of complexes on a qualitative level, an increased accuracy compared to a standard CASSCF calculation is most often not needed to improve the obtained parameters. LFT was never meant to be a predictive tool and regarding this, it is valid to focus on qualitative results.

Compared to the experimental data, CASSCF calculations have the inherent advantage of being conceptually very close to ligand field theory. The identification of electronic states is naturally given, while it is a difficult task to assign experimental electronic transitions. An active space of d orbitals corresponds almost exactly to the ligand field basis, leading to a similar CI matrix. Another advantage is the possibility to interpret the LFT parameterization from an MO perspective. By examining the MO coefficients, the

⁵With two exceptions in chapter 5.

ligand admixture can be quantified directly and cases of strong differential covalency or d-s mixing can be identified, as shown in section 5.3.

4 History of the Angular Overlap Model

The purpose of this chapter is to provide an overview of the development of the angular overlap model. It is not exhaustive, but I do not want to list publications with arbitrary experimental data; it can rather be seen as a short trip through different applications and developments.

4.1 Origins

The first formulation of the angular overlap model by Schäffer and Jørgensen was published in 1965,^[14] after preliminary conceptual work by Yamatera^[37,38], McClure^[39] and Jørgensen, Schmidtke *et al.*,^[40–42] who related ligand field parameters to interaction types, regarding the ligand positions. Models that were very similar to the AOM were thus in use before and Smith stated in a later review, that “*There is still a widespread feeling that the AOM is distinguished more for its elegance and simplicity than for its practical utility in the solution of chemical problems.*”^[43] The actual achievement of Schäffer and Jørgensen might be seen in be the clearer presentation and unification of the existing local approaches. Notations commonly seen in older local ligand field parameterizations are the Ξ^2 model, where Ξ represented a geometrical factor similar to F in the AOM notation,^[41,43,44] and the usage of $\delta\sigma$ and $\delta\pi$ parameters, which account for whole energy levels affected by σ and π bonding, respectively.^[39]

As in the publication of Jørgensen *et al.*, the AOM employed the Wolfsberg-Helmholz model for orbital overlap considerations.^[45] When specifying the metal-ligand overlap operator in the derivation of the AOM, we implicitly used this model to derive the proportionality $e_\lambda \sim S^2$.

From today’s perspective it is remarkable that the title of the 1965 publication contains “*an attempt to revive the ligand field approaches*”, which shows that at least a part of the ligand field community was concerned about the LCAO approach superseding LFT as a more powerful but somewhat complicated model.^[46] Schäffer himself stated that the idea of the AOM was the inclusion of “*the approximate consequences of molecular orbital models*” into ligand field parameters.^[26] With this in mind, our interpretation of LFT from an MO perspective in the theory chapter might be actually close to what the authors originally intended.

The AOM was successfully applied to numerous problems, so many that an attempt to provide an overview here would be futile. It was common from the beginning to omit the e_δ parameters, although some authors formally correctly defined $e'_\lambda = e_\lambda - e_\delta$.^[43] Several applications are discussed chapter 5, where original research papers are cited for

comparisons. A selection of reviews discussing experimental data can be found that often also contain parts of the derivation of the AOM.^[13,29,43,47,48]

4.2 AOM for f-shell elements

Going back to the derivation of the AOM, we saw that the overlap factors F are basically rotations in a basis of real spherical harmonics. Since we are interested in the transition metals with partly filled d shells, we used the corresponding Wigner matrices for $l = 2$. Using the rotations for real spherical harmonics with $l = 3$ will yield overlap factors for f orbitals, as originally derived by Urland in 1976,^[49] and slightly later by Warren in 1977.^[50]¹ It is perhaps interesting that one of the most important preliminary works that led to the AOM was in fact concerned with the treatment of lanthanoides.^[41]

Much of the early work on the AOM of f elements was performed by Urland^[52-54] (although he also contributed to the coordination chemistry of d elements^[55]) and Warren^[56,57], followed by many others.

The extension of the AOM to f elements can be considered to be established and proven to work at many occasions. As of today, there is still research complemented by the AOM.^[30,58-63] As a final remark on f elements, investigating them with ligand field theory comes with a catch: as Bendix pointed out in a conference talk, f element chemists are always 87% more frustrated than d element chemists. That is because the one electron ligand field operator has 28 uniquely defined elements for f orbitals, as opposed to 15 when treating d orbitals.^[64]

4.3 The divide

In 1977, Smith published a paper where he investigated different chlorocuprates and found that using the standard AOM parameterization, he could not fit experimental data to a satisfactory precision.^[33] Complexes with near-planar geometries showed an unexpectedly low energy for the d_{z^2} orbital, which the usual AOM parameters could not account for. Smith proposed that due to the symmetry of the complexes (D_{4h} , D_{2d} and D_{3h}), where the d_{z^2} orbital transforms in the same irreducible representation as the metal s orbitals, a mixing between 3d and 4s orbitals could occur, lowering the energy of the d_{z^2} orbital. A similar mechanism would be possible for 3d and 4p orbitals, as long as they transform in the same representation. This idea of d-s mixing was mentioned by Schäffer a few years earlier, but he dismissed it as not being helpful.^[65]

Interestingly, another paper by Cruse and Gerloch was published in the same year, who fitted AOM parameters to the $[\text{CuCl}_4]^{2-}$ subunit in Cs_2CuCl_4 , not mentioning the low energy of the d_{z^2} orbital.^[66] The experimental data used by them was the same as in the publication by Smith.^[67,68]

The concept of d-s and d-p mixing proposed by Smith was apparently not acceptable for Gerloch and Woolley, who had strong objections towards any molecular orbital interpreta-

¹Warren cites ref. [51] for originally deriving the overlap factors, but it is not obtainable any more.

tion of LFT and promoted a view that used electron density considerations only.² Instead of the mixing of metal orbitals, they favoured the idea of coordination voids, where a coordination position could have a (negative) σ parameter assigned despite the absence of a ligand.^[70,71] They eventually came up with an alternative name for their interpretation of LFT and the AOM: cellular ligand field (CLF).^[72,73] This interpretation is often called the Gerloch–Woolley (GW) picture in opposition to the Schäffer–Jørgensen (SJ) one.

In the following years, Gerloch, Woolley and also Deeth tried to justify the CLF and the coordination void concept on many occasions.^[36,74–78] Others preferred the concept of d–s mixing, refined it and equally successfully used AOM parameter sets including e_{ds} .^[34,35,79–82]

As a personal impression, the tone of discussion that was used by its protagonists, GW and SJ, was harsh and sometimes personal. An example is Schäffer's critique of the CLF: "From a parametric point of view the void with its negative e_{σ} parameter is no different from a negative energy correction on the d_{z^2} orbital's energy, but Gerloch and co-workers are able to see interesting chemistry in the void."^[82]

This dispute dominated many of their publications in the 80s and 90s and one has to be aware of the different interpretations of ligand field theory by authors that might be in favour of either the GW or the SJ picture. The disagreement was never really settled, although some observations that were made throughout the years are in favour of the original SJ picture of the AOM:

- The CLF assumes the metal d orbitals not to participate in metal-ligand bonding. Instead, the bonds are mainly formed with the higher-lying s and p orbitals. This assumption can be considered wrong: quantum chemical calculations clearly show a significant d contribution to metal-ligand MOs, which is confirmed by all ground state and excited state calculations in this work. Experimental evidence for metal-ligand bonding via the metal d orbitals is also available by XAS studies.^[83]
- Quantum chemical calculations also show that d orbitals in a CASSCF calculation mix exactly as they are expected to in the SJ picture. Metal s character is consistently found in d orbitals for cases where d–s mixing parameters are required and vice versa.
- On a technical level, it is unclear where to place the coordination voids that are required in the CLF in order to account for low d orbital energies. The only successful applications were performed for planar complexes, where it is intuitive to place a void cell on top and below the complex; more complicated examples do not provide these obvious positions.

It is, however, impossible to prove or disprove one of the two interpretations. Both parameterizations do work for the same cases, but this does not tell anything about their validity. There are also cases that do not allow for a fit because they are too complicated or the ligand field approach in general is unsuitable. Both approaches do fail in these

²Direct quote: "[...] *the molecular orbital model has no role in the ligand-field theory of transition-metal complexes.*"^[69]

cases. For many complexes they yield the same set of parameters and are practically indistinguishable. Nowadays, it seems as if the GW interpretation is declining, with Deeth being the only active advocate of the coordination void.^[84,85]

4.4 Phase-coupled ligation

When the AOM was not yet formulated as such, Orgel published a paper in 1961, where he discussed the effect of planar, multidentate ligands with a delocalized π system on a ligand field and predicted that these ligands should create a characteristic d orbital splitting.^[86] It was rooted in the idea that the orbital phases of HOMOs and LUMOs at the ligating orbitals of conjugated π -systems would be symmetric and antisymmetric. This means there are two π -interactions for the metal with each ligating atom, that affect the d orbitals differently. This effect was called *phase-coupled ligation* or later occasionally *Orgel effect*. Several orbital energy splittings could be explained by phase-coupled ligation,^[87–89] and Ceulemans and Vanquickenborne provided the first AOM treatment of this effect in their publications in 1985.^[90,91] Their approach was refined, but the general idea of differentiating between an in-phase and an out-of-phase π interaction remained.^[92–94]

It is not surprising that Gerloch and Woolley refused the concept of phase-coupled ligation, as it emerged from an orbital mixing perspective.^[36,77] Deeth recently attributed the observed effect to π interactions of coordination voids.^[84] While this interpretation may be questionable, it highlighted the odd observation that planar complexes with non-coupled, monodentate ligands show orbital energy sequences that resemble the Orgel effect. This observation is confirmed for similar complexes in section 5.3, where *cis* and *trans* complexes show a different orbital energy splitting, although they should be equal when assuming identical AOM parameters. This difference should be spectroscopically observable due to the different electronic states that emerge, but experimental evidence for the particular ligand field splitting and a sound explanation are lacking.

4.5 LFT from a computational perspective

While the quantum chemical character of ligand field theory was always clear, its purpose was the parameterization of experimental data. Computational methods were for a long time not accurate enough to produce relevant data and rather used to verify assignments of electronic spectra.^[95] We have to keep in mind that KS-DFT and HF are methods that are designed to predict the electronic ground state energies. They are not well suited for excited state energies, and additional procedures like the Slater transition state method need to be applied.^[96,97] It was clear that excited determinants would be necessary to obtain more accurate state energies.^[98]

In the 2000s, two groups worked on employing KS-DFT to predict d-d electronic transition energies for subsequent ligand field theory parameterizations. Atanasov and Daul on the one hand developed an approach that they called ligand field DFT (LFDFT).^[99–102] On the other hand, Anthon, Schäffer and Bendix developed a connection between LFT

and DFT without giving it a specific name.^[103–106] The two approaches are very similar in the sense that they start from a ground-state determinant that was optimized by KS-DFT and create excited determinants without further optimization from this ground-state determinant. It can be seen as similar to a ground-state-specific CASSCF calculation with KS-DFT as the underlying method. Since the results of multi-determinant methods depend on the reference determinant, this approach yields different energies compared to the use of an HF-optimized determinant.

Abandoning DFT as reference for excited determinants, Atanasov and Neese started to focus on MCSCF methods to obtain excited state wave functions. This first-principles approach was termed *ab initio* LFT (aiLFT) in their publication in 2011.^[16] *Ab initio* ligand field theory focuses on the connection of the CASSCF method and LFT, and other than the preceding methods based on KS-DFT, there is no empirical component to aiLFT. The method is available in the ORCA quantum chemistry package since version 4,^[107,108] and has been refined to work with several extensions since ORCA 5.^[109] It has been successfully applied to a variety of complexes,^[60,61,110–112] and represents the backbone of this work.

4.6 AOM and molecular mechanics

Molecular mechanics (MM) simulations are well known for organic molecules of any size, but also transition metal complexes have been investigated for a long time.^[113–115] Due to the variety of coordination numbers and bond angles and the ligand field stabilization depending on the d electronic configuration, it is difficult to create general force fields that work for multiple complexes. There are very well investigated systems, but the problem remains that specialized force fields need to be defined specifically for particular complexes.

A combination of MM with the AOM was employed by Bernhardt and Comba, who used specific force fields to sample molecular geometries and the AOM to predict electronic spectra and EPR g values.^[116–120] The AOM was used here in conjunction with molecular mechanics, but not to improve the force fields themselves. Deeth *et al.* presented an approach that incorporated the AOM into force fields to account for the ligand field stabilization energy.^[121–123] The AOM with its local parameters is attractive in the regard that it represents the effect of single ligands on the ligand-field stabilization energy. Although this contribution is always only a part of a coordination complex force field, a systematic treatment seems promising. Several implementations of ligand field parameters (mainly AOM) were published during the last two decades, with Deeth being the most active researcher in the field.^[27,124–127]

As it will become apparent in chapter 5, AOM parameters are in fact not separate in the same complex, although they formally parameterize a single metal-ligand interaction each. Ligand-ligand interactions are clearly observable in many complexes and make a transferable force field parameterization complicated. This was mentioned by Comba on several occasions, although he considered the error to be acceptable.^[116,117,119]

4.7 Concluding remarks

As of today, the AOM has its place in ligand field theory for more than 70 years now. It has been a valuable tool for the interpretation of electronic spectra and magnetic properties and is often part of the basic knowledge of inorganic chemists. It is generally used complementary to experiments and calculations and provides a means to clarify results and make them understandable to other chemists. As often stated by Neese in different variations: “*A model gives scientists a language in which they can express their ideas.*” Despite all inaccuracies and dispute, this is greatly achieved by the angular overlap model.

5 Results and Discussion

The results of this work and their discussion were published in peer-reviewed publications that are presented in this chapter. Each of these publications is summarized in the next sections. On a sidenote, due to the margins in this document, the embedded publications are scaled down to fit the page size. If a publication is desired in higher quality, they can be found on the publishers websites.

5.1 Revisiting the Fundamental Nature of Metal-Ligand Bonding: An Impartial and Automated Fitting Procedure for Angular Overlap Model Parameters


M. Buchhorn, R. J. Deeth, V. Krewald, *Chemistry - A European Journal* **2022**, 28, e202103775, 10.1002/chem.202103775

Since the establishment of *ab initio* ligand field theory by Atanasov, Neese and co-workers, several publications showed the general feasibility of their approach.^[60,111,129] The implementation of a ligand field analysis in the ORCA software package made it even easier to access ligand field parameters from CASSCF calculations, as it directly yields the ligand field matrix V_{LF} . The general problem of overparameterization for highly symmetric complexes remained. In an interesting publication, Singh *et al.* fitted AOM parameters to octahedral structures by lowering their symmetry towards a trigonal distorted complex.^[112] This distorted complex is asymmetric enough to allow for an unambiguous fit of e_σ and e_π .

In the presented publication, we pursue a very similar approach, although more generalized. Using aiLFT to obtain the ligand field matrix from CASSCF calculations, we employed asymmetric distortions that do not depend on the original symmetry of the molecule. These distortions are random, so the obtained point group should be C_1 in most of the cases. To preserve the transferability, i.e. ensure that the parameters obtained from the distorted structure are the same as for the original, the distortions are very small and do not affect the bond lengths. For testing purposes, we investigated series of tetrahedral metal halides and were able to reproduce expected trends to full extent. We showed that the impact of the distortions on the AOM parameters is small in the sense that they are mostly stable for different structural samples of the same complex. Although small, it is also shown that the distortions are enough to lift the degeneracy problem of the ligand field matrix such that unambiguous fits to otherwise highly symmetric complexes could be made. The initial series served as a confirmation that the asymmetry approach

works, and we further demonstrated some computational experiments that are difficult to do experimentally. Bond length scans were performed and substitutions of metals and ligands were investigated. We showed that the dependence of AOM parameters on metal-ligand bond lengths is different for σ and π interactions and can be correlated to the hardness of the ligands. We also investigated the effects of different ligands on each other in heteroleptic complexes and discovered an interesting correlation between AOM parameter and Pearson's hardness of halide ligands.

The work published in Chem. Eur. J. served as a proof of concept. We showed that the approach using distorted molecules of minimal symmetry is able to reproduce expected results to a reasonable precision. Remaining deviations from the experiment are likely caused by the inaccuracy of the underlying quantum chemical calculation and not by the AOM parameterization. As stated at the very end of the theory chapter, this is not concerning, since all expected trends are successfully reproduced.



Revisiting the Fundamental Nature of Metal-Ligand Bonding: An Impartial and Automated Fitting Procedure for Angular Overlap Model Parameters

Moritz Buchhorn,^[a] Robert J. Deeth,^[b] and Vera Krewald^{*[a]}

Abstract: The properties and reactivities of transition metal complexes are often discussed in terms of Ligand Field Theory (LFT), and with *ab initio* LFT a direct connection to quantum chemical wavefunctions was recently established. The Angular Overlap Model (AOM) is a widely used, ligand-specific parameterization scheme of the ligand field splitting that has, however, been restricted by the availability and resolution of experimental data. Using *ab initio* LFT, we present here a generalised, symmetry-independent and automated fitting procedure for AOM parameters that is even applicable to formally underdetermined or experimentally inaccessible systems. This method allows quantitative evalua-

tions of assumptions commonly made in AOM applications, for example, transferability or the relative magnitudes of AOM parameters, and the response of the ligand field to structural or electronic changes. A two-dimensional spectrochemical series of tetrahedral halido metalates ($[M^II X_4]^{2-}$, $M = Mn-Cu$) served as a case study. A previously unknown linear relationship between the halide ligands' chemical hardness and their AOM parameters was found. The impartial and automated procedure for identifying AOM parameters introduced here can be used to systematically improve our understanding of ligand-metal interactions in coordination complexes.

Introduction

Transition metal compounds are relevant in many areas of chemistry; they serve as catalysts, pigments, photosensitisers, and drugs to name a few. They show an immense variance in their properties, reactivities and stabilities, which is rooted in the malleability of their electronic structures. Many examples in the literature have shown that the interplay of synthesis, spectroscopy and theory is essential for the targeted electronic structure design of transition metal complexes with improved properties.^[1–6] An early and well-known example is the electronic structure analysis of vanadyl in terms of a molecular orbital picture.^[7] This interplay rests on chemical concepts, which are often derived from quantum mechanics or accurate measurements, but are commonly applied and used in an intuitive manner. With quantum chemistry being able to predict electronic structures and thus contributing to explain exper-


imental observations,^[3,8–12] detailed connections to established chemical concepts can be made to quantitatively evaluate their scope and limitations.


Ligand Field Theory (LFT) is one of the most successful models in chemistry: by connecting readily available information on structure, symmetry and chemical building blocks, it can predict spectroscopic and magnetic properties of a vast array of transition metal complexes.^[13–15] LFT evaluates the effect of ligands, or more specifically of the electrostatic field created by the ligands, on the d or f electrons of a central metal. When ligands are considered as point charges in a purely ionic picture of bonding, Crystal Field Theory (CFT) emerges as an extreme scenario within LFT.^[13,16] While CFT can be deduced from fundamental principles and therefore considered *ab initio*, the representation of ligands as point charges or point dipoles is a poor approximation to real electron distributions and CFT gives d orbital splittings which are in quantitatively poor agreement with experiment.^[17]


LFT has been interpreted differently by various authors.^[18–23] It can be considered as a parameterization scheme that is intended to capture the interaction of the metal d orbitals with the ligands empirically. Ideally, these empirical parameters can be interpreted chemically. Which kind of parameterization is used depends on the complex considered. For example, the ligand-field splitting parameter Δ is valid for homoleptic cubic octahedral and tetrahedral complexes, but becomes ill-defined for other geometries. Many parameterizations are global, which means they apply to a whole complex and cannot be transferred to another. The utility of such a global scheme lies in the fact that the respective parameters such as ligand field stabilization energy, interelectronic repulsion, etc. can be meaningfully compared between complexes. However, global

[a] M. Buchhorn, Prof. Dr. V. Krewald
TU Darmstadt, Department of Chemistry, Theoretical Chemistry, Alarich-Weiss-Straße 4, 64287 Darmstadt (Germany)
E-mail: krewald@chemie.tu-darmstadt.de

[b] Prof. Dr. R. J. Deeth
University of Warwick, Department of Chemistry, University of Warwick, Gibbet Hill, Coventry, CV4 7AL (United Kingdom)

 Supporting information for this article is available on the WWW under <https://doi.org/10.1002/chem.202103775>

 Part of the Chemistry Europe joint Special Collection on Quantum Bioinorganic Chemistry.

 © 2022 The Authors. Chemistry - A European Journal published by Wiley-VCH GmbH. This is an open access article under the terms of the Creative Commons Attribution Non-Commercial License, which permits use, distribution and reproduction in any medium, provided the original work is properly cited and is not used for commercial purposes.

schemes are not intended to capture the impact of single M–L bonds, so they do not allow for an interpretation in terms of functional groups.

The Angular Overlap Model (AOM) is a parameterization scheme within LFT, which was developed by Schäffer and Jørgensen.^[24] An appealing characteristic of the AOM is the description of metal–ligand interactions in terms of local parameters. The complex is divided into spatial regions that are centered around the metal–ligand bonds and are characterized in terms of σ and π interactions between metal and ligand.^[20,25] The fundamental idea is to consider the field imposed by the ligands on the metal d orbital energies as a perturbation and thus fit parameters for the individual metal–ligand interaction to the d orbital energy differences.^[26] Besides the intuitive chemical interpretation, the definition and quantification of individual interactions may in principle permit a transfer of the corresponding parameters to other complexes with the same metal–ligand bond.^[27] While the AOM parameterization is well established for ionic metal–ligand interactions, an often quoted limitation is its failure for systems with strong differential orbital covalency, which has been defined as the difference in the metal d character in different types of d orbital.^[25,28] We note here that in the puristic ligand field model, the d orbitals remain pure and therefore the concept of differential orbital covalency cannot be included in this model.^[13,29,30] However, other interpretations of covalency in the ligand field and AOM context have been given.^[31–33] As discussed in more detail below, large non-spherical contributions to the ligand field matrix are outside the remit of the AOM model.^[13]

Historically and today, AOM parameter fitting procedures make use of experimental data sensitive to the valence orbitals of predominant d or f orbital character, e.g. UV-vis spectra or magnetic data.^[34–38] Although it has in principle always been within the scope of the AOM to describe complexes with arbitrary or no symmetry, this was almost impossible to achieve, mainly because experimental data provides limited information. For instance, data on optical transitions in transition metal complexes are generally limited to at most four d orbital energy differences. This limits the number of fittable parameters dramatically, and very often resulted in assumptions about the AOM parameters. These assumptions or constraints were usually not generally applicable and hence not transferrable to related complexes. In some cases, assumptions were made to reduce complexity, e.g. neglecting π -interactions for ammine ligands^[20] or imposing constraints such as $e_{\sigma} \approx 4e_{\pi}$.^[39,40] In other cases, an additional parameter was introduced to account for the otherwise inexplicable positioning of a d orbital energy level. The most prominent example for this is the low energy of the d_{z^2} orbital in square planar $[\text{CuCl}_4]^{2-}$. The attempts to explain and parameterize this observation eventually divided the AOM formalism into two models: the AOM and a branch called Cellular Ligand Field (CLF) model.^[41,42] The introduction of coordination voids was criticised,^[18] although recent work by one of us (R.J.D.) has sought to rejustify the void cell concept.^[43,44] For the parameterization scheme utilized in this work, the models are identical.

Even with the predictive power that single- and multi-determinantal quantum chemistry methods have now reached, LFT and the AOM have not become obsolete.^[45–49] Quite in contrast, the implementation of *ab initio* LFT (aiLFT)^[31,50,51] has been a significant success that illustrates the need for straightforward chemical interpretations of complex quantum chemical data.^[32,52–55] The aiLFT approach can be understood as a way of translating the multidimensional information of a CASSCF or CASSCF/NEVPT2 wavefunction into concepts that are readily understood by experimental and theoretical chemists.^[31,50,51,56] Naturally, such a compression of information comes at a certain cost; in this instance it is the model Hamiltonian that recovers only a specific part of the full complexity of the much more general *ab initio* wavefunction and energies. It cannot be used, for example, to treat charge transfer transitions which would require explicit inclusion of the ligand orbitals.^[50] This simplification is desired, however, since aiLFT's focus on the metal–ligand interactions means that they can be described in terms of chemically intuitive σ and π interactions. The loss of generality is the price to pay for a simple and understandable model.

The aiLFT analysis delivers the ligand field matrix. However, a standardized and impartial way for obtaining AOM parameters from a quantum chemical calculation of an arbitrary coordination complex is not yet available. In this work, we introduce such an automated fitting procedure for AOM parameters derived from aiLFT. We employ systematic asymmetric distortions of the ligand sphere to obtain a large number of independent matrix elements and thereby overcome the limitations imposed on fits to experimental data. Importantly, the approach proposed in this work differs from AOM parameter fitting procedures employed previously in that it does not rely on symmetry considerations or experimental data. The procedure introduced here can be applied to a variety of complexes as long as the requirements for the underlying aiLFT analysis are met, i.e. a reasonable representation of the electronic structure with an active space containing only the metal d or f orbitals. Naturally, this excludes complexes with non-innocent ligands.^[57,58] Our concept and its success are illustrated with tetrahedral metal halides that form a two-dimensional spectrochemical series. Additionally, a linear relationship between Pearson's chemical hardness^[59,60] and the AOM parameters is found. This previously unknown relationship connects the AOM parameters with a measurable chemical quantity and may provide further avenues for the classification and interpretation of quantum chemical calculations of transition metal complexes and their ligand fields.

Methodology

The ligand field potential

Ab initio ligand field theory, developed and implemented in ORCA,^[61] makes a direct connection between ligand field theory and the electronic energies computed with complete active space self consistent field (CASSCF) theory, optionally with a

subsequent perturbation theory treatment (NEVPT2). The details of this procedure are presented elsewhere,^[31,50,62] so that only a brief summary is given below. The key feature is the construction of an effective ligand field Hamiltonian that acts on a d orbital basis.^[50,62] In LFT, this Hamiltonian is derived from experimentally observed d–d transitions, whereas in aiLFT, the respective states are obtained from a CASSCF calculation. The LFT model Hamiltonian consists of a one-electron part, \hat{V} , and a two-electron part, \hat{G} :

$$\hat{H}_{LF} = \sum_i \hat{V}_{LF}(i) + \sum_{i<j} \hat{G}(i,j) \quad (1)$$

Acting on a d orbital basis, the one-electron operator yields a matrix which is called the *one-electron ligand field matrix* or *ligand field potential* V_{LF} , the elements of which are defined as:

$$v_{ij} = \langle d_i | \hat{V}_{LF} | d_j \rangle \quad (2)$$

In the equation above, the ligand field potential is expressed in terms of a d orbital basis, although one can construct \hat{H}_{LF} (or \hat{V}_{LF} , respectively) for an f orbital basis in order to perform a ligand field analysis.^[33,38,45] When d orbitals are mentioned in this work, we always refer to the valence d orbitals. V_{LF} is obtained by a CASSCF calculation with subsequent aiLFT analysis as implemented in the ORCA quantum chemistry package (see Computational Details).

AOM equations

The AOM can be used as a parameterized fitting scheme for the V_{LF} matrix.^[20,41,50] The matrix elements are expressed in terms of the angular overlap factors $F(\theta, \phi, \psi)$, which are determined by the angular positions of the ligands L and the AOM parameters $e_{\lambda}(r)$:

$$v_{ij} = \sum_L \sum_{\lambda} F_{Lij} F_{Lij} e_{L\lambda} - \sum_L F_{dsi} \sqrt{e_{Lds}} \cdot \sum_L F_{dsj} \sqrt{e_{Lds}} \quad (3)$$

with $\lambda = \sigma, \pi_x, \pi_y$ and $i, j = 0, 1, 2, 3, 4 = xy, yz, z^2, xz, x^2 - y^2$. The equations for F can be found in the Supporting Information; a visualization of the interaction including different interaction types is shown schematically in Figure 1. Note that the d–s mixing contribution cannot be included in the first sum, since it is a second order effect and the summations are executed before the multiplication. Deeth and Foulis provided a detailed overview of the d–s mixing formalism.^[63]

For ligands without cylindrical symmetry, π_x and π_y interactions must be distinguished. All ligands treated in this work have cylindrical symmetry, so the two interactions are indistinguishable and therefore the labels x and y are dropped in the discussions below. In $F(\theta, \phi, \psi)$, ψ is the rotational angle along the bond axis and can be set to an arbitrary value; we assume ψ to be 0.

Equation 4 shows the 5×5 one-electron ligand field matrix in more detail:

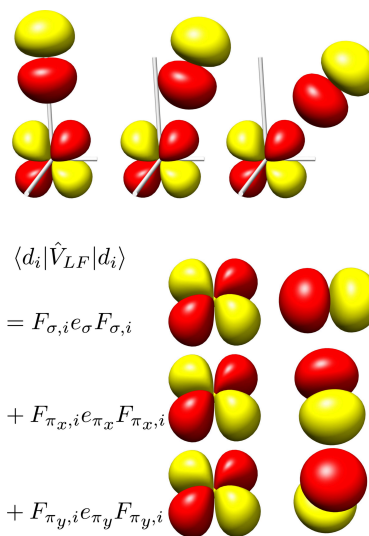


Figure 1. Top: Visualization of the σ -interaction of an arbitrary d orbital with a ligand orbital and its dependency on the polar angle. The square of the angular overlap factor $F_{\sigma,i}^2$ is zero for the left frame, increases in the center and is at its maximum in the right frame. Bottom: Visualization of the interaction between an arbitrary d orbital and ligand orbitals alongside the respective AOM parametrization.

$$H_{LF} = V_{LF} + E \cdot \mathbf{1}$$

$$= \begin{pmatrix} v_{00} + E & v_{01} & v_{02} & v_{03} & v_{04} \\ v_{10} & v_{11} + E & v_{12} & v_{13} & v_{14} \\ v_{20} & v_{21} & v_{22} + E & v_{23} & v_{24} \\ v_{30} & v_{31} & v_{32} & v_{33} + E & v_{34} \\ v_{40} & v_{41} & v_{42} & v_{43} & v_{44} + E \end{pmatrix} \quad (4)$$

$$h_{ij} = \langle d_i | V_{ij} | d_j \rangle + E \delta_{ij} \quad (5)$$

Here, E is the d orbital energy affected by the spherical contribution of the ligand field, $\mathbf{1}$ is the identity matrix. Since $v_{ij} = v_{ji}$ and no complex numbers occur, the ligand field matrix is always hermitian and therefore diagonalizable. When the matrix in equation 4 is diagonalized, the resulting eigenvalues are the perturbed d orbital energies. The eigenvalues represent the increase in energy of the d_i orbital due to ligand field effects. From the symmetric 5×5 matrix V_{LF} , a maximum of 15 independent matrix elements can be fitted. Since one parameter is always the d orbital energy affected by spherical field contributions E , a maximum of 14 AOM parameters can result from the fit. To meet this maximum, a totally asymmetric ligand environment around the central metal is required.

On the parameter E

The parameter E in equation 4 is rarely mentioned in the AOM literature, because it is irrelevant for the interpretation of the $e_{\lambda}(r)$ AOM parameters. In the matrix H_{LF} from aiLFT, the one-electron energy of the d orbitals is included, and hence it also contains the energy which is implicitly assumed to be the ground level in the AOM picture. In previous schemes for obtaining AOM parameters, E usually cancelled out and was therefore not easily available for interpretation. Since E is explicitly included in the procedure presented here, specifically in the way the equation systems are set up, we want to elaborate on the connection between the AOM equations with and without E a little further.

When H_{LF} as shown in equation 4 is diagonalized, the respective eigenvalues contain $+E$. Since the AOM is only interested in orbital energy differences rather than absolute energies and experimental data can also only yield relative energies, these eigenvalues are subtracted from each other, leaving four equations in which E is cancelled out. So while representing the energy of the degenerate $d_{x^2-y^2}$ and d_{z^2} orbitals in octahedral symmetry as $\varepsilon(x^2 - y^2) = \varepsilon(z^2) = 3e_{\sigma}$, is not inherently wrong, it implies that E will be cancelled out by taking the difference between this and other equations. From a mathematical perspective, there is no justification to say that we could not solve this equation. So the puristic way to write the AOM equations for octahedral symmetry would be:

$$\varepsilon(x^2 - y^2) = \varepsilon(z^2) = E + 3e_{\sigma} \quad (6)$$

$$\varepsilon(xz) = \varepsilon(yz) = \varepsilon(xy) = E + 4e_{\pi} \quad (7)$$

$$\Rightarrow \Delta = 3e_{\sigma} - 4e_{\pi} \quad (8)$$

It is immediately clear from these equations that the system is underdetermined and has no single solution. In Figure 2, the classical d orbital energy change due to the ligand field is shown, where the energy levels are labelled as in equation 6 and 7. At this point we want to emphasize that E is *not* the d orbital energy of the free ion. In fact, E is a function of the M–L bond length and resembles a spherical ligand field potential, while the e_{λ} parameters represent non-spherical contributions only. As shown below, the response of E to variations in the ligand field is easily accessible with the fitting procedure presented here.

Obtaining aiLFT-AOM parameters

Since a generalised black-box procedure for obtaining AOM parameters from the aiLFT analysis was missing, we introduce here how the AOM parameters are calculated starting from an optimized structure of the compound of interest. The next sections refer to Figure 3. The program we developed for fitting the AOM parameters is available upon request.

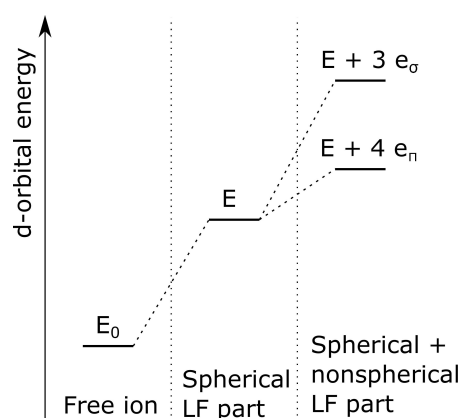


Figure 2. Schematic change of d orbital energies from a free ion to a homoleptic octahedral complex, labelled with the puristic style of AOM equations as in Equations 6 and 7.

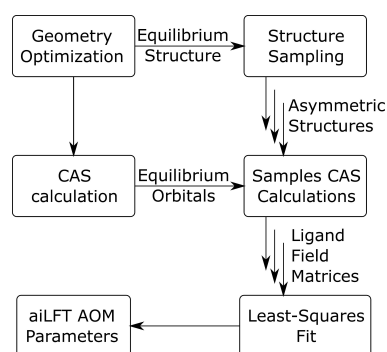


Figure 3. Schematic representation of the AOM fitting procedure.

Asymmetric distortions

The more symmetric a complex is, the fewer independent equations are available in the AOM fitting scheme. In order to avoid underdetermination even in the many highly symmetric complexes, small distortions have to be applied to the structure, while still assuming that the parameters obtained for the minimally distorted molecule are the same as for the initial structure. A similar procedure was already employed by Atanasov et al.^[50] and Singh et al.,^[31] although the distortions they applied were of a certain symmetry. We set three requirements for the distortions that are applied automatically in our black-box procedure:

1. It should be asymmetric, since high symmetry reduces the number of independent equations.^[64,65]
2. It should be small, so it can be safely assumed that the parameters do not change significantly.

3. It should not lead to a geometry in which the electronic structure differs significantly from the equilibrium geometry.

To meet the requirements, we employ a sampling procedure where the M–L bond lengths are varied and at each step a small, arbitrary angular distortion is imposed, thereby satisfying criterion 1. While the bond length variation can be chosen freely, the angle is varied by about 1° , which is sufficient for having more independent matrix elements and small enough to meet requirement 2.

The last requirement is met for every case covered in this work, but not generally. For chelating ligands, the sampling process must ensure that the displacements of the ligating atoms preserve the remainder of the ligand structure, and for bulky ligands the independent displacements must avoid structural clashes. For the small ligands explored in this proof-of-concept work, requirement 3 is well met. The structure sampling step is in the top right corner of Figure 3.

CASSCF calculations

A CASSCF calculation of the equilibrium structure is needed in which the active space consists of the valence d orbitals. Only one successful CASSCF calculation needs to be supplied by the user since the orbital projection feature of ORCA is employed for the subsequent CASSCF calculations on the structures obtained from the sampling process via asymmetric distortions. Compared to the equilibrium geometry, the sampled structures are sufficiently similar to ensure that the projection is successful. In this way, the aiLFT analysis and hence all quantum chemical information for the fitting procedure can be obtained very efficiently. These steps are placed in the center boxes of Figure 3.

Fitting procedure

The actual parameter fit is the bottom part of Figure 3. For every sampled structure, the one-electron ligand field matrix is extracted. Each matrix element corresponds to one equation. The resulting equation system is in general overdetermined and inconsistent, so the solution is approximated via a least-squares fit. The cost of the fit S is subject to minimization and defined as the sum of the squared differences between the found solution and the best solution of each equation. This difference is also called the residue r_i .^[66]

$$S = \sum_i (s_{i,\text{fit}} - s_{i,\text{ideal}})^2 = \sum_i r_i^2 \quad (9)$$

In general, better results at lower fitting costs are obtained when treating every ligand with its own set of parameters. This may however lead to overparameterizing the problem on a mathematical level. When fitting the parameters, different ligands may therefore be set to share a set of AOM parameters; this is referred to as *grouping*. Exemplifying this with the compounds studied in this work, they have four ligands and d-

s mixing is not relevant for the (near) tetrahedral symmetry. With grouped ligands, there are three parameters: E , e_σ and e_π , where E is global and e_σ and e_π are shared by all ligands. When assigning a unique parameter set to each ligand, there are nine parameters: E and four sets of e_σ and e_π parameters. Since up to 15 unique equations are available from V_{LF} , we can perform such an *ungrouped* fit.

Limitations

Ungrouped fitting is not always feasible since V_{LF} is limited to a maximum of 15 equations. When considering complexes with more ligands, distinguishable π_x and π_y interactions and/or a relevant d–s mixing contribution, this limit is easily exceeded. Ligands must then be treated with the same set of parameters, which imposes constraints on the system. Trial calculations show that assigning the same parameter set to several ligands is only successful for perfectly equivalent ligands. Even the small distortions employed in the presented sampling scheme interfere with this requirement because of their totally asymmetric nature.

An inherent problem comes with the underlying equation system, that is the main diagonal elements are clearly defined and have large values, and hence they dominate the fit. They roughly lead to the relationship for Δ and the AOM parameters in a tetrahedral complex. The off-diagonal elements should then help to find the exact minimum on this line, but they have very low numbers and the identified minima can scatter. The behaviour is illustrated in Figure 4, for which ligand grouping was used and the equation system was reformulated in order to reduce the problem to three dimensions. The same concept holds for larger parameter sets, but the ten-dimensional equation system cannot be depicted in human-readable form anymore. More details are given in the Supporting Information.

Computational details

The ORCA 4.2.1 quantum chemistry package^[61,67] was used for all calculations except the AOM parameter fitting. Geometries were optimized using the unrestricted Kohn–Sham formalism with the BP86 functional^[68,69] and the def2-SVP basis set.^[70] The electronic states corresponding to the d orbitals were calculated using the CASSCF procedure^[71,72] with the def2-TZVP basis set. The subsequent second-order N -electron valence state perturbation theory (NEVPT2)^[73–76] was employed for the calculations in the section “AOM parameters for complexes of the type $[\text{CoX}_4]^{2-}$ ”. The active space was chosen to contain the d orbitals and d electrons, which makes up e.g. a CAS(7,5) space in the cobalt complexes considered. The *ab initio* ligand field theory module^[50] was then employed to construct the effective ligand field Hamiltonian from the calculated states. The AOM was used to fit the one-electron part of the ligand field Hamiltonian according to our fitting procedure described above.^[24,41] For testing purposes, calculations with solvation models and differ-

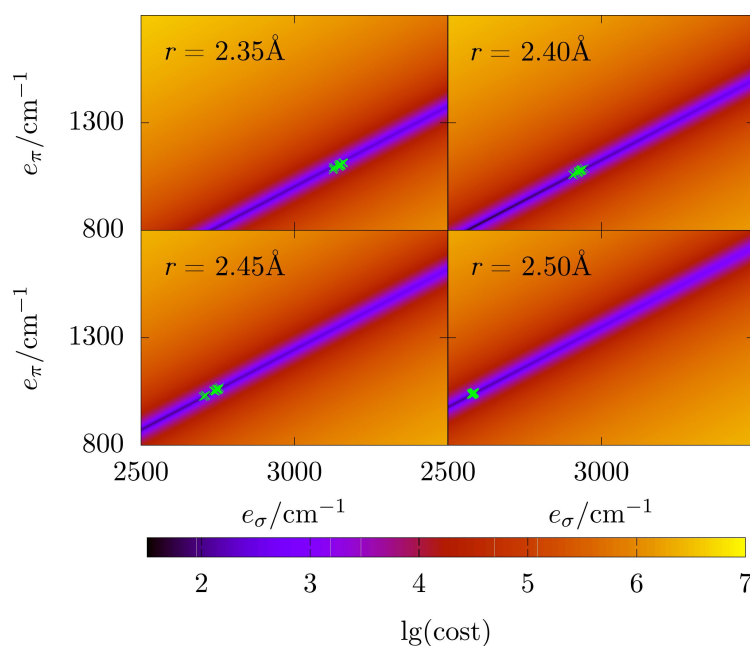


Figure 4. Fitting costs for $[\text{CoCl}_4]^{2-}$, calculated with a reduced equation system. Matrix elements on the main diagonal are subtracted from each other in order to cancel out E , all chloride ligands are grouped. The plot shows the dependence of the fitting cost S (see Equation 9) of a certain parameter set on the two parameters e_σ and e_π . Fitting costs are shown on a logarithmic scale as a colour gradient. Each green point represents the results of an individual fit. The four plots correspond to different M–Cl distances as labelled in the insets.

ent basis sets were run as stated in the main text and Supporting Information.

Results

For this study, (near-)tetrahedral metal halide complexes of the type $[\text{MX}_4]^{2-}$ in a two-dimensional spectrochemical series with $\text{M} = \text{Mn-Cu}$ and $\text{X} = \text{F-Cl}$ were selected. The series allows two simplifications: the cylindrical symmetry of the halide ligands with respect to the M–L bond implies that the π_x and π_y interactions need not be distinguished, but can be subsumed as a π interaction. Secondly, all complexes considered are of (near) tetrahedral symmetry, therefore no or quite limited d–s mixing is expected and the d–s mixing parameter can be neglected in most cases.

The principles of our automated fitting procedure are demonstrated with $[\text{CoX}_4]^{2-}$ complexes, for which ideal tetrahedral coordination environments and no d–s mixing are expected. Experimental data are available for most members of the $[\text{CoX}_4]^{2-}$ series. $[\text{CoCl}_4]^{2-}$ is readily formed from CoCl_2 in hydrochloric acid,^[77] can be synthesized in different organic solvents,^[78] and crystal structures are well known and spectroscopically investigated.^[79,80] For $[\text{CoBr}_4]^{2-}$, the ion in solution was not reported, but crystals have been analysed spectroscopically,^[80] and the $[\text{CoBr}_4]^{2-}$ units were found to be

almost tetrahedral.^[81,82] The data thin out a little for $[\text{CoI}_4]^{2-}$: crystals with almost tetrahedral $[\text{CoI}_4]^{2-}$ units are known,^[81,83,84] but no electronic spectroscopy data was collected. The only homoleptic anion we must assume to be fictitious is $[\text{CoF}_4]^{2-}$. Fluoro complexes of cobalt have been reported with higher cobalt oxidation states of +III and +IV.^[85] Publications on the synthesis and characterization of gaseous CoF_3 , CoF_4 , CoF_4^- and respective cations are known.^[86,87]

AOM parameters for complexes of the type $[\text{CoX}_4]^{2-}$

In the literature, we can find AOM parameters fitted to experimental data, but they always come with a catch: it is basically impossible to distinguish the split components of the tetrahedral ${}^4\text{A}_2(4\text{F})$, ${}^4\text{T}_2(4\text{F})$, ${}^4\text{T}_1(4\text{F})$ and ${}^4\text{T}_1(4\text{P})$ states.^[88] The slight distortions to the tetrahedral units in many crystals are not large enough to affect the spectra significantly. That means even in these distorted environments, there is only one experimental value to fit two parameters on: $\Delta = \frac{4}{3}e_\sigma - \frac{16}{9}e_\pi$. Consequently, it has not been possible to reliably determine experimental AOM parameters for tetrahedral $[\text{CoX}_4]^{2-}$ systems. Published data depends either on an additional constraint for the ratio of e_σ and e_π ,^[39] or is even chosen randomly.^[88] Therefore review articles and book chapters listing the parameters have to be read with some caution.^[27]

The fitting procedure outlined above was applied to the series of cobalt halide complexes. The e_o and e_π parameters in Table 1 show the expected trend of $F^- > Cl^- > Br^- > I^-$ according to their donor capabilities and positioning in the spectrochemical series. The parameters fitted to the matrices based on the CASSCF and NEVPT2 data follow the same trend, but do show some numerical differences that are discussed in some more detail in the Supporting Information. A comparison with experimental and computational ligand field splitting values is also provided in the Supporting Information.

Having the e_o and e_π parameters in hand, we calculated the ratio e_o/e_π . This is the first time that this ratio has been calculated from individually obtained parameters, as opposed to requiring the parameters to meet a predefined ratio.^[39,40] The values found, see Table 1, lie within the expected range for halide ligands in various complexes, ranging roughly from 2 to 5.^[27] Most notably, the often assumed ratio of 4 for cobalt halide complexes is not reproduced here.

As a side note, the fitting procedure confirms the expectation of d-s mixing not being relevant: when fitting the systems

with e_{ds} , the parameter restraints are hit and the parameter has no influence on the cost of the fit.

Dependence on the bond length

The ligand field splitting is a function of the metal-ligand distance r . Crystal field theory predicts that:^[25,p.38]

$$\Delta_{\text{tet}} = \frac{20ze^2(q^4)}{27r^5}, \quad (10)$$

whereas taking the ligand as a dipole instead of a point charge would result in a distance dependence of r^{-6} .^[25,p.39] Here, ze^2 refers to the charge of a ligand and a d electron, and a to the radius of the d shell. While the relation was derived for octahedral symmetry, the only difference in tetrahedral symmetry is a factor of 4/9. Since there is no such simple equation for ligands with more complicated charge distributions, the equation was generalised in the form^[40,89-91]

$$\Delta \propto r^{-n}, \quad (11)$$

with n as a fitting parameter and an undefined proportionality constant.

The fitting procedure described herein allows us to quantitatively evaluate the distance dependence of all AOM parameters. The variation of the ligand field splitting Δ across the series of homoleptic cobalt halide complexes and point charges is shown in Figure 5. Rodriguez and Moreno state that the parameters A and n in $10Dq = Ar^{-n}$ are not necessarily constant over a wide range of r . They assume that the description applies in an interval of $\pm 0.1 \text{ \AA}$ around a given r .^[90]

Method	Complex	$E [\text{cm}^{-1}]$	$e_o [\text{cm}^{-1}]$	$e_\pi [\text{cm}^{-1}]$	e_o/e_π
CASSCF	$[\text{CoF}_4]^{2-}$	-1 211 563(52)	5432(26)	2298(20)	2.36(2)
	$[\text{CoCl}_4]^{2-}$	-1 224 735(19)	3146(10)	1101(9)	2.86(3)
	$[\text{CoBr}_4]^{2-}$	-1 229 806(54)	2662(27)	872(21)	3.05(8)
	$[\text{CoI}_4]^{2-}$	-1 237 432(44)	2090(22)	630(17)	3.32(10)
NEVPT2	$[\text{CoF}_4]^{2-}$	-1 213 192(71)	5274(36)	2225(27)	2.37(3)
	$[\text{CoCl}_4]^{2-}$	-1 226 664(41)	3150(21)	1118(16)	2.82(4)
	$[\text{CoBr}_4]^{2-}$	-1 231 835(86)	2717(44)	917(33)	2.96(12)
	$[\text{CoI}_4]^{2-}$	-1 239 611(111)	2216(56)	719(43)	3.08(20)

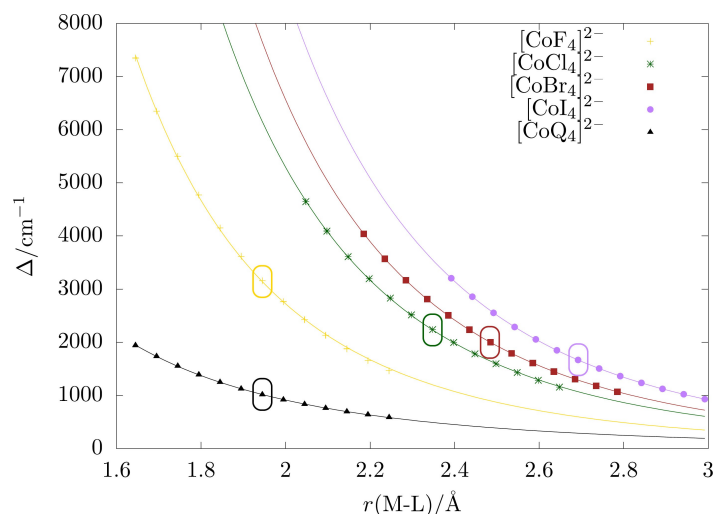


Figure 5. Δ of homoleptic cobalt halides for different bond lengths, calculated with $\Delta = \varepsilon(t_2) - \varepsilon(e) = \frac{4}{3}e_o - \frac{16}{9}e_\pi$. The respective equilibrium bond lengths are highlighted with boxes around the data points. Q denotes a point charge.

Our data shows that an excellent fit is obtained even with variations of $\pm 0.2 \text{ \AA}$ around the equilibrium bond lengths. The exponent n increases from 5.12 in the fluoride complex to 5.53 in the iodide complex, in full agreement with the range determined experimentally. At first glance, this also fits to the assumption of an r^{-5} distance dependence for point charges and a r^{-6} relationship for dipoles: the hard fluoride ligand is usually seen as barely polarizable and therefore expected to act similar to a point charge. The softer and more polarizable the halide is, the more it is expected to act as a dipole. However, the aiLFT-AOM parameter fit for point charges at the positions of the fluoride ions in $[\text{CoF}_4]^{2-}$ yields an even lower value of $n = 3.83$. By this measure, fluoride thus appears to be much more polarizable than an actual point charge. Even though there are no immediately obvious practical implications of this knowledge, being able to quantitatively compare ligands in this way may be useful in other settings.

The proportionality constant A shows a trend too, with softer ligands yielding larger constants as shown in Table 2. Since the charge of the ligands is constant, we put forward the interpretation that A corresponds to the d shell radius a in equation 10. The harder the ligand, the smaller is A and therefore the extent of the pure d orbitals in the ligand field picture.

Experimentally, different methods have been used to study the bond length dependence of Δ . It is calculated by measuring electronic transitions through UV-vis or photoluminescence spectroscopy. The bond length changes are achieved by compression experiments of crystals,^[92–94] observations in different crystal lattices,^[90,95] and comparisons of different ligands with the same donor atom.^[96,97] Compression and lattice variation experiments have shown Δ dependencies of r^{-5} to r^{-6} . The third method depending on the donor atom is inherently flawed, because it mixes the effect of the bond length and of the different electronic properties of the ligands into the same interpretation; Bertini et al. call it “extremely simplified and rough”.^[96]

The fitting procedure introduced here allows us to separate electronic and structural effects and compute the distance dependence individually for the different AOM parameters. We studied the bond length dependence of AOM parameters for homoleptic and heteroleptic complexes. Because the situation is much more complicated for heteroleptic complexes, we focus on homoleptic ones below; additional data sets are shown in the Supporting Information.

Starting with the behaviour of E for different bond lengths r , see Figure 6, a first surprising observation is made: E decays as

Table 2. Fitting parameters of $\Delta(r) = Ar^{-n}$ shown in Figure 5. Q denotes a point charge.

Complex	n	A
$[\text{CoQ}_4]^{2-}$	3.88	13402
$[\text{CoF}_4]^{2-}$	5.12	94482
$[\text{CoCl}_4]^{2-}$	5.39	221487
$[\text{CoBr}_4]^{2-}$	5.48	293771
$[\text{CoI}_4]^{2-}$	5.53	398624

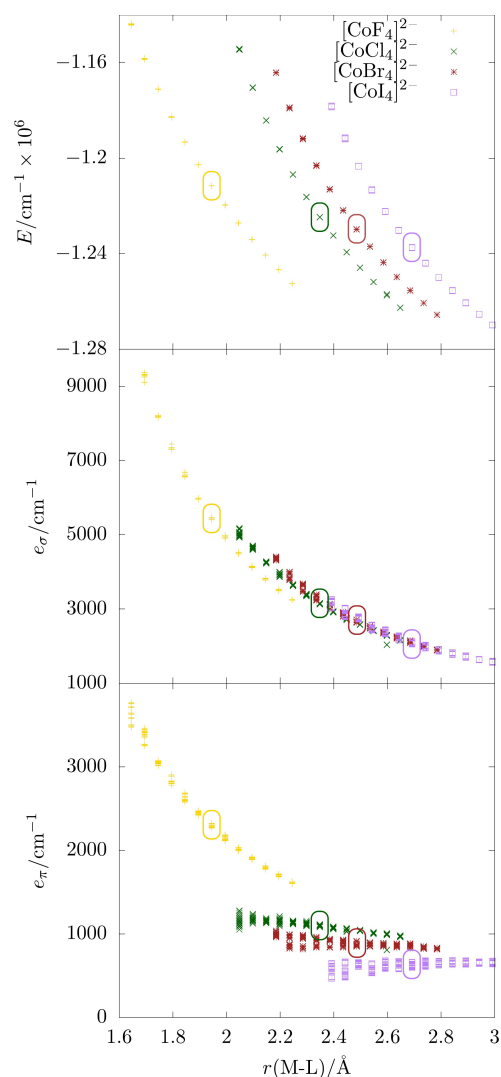


Figure 6. E , e_o and e_π of homoleptic cobalt halides for different bond lengths. The respective equilibrium bond lengths are highlighted with boxes around the data points. Note that analogous plots are shown in the Supporting Information for Mn–Cu.

the bond length increases, but vastly different values for E are found at the same bond length for different halides. This finding might reflect variations in the spherical potential the central metal is subjected to and may be an effect of differences in the charge screening or charge distribution in the different halides.

The parameter e_o decreases with increasing r with very little variation across the series of halide ligands, see Figure 6. This suggests that e_o is only a function of r and independent of the

halide element. The variation in e_π depends on the nature of the halide: for the heavier elements Cl, Br⁻ and I⁻, e_π is almost constant. A plausible explanation might be that the increased σ -donation at shorter distances is compensated with reduced π -donation, thus ensuring electroneutrality. Therefore the π -interaction does not increase as may have been expected, but stays the same. For the lightest halide, F⁻, e_π decays monotonically with increasing bond length. Fluoride is known to be much harder than the other halides and very often shows a unique chemical behaviour. Congruent with the above interpretation, fluoride appears less capable of ensuring electroneutrality, which we can trace back to its π -interaction with the central metal.

Transferability

Transferability of AOM parameters for the same ligand or ligand type between different complexes is an often assumed or expected feature, although it was also shown that it is not generally applicable.^[42,64,96,98,99] It is usually applied to systems where the chemical environment of a certain M–L bond is seen as very similar.^[20,42] For many heteroleptic complexes, the equation system will be underdetermined, precluding an individual fit for every AOM parameter. With the procedure presented herein, we are able to obtain V_{if} with a high or complete degree of independent matrix elements. Our method can thus investigate heteroleptic complexes with highly symmetric equilibrium structures, which allows us to quantitatively evaluate the transferability of AOM parameters.

We investigated complexes of the type $[\text{CoX}_n\text{Y}_{4-n}]^{2-}$, where X and Y are different halides. All XY combinations with the exception of $[\text{CoF}_3\text{I}]^{2-}$ are considered. Geometries are optimized without restraints and a bond length scan is performed. The results of the bond length scan are shown exemplarily for e_σ of the Co–Cl bond in Figure 7.

Despite the outliers occasionally found, there is a clear correlation between bond length and AOM parameter: shorter bond lengths lead to larger e_σ values. With regard to the stoichiometry, no clear trend can be observed. For F⁻, e_σ decreases with an increasing portion of fluoride heteroligands. In the cases of bromide or iodide heteroligands, no such trend can be determined. Still, the heteroligand has an impact on the bond length of the subject ligand: soft halides tend to have longer bond lengths when another hard halide is present in the complex and vice versa.

To distinguish the effects of the M–X bond length and influence of the heteroligand, additional calculations were performed where each metal–ligand bond length in the complexes $[\text{CoX}_n\text{Y}_{4-n}]^{2-}$ is fixed at the equilibrium bond length of the respective homoleptic complex. Accordingly, the M–X bonds are as long as the bonds in $[\text{MX}_4]^{2-}$ and the M–Y bonds have the same length as in $[\text{MY}_4]^{2-}$. The obtained AOM parameters refer to the Co–X bond. The results are shown in Table 3 and can be summarized for both e_σ and e_π as follows: the harder the ligand X, the less noticeable are possible trends; the harder the heteroligand Y, the smaller are the AOM

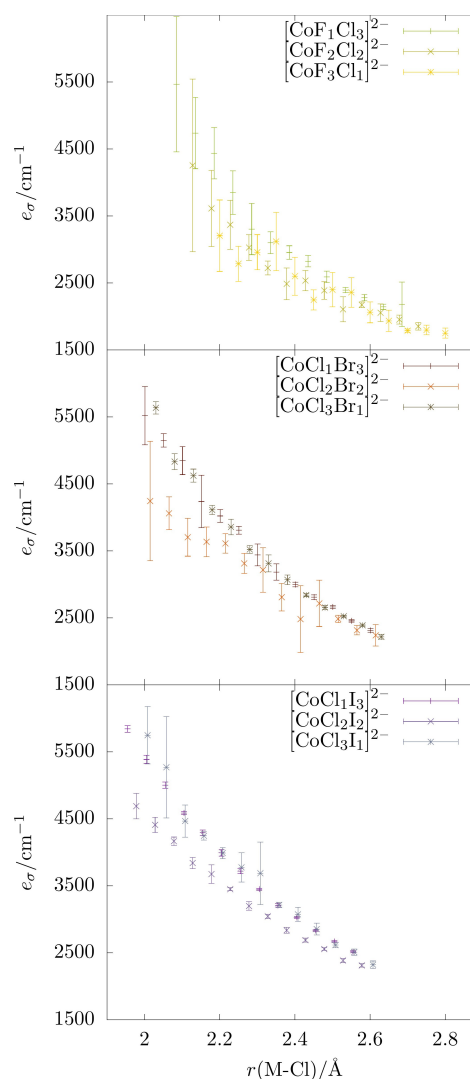


Figure 7. e_σ parameter of the Co–Cl bond in various complexes. Three outliers were removed, see Supporting Information for details.

parameters. Parameters for neighbouring Y are of similar size and almost never differ by more than 200 cm^{-1} .

Compared to the data of the optimized structures (see the Supporting Information) it seems that the influence of the heteroligand is mainly caused by the change in bond length. The obvious exception is fluoride, which has a significant impact at any bond length and every complex. This has two implications: many qualitative effects are already captured by the simple crystal field approach, in which only the charge or dipole moment at the ligands is relevant. On the other hand,

Table 3. AOM parameters for the Co–X bond in different complexes of the type $\text{CoX}_n\text{Y}_{4-n}$ with $r(\text{M–L})$ being the equilibrium bond length of the homoleptic complexes. The subject ligand X is printed in bold letters on the far left of the Table, n_x is its count in the respective complex. Y denotes the type of the hetero ligand, given in the second column. Parameters of homoleptic complexes with $n_x=4$ are shown in italics for easier comparison. All numbers are the average of five data points with the standard deviation given in parentheses. Rows show the parameter change with the stoichiometry, with the homoleptic complex on the right. Columns show the parameter change in the same stoichiometry but with changing heteroligands; the entry for the homoleptic complex is the one where the heteroligand is the same as the subject ligand.

X	Y	e_σ/cm^{-1}				e_π/cm^{-1}			
		n_x 1	2	3	4	n_x 1	2	3	4
F	F	5432(26)	5432(26)	5432(26)	5432(26)	2298(20)	2298(20)	2298(20)	2298(20)
	Cl	5330(65)	5325(101)	5385(82)	5432(26)	2387(53)	2322(82)	2309(75)	2298(20)
	Br	5322(42)	5365(64)	5474(423)	5432(26)	2436(41)	2384(54)	2399(326)	2298(20)
	I	5372(150)	5352(162)	5178(151)	5432(26)	2538(112)	2418(123)	2208(115)	2298(20)
Cl	F	2997(92)	3045(101)	3116(67)	3146(10)	879(47)	946(83)	1027(56)	1101(9)
	Cl	3146(10)	3146(10)	3146(10)	3146(10)	1101(9)	1101(9)	1101(9)	1101(9)
	Br	3204(28)	3179(65)	3042(304)	3146(10)	1184(22)	1142(52)	1030(224)	1101(9)
	I	3227(55)	3089(117)	3216(52)	3146(10)	1281(55)	1131(92)	1186(53)	1101(9)
Br	F	2463(421)	2504(69)	2594(61)	2662(27)	565(306)	643(70)	763(58)	872(21)
	Cl	2469(288)	2610(63)	2635(27)	2662(27)	667(227)	793(49)	834(28)	872(21)
	Br	2662(27)	2662(27)	2662(27)	2662(27)	872(21)	872(21)	872(21)	872(21)
	I	2764(174)	2711(93)	2669(94)	2662(27)	1021(139)	953(81)	895(77)	872(21)
I	F	1427(151)	1869(186)	2086(193)	2090(22)	–45(91)	341(159)	558(155)	630(17)
	Cl	1956(64)	1848(110)	2047(32)	2090(22)	415(58)	361(77)	553(32)	630(17)
	Br	2015(99)	2075(103)	2107(160)	2090(22)	501(71)	561(83)	614(120)	630(17)
	I	2090(22)	2090(22)	2090(22)	2090(22)	630(17)	630(17)	630(17)	630(17)

the bond lengths change in real complexes, so while it would be valid to assume roughly the same $e_i(r)$ for a certain M–L bond in different complexes, r will not be identical.

Summed up, transferability in the given systems is at least questionable. Because ligands have a significant influence on each others bond lengths and they mutually influence their interaction with the metal, their AOM parameters are likely to differ in different chemical settings. Having shown that the black-box fitting procedure presented herein facilitates not only the identification of an ideal AOM parameter set for a given system, but also the distance dependence of one or more ligands, it is now possible to evaluate the error made when transferring the AOM parameters of a particular ligand type between complexes. In any case, the parameters in a specific complex can be used to assess the electronic properties of a ligand in a certain environment in a qualitative and chemically understandable way.

Two-Dimensional Spectrochemical Series and Chemical Hardness

Having shown with a thorough investigation of $[\text{CoX}_4]^{2-}$ complexes and their heteroleptic variants that our fitting procedure provides reliable results that agree with experiment and offer various opportunities for chemical interpretation, we now discuss the two-dimensional spectrochemical series $[\text{M}^n\text{X}_4]^{2-}$ with $\text{M}=\text{Mn, Fe, Co, Ni, Cu}$, and $\text{X}=\text{F, Cl, Br, I}$. The metals form the Irving–Williams series, for which the observed ‘double-bump’ trend in the hydration enthalpies is explained with differences in their ligand field stabilisation energies.^[100–102] While the d^7 configuration of Co^{2+} leads to perfectly tetrahedral structures that are straightforward to analyse and interpret, there are a few caveats for other members of the series. The Fe,

Ni and Cu complexes are subject to Jahn–Teller distortion, the exact shape of which depends on the metals. For Fe, there is a slight change in bond angles, the Ni complexes have two shorter and two longer bond lengths, whereas the Cu complexes are ‘flattened’ and have D_{2d} symmetry. Experimental references for these complexes are listed in the Supporting Information.

As shown in Table 4, the general trends for E , e_σ and e_π are the same even for the more asymmetric structures. Of note is the sensitivity of the method, which for instance discerns the different e_π parameters in the nickel halides as the metal-halide bond is varied, see graphs in the Supporting Information analogous to Figure 6. Overall, Table 4 shows that the AOM

Table 4. AOM parameters E , e_σ and e_π for homoleptic metal halides with the metals Mn, Fe, Co, Ni, Cu.

Complex	E/cm^{-1}	e_σ/cm^{-1}	e_π/cm^{-1}	e_σ/e_π
$[\text{MnF}_4]^{2-}$	–715 961(98)	5988(52)	2560(42)	2.34(4)
$[\text{MnCl}_4]^{2-}$	–734 463(64)	3422(33)	1258(27)	2.72(6)
$[\text{MnBr}_4]^{2-}$	–741 496(48)	2825(26)	982(27)	2.88(8)
$[\text{MnI}_4]^{2-}$	–749 106(25)	2265(16)	750(20)	3.02(8)
$[\text{FeF}_4]^{2-}$	–945 787(68)	6900(91)	2920(106)	2.36(9)
$[\text{FeCl}_4]^{2-}$	–966 124(81)	3427(35)	1252(28)	2.74(7)
$[\text{FeBr}_4]^{2-}$	–971 604(144)	2796(51)	943(44)	2.97(15)
$[\text{FeI}_4]^{2-}$	–979 423(273)	2151(27)	656(25)	3.28(13)
$[\text{CoF}_4]^{2-}$	–1 211 563(52)	5359(168)	2252(111)	2.38(14)
$[\text{CoCl}_4]^{2-}$	–1 224 735(19)	3146(10)	1101(9)	2.86(3)
$[\text{CoBr}_4]^{2-}$	–1 229 806(54)	2662(27)	872(21)	3.05(8)
$[\text{CoI}_4]^{2-}$	–1 237 432(44)	2043(135)	594(103)	3.44(64)
$[\text{NiF}_4]^{2-}$	–1 492 974(30)	5213(162)	2248(140)	2.32(16)
$[\text{NiCl}_4]^{2-}$	–1 503 065(45)	3128(98)	1144(95)	2.73(24)
$[\text{NiBr}_4]^{2-}$	–1 507 380(69)	2671(92)	920(101)	2.90(33)
$[\text{NiI}_4]^{2-}$	–1 513 307(61)	2121(84)	672(84)	3.16(41)
$[\text{CuF}_4]^{2-}$	–1 823 377(19)	5331(179)	2353(162)	2.27(17)
$[\text{CuCl}_4]^{2-}$	–1 835 433(26)	3035(51)	1124(48)	2.70(12)
$[\text{CuBr}_4]^{2-}$	–1 841 224(38)	2507(41)	876(31)	2.86(11)
$[\text{CuI}_4]^{2-}$	–1 847 959(14)	1930(36)	623(26)	3.10(14)

parameters are mainly influenced by the ligand, while the metal series show rather subtle differences. The only exception is $[\text{FeF}_4]^{2-}$ with notably larger e_σ and slightly larger e_π values than seen in the rest of the series. Compared with an earlier study based on Average-of-Configuration-KS-DFT, we find smaller e_σ values and e_σ/e_π ratios (e.g. for $[\text{FeCl}_4]^{2-}$: $e_\sigma = 0.471(4) \mu\text{m}^{-1}$, $e_\sigma/e_\pi = 3.00$).^[103] It will be interesting to study such a 2D-spectrochemical series for octahedral coordination environments, where the influence of the metal is expected to be much more pronounced for differential occupation of the σ - e_g and π - t_{2g} sets since the σ and π bonding modes are more cleanly separated than in tetrahedral systems.

Two-dimensional spectrochemical series separate and compare the σ and π contribution in a metal-ligand interaction.^[104,105] The e_σ and e_π parameters obtained from our procedure are plotted against each other, see Figure 8, as is commonly done for such series.^[22] The points show a linear relationship and can be fitted almost perfectly with a common regression line, pointing out again the above finding that the spectrochemical series for the metals is much less pronounced in the present cases than for the halides. Our data show that there is one equation that relates e_σ and e_π for all complexes investigated here. This finding can be used as a constraint that complements the relationship between Δ and the e-parameters ($\Delta = \varepsilon(t_2) - \varepsilon(e)$), and thus enables AOM parameter fits for perfectly tetrahedral $[\text{MX}_4]^{2-}$ complexes without information on the off-diagonal elements. In contrast to the approach using empirical ratios mentioned in the introduction (e.g. $e_\pi = 4e_\sigma$ for $\text{Cl}^{-[40]}$), this observation includes all halides. Studies on $[\text{V}^{\text{II}}\text{X}_4]^{-}$ and $[\text{Cr}^{\text{IV}}\text{X}_4]^{106}$ $[\text{M}^{\text{III}}\text{Cl}_6]^{2-}$ with $\text{M} = \text{Cr}, \text{Mo}, \text{W}$, $[\text{CrX}_6]^{3-}$ with $\text{X} = \text{CN}^-, \text{NH}_3, \text{F}^-, \text{Cl}^-, \text{Br}^-, \text{I}^-$,^[31] and Ni^{II} complexes^[107] had found similar relationships for other ligand types and metal charges. Even though a direct comparison is not possible due to the

different protocols used here and in the previous examples, the correlation lines for different ligand types but the same metal appear to lie parallel to each other.

In the previous sections, we often referred to chemical hardness in a qualitative way to rationalize and compare the effect of different ligands. In order to probe whether the concept can be applied quantitatively, the Pearson hardness of the halides is plotted against their AOM parameters in the homoleptic complexes at their equilibrium geometries in Figure 9.^[60] The plots are essentially perfectly linear for the σ and π parameters, showing that the concept of chemical hardness is suitable to explain the observed effects. Since the AOM parameters are very similar for the different metals, the resulting regression lines lie close to each other; as mentioned above, $[\text{FeF}_4]^{2-}$ is an exception here. While for each metal series, a linear relationship between the hardness of the halide ligands and the AOM parameters is obtained, it will have to be evaluated whether this holds for other types of ligand. It cannot be expected that all ligands will fall on the same line, but series of ligands with similar donor capabilities may show a correlation within the series.

Conclusions

Ligand Field Theory and the Angular Overlap Model are powerful ideas that allow chemists to intuitively interpret the electronic structures of coordination complexes based on their building blocks. With the aiLFT analysis now readily available to translate complex quantum chemical wavefunctions into a ligand field picture,^[50] chemists can study arbitrary coordination complexes in great detail from a ligand field perspective.^[32,35,52-55] The AOM provides ligand-specific parame-

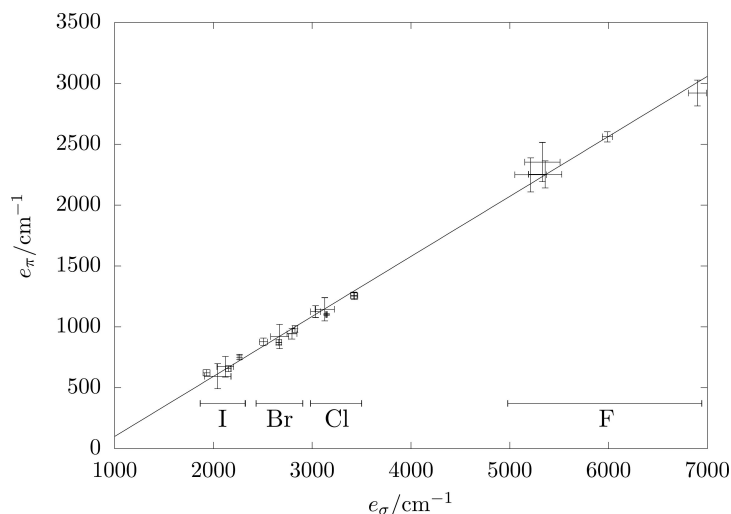


Figure 8. e_σ vs. e_π for different metal halides, all metals shown in the same color and fitted with a common regression line. Error bars indicate the standard deviation. The regression line is the function $e_\pi = 0.4929e_\sigma - 394 \text{ cm}^{-1}$. Regression lines for the individual metal series are given in the Supporting Information.

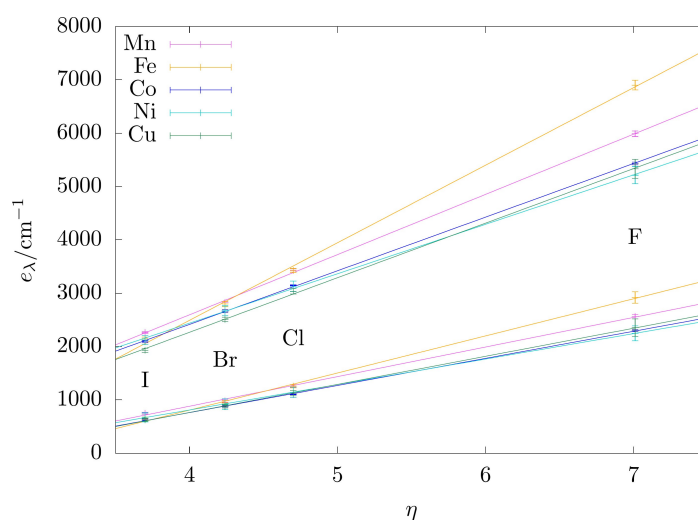


Figure 9. Calculated AOM parameters of various halido metalates versus the chemical hardness η of X with their respective linear regression lines. The hardness values are taken from [60].

ters, e_{σ} and e_{π} , that describe the individual ligand–metal interactions in terms of the widely used σ - and π -terminology. However, obtaining AOM parameters for such complexes previously required detailed knowledge of the underlying equation systems and significant experience in applying and solving them. Therefore, we have developed an automated fitting procedure for AOM parameters based on a scheme for generating asymmetric coordination environments with subsequent aiLFT analyses.

The protocol established here provides AOM parameters for any complex the model is applicable to, and is not limited by the availability or resolution of experimental data, that is, AOM parameters can even be generated for complexes where fits were not possible before. In addition, the procedure used herein naturally includes the spherical ligand field potential E , which was not considered in any of the fitting schemes previously reported in the literature. We are confident that having easy access to the AOM parameters e_{σ} , e_{π} and e_{δ} for any complex that falls under the remit of the AOM and aiLFT analyses, including any structural distortions or modifications that may be useful to answer a given chemical question, will help in better understanding their electronic structures and coordination chemistry.

With a series of tetrahedral cobalt halide complexes as a case study, we have shown that the numerical values found with our procedure are in agreement with experimental data and have standard deviations much below the uncertainties that were previously commonly accepted. We quantitatively evaluated how the bond length r affects the ligand field splitting Δ , the spherical ligand field potential E and the AOM parameters e_{σ} and e_{π} . The behaviour of fluoride differs from that of the heavier halides, which led us to conclude that it is

much less capable of ensuring electroneutrality in these complexes. Given the often unusual behaviour of fluoride ligands, it will be interesting to verify this effect in other series of halide complexes, ideally in conjunction with spectroscopy methods that are sensitive to the charge distribution around the central metal.

Due to the limited number of independent matrix elements available for fitting, a commonly used practice is to transfer the AOM parameters found for a particular ligand type from one complex to another. We evaluated how sensitive the AOM parameters of the halide ligands are to the overall composition of the complex and showed that this practice is at least inaccurate. As a common rule, we deduced that in cases where the other ligands have high donor or acceptor capabilities compared to the ligand for which the parameters are to be transferred, AOM parameter transfer is prone to failure. The fitting procedure presented herein allows a detailed quantification of the errors made when AOM parameter transfer cannot be avoided, e.g. in cases where too few matrix elements are available for fitting.

Pearson's principle of hard and soft acids and bases relies on the chemical hardness, a quantity that is calculated as the average of a species' ionisation potential and electron affinity.^[59,60] As such, it can in principle be measured with high accuracy, even though the HSAB concept is used rather intuitively in everyday chemistry arguments. We found a previously unknown linear relationship between the chemical hardness of the ligands and their AOM parameters for all series of metal complexes in the two-dimensional spectrochemical series from Mn–Cu. It will be interesting to explore whether this relationship holds for other types of ligand, which may provide an additional aspect to the comparison and quantification of

ligand character in coordination complexes. Within the two-dimensional spectrochemical series involving all halides of Mn–Cu, we found a common relationship between e_{σ} and e_{π} . This finding can act as an additional constraint in future fitting procedures. Comparison with similar series in the literature showed that other types of ligand fall on approximately parallel lines. The e_{σ} – e_{π} relationship can thus serve as a tool for characterising the metal–ligand interaction in a two-dimensional map, which might be particularly useful in the context of developing structure–property relationships.

The above examples illustrate a few avenues in which the AOM parameter fitting scheme can be used to better understand the ligand–metal interactions and cooperative effects in coordination complexes. Future work will involve more complex ligands, e.g. ligands in which e_{x_2} and e_{y_2} will be differentiated and multidentate ligands. With the capability of fitting AOM parameters in an unbiased and automated fashion, several other ideas can be studied quantitatively in future, e.g. d–s mixing (or coordination voids) and misdirected bonding effects, which have previously been accounted for by introducing new parameters. Since the procedure introduced here will allow us to avoid overparameterisation and quantify the uncertainty associated with each parameter, we will be able to carefully evaluate their physical and chemical meaning.

Going beyond the specific interpretations of individual AOM parameters, we are convinced that having access to an automated AOM parameter fitting scheme will make it much easier for chemists to interpret electronic structures or design desirable electronic structures by evaluating the effects of ligand substitution patterns and changes in coordination geometry through the AOM lens, whether these are specific design criteria for catalysis, molecular magnetism or other desirable ground state properties.

Acknowledgements

Calculations for this research were conducted on the Lichtenberg high performance computer of the TU Darmstadt. Open Access funding enabled and organized by Projekt DEAL.

Conflict of Interest

The authors declare no conflict of interest.

Data Availability Statement

The data that support the findings of this study are available from the corresponding author upon reasonable request.

Keywords: *ab initio* calculations · angular overlap model · ligand effects · ligand field theory · transition metal complexes

[1] D. J. Durand, N. Fey, *Chem. Rev.* **2019**, *119*, 6561–6594.

- [2] F. Neese, *Coord. Chem. Rev.* **2009**, *253*, 526–563.
[3] F. Neese, T. Petrenko, D. Ganyushin, G. Olbrich, *Coord. Chem. Rev.* **2007**, *251*, 288–327.
[4] R. Francke, B. Schille, M. Roemelt, *Chem. Rev.* **2018**, *118*, 4631–4701.
[5] P. Comba, B. Martin in *Adv. Inorg. Chem. Vol. 73*, Elsevier, **2019**, pp. 305–322.
[6] C.-H. Wang, S. DeBeer, *Chem. Soc. Rev.* **2021**, *50*, 8743–8761.
[7] C. J. Ballhausen, H. B. Gray, *Inorg. Chem.* **1962**, *1*, 111–122.
[8] T. Helgaker, S. Coriani, P. Jørgensen, K. Kristensen, J. Olsen, K. Ruud, *Chem. Rev.* **2012**, *112*, 543–631.
[9] C. J. Cramer, D. G. Truhlar, *Phys. Chem. Chem. Phys.* **2009**, *11*, 10757–10816.
[10] L. González, D. Escudero, L. Serrano-Andrés, *ChemPhysChem* **2012**, *13*, 28–51.
[11] J. P. Malrieu, R. Caballol, C. J. Calzado, C. de Graaf, N. Guihéry, *Chem. Rev.* **2014**, *114*, 429–492.
[12] V. Krewald, M. Retegan, F. Neese, W. Lubitz, D. A. Pantazis, N. Cox, *Inorg. Chem.* **2016**, *55*, 488–501.
[13] M. Gerloch, *Magnetism and Ligand-Field Analysis*, Cambridge University Press, New York, **1983**.
[14] C. J. Ballhausen, *Introduction to ligand field theory*, McGraw-Hill, New York, **1962**.
[15] J. S. Griffith, L. E. Orgel, *Q. Rev. Chem. Soc.* **1957**, *11*, 381.
[16] L. E. Orgel, *J. Chem. Soc.* **1952**, 4756.
[17] W. H. Kleiner, *J. Chem. Phys.* **1952**, *20*, 1784–1791.
[18] C. E. Schäffer, *Inorg. Chim. Acta* **1995**, *240*, 581–592.
[19] C. E. Schäffer, H. Yamatera, *Inorg. Chem.* **1991**, *30*, 2840–2853.
[20] M. Gerloch, R. G. Woolley, *J. Chem. Soc. Dalton Trans.* **1981**, 1714.
[21] M. Gerloch, J. H. Harding, R. G. Woolley in *Inorganic Chemistry*, Springer, Berlin, **1981**, pp. 1–46.
[22] C. Anthon, J. Bendix, C. E. Schäffer, *Inorg. Chem.* **2004**, *43*, 7882–7886.
[23] R. Deeth in *Comprehensive Coordination Chemistry II*, Elsevier, **2003**, pp. 439–442.
[24] C. E. Schäffer, C. K. Jørgensen, *Mol. Phys.* **1965**, *9*, 401–412.
[25] B. N. Figgis, M. A. Hitchman, *Ligand Field Theory and Its Applications*, 1st ed., Wiley, New York, **2000**.
[26] C. E. Schäffer, *Pure Appl. Chem.* **1970**, *24*, 361–392.
[27] A. Bencini, C. Benelli, D. Gatteschi, *Coord. Chem. Rev.* **1984**, *60*, 131–169.
[28] E. C. Wasinger, F. M. F. de Groot, B. Hedman, K. O. Hodgson, E. I. Solomon, *J. Am. Chem. Soc.* **2003**, *125*, 12894–12906.
[29] M. Gerloch, R. G. Woolley in *Progress Inorganic Chemistry* Wiley, New York, **1984**, pp. 371–446.
[30] A. Ceulemans, M. Dendooven, L. G. Vanquickenborne, *Inorg. Chem.* **1985**, *24*, 1153–1158.
[31] S. K. Singh, J. Eng, M. Atanasov, F. Neese, *Coord. Chem. Rev.* **2017**, *344*, 2–25.
[32] D. Schweinfurth, M. G. Sommer, M. Atanasov, S. Demeshko, S. Hohloch, F. Meyer, F. Neese, B. Sarkar, *J. Am. Chem. Soc.* **2015**, *137*, 1993–2005.
[33] J. Jung, M. Atanasov, F. Neese, *Inorg. Chem.* **2017**, *56*, 8802–8816.
[34] G. Charron, F. Bellot, F. Cisnetti, G. Pelosi, J.-N. Rebilly, E. Rivière, A.-L. Barra, T. Mallah, C. Policar, *Chem. Eur. J.* **2007**, *13*, 2774–2782.
[35] J. Krzystek, D. C. Swenson, S. A. Zvyagin, D. Smirnov, A. Ozarowski, J. Telsner, *J. Am. Chem. Soc.* **2010**, *132*, 5241–5253.
[36] A. Bronova, N. Kannengießer, R. Glaum, *Inorg. Chem.* **2017**, *56*, 9235–9246.
[37] N. Kannengießer, M. Jähnig, R. K. Kremer, R. Glaum, *Eur. J. Inorg. Chem.* **2021**, *2021*, 1722–1735.
[38] M. Suta, F. Cimpoesu, W. Urland, *Coord. Chem. Rev.* **2021**, *441*, 213981.
[39] D. A. Cruse, M. Gerloch, *J. Chem. Soc. Dalton Trans.* **1977**, 1617.
[40] R. Glaum, M. A. Hitchman, *Aust. J. Chem.* **1996**, *49*, 1221.
[41] R. G. Woolley, *Mol. Phys.* **1981**, *42*, 703–720.
[42] M. Gerloch in *Understanding Molecular Properties*, **1987**, pp. 111–142.
[43] R. J. Deeth, *Dalton Trans.* **2020**, *49*, 9641–9650.
[44] R. J. Deeth, *Eur. J. Inorg. Chem.* **2020**, *2020*, 1960–1963.
[45] M. Atanasov, C. Daul, H. U. Güdel, T. A. Wesolowski, M. Zbiri, *Inorg. Chem.* **2005**, *44*, 2954–2963.
[46] M. Atanasov, C. A. Daul, C. R. Chim. **2005**, *8*, 1421–1433.
[47] C. E. Schäffer, C. Anthon, J. Bendix, *Coord. Chem. Rev.* **2009**, *253*, 575–593.
[48] C. Daul, *Chimia* **2014**, *68*, 633–641.
[49] F. Vlahović, M. Perić, M. Gruden-Pavlović, M. Zlatar, *J. Chem. Phys.* **2015**, *142*, 214111.

- [50] M. Atanasov, D. Ganyushin, K. Sivalingam, F. Neese in *Molecular Electronic Structures of Transition Metal Complexes II, Structure and Bonding* 2011, pp. 149–220.
- [51] L. Lang, M. Atanasov, F. Neese, *J. Phys. Chem. A* 2020, 124, 1025–1037.
- [52] E. A. Suturina, D. Maganas, E. Bill, M. Atanasov, F. Neese, *Inorg. Chem.* 2015, 54, 9948–9961.
- [53] Y. Rechkemmer, F. D. Breitgoff, M. van der Meer, M. Atanasov, M. Haki, M. Orlita, P. Neugebauer, F. Neese, B. Sarkar, J. van Slageren, *Nat. Commun.* 2016, 7, 10467.
- [54] M. A. Palacios, I. F. Diaz-Ortega, H. Nojiri, E. A. Suturina, M. Ozerov, J. Krzystek, E. Colacio, *Inorg. Chem. Front.* 2020, 7, 4611–4630.
- [55] S. E. Stavretis, M. Atanasov, A. A. Podlesnyak, S. C. Hunter, F. Neese, Z.-L. Xue, *Inorg. Chem.* 2015, 54, 9790–9801.
- [56] M. Atanasov, D. Aravena, E. Suturina, E. Bill, D. Maganas, F. Neese, *Coord. Chem. Rev.* 2015, 289–290, 177–214.
- [57] V. Lyaskovskyy, B. de Bruin, *ACS Catal.* 2012, 2, 270–279.
- [58] O. R. Luca, R. H. Crabtree, *Chem. Soc. Rev.* 2013, 42, 1440–1459.
- [59] R. G. Pearson, *J. Am. Chem. Soc.* 1963, 85, 3533–3539.
- [60] R. G. Pearson, *J. Am. Chem. Soc.* 1988, 110, 7684–7690.
- [61] F. Neese, *Wiley Interdiscip. Rev.: Comput. Mol. Sci.* 2012, 2, 73–78.
- [62] V. G. Chilkuri, S. DeBeer, F. Neese, *Inorg. Chem.* 2017, 56, 10418–10436.
- [63] R. J. Deeth, D. L. Foulis, *Phys. Chem. Chem. Phys.* 2002, 4, 4292–4297.
- [64] R. G. Woolley, *Int. Rev. Phys. Chem.* 1987, 6, 93–141.
- [65] R. J. Deeth, A. Anastasi, C. Diedrich, K. Randell, *Coord. Chem. Rev.* 2009, 253, 795–816.
- [66] W. H. Press, *Numerical Recipes: The Art of Scientific Computing*, 3rd ed., Cambridge University Press, Cambridge, 2007.
- [67] F. Neese, *WIREs Comput. Mol. Sci.* 2018, 8, e1327.
- [68] A. D. Becke, *Phys. Rev. A* 1988, 38, 3098–3100.
- [69] J. P. Perdew, *Phys. Rev. B* 1986, 33, 8822–8824.
- [70] F. Weigend, R. Ahlrichs, *Phys. Chem. Chem. Phys.* 2005, 7, 3297.
- [71] P. Siegbahn, A. Heiberg, B. Roos, B. Levy, *Phys. Scr.* 1980, 21, 323–327.
- [72] B. O. Roos, P. R. Taylor, P. E. Siegbahn, *Chem. Phys.* 1980, 48, 157–173.
- [73] C. Angeli, R. Cimiraglia, J.-P. Malrieu, *Chem. Phys. Lett.* 2001, 350, 297–305.
- [74] C. Angeli, R. Cimiraglia, S. Evangelisti, T. Leininger, J.-P. Malrieu, *J. Chem. Phys.* 2001, 114, 10252–10264.
- [75] C. Angeli, R. Cimiraglia, J.-P. Malrieu, *J. Chem. Phys.* 2002, 117, 9138–9153.
- [76] C. Angeli, R. Cimiraglia, *Theor. Chem. Acc.* 2002, 107, 313–317.
- [77] N. M. Barrera, J. L. McCarty, V. Dragojlovic, *Chem. Educ.* 2002, 7, 142–145.
- [78] S. Buffagni, T. M. Dunn, *Nature* 1960, 188, 937–938.
- [79] N. Fogel, C. C. Lin, C. Ford, W. Grindstaff, *Inorg. Chem.* 1964, 3, 720–726.
- [80] K. Kojima, J. Matsuda, *Bull. Chem. Soc. Jpn.* 1986, 59, 859–863.
- [81] M. R. Pressprich, R. D. Willett, *Acta Crystallogr. Sect. C Cryst. Struct. Commun.* 1991, 47, 1188–1191.
- [82] Y. Nishihata, A. Sawada, H. Kasatani, H. Terauchi, *Acta Crystallogr. Sect. C Cryst. Struct. Commun.* 1993, 49, 1939–1941.
- [83] V. V. Sharutin, V. S. Senchurin, O. K. Sharutina, O. A. Fastovets, A. P. Pakusina, *Russ. J. Inorg. Chem.* 2010, 55, 1410–1414.
- [84] V. V. Sharutin, V. S. Senchurin, O. K. Sharutina, B. B. Kunkurdonova, *Russ. J. Inorg. Chem.* 2011, 56, 1384–1389.
- [85] W. Klemm, W. Brandt, R. Hoppe, *Z. Anorg. Allg. Chem.* 1961, 308, 179–189.
- [86] J. V. Rau, N. S. Chilingarov, L. N. Sidorov, *Rapid Commun. Mass Spectrom.* 1997, 11, 1977–1979.
- [87] M. I. Nikitin, A. S. Alikhanyan, *Russ. J. Inorg. Chem.* 2020, 65, 199–204.
- [88] W. D. Horrocks, D. A. Burlone, *J. Am. Chem. Soc.* 1976, 98, 6512–6516.
- [89] M. Bermejo, L. Pueyo, *J. Chem. Phys.* 1983, 78, 854–857.
- [90] F. Rodríguez, M. Moreno, *J. Chem. Phys.* 1986, 84, 692–697.
- [91] P. V. Bernhardt, P. Comba, *Inorg. Chem.* 1993, 32, 2798–2803.
- [92] H. G. Drickamer, *J. Chem. Phys.* 1967, 47, 1880.
- [93] D. W. Smith, *J. Chem. Phys.* 1969, 50, 2784.
- [94] D. R. Stephens, H. G. Drickamer, *J. Chem. Phys.* 1961, 35, 427–429.
- [95] M. C. M. de Lucas, F. Rodríguez, H. U. Güdel, N. Furer, *J. Lumin.* 1994, 60–61, 581–584.
- [96] I. Bertini, D. Gatteschi, A. Scozzafava, *Inorg. Chem.* 1976, 15, 203–207.
- [97] A. B. P. Lever, I. M. Walker, P. J. McCarthy, K. B. Mertes, A. Jircitano, R. Sheldon, *Inorg. Chem.* 1983, 22, 2252–2258.
- [98] M. Gerloch, R. F. McMeeking, A. M. White, *J. Chem. Soc. Dalton Trans.* 1976, 655–660.
- [99] R. J. Deeth, M. Gerloch, *Inorg. Chem.* 1985, 24, 1754–1758.
- [100] D. A. Johnson, P. G. Nelson, *Inorg. Chem.* 1995, 34, 3253–3259.
- [101] D. A. Johnson, P. G. Nelson, *J. Chem. Soc. Dalton Trans.* 1995, 3483–3488.
- [102] R. J. Deeth, K. Randell, *Inorg. Chem.* 2008, 47, 7377–7388.
- [103] C. E. Schäffer, C. Anthon, J. Bendix, *Aust. J. Chem.* 2009, 62, 1271.
- [104] D. S. McClure in *Solid State Physics*, (Eds.: D. Turnbull, H. Ehrenreich), Elsevier, Burlington, 1959, pp. 399–525.
- [105] W. W. Fee, J. N. Harrowfield, *Aust. J. Chem.* 1970, 23, 1049.
- [106] C. Anthon, J. Bendix, C. E. Schäffer in *Optical Spectra and Chemical Bonding in Transition Metal Complexes* (Ed.: T. Schönherl), Springer, Berlin, 2004, pp. 207–301.
- [107] M. Atanasov, P. Comba, S. Helmlé, D. Müller, F. Neese, *Inorg. Chem.* 2012, 51, 12324–12335.

Manuscript received: October 19, 2021
Accepted manuscript online: January 3, 2022
Version of record online: February 2, 2022

Chemistry–A European Journal

Supporting Information

Revisiting the Fundamental Nature of Metal-Ligand Bonding: An Impartial and Automated Fitting Procedure for Angular Overlap Model Parameters

Moritz Buchhorn, Robert J. Deeth, and Vera Krewald*

Angular Overlap Factors

Table 1: Angular overlap factors $F_{\sigma i}(\theta, \phi)$ as in [1].

i	$F_{\sigma i}(\theta, \phi)$
xy	$\frac{\sqrt{3}}{4} \sin(2\phi)(1 - \cos(2\theta))$
yz	$\frac{\sqrt{3}}{2} \sin(\phi) \sin(2\theta)$
z^2	$\frac{1}{4}(1 + 3 \cos(2\theta))$
xz	$\frac{\sqrt{3}}{2} \cos(\phi) \sin(2\theta)$
$x^2 - y^2$	$\frac{\sqrt{3}}{4} \cos(2\phi)(1 - \cos(2\theta))$

Table 2: Angular overlap factors $F_{\pi xi}(\theta, \phi, \psi)$ as in [1].

i	$F_{\pi xi}(\theta, \phi, \psi)$
xy	$\cos(2\phi) \sin(\theta) \sin(\psi) + \frac{1}{2} \sin(2\phi) \sin(2\theta) \cos(\psi)$
yz	$\cos(\phi) \cos(\theta) \sin(\psi) + \sin(\phi) \cos(2\theta) \cos(\psi)$
z^2	$-\frac{\sqrt{3}}{2} \sin(2\theta) \cos(\psi)$
xz	$-\sin(\phi) \cos(\theta) \sin(\psi) + \cos(\phi) \cos(2\theta) \cos(\psi)$
$x^2 - y^2$	$-\sin(2\phi) \sin(\theta) \sin(\psi) + \frac{1}{2} \cos(2\phi) \sin(2\theta) \cos(\psi)$

Table 3: Angular overlap factors $F_{\pi yi}(\theta, \phi, \psi)$ as in [1].

i	$F_{\pi yi}(\theta, \phi, \psi)$
xy	$\cos(2\phi) \sin(\theta) \cos(\psi) - \frac{1}{2} \sin(2\phi) \sin(2\theta) \sin(\psi)$
yz	$\cos(\phi) \cos(\theta) \cos(\psi) - \sin(\phi) \cos(2\theta) \sin(\psi)$
z^2	$\frac{\sqrt{3}}{2} \sin(2\theta) \sin(\psi)$
xz	$-\sin(\phi) \cos(\theta) \cos(\psi) - \cos(\phi) \cos(2\theta) \sin(\psi)$
$x^2 - y^2$	$-\sin(2\phi) \sin(\theta) \cos(\psi) - \frac{1}{2} \cos(2\phi) \sin(2\theta) \sin(\psi)$

Table 4: Simplified angular overlap factors $F_{\pi i}(\theta, \phi) = F_{\pi xi}(\theta, \phi, \psi = 0) + F_{\pi yi}(\theta, \phi, \psi = 0)$.

i	$F_{\pi i}(\theta, \phi)$
xy	$\cos(2\phi) \sin(\theta) + \frac{1}{2} \sin(2\phi) \sin(2\theta)$
yz	$\cos(\phi) \cos(\theta) + \sin(\phi) \cos(2\theta)$
z^2	$-\frac{\sqrt{3}}{2} \sin(2\theta)$
xz	$-\sin(\phi) \cos(\theta) + \cos(\phi) \cos(2\theta)$
$x^2 - y^2$	$-\sin(2\phi) \sin(\theta) + \frac{1}{2} \cos(2\phi) \sin(2\theta)$

Discussion of Δ -values

A limited comparison with experimental data is possible for the values of Δ calculated from the AOM parameters. In the AOM, the d-orbital energy difference Δ in a tetrahedral complex is given as:

$$\Delta = \epsilon(t_{2g}) - \epsilon(e_g) = \frac{4}{3}e_{\sigma} - \frac{16}{9}e_{\pi} \quad (1)$$

Since orbitals and their energies are not observables, there is no direct connection with experiment. The approximation used most often is to resort to the first electronic transition: [1]

$$\Delta = E(^4T_2) - E(^4A_2) \quad (2)$$

In the special case of a tetrahedral d^7 -system, the Tanabe-Sugano diagram for $B = 918 \text{ cm}^{-1}$ and $C/B = 4.5$, the line of the $^4T_2(F)$ state is linear with a slope of 1.[2] In this case, the definitions of Δ are coincidentally equal. Table 5 shows calculated and experimental values for the ligand field splitting. While the ligand field splitting according to the AOM parametrization shows the correct trend, smaller splittings for heavier halides, the absolute values are consistently underestimated. The same observation can already be made in the ligand field splitting values calculated directly from the CASSCF and NEVPT2 states, although the NEVPT2 correction approaches the experimental value to within 200 cm^{-1} . An apparent mismatch arises from the fact that the CASSCF and NEVPT2 transition energies differ, although the fit of \mathbf{V}_{LF} yields almost the same AOM parameters (see main text). The methods predict different Racah parameters (CASSCF: $B = 1200 \text{ cm}^{-1}$, $C/B = 3.7$, NEVPT2: $B = 1000 \text{ cm}^{-1}$, $C/B = 4.0$), so while the one-electron part of the ligand field Hamiltonian remains almost unaltered, the two-electron part changes significantly. Arguing with the Tanabe-Sugano diagrams this would mean different diagrams are necessary for both cases and Δ in Equation 2 is different to Δ in Equation 1. Consequently, the values cannot be compared directly. The trend in Δ , regardless of its definition, is reproduced by all of the calculations.

Table 5: Calculated and experimental values for Δ in cm^{-1} . Note that the theoretical and experimental definitions of Δ differ.

Complex	$\Delta_{\text{AOM}}/\text{cm}^{-1}$	${}^4A_{2g} \Rightarrow {}^4T_{2g}/\text{cm}^{-1}$		$\Delta_{\text{exp.}}/\text{cm}^{-1}$	Source
		(CASSCF)	(NEVPT2)		
$[\text{CoCl}_4]^{2-}$	2237	2100	3000	2825 - 3330	[3], [4], [5]
$[\text{CoBr}_4]^{2-}$	1999	1850	2700	2800	[4]
$[\text{CoI}_4]^{2-}$	1667	1500	2500	2700	[6]

Additional metal halides

For the extended series of metal halide complexes, we researched which coordination compounds exist and have been reported. The list in Table 6 makes no claim to be complete, but shows that most of the investigated complexes exist, either as solvated ion or as a subunit in a crystal lattice. Only Mn^{III} compounds were found.[7] We were unable to find (near-)tetrahedral Fe^{II} compounds for halides other than fluoride. All Cu^{II} fluorides we found are octahedrally coordinated,[8, 9] and for $[\text{CuI}_4]^{2-}$ we found no reported synthesis or analysis.

The AOM parameters for the series of metal halides resulting from our fitting procedure are shown in the main text. The results of bond length scans analogous to that shown for the cobalt complex are shown in Figure 1 to 5, with an overview of all data presented in Figure 6.

The AOM parameters and their ratios are similar for the same halides, as was pointed out in the main text. Here, we will discuss the deviations from the model system $[\text{CoX}_4]^{2-}$. For manganese, the optimized geometry is tetrahedral, as expected for a d^5 high-spin system. All other metal complexes show Jahn-Teller distortions that lead to different symmetries. $[\text{FeX}_4]^{2-}$ shows slightly bent bond angles, nevertheless the fit yields AOM parameters that are roughly identical.

$[\text{NiX}_4]^{2-}$ is distorted in an interesting way: there are two short, one intermediate and one long bond in the molecule. The difference between the bond lengths is about 0.02 Å. In every calculation, the AOM parameters of the short bonds are larger than the average at the respective length. Vice versa, the AOM parameters of the longer bonds are smaller than the average at the respective

Table 6: Experimental references for the metal halides $[\text{MX}_4]^{2-}$ where available.

X	Mn	Fe	Ni	Cu
F	none	[10]	[11, 12]	none
Cl	[13–16]	none	[13, 17]	[13, 18]
Br	[13, 15, 16, 19]	none	[13, 20]	[13, 21, 22]
I	[13, 15, 16]	none	[13]	none

Table 7: Angular overlap parameters E , e_σ , e_π and e_{ds} for homoleptic copper halides $[\text{CuX}_4]^{2-}$. To avoid overparameterization, a grouped fit was performed where the additional restraint $e_{\lambda,L} = e_{\lambda,L'}$ is imposed.

X	E/cm^{-1}	e_σ/cm^{-1}	e_π/cm^{-1}	e_{ds}/cm^{-1}
F	-1 822 578(32)	5012(26)	2107(29)	402(31)
Cl	-1 835 247(26)	2949(37)	1069(29)	141(24)
Br	-1 841 118(51)	2457(35)	845(27)	85(32)
I	-1 847 925(25)	1919(34)	612(26)	20(27)

length. This illustrates the mutual influence of ligands on each other, and that not only their chemical nature, but also their relative bond length is important.

The copper complexes have D_{2d} symmetry, which would require the consideration of d-s mixing[23] or the introduction of coordination voids.[24] The least-squares fit is able to find a set of E , e_σ and e_π parameters which represent the d-orbital energies with the smallest deviation to the original V_{LF} . However, the overall fitting costs are very high and the d-orbital energies are reproduced less well than in the other examples. Inclusion of d-s mixing significantly improves the fit and lowers the cost. Preliminary results with an additional d-s mixing parameter e_{ds} for the copper halides are shown in Table 7. The equations used for the fit are derived and presented in [25].

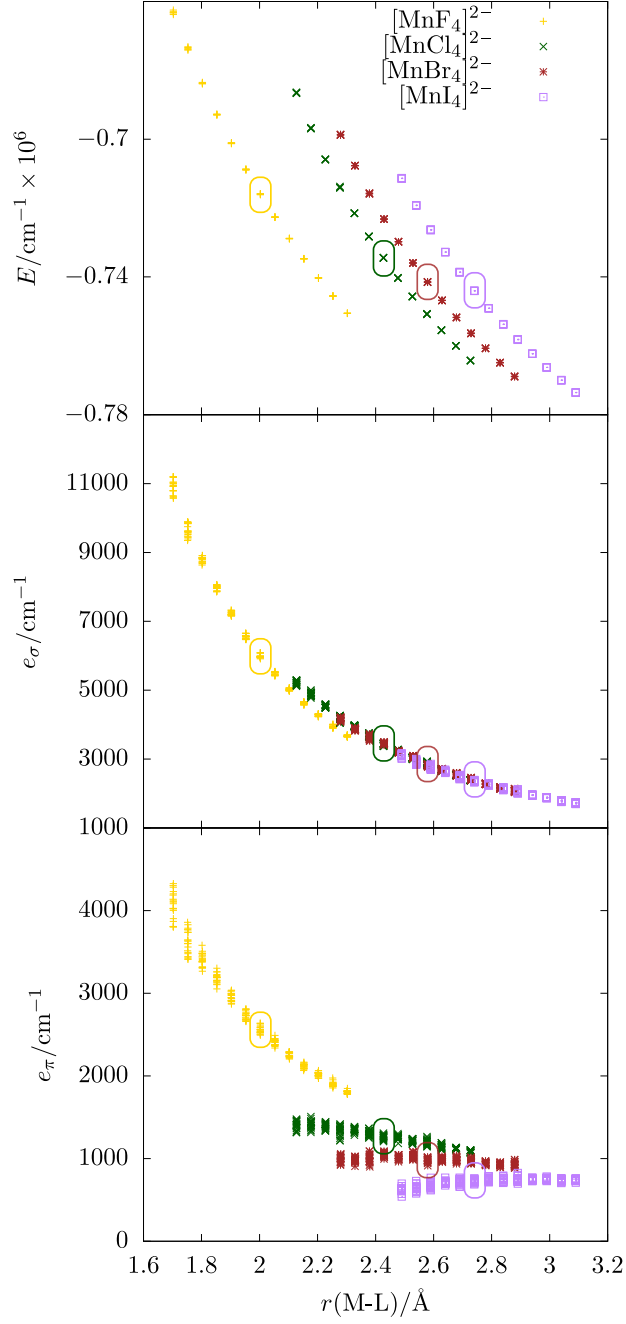


Figure 1: E , e_σ and e_π of homoleptic manganese halides for different bond lengths. The respective equilibrium bond lengths are highlighted with boxes around the data points.

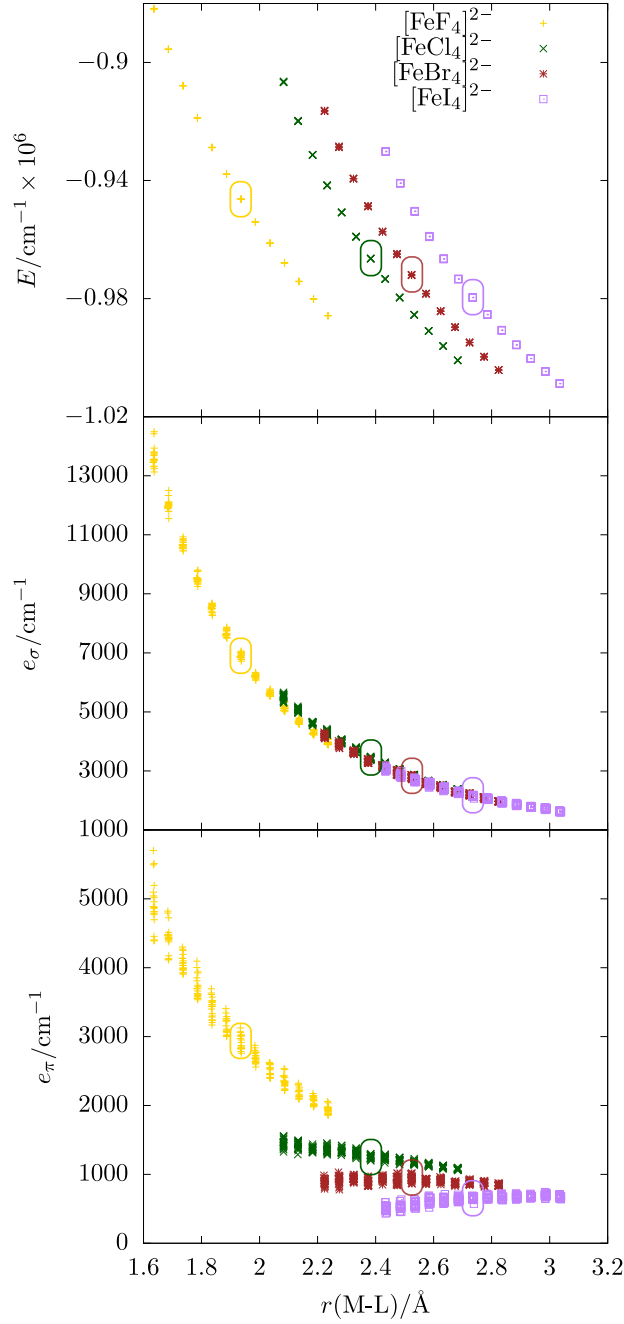


Figure 2: E , e_σ and e_π of homoleptic iron halides for different bond lengths. The respective equilibrium bond lengths are highlighted with boxes around the data points.

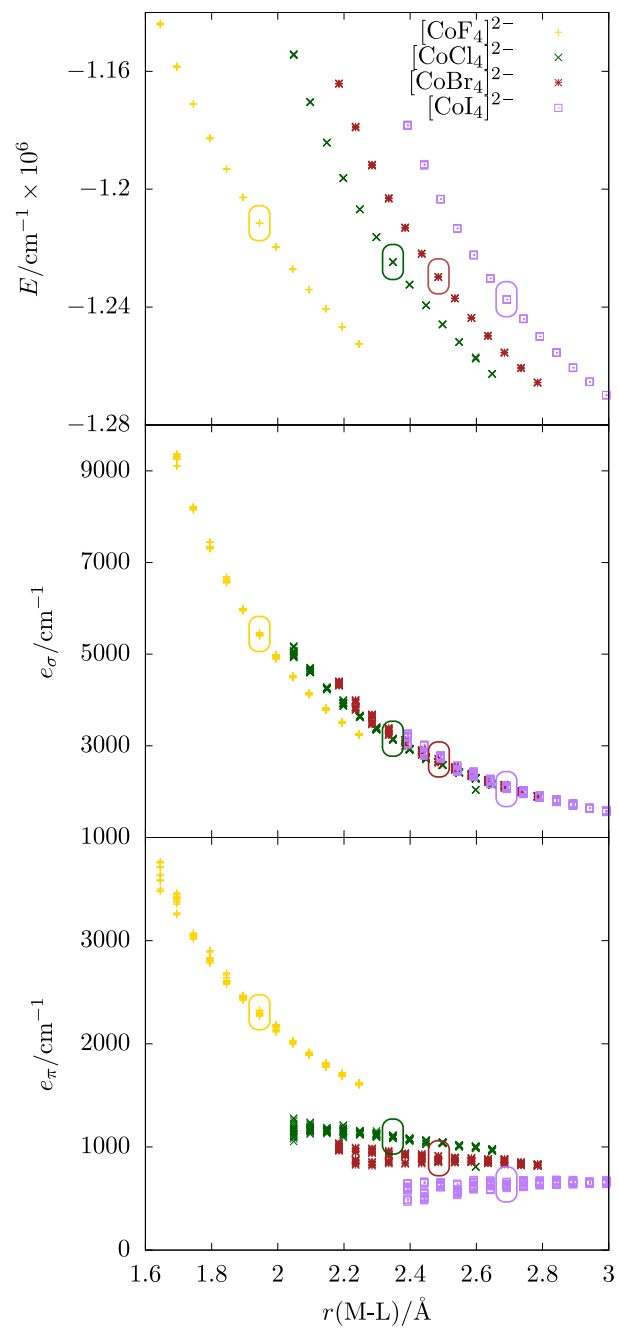


Figure 3: E , e_σ and e_π of homoleptic cobalt halides for different bond lengths. The respective equilibrium bond lengths are highlighted with boxes around the data points.

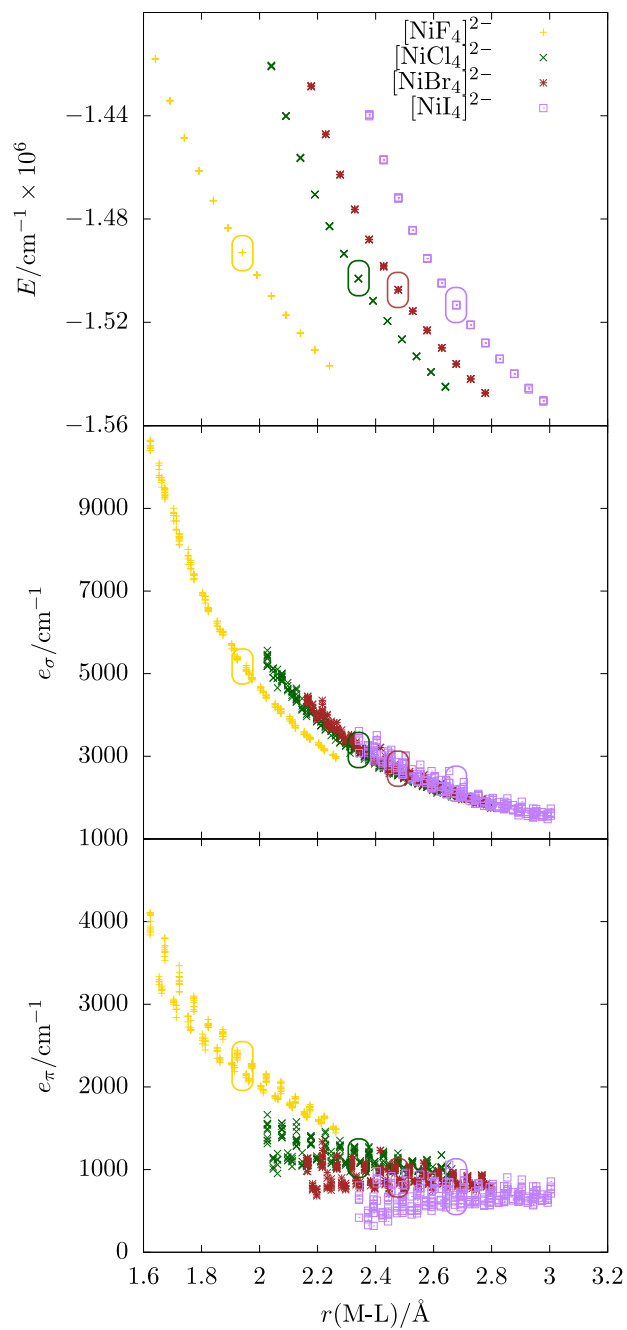


Figure 4: E , e_σ and e_π of homoleptic nickel halides for different bond lengths. The respective equilibrium bond lengths are highlighted with boxes around the data points.

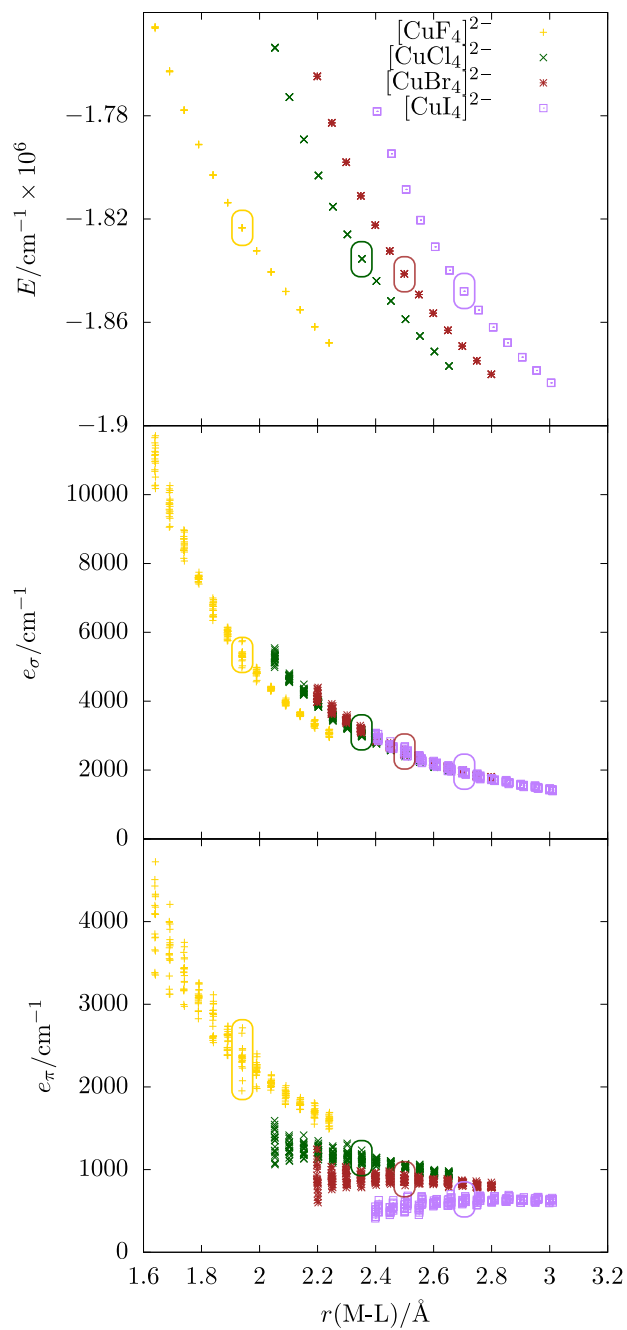


Figure 5: E , e_σ and e_π of homoleptic copper halides for different bond lengths. The respective equilibrium bond lengths are highlighted with boxes around the data points.

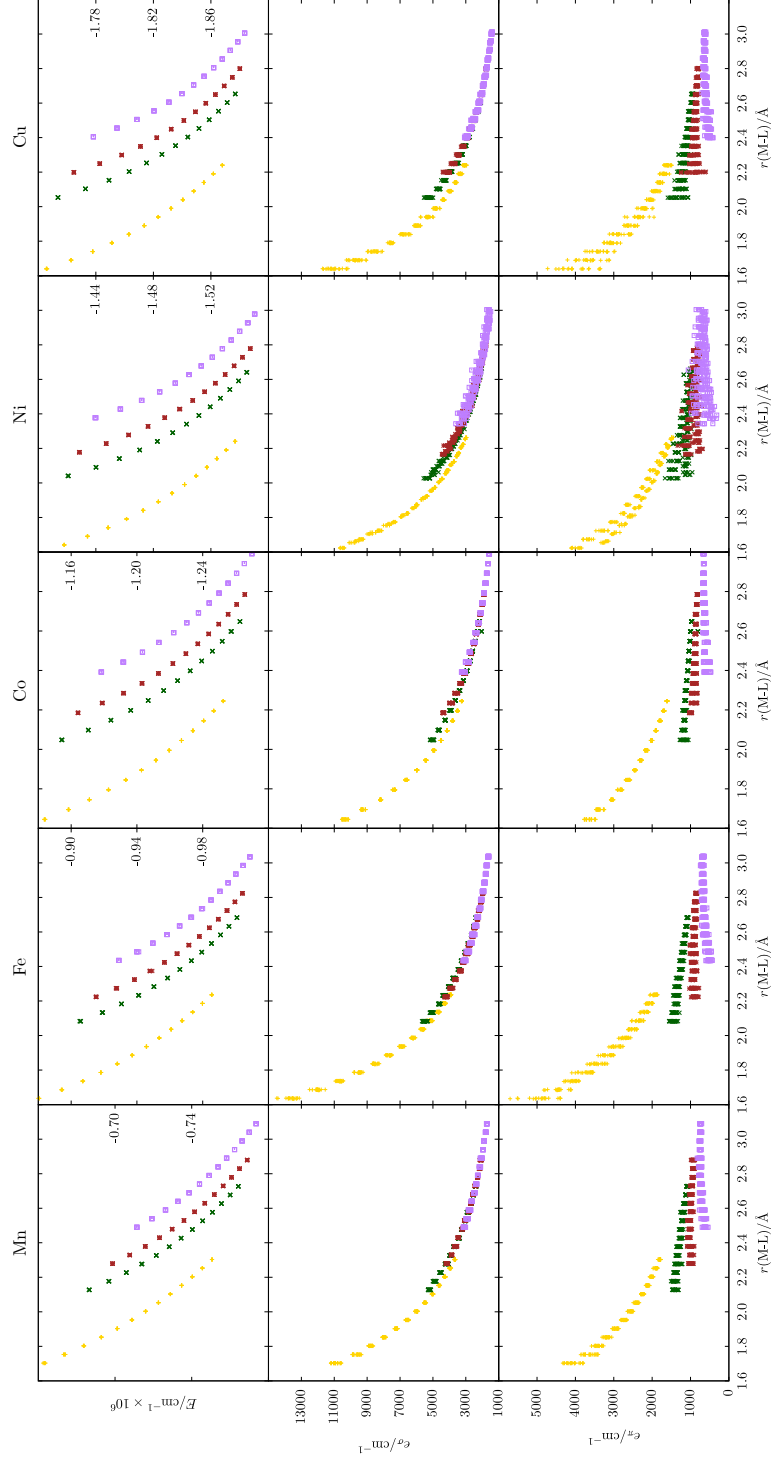


Figure 6: E , e_σ and e_π of homoleptic metal halides for different bond lengths as an overview of the preceding plots.

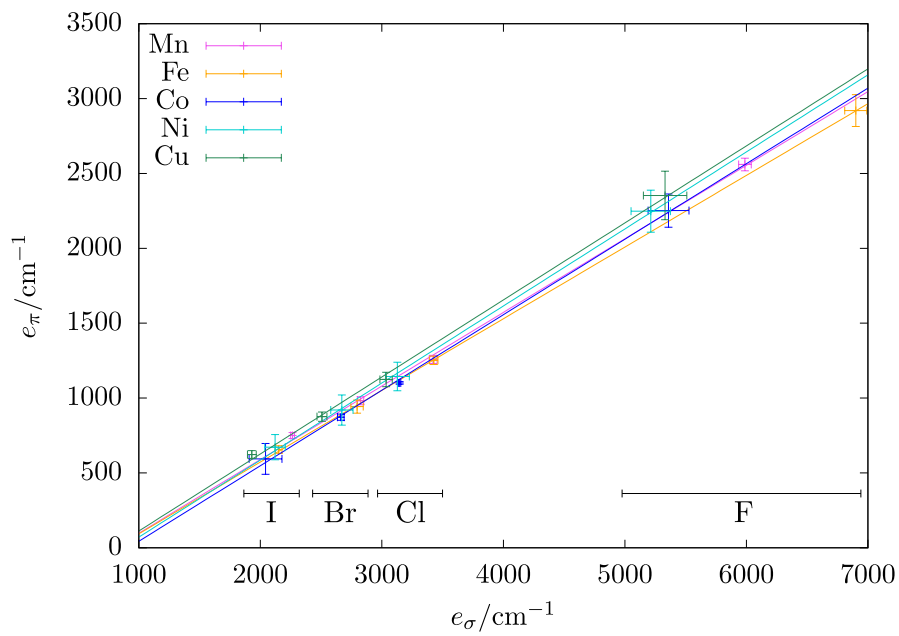


Figure 7: 2D-spectrochemical series for different metal halides, each metal with a different color. Error bars indicate the standard deviation. Regression line functions are:

$$\text{Mn: } e_{\pi} = 0.4915e_{\sigma} - 394\text{cm}^{-1}$$

$$\text{Fe: } e_{\pi} = 0.4786e_{\sigma} - 385\text{cm}^{-1}$$

$$\text{Co: } e_{\pi} = 0.5043e_{\sigma} - 461\text{cm}^{-1}$$

$$\text{Ni: } e_{\pi} = 0.5145e_{\sigma} - 443\text{cm}^{-1}$$

$$\text{Cu: } e_{\pi} = 0.5144e_{\sigma} - 403\text{cm}^{-1}$$

Discussion of technical details

Differences between CASSCF and NEVPT2

As the underlying wavefunction method, CASSCF or CASSCF/NEVPT2 can be chosen. Our results show that this choice does not alter the e_λ parameters significantly. It was observed already that CASSCF results are fitted more easily than NEVPT2 results.[26] We can confirm that observation, since the standard deviation is strictly smaller when fitting CASSCF results with the AOM compared to the NEVPT2 fit. There appears to be a problem with the NEVPT2 correction: according to Jung *et al.*, the energies of the states are changed in the order of energy, not in the order of states.[27] If the energetic ordering of the states were changed by the NEVPT2 correction, the aiLFT matrix elements would not be replaced accordingly. We found this to be a problem in some mixed halide calculations, leading to odd AOM parameter sets. For this reason, all shown results are fits of the CASSCF matrix without the NEVPT2 correction.

Choice of basis set

With CASSCF or CASSCF/NEVPT2 as the underlying wavefunction method, a basis set dependence is expected for the absolute energies. Table 8 shows the fitting results for $[\text{CoCl}_4]^{2-}$ with the Karlsruhe def2-SVP, def2-TZVP and def2-QZVP basis sets. E decreases with increasing basis set size, the other AOM parameters do not show a trend.

Influence of implicit solvation models

To assess the influence of environmental corrections on the AOM parameters, three different fits based on CASSCF calculations in vacuum and with the CPCM and SMD solvation models for water were made, see Figure 8. E is strongly affected, which is in good agreement with the concept of E being a spherical contribution assuming that the solvation shell is highly symmetric in the given geometry. In contrast, the AOM parameters show a very limited dependence on the solvation model.

The fact that the non-spherical contribution of the ligands is nearly independent of this (neglecting some outliers with the cpcm model) is also fitting. All calculations in the main text are performed without any solvation model,

Table 8: AOM parameters and E of $[\text{CoCl}_4]^{2-}$ for different basis sets.

basis set	E/cm^{-1}	E_{rel}/cm^{-1}	e_σ/cm^{-1}	e_π/cm^{-1}
def2-SVP	-1221831	4049	3235(15)	1183(14)
def2-TZVP	-1224735	1145	3146(10)	1101(9)
def2-QZVP	-1225880	0	3164(17)	1106(13)

but we note explicitly that a solvent model can be included without any loss in accuracy or notable increase in computational cost.

Origin of deviations in the fitted AOM parameters

At each bond length, five structures are generated by changing their bond angle, fulfilling the requirements stated in the main text. A separate set of parameters is assigned to each bond, so four AOM parameter sets are obtained per tetrahedral complex. For a homoleptic complex, 20 parameter sets are obtained. With the heteroleptic complexes, this number decreases, since the parameter sets then belong to different M-L bonds.

As already pointed out, an ideal tetrahedral system is underdetermined in terms of an AOM parameterization. The procedure employed here can solve this problem to some extent, but especially for the heteroleptic complexes, large deviations are found. Within a single calculation, parameters associated with the same ligand are always very close to each other, but in a set (same bond lengths, slightly different bond angles), the differences between the obtained parameters can be large. Most often, there is one strong outlier, while the other four calculations yield similar parameter sets. These outliers can be easily identified by looking at the data. In the plots in the main text, some of these outliers were removed. In the plots in the SI, all obtained data points are shown.

It is not entirely clear what the cause of the observed scattering of AOM parameters is, but some observations were made that indicate the origin of this problem to be rooted in the electronic structure of these complexes rather than the fitting procedure itself. The structures are extremely similar, no distinctive features can be found for structures with stark outliers. The d orbital energies (which are the eigenvalues of \mathbf{V}_{LF}) are unremarkable. The equation systems resulting from the structures do not show unexpected values, the least squares fit converges without errors and reliably finds the only minimum. Numerical precision does not seem to be an issue, since \mathbf{V}_{LF} rounded to fewer digits yields roughly the same AOM parameters.

We noted that the scattering becomes stronger at shorter bond lengths, where the molecule is in a chemically unrealistic situation. At short bond lengths, there is most often not only one strong outlier, but all the sets significantly differ from each other. We observed that the d orbitals at shorter bond lengths are not pure anymore, so it could be possible that aiLFT and the AOM cannot properly describe these molecules anymore. While the data sets presented in this contribution are obtained with equal bond length variations about the equilibrium distance, it is obviously equally possible to perform a bond length scan that contains more data points at longer bond lengths; this procedure would be expected to produce fewer outliers.

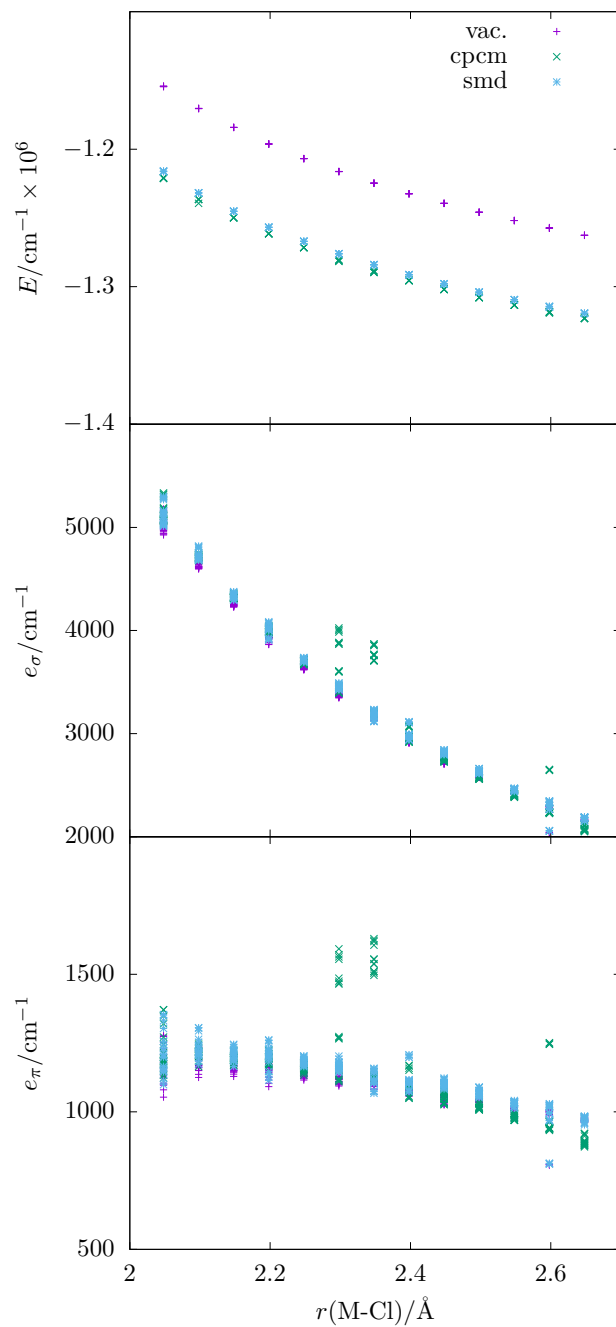


Figure 8: AOM parameters for $[\text{CoCl}_4]^{2-}$ with and without implicit solvation.

AOM parameters of mixed complexes

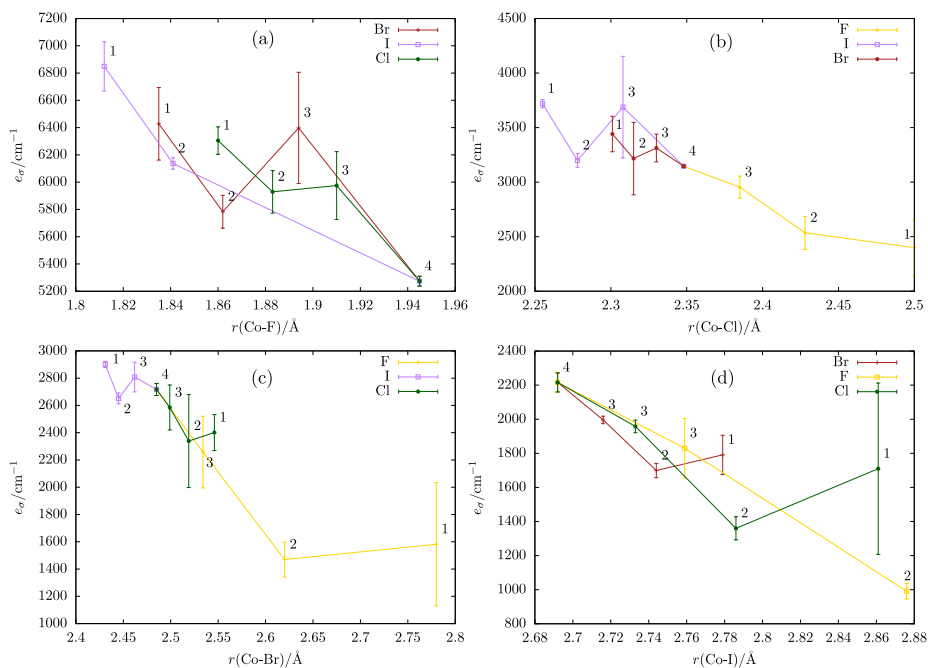


Figure 9: e_{σ} parameters with of Co-X for different, fully relaxed $[\text{CoX}_n\text{Y}_{4-n}]^{2-}$ complexes. The data shown are averaged over five data points each, and the error bars indicate the resulting standard deviation. The number at each data point indicates the X atom count, and the legend shows which other halide is present in the complex.

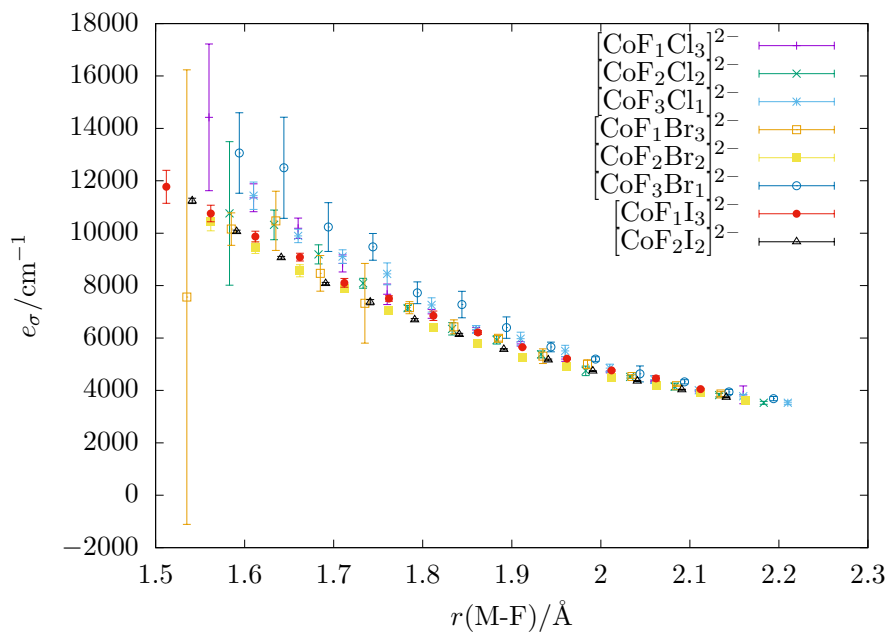


Figure 10: e_σ of the M-F bond length in various heteroleptic complexes.

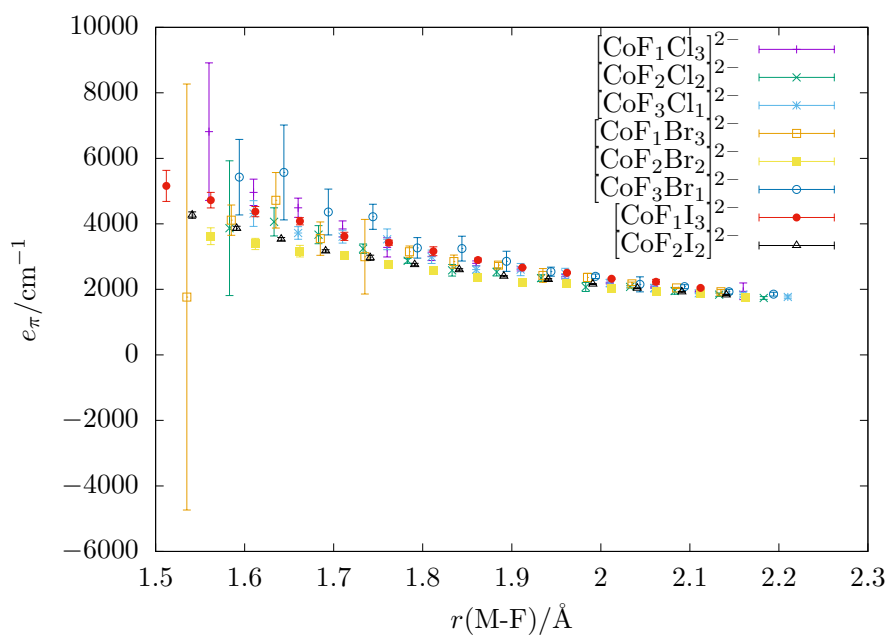


Figure 11: e_π of the M-F bond length in various heteroleptic complexes.

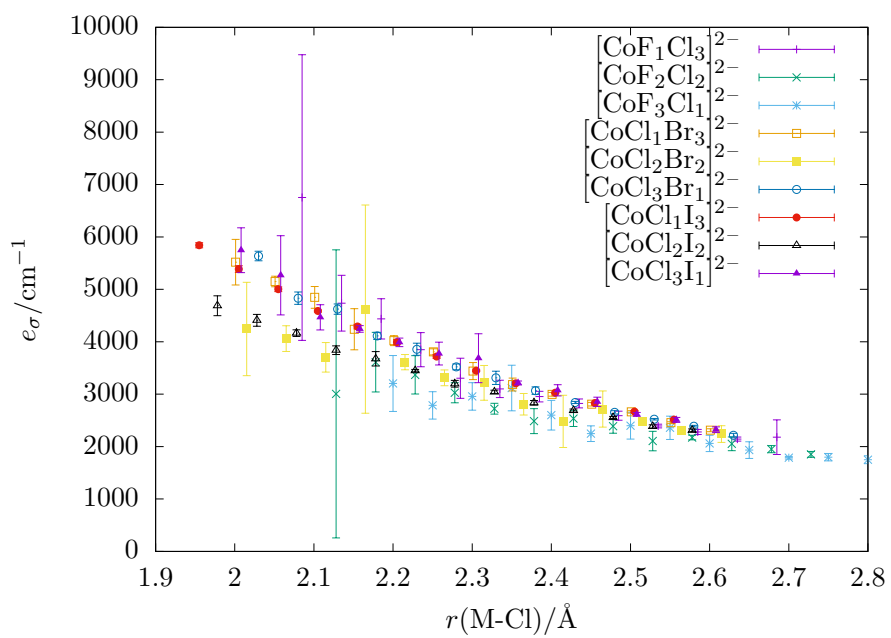


Figure 12: e_σ of the M-Cl bond length in various heteroleptic complexes.

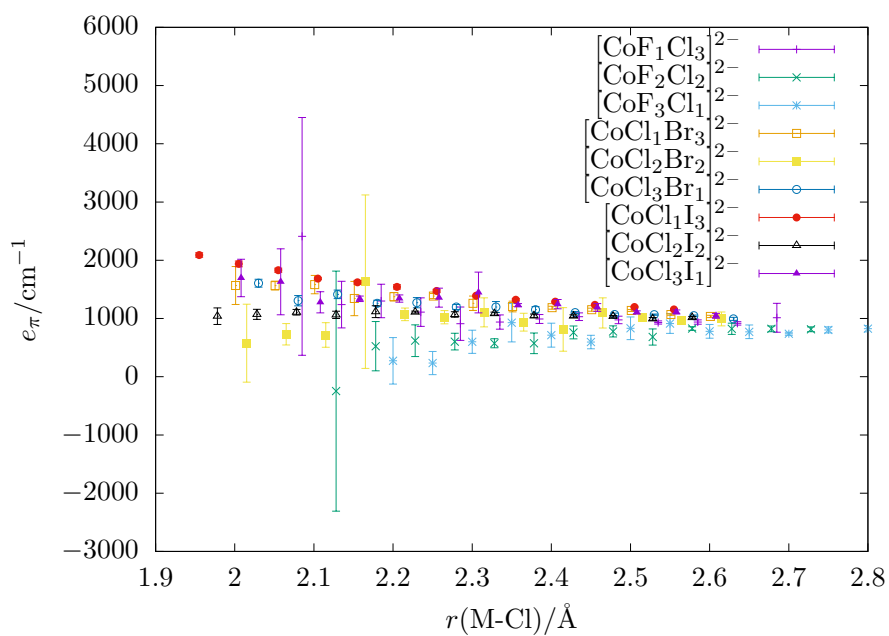


Figure 13: e_π of the M-Cl bond length in various heteroleptic complexes.

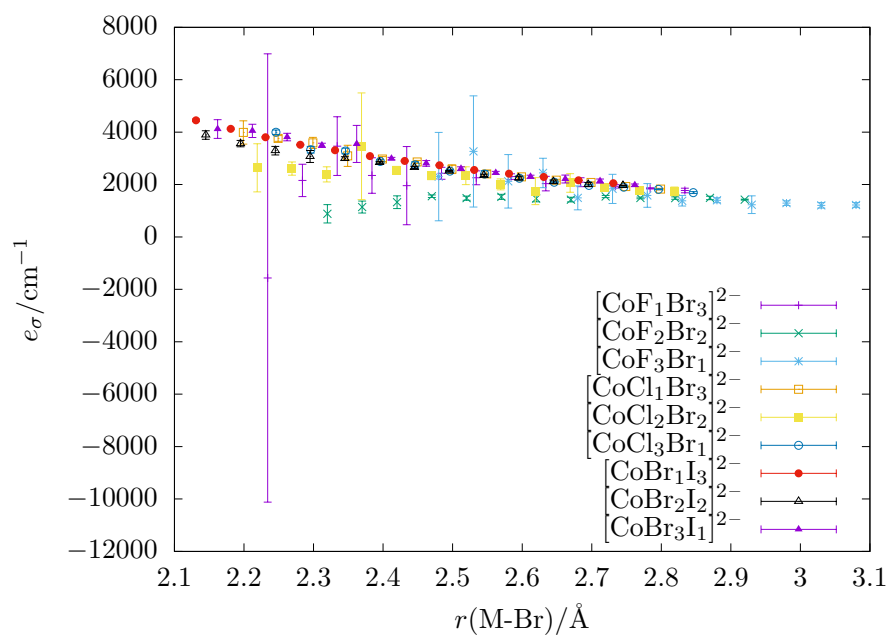


Figure 14: e_σ of the M-Br bond length in various heteroleptic complexes.

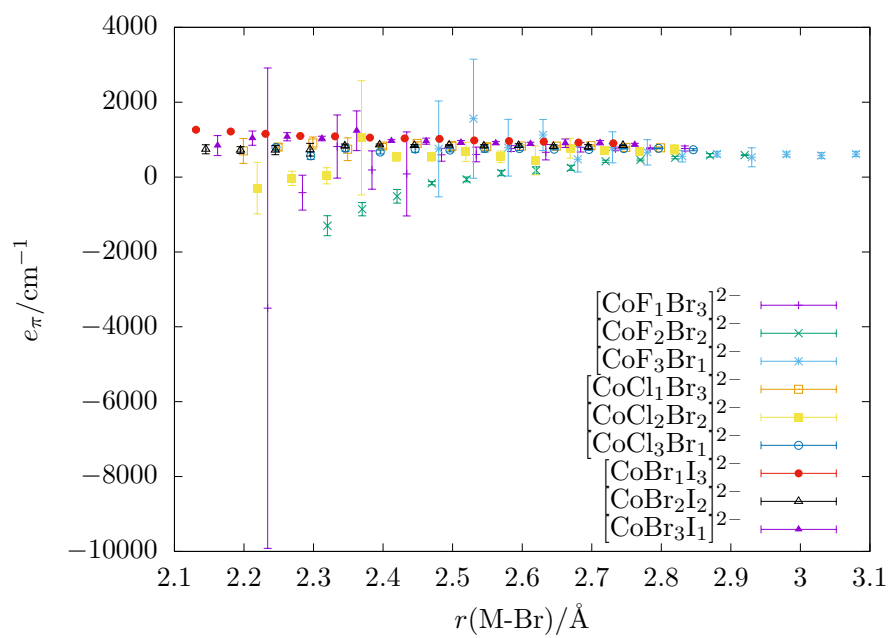


Figure 15: e_π of the M-Br bond length in various heteroleptic complexes.

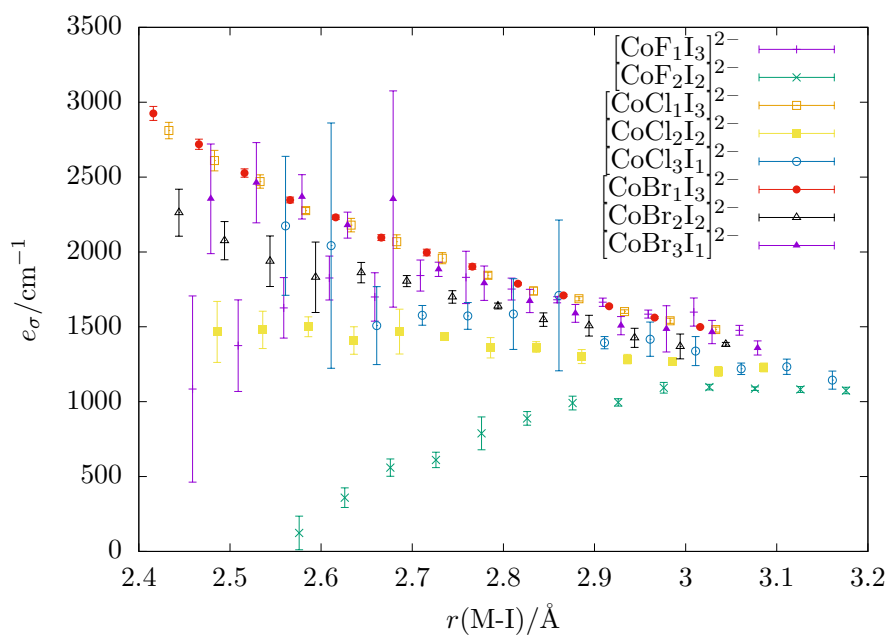


Figure 16: e_σ of the M-I bond length in various heteroleptic complexes.

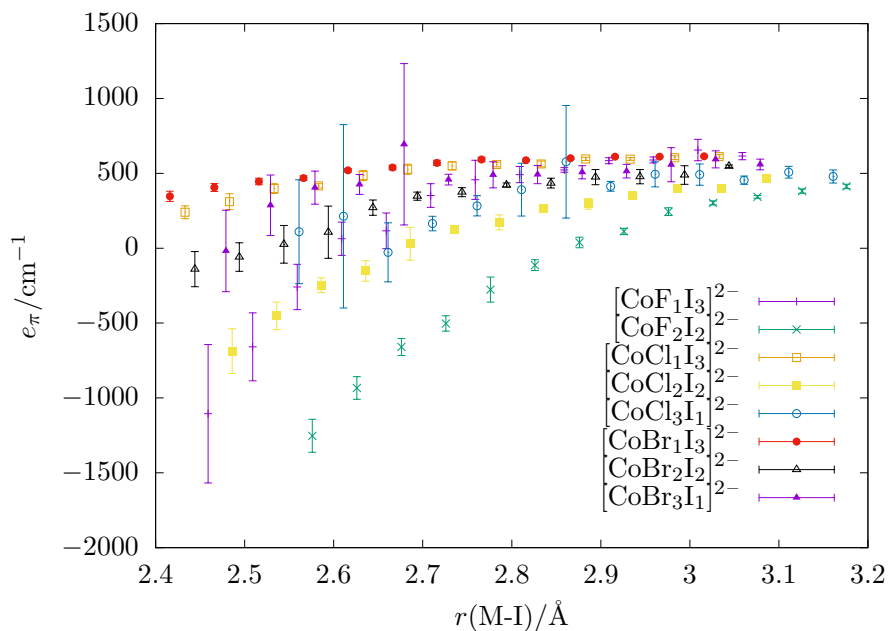


Figure 17: e_{π} of the M-I bond length in various heteroleptic complexes.

References

- [1] B. N. Figgis, M. A. Hitchman, *Ligand Field Theory and Its Applications*, 1st ed., Wiley-VCH, New York, **2000**.
- [2] Y. Tanabe, S. Sugano, *J. Phys. Soc. Japan* **1954**, *9*, 766–779.
- [3] S. Buffagni, T. M. Dunn, *Nature* **1960**, *188*, 937–938.
- [4] K. Kojima, J. Matsuda, *Bull. Chem. Soc. Jpn.* **1986**, *59*, 859–863.
- [5] W. D. Horrocks, D. A. Burlone, *J. Am. Chem. Soc.* **1976**, *98*, 6512–6516.
- [6] L. H. Gade, *Koordinationschemie*, Wiley-VCH, **1998**.
- [7] M. Molinier, W. Massa, *Z. Naturforsch. B* **1992**, *47*, 783–788.
- [8] K. Knox, *J. Chem. Phys.* **1959**, *30*, 991–993.
- [9] D. Babel, M. Otto, *Z. Naturforsch. B* **1989**, *44*, 715–720.
- [10] J. W. Lauher, J. A. Ibers, *Inorg. Chem.* **1975**, *14*, 348–352.
- [11] W. Rüdorff, J. Kändler, D. Babel, *Z. Anorg. Allg. Chem.* **1962**, *317*, 261–287.
- [12] M. K. Chaudhuri, S. K. Ghosh, Z. Hiese, *J. Chem. Soc. Dalton Trans.* **1984**, 1763.
- [13] N. S. Gill, R. S. Nyholm, *J. Chem. Soc.* **1959**, 3997.

-
-
- [14] F.-D. Tsay, L. Helmholz, *J. Chem. Phys.* **1969**, *50*, 2642–2650.
- [15] V. Morad, I. Cherniukh, L. Pötttschacher, Y. Shynkarenko, S. Yakunin, M. V. Kovalenko, *Chem. Mater.* **2019**, *31*, 10161–10169.
- [16] B. R. Sundheim, E. Levy, B. Howard, *J. Chem. Phys.* **1972**, *57*, 4492–4496.
- [17] M. B. Meredith, C. H. McMillen, J. T. Goodman, T. P. Hanusa, *Polyhedron* **2009**, *28*, 2355–2358.
- [18] L. Helmholz, R. F. Kruh, *J. Am. Chem. Soc.* **1952**, *74*, 1176–1181.
- [19] K. Hasebe, T. Asahi, K. Gesi, *Acta Cryst. C* **1990**, *46*, 759–762.
- [20] D. A. Fine, *Inorg. Chem.* **1965**, *4*, 345–350.
- [21] B. Morosin, E. C. Lingafelter, *Acta Cryst.* **1960**, *13*, 807–809.
- [22] P. S. Braterman, *Inorg. Chem.* **1963**, *2*, 448–452.
- [23] D. W. Smith, *Inorg. Chim. Acta* **1977**, *22*, 107–110.
- [24] R. J. Deeth, M. Gerloch, *Inorg. Chem.* **1984**, *23*, 3846–3853.
- [25] R. J. Deeth, D. L. Foulis, *Phys. Chem. Chem. Phys.* **2002**, *4*, 4292–4297.
- [26] S. K. Singh, J. Eng, M. Atanasov, F. Neese, *Coord. Chem. Rev.* **2017**, *344*, 2–25.
- [27] J. Jung, M. Atanasov, F. Neese, *Inorg. Chem.* **2017**, *56*, 8802–8816.

5.2 The π -interactions of ammonia ligands evaluated by *ab initio* ligand field theory

M. Buchhorn, V. Krewald, *Dalton Transactions* **2023**, 52, 6685–6692, 10.1039/D3DT00511A

The incentive to investigate the π interactions of ammine ligands was given by the fitting routine we developed for the first publication. While looking for good model systems, all encountered ammine complexes showed pronounced π parameters. At first, we thought this observation might be an artefact of the employed procedure, since it is common in the literature to assume ammine e_π to be close to zero. The parameters found made us worry that other parameters like the ones for halides might be unreliable, too. Due to the plausible results obtained for halides and a few other (unpublished) complexes, we started to question the assumption of zero- π amines. Hypothetical complexes with amines showed such significant π parameters that we decided to search for experimental evidence for our findings.

In square-planar complexes, any π interaction is evident by the splitting of the d_{xy} and d_{xz}/d_{yz} orbital energies. Cu^{2+} complexes tend to form such square-planar complexes and come with the convenient feature that due to their d^9 electron configuration, the d orbital energies and the state energies are identical. An experimental difficulty that prevents a clear assignment of spectroscopic bands to specific electronic states is the low energy of the d_{z^2} orbital, which lies in the same region as the d_{xy} and d_{xz}/d_{yz} orbitals. No clear orbital assignment could be made in the original publications of the experimental data. We were able to assign the spectroscopic bands without ambiguity, backed by other computational studies that yield the same results. This assignment shows that there is indeed a significant π interaction for ammine ligands and that there is actual spectroscopic evidence. This interaction is not small: we found $e_\pi > 1000 \text{ cm}^{-1}$ from the investigated experimental data.

With the experimental evidence that the unexpectedly large π parameters are no artefact of the computational method, we investigated a series of hexammine complexes, without further comparison to experimental data. The found parameters are consistently large and usually around 1000 cm^{-1} . A similar series employing chelating amines was not as successful; the misdirected valency of the ligands due to the chelation introduces complications for the fit that are not easily accounted for.



Cite this: DOI: 10.1039/d3dt00511a

The π -interactions of ammonia ligands evaluated by *ab initio* ligand field theory†Moritz Buchhorn  and Vera Krewald *

Ammonia and amine ligands are commonly assumed to be σ -only ligands in coordination chemistry, *i.e.* they are not expected to interact significantly with a metal *via* a π path. Ligand field analyses employing the Angular Overlap Model resulted in good fits to experimental data without a π parameter for ammonia ligands, thereby supporting this assumption. In this work, we challenge this assumption and suggest that it is an oversimplification. We use complete active space calculations for electronic structure analyses of copper ammine complexes that are in good agreement with the transitions observed in experimental UV-vis spectra. These findings lead to a reinterpretation of the experimental spectra that necessitates a significant π interaction of the ammonia ligands. The strength of the ammonia π interaction is evaluated by parameterizing the ligand field splittings of a series of metal hexammine complexes ($(M(\text{NH}_3)_6)^{n+}$ with $M = \text{Cr, Mn, Fe, Co, Ni, Ru, Os}$ and $n = 2, 3$) and selected tetrammine complexes ($(M(\text{NH}_3)_4)^{n+}$ with $M = \text{Cr, Mn, Fe, Co, Ni}$ and $n = 2$ or 3) with the Angular Overlap Model. The resulting π parameters show that ammonia is a π donor of similar strength as chloride.

Received 17th February 2023,
Accepted 7th April 2023

DOI: 10.1039/d3dt00511a

rsc.li/dalton

Introduction

In coordination chemistry, it is frequently assumed that the interaction between a metal centre and an ammonia ligand is characterised exclusively by σ character and thus that any π character is negligible.^{1–12} This can be rationalized in an orbital picture: ammonia does not have any molecular orbitals of π character; only the σ/σ^* molecular orbitals of the N–H bonds are partly oriented such that the metal–ammonia binding axis can lie in the nodal plane of a metal d orbital. Ammonia is therefore commonly classified as a σ -only ligand.

Metal–ligand interactions can be evaluated with ligand field theory. Besides global ligand field descriptors like the ligand field splitting Δ or Racah parameters, the Angular Overlap Model (AOM) provides a ligand-specific parameterisation that conforms to the familiar interpretation of chemistry in terms of functional groups. The AOM quantifies the metal–ligand interaction *via* σ and π overlaps, with an additional parameter for d–s mixing.^{2,13,14} The destabilisation of each pure metal d orbital with respect to the situation in the free ion is associated with a spherical component E and a directional component that is expressed with a specific number and magnitude of e_σ and e_π parameters depending on the coordination environment, see Fig. 1. The orbital splitting of

tetrahedral and octahedral coordination spheres does not allow for a distinction between e_σ and e_π .¹⁵ This means that neglecting e_π comes with the convenience of having an unambiguous relationship between e_σ and Δ . Lower symmetry coordination environments result in fewer orbital degeneracies which should provide a sufficient number of states to fit e_σ and e_π parameters simultaneously.

We recently developed an AOM parameter fitting procedure¹⁶ based on *ab initio* ligand field theory^{17–19} as a tool that provides insights into metal–ligand bonding situations. Notably, it is able to obtain AOM parameters for complexes for which previously the ligand field equation system would have been underdetermined. We showed that the method yields qualitatively correct parameters and reproduces expected chemical trends like the e_λ values of halide ligands being associated with their donor capacity and position in the spectrochemical series.¹⁶

In this paper, we present some incentives to rethink the assumption of amines being σ -only ligands. Firstly, we revisit the experimental UV-vis spectra of a square planar copper tetrammine and a pyramidal copper pentammine complex. They had been interpreted to not contain d–d transitions that would be expected if π interactions were present.⁵ Their analysis with *ab initio* ligand field theory calculations demonstrates the need for an ammine π interaction. Building on this, we present and discuss AOM parameters for a series of octahedral and tetrahedral ammine complexes obtained with our recently presented AOM parameter fitting procedure.¹⁶ We find that ammonia should be viewed as capable of significant π inter-

TU Darmstadt, Department of Chemistry, Theoretical Chemistry, Alarich-Weiss-Straße 4, 64287 Darmstadt, Germany. E-mail: vera.krewald@tu-darmstadt.de

† Electronic supplementary information (ESI) available. See DOI: <https://doi.org/10.1039/d3dt00511a>



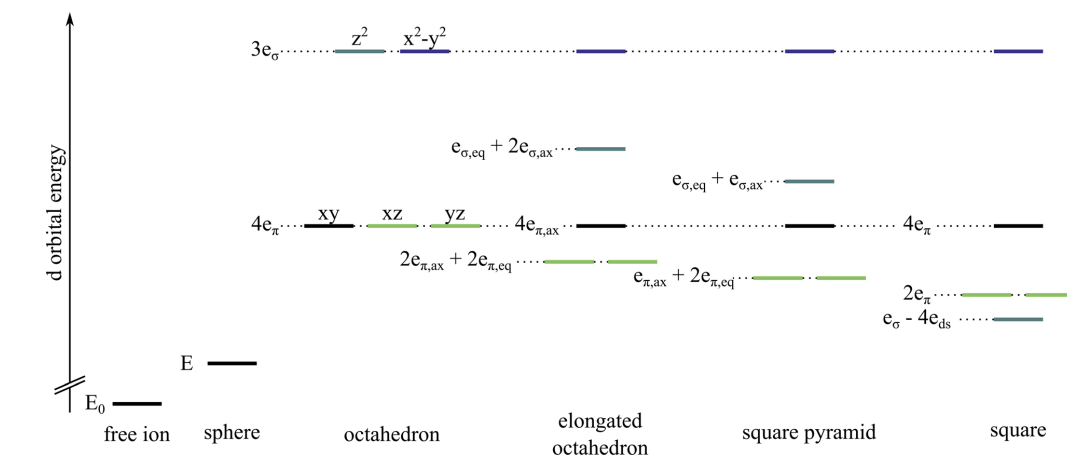


Fig. 1 Comparison of d orbital energy splittings for a free ion, a spherical potential and different coordination environments with the respective AOM parameters e_i . The orbital levels are coloured as follows, d_{z^2} teal, $d_{x^2-y^2}$ dark blue, d_{xy} black, d_{xz} and d_{yz} light green. For an elongated octahedron and a square pyramid, the ligands on the z-axis have parameters labelled ax, while the others in the xy-plane are labelled eq. For symmetries with at least one d orbital in the totally symmetric representation, d-s mixing must be considered which affects the orbital energy by an additional parameter e_{ds} . More details regarding d-s mixing are provided in the ESI.†

actions (ranging from about 400 cm^{-1} to more than 1000 cm^{-1}), which raises the question of whether a true σ -only ligand can exist.

Methodology and computational details

The ORCA 4.2.1 quantum chemistry package^{20,21} was used for all quantum chemical calculations. Geometries were optimized using the unrestricted Kohn-Sham formalism with the BP86 functional,^{22,23} the def2-SVP basis set,²⁴ and the def2/J auxiliary basis.²⁵ The resolution of identity approximation for the Coulomb term was used.^{26,27} Convergence criteria were NormalSCF for all self-consistent field calculations and TightOpt for geometry optimizations. The geometry optimizations employed the default integration grid (Accuracy 2: Lebedev 110 points) for optimization steps and the final SCF at the optimized geometry (Accuracy 4: Lebedev 302 points). Geometry optimizations of halide complexes of the type $[\text{MX}_6]^{3-/4-}$ with large negative charges additionally employed the CPCM/SMD solvation model with the parameters of water and an increased solvent radius of 3.0 \AA to aid convergence.^{28,29}

For square planar $[\text{Cu}(\text{NH}_3)_4]^{2+}$ and square pyramidal $[\text{Cu}(\text{NH}_3)_5]^{2+}$, the heavy atom positions were taken from the crystal structures (ICSD entries 14372 and 201229) and only the hydrogen atom positions were optimised with the settings stated above, but without employing a solvent model. The electronic states corresponding to the d orbitals were calculated using CASSCF^{30,31} in the *ab initio* ligand field theory

variant¹⁷⁻¹⁹ with the def2-TZVP basis set. The calculations on $[\text{Cu}(\text{NH}_3)_4]^{2+}$ and $[\text{Cu}(\text{NH}_3)_5]^{2+}$ also employed a subsequent perturbation theory treatment (NEVPT2).³²⁻³⁵ The active space was chosen to contain the five valence d orbitals and n d electrons, or in shorthand notation a $\text{CAS}(n,5)$ space. The *ab initio* ligand field theory module¹⁷ was employed to construct the effective ligand field Hamiltonian from the calculated states. For selected examples, spin-orbit coupling was considered using the spin-orbit mean field approach as implemented in ORCA.³⁶

The AOM was used to fit the one-electron part of the ligand field Hamiltonian^{13,37} according to our fitting procedure.¹⁶ The ligand field matrix contains up to 15 unique equations, which quickly results in underdetermined problems. For instance for six-coordinate complexes, one needs to fit 13 parameters of the ligand field potential: E , six e_σ and six e_π . Such a fit is in theory possible but in practice, linear dependencies can occur in the equation system so that the actual number of equations can be lower than 13, resulting in an underdetermined problem.

We address this restriction by grouping chemically equivalent ligands at similar bond lengths (*e.g.* in Jahn-Teller distorted $[\text{Mn}(\text{NH}_3)_6]^{3+}$, ligands are grouped into axial and equatorial parameter sets). In practice, grouping is achieved by adding additional equations to the system that require $0 = e_{\sigma,L} - e_{\sigma,L'}$. From a formal perspective, one could use these equations to require parameters to be strictly equal and thereby reduce their number. For solving the least squares problem of the overdetermined system, the addition of more equations has different consequences than the reduction of the number of parameters. Additional equations allow the



parameters $e_{\sigma,L}$ and $e_{\sigma,L'}$ to deviate, even if they are expected to be equal. This flexibility is important, since the asymmetric distortions generated during the fitting procedure render the ligands not perfectly equivalent so that small deviations are expected. If not stated otherwise, all ligands in the complexes studied are put into a single group. Complexes with significant differences in bond lengths due to Jahn–Teller distortions have two or more ligand groups as indicated by labels.

Results

Pyramidal copper pentammine

An explicit assessment of π interactions is only possible for symmetries lower than O_h or T_d , see Fig. 1. The $[\text{Cu}^{\text{II}}(\text{NH}_3)_5]^{2+}$ subunit in $\text{K}[\text{Cu}(\text{NH}_3)_5][\text{PF}_6]_3$ ³⁸ and $\text{NH}_4[\text{Cu}(\text{NH}_3)_5][\text{PF}_6]_3$ ³⁹ is approximately square pyramidal (point group: C_{2v}) and thus represents a suitable test case. Another convenient feature is its d^9 electronic configuration that results in four d–d transitions. The interelectronic repulsion within each electronic state is equal, and therefore the energy differences of these states can be equated with the energy differences of the d orbitals.

The electronic spectrum of $[\text{Cu}(\text{NH}_3)_5]^{2+}$ (see Fig. 2a) shows a band at $15\,300\text{ cm}^{-1}$ with a weak shoulder at $14\,000\text{ cm}^{-1}$

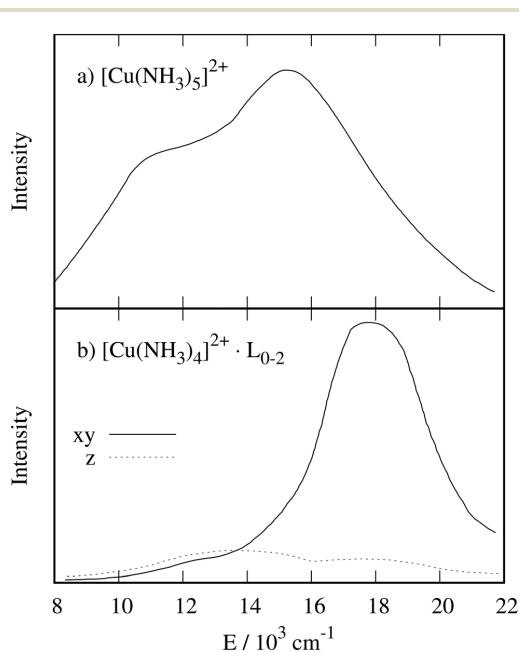


Fig. 2 Electronic spectrum of (a) $\text{NH}_4[\text{Cu}(\text{NH}_3)_5][\text{PF}_6]_3$, reprint from ref. 38 with permission from the Royal Society of Chemistry. Polarized electronic spectrum of (b) $\text{Na}_4[\text{Cu}^{\text{II}}(\text{NH}_3)_4\text{L}][\text{Cu}^{\text{I}}(\text{S}_2\text{O}_3)_2]_2$, reprint from ref. 41 with permission from the Royal Society of Chemistry. Please note the structural uncertainty of (b) discussed in the main text.

Table 1 Energies of the experimental and calculated d–d transitions for $[\text{Cu}(\text{NH}_3)_5]^{2+}$

	$d_{xz}, d_{yz} \rightarrow d_{x^2-y^2}/\text{cm}^{-1}$	$d_{xy} \rightarrow d_{x^2-y^2}/\text{cm}^{-1}$	$d_{z^2} \rightarrow d_{x^2-y^2}/\text{cm}^{-1}$
CASSCF	11 549–11 673	10 523	8 635
NEVPT2	16 145–16 308	15 341	11 687
Exp.	15 300	ca. 14 000	11 000

and a second band at $11\,000\text{ cm}^{-1}$, see Table 1. The shoulder is assigned to a $d_{xy} \rightarrow d_{x^2-y^2}$ transition by Duggan *et al.*,³⁸ implying a state splitting of 1300 cm^{-1} . Within the AOM, this splitting results in an e_{π} value of 1300 cm^{-1} in a perfect square pyramid or even a slightly larger value in a C_{2v} distorted square pyramid (see ESI† for details). Since the shoulder is not a very pronounced feature, the signal was interpreted later as “essentially unsplit”, ruling out a π interaction.⁵ With this interpretation, ammonia is viewed as a σ -only ligand. This assumption was also made for other complexes.^{6–12,40}

CASSCF/NEVPT2 calculations on the $[\text{Cu}(\text{NH}_3)_5]^{2+}$ subunit from the crystal structure yield an orbital ordering and d–d transitions in very good agreement with the measured ones, see Table 1. We note that while spin–orbit coupling (SOC) may be of importance for copper complexes (single-electron SOC parameter of ca. 830 cm^{-1} for free Cu^{2+}),¹⁵ inclusion of SOC does not qualitatively alter the picture, see ESI†. The calculations thus fully support the spectral assignments of Duggan *et al.*, and hence the need for an ammonia π interaction of about 1300 cm^{-1} .

Square planar copper tetrammine

As a second example, we selected the $[\text{Cu}^{\text{II}}(\text{NH}_3)_4]^{2+}$ subunit in the crystal structure of $\text{Na}_4[\text{Cu}^{\text{II}}(\text{NH}_3)_4][\text{Cu}^{\text{I}}(\text{S}_2\text{O}_3)_2]_2$.⁴² While initially, the crystal structure was thought to contain copper ions in a square-planar environment,⁴² later studies suggested that one or two axial ammonia ligands may weakly coordinate.⁴³ Although the precise structure is therefore not clear, there are two independently reported UV-vis spectra.^{41,44} Tomlinson *et al.* assigned the d–d transitions for the presumed square-planar complex using polarised electronic spectra, see Fig. 2b, leading to a one-electron orbital sequence of $d_{x^2-y^2} > d_{z^2} > d_{xy} \geq d_{xz}, d_{yz}$.⁴¹

To evaluate the electronic structure with CASSCF/NEVPT2 calculations as for the square-pyramidal system, hydrogen atoms were added to complete the ammonia ligands of the $[\text{Cu}(\text{NH}_3)_4]^{2+}$ subunit and their positions were optimized (see computational details). The influence of one or two axial ammonia ligands was evaluated explicitly, see below. Using CASSCF calculations that facilitate a direct assignment of configurations to states, we arrive at a different energetic ordering for the square planar complex, namely $d_{x^2-y^2} > d_{xy} > d_{xz}, d_{yz} \approx d_{z^2}$ in agreement with other computational studies.^{45–47} Giner *et al.* found this orbital ordering, notably including the pronounced energy difference between the d_{xy} and d_{xz}, d_{yz} levels, at different levels of theory that capture electron correlation



adequately, e.g. CCSD(T).⁴⁷ Atanasov *et al.* assigned an e_π of roughly 1200 cm^{-1} to NH_3 from an *ab initio* ligand field theory analysis.⁴⁸

There is some uncertainty surrounding the exact composition of the ligand field experienced by the copper ion in the crystal structure,^{42,43} where the gaps between the square planar $[\text{Cu}(\text{NH}_3)_4]^{2+}$ subunits are large enough to host ammonia molecules. These additional molecules would result in axial Cu–N distances of 2.88 \AA . We investigated these different possibilities with one or two ammonia ligands approaching the copper ion along the z -axis, see Fig. 3. In these scans, the position of the d_{xy} orbital is taken as the reference value for the d orbital energies. As expected, the energy difference $d_{xy} \rightarrow d_{x^2-y^2}$ remains constant to a good approximation, and the position of the d_{z^2} orbital is influenced significantly by the additional ligands on the z -axis. The energies of the d_{xz} and d_{yz} orbitals are lower in energy than the d_{xy} orbital. In the extreme case of a square planar $[\text{Cu}(\text{NH}_3)_4]^{2+}$ (Fig. 3, middle panel), the d_{z^2} orbital is found coincidentally at about the same energy as the d_{xz} and d_{yz} orbitals. Here, too, SOC does not qualitatively alter the picture, see ESI.† Tomlinson *et al.* probably investigated a mixture of structures, leading to the large line broadening of the lower intensity peak.⁴¹ It is not possible to determine a dominant composition with the present data.

With regard to a possible ammonia π interaction, the ligand field splitting of the square planar complex can be discussed as follows. If there was no π interaction at all, the $d_{xy}(b_{2g})$ and $d_{xz/yz}(e_g)$ orbital energies ε would be degenerate (see also ESI, Fig. 3†):

$$\varepsilon_{d_{xz}} = \varepsilon_{d_{yz}} = 2e_\pi = 0$$

$$\varepsilon_{d_{xy}} = 4e_\pi = 0$$

The d_{z^2} orbital energy depends on the extent of d–s mixing, and thus could be lower or roughly equal to the energy of the aforementioned orbitals. If there is a donating π interaction, the d_{xz} and d_{yz} orbitals are shifted up by $2e_\pi$ and the d_{xy} orbital is shifted up by $4e_\pi$. Indeed, the CASSCF calculation shows that the energy of the d_{xy} orbital is significantly higher than that of the d_{yz} and d_{xz} orbitals, while the energy of the d_{z^2} orbital is accidentally equal to the ones of the d_{yz} and d_{xz} orbitals. A similar orbital energy sequence ($d_{x^2-y^2} \gg d_{xy} > d_{z^2} > d_{xz}, d_{yz}$) was assigned to the D_{4h} $[\text{Cu}(\text{H}_2\text{O})_4]^{2+}$ subunits in meta-zeunerite ($\text{Cu}(\text{UO}_2)_2(\text{AsO}_4)_2 \cdot 8\text{H}_2\text{O}$) by Billing *et al.*⁴⁹ For this system, a significant π interaction from the equatorial water ligands was expected.⁴⁹ Ten years later, this sequence was still considered to be plausible only for strong π donors.⁵⁰

The energy difference between d_{xy} and d_{yz}, d_{xz} from the CASSCF calculation is independent of any specific AOM fitting routine and too large to be a computational artefact. Increasing the basis set size does not lead to a qualitatively different result, see ESI.† Additionally, the computational studies mentioned above^{45–48} find the same pronounced difference between the d_{xy} and d_{xz}, d_{yz} orbital energies using different levels of theory. In the AOM, the higher energy of the d_{xy} orbital can only be explained if $e_\pi > 0$. Therefore, we interpret this ligand field splitting as strong support for the existence of a π interaction for ammonia ligands.

Equilibrium AOM parameters

Having seen that a π interaction is relevant for ammonia ligands with experimental evidence and examples that do not rely on our previously introduced sampling procedure, we now

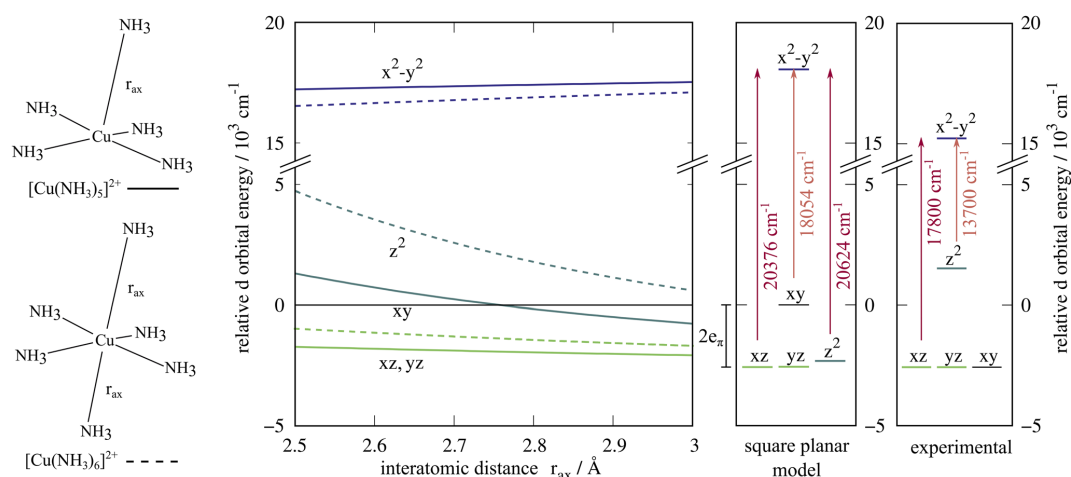


Fig. 3 Energy levels of the d orbitals in approximately square-pyramidal and octahedral ligand environments where the axial ligand positions r_{ax} are varied (left), the square planar case (middle), and the interpretation by Tomlinson, Hathaway *et al.* based on the observed UV-vis transitions (right).⁴¹ The gaps in the crystal structure⁴² might be filled with ammonia molecules, yielding a square pyramidal, elongated octahedral or square-planar case. The orbital energies are referenced to the d_{xy} orbital energy.



turn to a broader scope of complexes. Using our *ab initio* AOM sampling procedure, we evaluated a series of octahedral and tetrahedral complexes where all orbital energies affected by π interactions are degenerate so that the ammonia π interactions cannot be isolated. To this end, we chose complexes of the type $[M(\text{NH}_3)_6]^{n+}$, with $M = \text{Cr, Mn, Fe, Co, Ni, Ru, Os}$ and $n = 2, 3$. We note that some of the structures are Jahn–Teller distorted and therefore have different axial and equatorial AOM parameters. For strongly distorted structures, the ligands were grouped such that those at similar bond lengths are set to have equal parameters.

The average *ab initio* AOM parameters based on CASSCF calculations are listed in Table 2 for selected equilibrium structures. Note that the standard deviations result from the data points of five distinct calculations at similar structures. While the CASSCF calculation itself may carry a systematic error that could not be avoided even with a larger number of samples, the order of magnitude was shown to be reliable.^{16,18,51,52}

The *ab initio* AOM parameters identified with this procedure show a substantial π interaction for all complexes studied here. The data set is consistent with expectations and follows common trends, such as larger parameter values for higher oxidation states. Our findings for this more generalised data set thus contradict the widespread assumption of ammonia having only σ interactions.

Comparison to tetrahedral complexes

To rule out any conceivable sources of error for the chemically relevant magnitude of the ammonia π interactions we have identified above, we expanded the data set to tetrahedral complexes. This tests the possibility that artefacts arise due to the overlap of two adjacent σ potentials in an octahedral, square-planar or other setting with closely spaced ligands. This overlap would occur at a position which would be covered by a π parameter. In such cases, both σ and π would be artificially increased, while the spherical contribution E would be decreased correspondingly. Therefore, it should be tested whether ammonia π parameters also appear in complexes where the ligands are spaced further apart and thus overlapping σ potentials can be ruled out.

We chose complexes of the type $[M(\text{NH}_3)_4]^{2+/3+}$ with $M = \text{Cr, Mn, Fe, Co, Ni}$. These complexes are hypothetical; their only purpose is to provide more room for the ligands. The fits yield *ab initio* AOM parameters that are even larger than the ones obtained for the octahedral complexes, even though some scattering is observed. We note that d–s mixing needed to be included for some of the complexes where structural deviations from ideal tetrahedral symmetry were apparent (see ESI†). In conclusion, overlapping σ potentials can be ruled out as the origin for the observed ammonia π interaction in both the octahedral and tetrahedral complexes.

Scan and comparison to halido complexes

In order to verify that the order of magnitude obtained for the ammonia π parameters is reasonable, we replaced the ammonia ligands in $[\text{Cr}(\text{NH}_3)_6]^{3+}$ with chloride ligands in exactly the same positions. Since it is widely accepted that halides and metals interact *via* a considerable π path, this data set allows a meaningful comparison with the metal–ammine parameters.

Indeed, the chloride ligands show e_π values that are even smaller than those of the ammonia ligands (e_π chloride: 313 (524) cm^{-1} , e_π ammonia: 1027(255) cm^{-1}). However, the M–NH₃ bonds in these complexes are much shorter than M–Cl bonds would be in fully relaxed complexes. For instance, the Co–NH₃ bond length in $[\text{Co}(\text{NH}_3)_6]\text{Cl}_2$ is 2.11 Å,⁵³ whereas the Co–Cl bond length in CoCl_2 is 2.51 Å.⁵⁴ The metal–chloride distance when placing the chloride ions at the nitrogen atom positions of the relaxed $[\text{Cr}(\text{NH}_3)_6]^{3+}$ complexes is thus unnaturally short, which presumably leads to the broad scattering of the parameters and the unexpectedly small e_π parameters. We observed this behaviour already in our previous study on tetrahedral halido metalates, where e_π decreases at shorter bond lengths.¹⁶ Calculations on relaxed $[\text{MCl}_6]^{3-/4-}$ complexes yield bond lengths in the range of 2.43 Å to 2.53 Å and e_π parameters around 500 cm^{-1} with significantly less scatter (see ESI†). Scanning the metal–ligand distances in these examples from the equilibrium bond length of Cr–NH₃ to that of Cr–Cl, see Fig. 4, shows the similar order of magnitude for the e_π parameters in these two scenarios. The comparison thus confirms that the π interaction of ammonia is unlikely to be an

Table 2 Ligand field parameters e_σ and e_π for complexes $[M(\text{NH}_3)_6]^{2+/3+}$ with optimized bond lengths r in Å. The multiplicity $2S + 1$ refers to the multiplicity of the optimized ground state, ΔE (kJ mol^{-1}) is the relative energy to the spin ground state structure. The ligand field parameters are calculated as averages from five asymmetric structures each; the resulting standard deviations are given in parentheses

M	$2S + 1$	$\Delta E/\text{kJ mol}^{-1}$	$r/\text{Å}$	e_σ/cm^{-1}	e_π/cm^{-1}
M(II)					
Mn	6	0	2.34	3613(213)	894(159)
Fe	1	5	2.05	5491(324)	710(243)
Fe	3	43	2.03 ^{ax}	6011(352)	1051(263)
Fe	3	43	2.25 ^{eq}	3772(385)	826(265)
Fe	5	0	2.28	3598(229)	851(171)
Co	4	0	2.23	3471(62)	770(19)
Co	2	7	2.39 ^{ax}	1818(379)	591(284)
Co	2	7	2.02 ^{eq}	5857(379)	1024(285)
Ni	3	0	2.18	3024(355)	412(266)
Ru	1	0	2.16	9755(203)	799(152)
Os	1	0	2.18	11 271(156)	594(120)
M(III)					
Cr	4	0	2.14	6743(341)	1027(255)
Mn	5	0	2.36 ^{ax}	3285(360)	576(270)
Mn	5	0	2.12 ^{eq}	6707(359)	1046(270)
Fe	6	56	2.23	6532(915)	2052(683)
Fe	4	47	2.32 ^{ax}	3909(907)	972(679)
Fe	4	47	2.08 ^{eq}	7452(909)	1433(682)
Fe	2	0	2.06	7042(92)	1087(74)
Co	1	0	2.02	6788(408)	698(307)
Ni	4	0	2.15 ^a	7515(1628)	1971(1238)
Ni	4	0	2.18 ^b	7500(1420)	2349(1060)
Ni	4	0	2.22 ^c	6804(1058)	2665(792)
Ru	2	0	2.16	10 749(417)	649(311)
Os	2	0	2.18	11 686(170)	194(149)



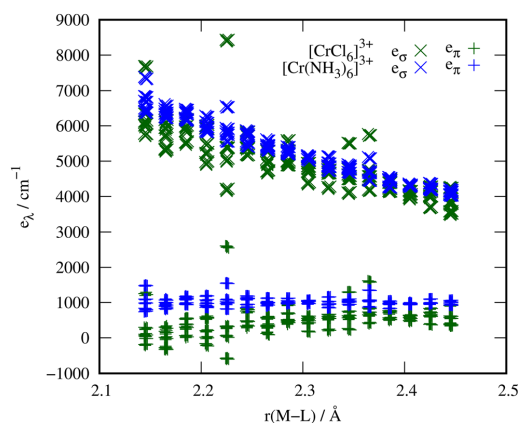


Fig. 4 Bond length scans of $[\text{Cr}(\text{NH}_3)_6]^{3+}$ and $[\text{CrCl}_6]^{3-}$ from the optimized metal–ligand bond length of the ammine complex to that of the chloride complex. The upper data points ($>3000\text{ cm}^{-1}$) are e_σ parameters and the lower set of data points are e_π parameters.

artefact, since the chloride interactions predicted at the same bond lengths match expectations and are qualitatively correct.

Monodentate amine ligands

To better understand the origin of the π interaction of ammonia, we studied the influence of the substituent R in $-\text{NR}_3$ on the π interaction, specifically comparing $-\text{NH}_3$ and $-\text{NMe}_3$. Complexes with different amine ligands can be compared in terms of their ligand field splitting or *via* AOM parameterization. A problem arising for such comparisons is that the bond lengths vary and hence the observed splitting is

influenced by the bond length and the ligand field strength of the amine itself. While these effects cannot be disentangled fully in experimental data, it appears that the bond length is the more dominant factor in a study by Lever *et al.*⁴

Due to the bulkiness of the methylamine ligand, it is not possible to obtain reasonable structures for $[\text{M}(\text{NMe}_3)_6]^{n+}$ complexes. Therefore, we chose to study heteroleptic complexes of the type $[\text{M}(\text{NH}_3)_4(\text{NMe}_3)_2]^{n+}$, with the methylamine ligands positioned *trans* to each other, see Table 3. For all complexes, the e_σ parameters of the ammonia ligands are larger than those of the amine ligands, whereas the magnitudes of the e_π parameters are comparable or larger.

To evaluate the influence of the M–N bond length on the AOM parameters, we set the M–N bond lengths with ammonia ligands to the value of the M–NMe₃ distances. As expected, the e_σ and e_π parameters of the ammonia ligands decrease so that the AOM parameters of $-\text{NMe}_3$ are consistently larger than those of $-\text{NH}_3$. In the hexammine reference complex with all ammonia ligands at the same distance as the amine ligands in the relaxed structure, the ammonia ligands have very similar AOM parameters as in the mixed complex with fixed ammonia bond lengths. We can therefore conclude that amine ligands have intrinsically higher e_π parameters than ammonia ligands. This comparison furthermore points towards hyperconjugation of the N–R bonds as a possible origin of the π interaction for both amines and ammonia.

From a molecular orbital perspective, the chemical origin and a possible explanation for the considerable π interaction of ammonia ligands may lie in the hyperconjugation of the N–H bonds with the respective d orbitals. Hyperconjugation was already observed and interpreted by Mulliken^{55–57} and became an important tool for rationalizing formation and stabilization energies⁵⁸ and chemical shifts in NMR experiments.⁵⁹

Table 3 AOM parameters (cm^{-1}) of complexes of the type $[\text{MA}_4\text{B}_2]^{n+}$ and $[\text{MA}_6]^{n+}$ with A = NH_3 and B = NMe_3 . The methylamine ligands are placed *trans* to each other. The bond lengths $r(\text{M}-\text{L})$ (Å) are shown for each ligand type. For each metal ion, three sets of parameters are given: one for the fully optimized structure at the multiplicity indicated with a superscript, one for a structure where the equatorial M–NH₃ bonds are set to the optimized M–NMe₃ bond length,^a and one for a reference hexammine complex where all M–NH₃ bonds are fixed at this value^b

Complex		A = NH_3			B = NMe_3			
		Bond lengths	$r(\text{M}-\text{L})/\text{Å}$	e_σ/cm^{-1}	e_π/cm^{-1}	$r(\text{M}-\text{L})/\text{Å}$	e_σ/cm^{-1}	e_π/cm^{-1}
$^4[\text{CrA}_4\text{B}_2]^{3+}$	Optimized		2.13	8115(842)	1944(632)	2.34	6291(847)	1917(634)
	Fixed		2.34	5228(222)	1378(167)	2.34	6425(223)	1746(167)
	Fixed		2.34	5143(93)	1193(71)			
$^6[\text{MnA}_4\text{B}_2]^{2+}$	Optimized		2.33	3946(247)	1023(185)	2.53	2793(247)	905(185)
	Fixed		2.53	2667(63)	866(47)	2.53	2992(63)	975(47)
	Fixed		2.53	2667(21)	849(17)			
$^5[\text{FeA}_4\text{B}_2]^{2+}$	Optimized		2.25	4740(185)	1548(137)	2.48	3360(185)	1410(138)
	Fixed		2.48	2981(104)	1152(77)	2.48	3320(106)	1268(79)
	Fixed		2.48	2864(64)	1044(47)			
$^1[\text{CoA}_4\text{B}_2]^{3+}$	Optimized		2.00	8353(623)	1518(469)	2.29	5018(636)	1290(471)
	Fixed		2.29	4439(38)	992(28)	2.29	6032(39)	1365(29)
	Fixed		2.29	4531(84)	853(63)			

^a The NH_3 ligands were moved with no subsequent geometry optimization. ^b The NMe_3 ligands were replaced with NH_3 with subsequent optimization of the positions of the new hydrogen atoms.



Experimental NMR studies of $\text{Ru}(\text{NH}_3)_x$ complexes show that there is an interaction between N–H bonds and the metal d orbitals, leading to measurable hyperfine interactions. This interaction is explained by hyperconjugation of the N–H bonding orbital with the ruthenium d orbital.^{60–62}

An alternative view is offered by the interpretation of ligand field splittings in terms of electrostatic potentials as developed by Gerloch and Woolley.^{63–65} This picture is completely independent of molecular orbital theory and treats the influence of the ligands on the d orbital energies purely electrostatically. With this approach, the π interaction could be explained by the electron density of the N–H bond and the negative partial charge on the nitrogen atom exerting an influence on the metal d orbital energies.

Both interpretations are supported by the results for the methylamine complexes. The larger N–C bonding orbital of $-\text{NMe}_3$ compared to the N–H bonding orbitals of $-\text{NH}_3$ suggest a stronger hyperconjugation with the metal d orbitals. Likewise, the methyl groups are electron donating, leaving a higher electron density at the nitrogen and thus supporting the picture of an electrostatic ligand field interaction.

Chelating amine ligands

When applying the aiLFT procedure on ethylenediamine (en) and diethylenetriamine (dien), it is apparent that it is not possible to obtain a good fit to the d orbital energies with just e_σ and e_π . We attribute this to an effect called “misdirected valency” by Deeth *et al.*^{48,66–69} Misdirected valency is caused by bent bonding and non-bonding lone pairs where the centroid of the bond is not aligned with the metal–ligand axis, as depicted in ref. 66. For the chelating en and dien ligands, the M–N bond is bent because of the orientation of the carbon backbone. We note that methylamine, although not chelating, also shows slight off-axis bonding since the bulky $-\text{CH}_3$ groups prevent full alignment. The parameters found for chelating amines (shown in the ESI†) should therefore be interpreted with some caution.

If the metal–ligand interaction is asymmetric with respect to the bonding axis, it cannot be fully described by the set of parameters employed. It is in principle possible to include off-diagonal $e_{\sigma\pi}$ parameters in the AOM parameterisation.⁴⁸ Naturally, this would aggravate the underdetermination problem and hinder a clear interpretation of the results.

Conclusions

To summarise, we presented indications that the widespread assumption of ammonia being a σ -only ligand might be incorrect. Our findings question the reliability of published AOM parameters for ammonia complexes from previous fitting procedures applied to experimental and computational data where e_π was neglected, noting of course that this was often done to reduce the number of AOM parameters. Without this assumption, many cases would not have been solvable. Our

work furthermore raises the question whether any ligand can be considered a σ -only ligand.

Conflicts of interest

There are no conflicts to declare.

Acknowledgements

The authors thank R. J. Deeth for many fruitful discussions and valuable input. The reviewers' comments were greatly appreciated. This work was funded by the Deutsche Forschungsgemeinschaft (DFG, German Research Foundation) – CRC 1487, “Iron, upgraded!” – project number 443703006.

References

- 1 D. W. Smith, *J. Chem. Soc. A*, 1969, 1708–1712.
- 2 C. E. Schäffer, *Pure Appl. Chem.*, 1970, **24**, 361–392.
- 3 M. Gerloch, J. H. Harding and R. G. Woolley, *Inorganic Chemistry*, Berlin, Heidelberg, 1981, pp. 1–46.
- 4 A. B. P. Lever, I. M. Walker, P. J. McCarthy, K. B. Mertes, A. Jircitano and R. Sheldon, *Inorg. Chem.*, 1983, **22**, 2252–2258.
- 5 R. J. Deeth and M. Gerloch, *Inorg. Chem.*, 1984, **23**, 3846–3853.
- 6 M. Sano, T. Maruo, Y. Masuda and H. Yamatera, *Inorg. Chem.*, 1984, **23**, 4466–4469.
- 7 A. Bencini, C. Benelli and D. Gatteschi, *Coord. Chem. Rev.*, 1984, **60**, 131–169.
- 8 P. V. Bernhardt and P. Comba, *Inorg. Chem.*, 1993, **32**, 2798–2803.
- 9 T. Schönherr, M. Itoh and A. Urushiyama, *Bull. Chem. Soc. Jpn.*, 1995, **68**, 2271–2276.
- 10 M. Atanasov, P. Comba, S. Helmle, D. Müller and F. Neese, *Inorg. Chem.*, 2012, **51**, 12324–12335.
- 11 D. Schweinfurth, M. G. Sommer, M. Atanasov, S. Demeshko, S. Hohloch, F. Meyer, F. Neese and B. Sarkar, *J. Am. Chem. Soc.*, 2015, **137**, 1993–2005.
- 12 P. Comba, G. Nunn, F. Scherz and P. H. Walton, *Faraday Discuss.*, 2022, **234**, 232–244.
- 13 C. E. Schäffer and C. K. Jørgensen, *Mol. Phys.*, 1965, **9**, 401–412.
- 14 M. Suta, F. Cimpoesu and W. Urland, *Coord. Chem. Rev.*, 2021, **441**, 213981.
- 15 B. N. Figgis and M. A. Hitchman, *Ligand Field Theory and Its Applications*, Wiley-VCH, New York, 1st edn, 2000.
- 16 M. Buchhorn, R. J. Deeth and V. Krewald, *Chem. – Eur. J.*, 2022, **28**, e202103775.
- 17 M. Atanasov, D. Ganyushin, K. Sivalingam and F. Neese, *Molecular Electronic Structures of Transition Metal Complexes II*, Springer Berlin/Heidelberg, Berlin, Heidelberg, 2011/2012, pp. 149–220.



- 18 J. Jung, M. Atanasov and F. Neese, *Inorg. Chem.*, 2017, **56**, 8802–8816.
- 19 S. K. Singh, J. Eng, M. Atanasov and F. Neese, *Coord. Chem. Rev.*, 2017, **344**, 2–25.
- 20 F. Neese, *Wiley Interdiscip. Rev.: Comput. Mol. Sci.*, 2012, **2**, 73–78.
- 21 F. Neese, *Wiley Interdiscip. Rev.: Comput. Mol. Sci.*, 2018, **8**, e1327.
- 22 A. D. Becke, *Phys. Rev. A*, 1988, **38**, 3098–3100.
- 23 J. P. Perdew, *Phys. Rev. B: Condens. Matter Mater. Phys.*, 1986, **33**, 8822–8824.
- 24 F. Weigend and R. Ahlrichs, *Phys. Chem. Chem. Phys.*, 2005, **7**, 3297.
- 25 F. Weigend, *Phys. Chem. Chem. Phys.*, 2006, **8**, 1057–1065.
- 26 E. J. Baerends, D. E. Ellis and P. Ros, *Chem. Phys.*, 1973, **2**, 41–51.
- 27 O. Vahtras, J. Almlöf and M. W. Feyereisen, *Chem. Phys. Lett.*, 1993, **213**, 514–518.
- 28 V. Barone and M. Cossi, *J. Phys. Chem. A*, 1998, **102**, 1995–2001.
- 29 A. V. Marenich, C. J. Cramer and D. G. Truhlar, *J. Phys. Chem. B*, 2009, **113**, 6378–6396.
- 30 P. Siegbahn, A. Heiberg, B. Roos and B. Levy, *Phys. Scr.*, 1980, **21**, 323–327.
- 31 B. O. Roos, P. R. Taylor and P. E. Siegbahn, *Chem. Phys.*, 1980, **48**, 157–173.
- 32 C. Angeli, R. Cimiraglia and J.-P. Malrieu, *Chem. Phys. Lett.*, 2001, **350**, 297–305.
- 33 C. Angeli, R. Cimiraglia, S. Evangelisti, T. Leininger and J.-P. Malrieu, *J. Chem. Phys.*, 2001, **114**, 10252–10264.
- 34 C. Angeli, R. Cimiraglia and J.-P. Malrieu, *J. Chem. Phys.*, 2002, **117**, 9138–9153.
- 35 C. Angeli and R. Cimiraglia, *Theor. Chem. Acc.*, 2002, **107**, 313–317.
- 36 F. Neese, *J. Chem. Phys.*, 2005, **122**, 34107.
- 37 R. G. Woolley, *Mol. Phys.*, 1981, **42**, 703–720.
- 38 M. Duggan, N. Ray, B. Hathaway, G. Tomlinson, P. Brint and K. Pelin, *J. Chem. Soc., Dalton Trans.*, 1980, 1342.
- 39 B. J. Hathaway and A. Tomlinson, *Coord. Chem. Rev.*, 1970, **5**, 1–43.
- 40 R. J. Deeth and C. M. Kemp, *J. Chem. Soc., Dalton Trans.*, 1992, 2013–2017.
- 41 A. A. G. Tomlinson, B. J. Hathaway, D. E. Billing and P. Nichols, *J. Chem. Soc. A*, 1969, 65.
- 42 A. Ferrari, A. Braibanti and A. Tiripicchio, *Acta Crystallogr.*, 1966, **21**, 605–610.
- 43 B. Morosin and A. C. Larson, *Acta Crystallogr., Sect. B: Struct. Crystallogr. Cryst. Chem.*, 1969, **25**, 1417–1419.
- 44 B. J. Hathaway and F. Stephens, *J. Chem. Soc. A*, 1970, 884.
- 45 F. Neese, *Magn. Reson. Chem.*, 2004, **42**, 187–198.
- 46 S. Vancoillie and K. Pierloot, *J. Phys. Chem. A*, 2008, **112**, 4011–4019.
- 47 E. Giner, D. P. Tew, Y. Garniron and A. Alavi, *J. Chem. Theory Comput.*, 2018, **14**, 6240–6252.
- 48 M. Atanasov, P. Comba, C. A. Daul and F. Neese, *Models, mysteries, and magic of molecules*, Springer, Dordrecht, The Netherlands, 2008, pp. 411–445.
- 49 D. E. Billing, B. J. Hathaway and P. Nicholls, *J. Chem. Soc. A*, 1969, 316.
- 50 Y. Nishida and S. Kida, *Coord. Chem. Rev.*, 1979, **27**, 275–298.
- 51 D. Aravena, M. Atanasov and F. Neese, *Inorg. Chem.*, 2016, **55**, 4457–4469.
- 52 L. Lang, M. Atanasov and F. Neese, *J. Phys. Chem. A*, 2020, **124**, 1025–1037.
- 53 M. T. Barnet, B. M. Craven, H. C. Freeman, N. E. Kime and J. A. Ibers, *Chem. Commun.*, 1966, 307–308.
- 54 H. Grime and J. A. Santos, *Z. Kristallogr. - Cryst. Mater.*, 1934, **88**, 136–141.
- 55 R. S. Mulliken, *Phys. Rev.*, 1933, **43**, 279–302.
- 56 R. S. Mulliken, *J. Chem. Phys.*, 1939, **7**, 339–352.
- 57 R. S. Mulliken, C. A. Rieke and W. G. Brown, *J. Am. Chem. Soc.*, 1941, **63**, 41–56.
- 58 J. I.-C. Wu and P. v. R. Schleyer, *Pure Appl. Chem.*, 2013, **85**, 921–940.
- 59 J. W. de M. Carneiro, J. F. Dias, J. G. R. Tostes, P. R. Seidl and C. A. Taft, *Int. J. Quantum Chem.*, 2003, **95**, 322–328.
- 60 M. L. Naklicki, C. A. White, V. V. Kondratiev and R. J. Crutchley, *Inorg. Chim. Acta*, 1996, **242**, 63–69.
- 61 B. R. McGarvey, N. C. Batista, C. W. B. Bezerra, M. S. Schultz and D. W. Franco, *Inorg. Chem.*, 1998, **37**, 2865–2872.
- 62 W. M. Laidlaw, R. G. Denning, J. C. Green, J. Boyd, J. Harmer and A. L. Thompson, *Inorg. Chem.*, 2013, **52**, 7280–7294.
- 63 R. J. Deeth and M. Gerloch, *J. Chem. Soc., Dalton Trans.*, 1986, 1531–1534.
- 64 R. G. Woolley, *Int. Rev. Phys. Chem.*, 1987, **6**, 93–141.
- 65 M. Gerloch, *Understanding Molecular Properties*, D. Reidel Publishing Company, Dordrecht, 1987, pp. 111–142.
- 66 R. J. Deeth, M. J. Duer and M. Gerloch, *Inorg. Chem.*, 1987, **26**, 2573–2578.
- 67 R. J. Deeth, M. J. Duer and M. Gerloch, *Inorg. Chem.*, 1987, **26**, 2578–2582.
- 68 R. J. Deeth and M. Gerloch, *Inorg. Chem.*, 1987, **26**, 2582–2585.
- 69 M. J. Duer, N. D. Fenton and M. Gerloch, *Int. Rev. Phys. Chem.*, 1990, **9**, 227–280.



Supporting Information:
The π -Interactions of Ammonia Ligands
Evaluated by *ab initio* Ligand Field Theory

Moritz Buchhorn¹ and Prof. Dr. Vera Krewald^{1*}

¹TU Darmstadt, Department of Chemistry, Theoretical Chemistry,
Alarich-Weiss-Straße 4, 64287 Darmstadt, Germany

*vera.krewald@tu-darmstadt.de

Contents

1	A few comments on d-s mixing	2
2	Influence of implicit solvation models	2
3	Square pyramidal copper pentammine	3
3.1	Influence of spin-orbit coupling	4
4	Square planar copper tetrammine	6
4.1	Influence of spin-orbit coupling	7
5	Table data and plots for octahedral hexammines	9
6	Comparison of chloride and ammine ligands	13
7	Table data for tetrammines	19
8	Table data for en and dien complexes	20

List of Figures

1	Spin-orbit coupled energy levels of $[\text{Cu}(\text{NH}_3)_5]^{2+}$	5
2	Spin-orbit coupled energy levels of $[\text{Cu}(\text{NH}_3)_4]^{2+}$	7
3	Orbital energy schemes for square planar complexes.	9
4	AOM parameters of M^{II} hexammine complexes vs. bond length.	11
5	AOM parameters of M^{III} hexammine complexes vs. bond length.	12
6	AOM parameters of M^{II} hexachloride complexes vs. bond length.	14

7	AOM parameters of M^{III} hexachloride complexes vs. bond length.	15
8	e_σ vs. e_π for M^{II} hexachloride complexes.	16
9	e_σ vs. e_π for M^{III} hexachloride complexes.	17
10	Plots 8 and 9 combined.	18

List of Tables

1	Experimental bond lengths (\AA) and angles ($^\circ$) for $\text{Cu}(\text{NH}_3)_5$.	4
2	SOC electronic states of $[\text{Cu}(\text{NH}_3)_5]^{2+}$ with orbital compositions.	6
3	Experimental and calculated d-d transitions for $[\text{Cu}(\text{NH}_3)_4]^{2+}$.	6
4	Calculated d-d transitions for different basis sets and corrections.	7
5	SOC electronic states of $[\text{Cu}(\text{NH}_3)_4]^{2+}$ with orbital compositions.	8
6	AOM parameters for $[\text{M}(\text{NH}_3)_6]^{n+}$.	10
7	AOM parameters for $[\text{MCl}_6]^{n-6}$.	13
8	AOM parameters for $[\text{M}(\text{NH}_3)_4]^{n+}$.	19
9	AOM parameters for $[\text{M}(\text{en})_3]^{n+}$.	20
10	AOM parameters for $[\text{M}(\text{dien})_2]^{n+}$.	21

1 A few comments on d-s mixing

In the Introduction, Fig. 1, we labelled the d_{z^2} orbital energy with a d-s mixing contribution. d-s mixing generally needs to be considered if at least one d orbital transforms in the totally symmetric irreducible representation of the molecular point group. It is best known in square planar complexes, but also the elongated octahedron and the square pyramid have d-s mixing contributions to the d_{z^2} orbital energy:

$$\begin{aligned} \text{elong. oct.} \quad \Delta_{ds}\varepsilon_{z^2} &= -(2e_{ds,ax} - 2e_{ds,eq})^2 \\ \text{sq. pyr.} \quad \Delta_{ds}\varepsilon_{z^2} &= -(e_{ds,ax} - 2e_{ds,eq})^2 \end{aligned}$$

Deeth, Gerloch and Woolley showed that in the square planar case, the introduction of d-s mixing is equivalent to placing σ -only pseudo ligands on the z-axis, termed coordination voids. These voids then have negative e_σ parameters and account for the lower d_{z^2} orbital energy. Consequently, an elongated octahedron automatically covers the effect of d-s mixing by having a reduced e_σ for the axial ligands and one may drop the d-s mixing term.

2 Influence of implicit solvation models

As stated in the methodology section, we do not employ solvation models for our CASSCF calculations. Tests with and without solvation yield roughly the same AOM parameters at higher computational costs. The difference between the parameters is less than 100 cm^{-1} and all trends are the same. Another effect of implicit solvation is a change in some orbital energies for complexes with empty

coordination sites. For square planar complexes, the d_{z^2} orbital energy increases significantly when implicit solvation is included. The empty sites are covered by the polarizable solvent surface and act similar to an additional ligand. This is an undesired effect when comparing with the experimental crystal structure data.

For geometry optimizations of complexes of the type $[\text{MCl}_6]^{3/4-}$, the inclusion of an implicit solvation model is necessary because of the large negative charge. Without a solvation model, the charge leads the ligands to repel each other, leading to asymmetric structures, if convergence is achieved at all. The CASSCF calculations are still conducted without a solvation model.

3 Square pyramidal copper pentammine

The experimental structure of the $\text{Cu}(\text{NH}_3)_5$ unit is roughly square pyramidal, with the structural parameters given in Table 1. Assuming a perfect square pyramid (C_{4v}), we obtain the following AOM parameterization for V_{LF} :

$$V_{LF} = \begin{bmatrix} 4.0e_\pi & 0 & 0 & 0 & 0 \\ 0 & 3.0e_\pi & 0 & 0 & 0 \\ 0 & 0 & 2.0e_\sigma - 1.0e_{ds} & 0 & 0 \\ 0 & 0 & 0 & 3.0e_\pi & 0 \\ 0 & 0 & 0 & 0 & 3.0e_\sigma \end{bmatrix}$$

which directly yields the following eigenvalues on the diagonal:

$$\begin{aligned} E_{d_{xy}} &= 4.0e_\pi \\ E_{d_{yz}} &= 3.0e_\pi \\ E_{d_{z^2}} &= 2.0e_\sigma - 1.0e_{ds} \\ E_{d_{xz}} &= 3.0e_\pi \\ E_{d_{x^2-y^2}} &= 3.0e_\sigma \end{aligned}$$

It is apparent that the energy difference between the d_{yz}/d_{xz} orbitals and the d_{xy} orbital is e_π . Plugging in the measured energy difference of 1300 cm^{-1} , we obtain the same value for the π parameter.

The above calculation relies on a square pyramidal structure with right angles and equal bond lengths. When using the actual structure data in Table 1, we arrive at a different ligand field potential and the diagonalized matrix is much more complicated:

$$V_{LF} = \begin{bmatrix} 3.93e_\pi & 0 & 0 & 0 & 0 \\ 0 & 2.88e_\pi + 0.113e_\sigma & 0 & 0 & 0 \\ 0 & 0 & -0.8e_{ds} + 0.207e_\pi + 1.897e_\sigma & 0 & 0.005e_{ds} + 0.011e_\pi - 0.011e_\sigma \\ 0 & 0 & 0 & 2.914e_\pi + 0.094e_\sigma & 0 \\ 0 & 0 & 0.005e_{ds} + 0.011e_\pi - 0.011e_\sigma & 0 & 0.069e_\pi + 2.895e_\sigma \end{bmatrix}$$

$$E_{d_{xy}} = 3.93e_\pi$$

$$E_{d_{yz}} = 2.88e_\pi + 0.113e_\sigma$$

$$E_{d_{z^2}} = -0.4e_{ds} + 0.138e_\pi + 2.4e_\sigma$$

$$- 0.632 (0.401e_{ds}^2 - 0.138e_{ds}e_\pi + e_{ds}e_\sigma + 0.0122e_\pi^2 - 0.173e_\pi e_\sigma + 0.624e_\sigma^2)^{0.5}$$

$$E_{d_{xz}} = 2.91e_\pi + 0.0938e_\sigma$$

$$E_{d_{x^2-y^2}} = -0.4e_{ds} + 0.138e_\pi + 2.4e_\sigma$$

$$+ 0.632 (0.401e_{ds}^2 - 0.138e_{ds}e_\pi + e_{ds}e_\sigma + 0.0122e_\pi^2 - 0.173e_\pi e_\sigma + 0.624e_\sigma^2)^{0.5}$$

Even this is still a simplification, since we subsume the parameters of the first nitrogen atom with the ones of the other four nitrogen atoms. Without going into further detail, the orbital energy difference between d_{yz}/d_{xz} and d_{xy} is roughly $e_\pi - 0.1e_\sigma$, leading to a π parameter that is slightly larger than the measured energy gap of 1300 cm^{-1} .

Table 1: Experimental bond lengths (\AA) and angles ($^\circ$) for $\text{Cu}(\text{NH}_3)_5$.

Bond lengths / \AA	
Cu-N ₁	2.19
Cu-N ₂	2.01
Cu-N ₃	2.01
Cu-N ₄	2.05
Cu-N ₅	2.05
Angles / $^\circ$	
N ₁ -Cu-N ₂	98
N ₁ -Cu-N ₃	98
N ₁ -Cu-N ₄	97
N ₁ -Cu-N ₅	97
N ₂ -Cu-N ₃	164
N ₄ -Cu-N ₅	166

3.1 Influence of spin-orbit coupling

In $[\text{Cu}(\text{NH}_3)_5]^{2+}$, SOC only couples the states with singly occupied d_{xy} , d_{xz} and d_{yz} orbitals, and the spin-orbit coupled states have an energetic ordering

very similar to that of the uncoupled case.

Although the assignment is not as clear-cut as without SOC, we note that the energy difference between the second excited state (d_{xy} orbital contribution 68%) and the fourth excited state (d_{xz} and d_{yz} orbital contribution 37% and 59%) can only be explained by an ammonia π interaction.

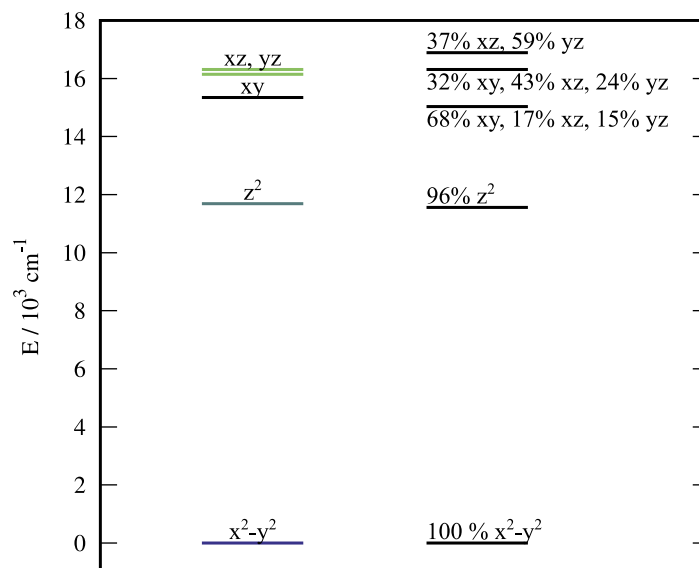


Figure 1: Energy levels of $[\text{Cu}(\text{NH}_3)_5]^{2+}$ with NEVPT2 correction (left) and upon consideration of spin-orbit coupling (right). Due to the coupling, the assignment of orbital occupations to electronic states is not as clear anymore.

Table 2: Electronic states of $[\text{Cu}(\text{NH}_3)_5]^{2+}$ and their orbital compositions with spin-orbit coupling. The configuration contribution is written in terms of the singly occupied orbital in the uncoupled contribution. Since the uncoupled states consist of (almost) a single configuration each, we use the orbital-based assignments also in the coupled states.

Energy / cm^{-1}	configuration contributions				
	d_{xy}	d_{yz}	d_{z^2}	d_{xz}	$d_{x^2-y^2}$
CASSCF					
0	0.00	0.00	0.00	0.00	0.99
8456	0.00	0.03	0.93	0.03	0.00
10305	0.73	0.13	0.00	0.13	0.00
11684	0.26	0.30	0.00	0.43	0.00
12374	0.00	0.54	0.07	0.39	0.00
CASSCF + NEVPT2					
0	0.00	0.00	0.00	0.00	1.00
11560	0.00	0.00	0.96	0.00	0.00
15032	0.68	0.15	0.00	0.17	0.00
16308	0.32	0.24	0.00	0.43	0.00
16892	0.00	0.59	0.03	0.37	0.00

4 Square planar copper tetrammine

Table 3: Experimental and calculated d-d transitions for $[\text{Cu}(\text{NH}_3)_4]^{2+}$.

	$E(B_{1g} \rightarrow A_{1g})$ / cm^{-1}	$E(B_{1g} \rightarrow B_{2g})$ / cm^{-1}	$E(B_{1g} \rightarrow E_g)$ / cm^{-1}
CASSCF	14992 - 14995	12262	14990
NEVPT2	20617 - 20631	18055	20376
Experimental	13600 - 13700		17400 - 17800

Table 4: Calculated d-d transitions for square planar $[\text{Cu}(\text{NH}_3)_4]^{2+}$ with and without NEVPT2 correction and with different basis sets. The acceptor orbital in each transition is $d_{x^2-y^2}$, so only the donor orbital is given.

method	basis set	$d_{xz} \rightarrow$ /cm ⁻¹	$d_{yz} \rightarrow$ /cm ⁻¹	$d_{z^2} \rightarrow$ /cm ⁻¹	$d_{xy} \rightarrow$ /cm ⁻¹
CASSCF	def2-SVP	14964	14966	14890	12452
	def2-TZVP	14992	14995	14990	12262
	def2-QZVP	14959	14960	14981	12227
NEVPT2	def2-SVP	19832	19831	19543	17495
	def2-TZVP	20617	20631	20376	18055
	def2-QZVP	20463	20464	20177	17980

4.1 Influence of spin-orbit coupling

In $[\text{Cu}(\text{NH}_3)_4]^{2+}$, SOC only couples the states with singly occupied d_{z^2} , d_{xz} and d_{yz} orbitals, leading to four excited states with relatively small energy differences. It is apparent that the first excited state is still clearly dominated by a singly occupied d_{xy} orbital. Again, the energy difference between this and the higher excited states can only be explained with an ammonia π interaction.

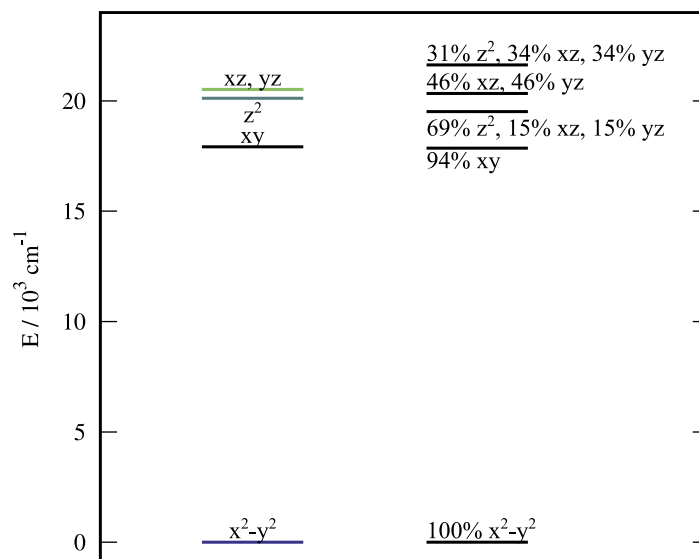


Figure 2: Energy levels of $[\text{Cu}(\text{NH}_3)_4]^{2+}$ with NEVPT2 correction (left) and upon consideration of spin-orbit coupling (right). Due to the coupling, the assignment of orbital occupations to electronic states is not as clear anymore.

Table 5: Electronic states of $[\text{Cu}(\text{NH}_3)_4]^{2+}$ and their orbital compositions with spin-orbit coupling. Configuration contribution is written in terms of the singly occupied orbital in the uncoupled contribution. Since the uncoupled states consist of (almost) a single configuration each, we convey the orbital assignments to the coupled states.

Energy / cm^{-1}	configuration contributions				
	d_{xy}	d_{yz}	d_{z^2}	d_{xz}	$d_{x^2-y^2}$
CASSCF					
0	0.00	0.00	0.00	0.00	0.99
12234	0.94	0.02	0.00	0.02	0.00
14203	0.00	0.19	0.61	0.19	0.00
14826	0.06	0.47	0.00	0.47	0.00
16232	0.00	0.31	0.38	0.31	0.00
CASSCF + NEVPT2					
0	0.00	0.00	0.00	0.00	1.00
17855	0.94	0.02	0.00	0.02	0.00
19514	0.00	0.15	0.69	0.15	0.00
20331	0.06	0.46	0.00	0.46	0.00
21636	0.00	0.34	0.31	0.34	0.00

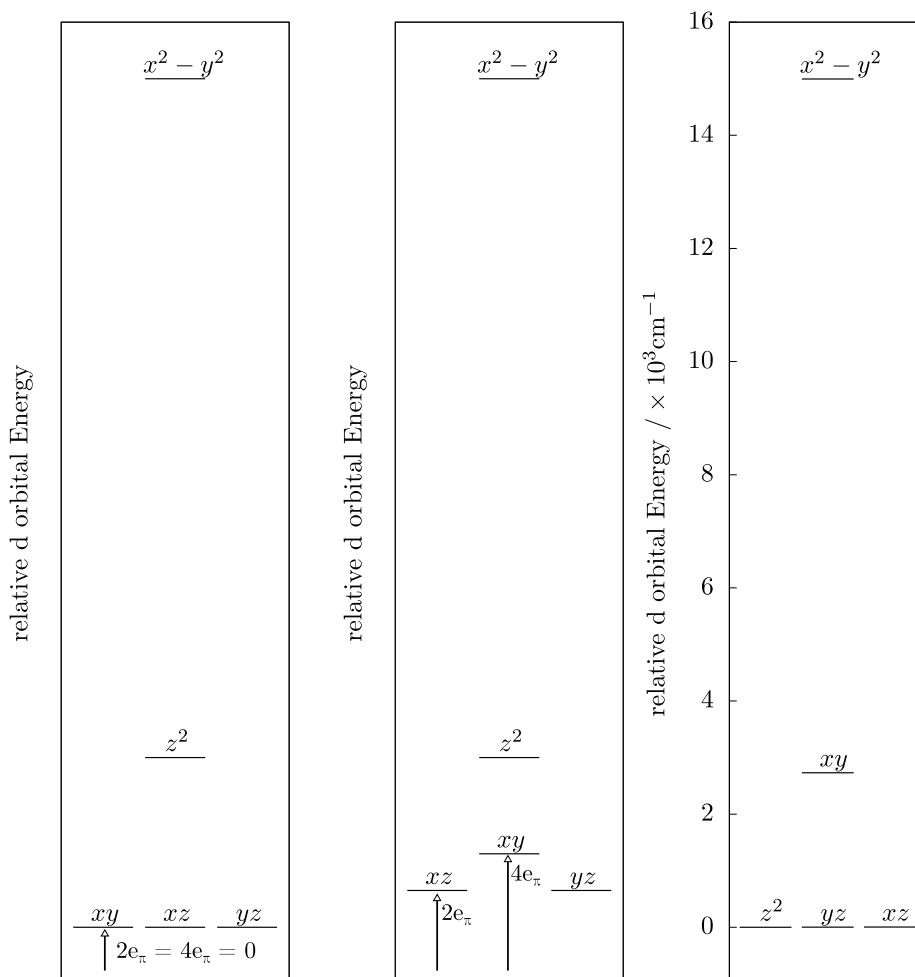


Figure 3: Expected d orbital energies for square planar complexes without π interaction (left), with π interaction (centre) and the energy levels for $[\text{Cu}(\text{NH}_3)_4]^{2+}$ from CASSCF calculations (right). The position of the z^2 orbital in the schemes on the left and centre is incompletely defined and depends on the parameter e_{ds} . It is noteworthy that the degeneracy in the left and right panel is no symmetry feature, as the d_{xz} and d_{yz} orbitals transform in the E_g representation of D_{4h} , while the d_{xy} and d_{z^2} orbital transform in the B_{2g} and A_{1g} representation, respectively.

5 Table data and plots for octahedral hexamines

It is apparent that some of the parameters (Cr^{2+} , intermediate spin Mn^{3+} , Ni^{3+} , i.e. chemically unrealistic or very challenging to obtain complexes) have uncom-

fortably large standard deviations, up to a level where the data point must be considered unreliable. The reason for the large scattering of parameters probably reflects the improbability of finding the compound in reality which poses a challenge for our procedure that may not be applicable to every hypothetical coordination compound. Nonetheless, most of the parameters have reasonable standard deviations that justify an interpretation, and ligand field splittings generally match expectations.

Table 6: AOM parameters for $[\text{M}(\text{NH}_3)_6]^{n+}$. Multiplicity refers to the multiplicity of the optimized ground state, ΔE is the energy difference to the ground state.

Complex	$2S + 1$	$\Delta E/\text{kJ mol}^{-1}$		bond length / Å	e_σ/cm^{-1}	e_π/cm^{-1}
$[\text{Cr}(\text{NH}_3)_6]^{2+}$	3	0	1	2.173(0.005)	6594(2760)	1527(2070)
$[\text{Cr}(\text{NH}_3)_6]^{3+}$	4	0	1	2.145(0.001)	6743(341)	1027(255)
$[\text{Mn}(\text{NH}_3)_6]^{2+}$	6	0	1	2.349(0.002)	3613(213)	894(159)
$[\text{Mn}(\text{NH}_3)_6]^{3+}$	3	5	1	2.099(0.003)	8917(4505)	2584(3378)
$[\text{Mn}(\text{NH}_3)_6]^{3+}$	5	0	ax	2.369(0.002)	3285(360)	576(270)
$[\text{Mn}(\text{NH}_3)_6]^{3+}$	5	0	eq	2.127(0.002)	6707(359)	1046(270)
$[\text{Fe}(\text{NH}_3)_6]^{2+}$	1	5	1	2.059(0.000)	5491(324)	710(243)
$[\text{Fe}(\text{NH}_3)_6]^{2+}$	3	43	ax	2.038(0.000)	6011(352)	1051(263)
$[\text{Fe}(\text{NH}_3)_6]^{2+}$	3	43	eq	2.250(0.016)	3772(385)	826(265)
$[\text{Fe}(\text{NH}_3)_6]^{2+}$	5	0	1	2.282(0.002)	3598(229)	851(171)
$[\text{Fe}(\text{NH}_3)_6]^{3+}$	6	56	1	2.237(0.003)	6532(915)	2052(683)
$[\text{Fe}(\text{NH}_3)_6]^{3+}$	4	47	ax	2.323(0.000)	3909(907)	972(679)
$[\text{Fe}(\text{NH}_3)_6]^{3+}$	4	47	eq	2.081(0.002)	7452(909)	1433(682)
$[\text{Fe}(\text{NH}_3)_6]^{3+}$	2	0	1	2.061(0.003)	7042(92)	1087(74)
$[\text{Co}(\text{NH}_3)_6]^{2+}$	4	0	1	2.233(0.008)	3471(62)	770(19)
$[\text{Co}(\text{NH}_3)_6]^{2+}$	2	7	ax	2.391(0.002)	1818(379)	591(284)
$[\text{Co}(\text{NH}_3)_6]^{2+}$	2	7	eq	2.022(0.000)	5857(379)	1024(285)
$[\text{Co}(\text{NH}_3)_6]^{3+}$	1	0	1	2.024(0.000)	6788(408)	698(307)
$[\text{Ni}(\text{NH}_3)_6]^{2+}$	3	0	1	2.182(0.000)	3024(355)	412(266)
$[\text{Ni}(\text{NH}_3)_6]^{3+}$	4	0	1	2.153(0.000)	7515(1628)	1971(1238)
$[\text{Ni}(\text{NH}_3)_6]^{3+}$	4	0	2	2.222(0.000)	6804(1058)	2665(792)
$[\text{Ni}(\text{NH}_3)_6]^{3+}$	4	0	3	2.181(0.000)	7500(1420)	2349(1060)
$[\text{Ru}(\text{NH}_3)_6]^{2+}$	1	0	1	2.164(0.003)	9755(203)	799(152)
$[\text{Ru}(\text{NH}_3)_6]^{3+}$	2	0	1	2.168(0.005)	10749(417)	649(311)
$[\text{Os}(\text{NH}_3)_6]^{2+}$	1	0	1	2.182(0.005)	11271(156)	594(120)
$[\text{Os}(\text{NH}_3)_6]^{3+}$	2	0	1	2.186(0.004)	11686(170)	194(149)

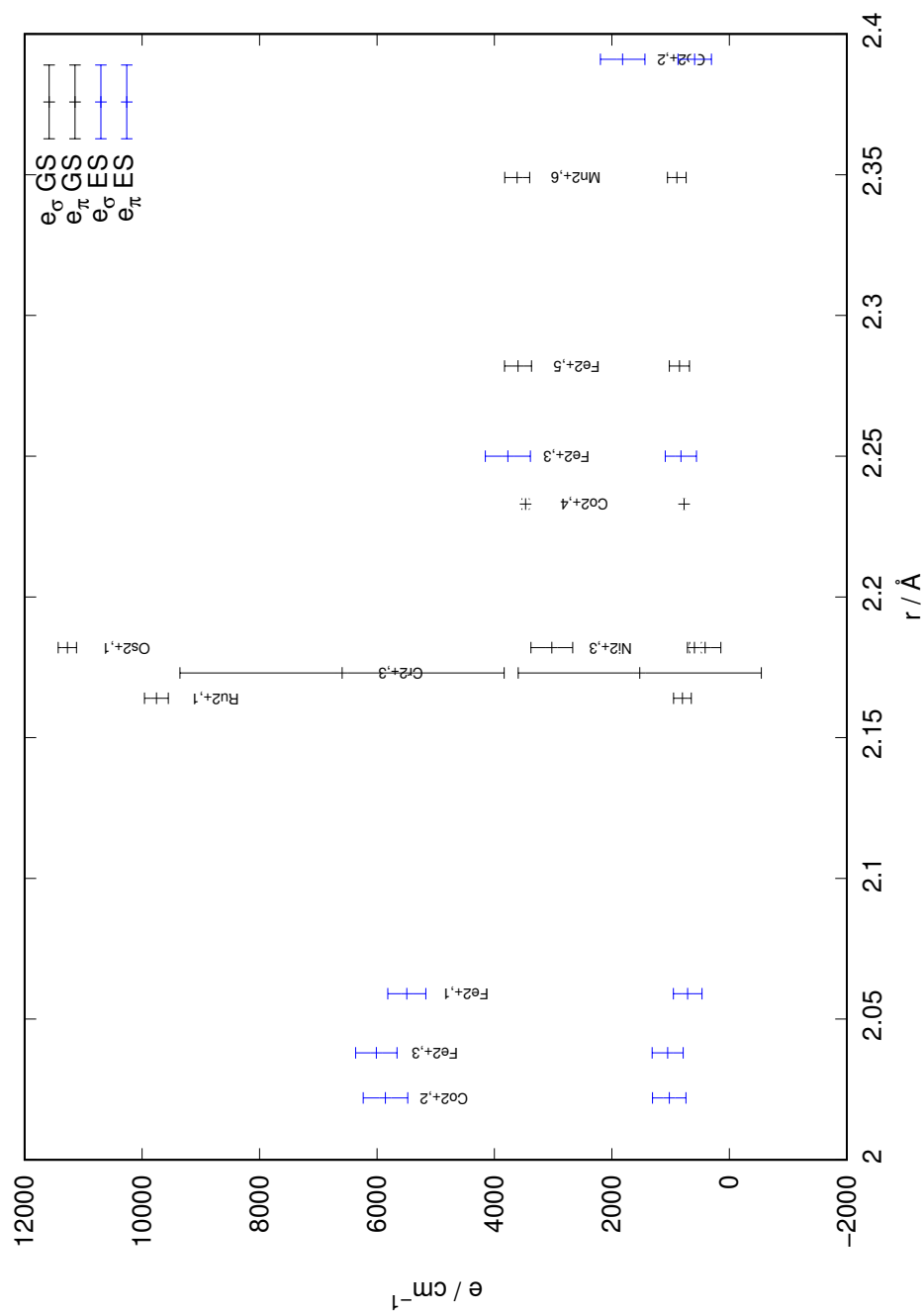


Figure 4: AOM parameters of M^{II} hexammine complexes plotted versus the corresponding bond length. The upper set of points represents σ parameters, the lower set of points π parameters. Data points of the ground spin state structures (GS) and of structures with less stabilised multiplicities (ES) are colored black and blue, respectively. The error bars show the standard deviations resulting from sampled calculations. Labels indicate the metal with formal charge and multiplicity.

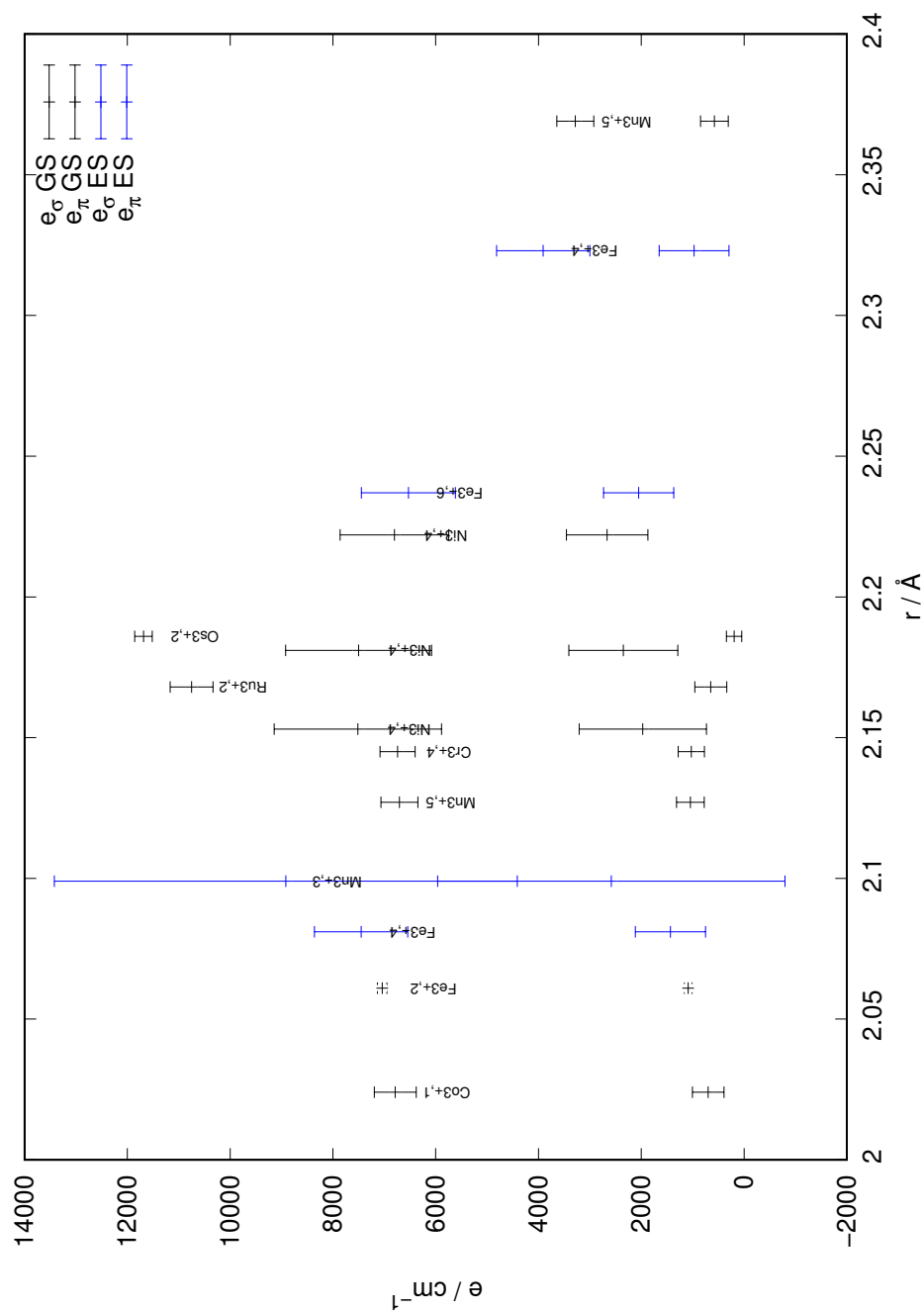


Figure 5: AOM parameters of M^{III} hexammine complexes plotted versus the corresponding bond length. The upper set of points represents σ parameters, the lower set of points π parameters. Data points of the ground spin state structures (GS) and of structures with less stabilised multiplicities (ES) are colored black and blue, respectively. The error bars show the standard deviations resulting from sampled calculations. Labels indicate the metal with formal charge and multiplicity.

6 Comparison of chloride and ammine ligands

For the parameters that do not have an overly large standard deviation, some patterns can be seen: Both σ and π parameters are larger for ammine ligands than for chloride ligands. Shorter bond lengths lead to higher σ parameters, but not necessarily to higher π parameters. Plotting the parameters of Cl^- ligands against the ones of NH_3 ligands shows absolutely no correlation. No rule in the sense of a parameter ratio can be derived from the calculations.

Table 7: AOM parameters for $[\text{MCl}_6]^{3-/4-}$, optimized with BP, def2-SVP, Grid5, CPCM(Water).

Complex	$2S + 1$	$\Delta E/\text{kJ mol}^{-1}$		bond length / Å	e_σ/cm^{-1}	e_π/cm^{-1}
$[\text{CrCl}_6]^{3-}$	4	0	1	2.410(04)	3987(72)	537(39)
$[\text{MnCl}_6]^{4-}$	6	0	1	2.639(05)	1930(31)	516(13)
$[\text{MnCl}_6]^{3-}$	3	0	1	2.376(04)	3892(110)	435(74)
$[\text{FeCl}_6]^{4-}$	5	0	ax	2.619(00)	1659(15)	410(11)
$[\text{FeCl}_6]^{4-}$	5	0	eq	2.583(02)	1836(18)	448(12)
$[\text{FeCl}_6]^{3-}$	6	0	1	2.454(08)	3363(86)	462(24)
$[\text{CoCl}_6]^{4-}$	4	0	1	2.529(02)	1928(22)	501(16)
$[\text{CoCl}_6]^{4-}$	4	0	2	2.635(00)	1416(21)	393(16)
$[\text{CoCl}_6]^{3-}$	1	2	1	2.329(05)	3975(67)	312(17)
$[\text{CoCl}_6]^{3-}$	5	0	1	2.437(04)	3425(52)	414(20)
$[\text{CoCl}_6]^{3-}$	3	19	ax	2.302(00)	4711(118)	606(88)
$[\text{CoCl}_6]^{3-}$	3	19	eq	2.436(16)	3087(211)	245(94)
$[\text{NiCl}_6]^{4-}$	3	0	ax	2.491(00)	1813(49)	430(37)
$[\text{NiCl}_6]^{4-}$	3	0	eq	2.553(04)	1517(52)	367(37)
$[\text{NiCl}_6]^{3-}$	2	0	ax	2.563(00)	1391(465)	-129(349)
$[\text{NiCl}_6]^{3-}$	2	0	eq	2.295(02)	4720(466)	423(349)
$[\text{RuCl}_6]^{4-}$	1	0	1	2.488(08)	4678(104)	378(19)
$[\text{RuCl}_6]^{3-}$	2	0	ax	2.441(00)	6236(143)	306(107)
$[\text{RuCl}_6]^{3-}$	2	0	eq	2.407(01)	6849(144)	404(107)
$[\text{RuCl}_6]^{3-}$	4	68	ax	2.679(00)	3068(547)	103(409)
$[\text{RuCl}_6]^{3-}$	4	68	eq	2.417(02)	7345(547)	742(410)
$[\text{OsCl}_6]^{4-}$	1	0	1	2.518(07)	5224(120)	256(55)
$[\text{OsCl}_6]^{3-}$	2	0	ax	2.468(00)	6903(216)	356(162)
$[\text{OsCl}_6]^{3-}$	2	0	eq	2.428(01)	7674(218)	457(162)

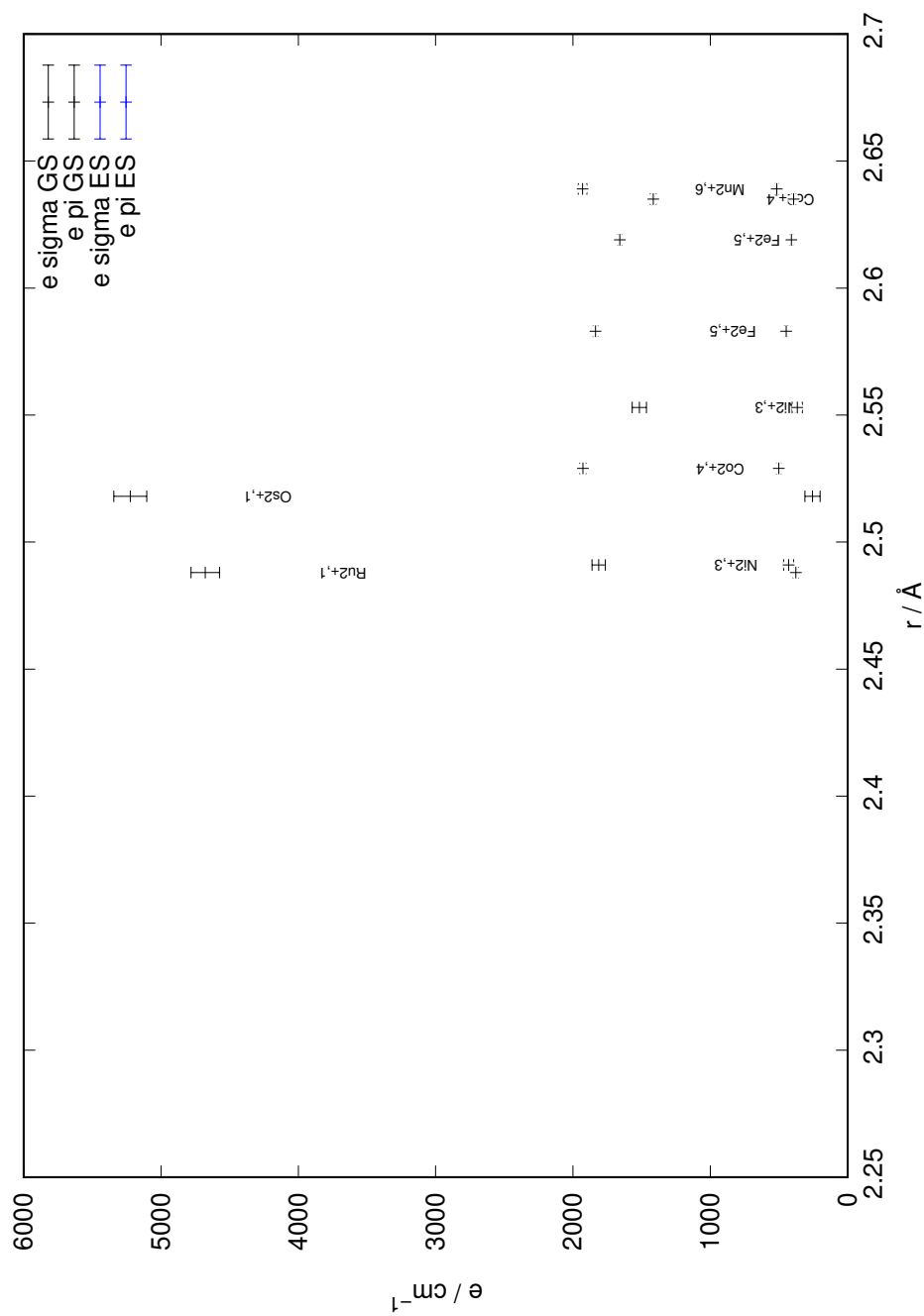


Figure 6: AOM parameters of M^{II} hexachloride complexes plotted versus the corresponding bond length. The upper set of points represents σ parameters, the lower set of points π parameters. Data points of the ground spin state structures (GS) and of structures with less stabilised multiplicities (ES) are colored black and blue, respectively. The error bars show the standard deviations resulting from sampled calculations. Labels indicate the metal with formal charge and multiplicity.

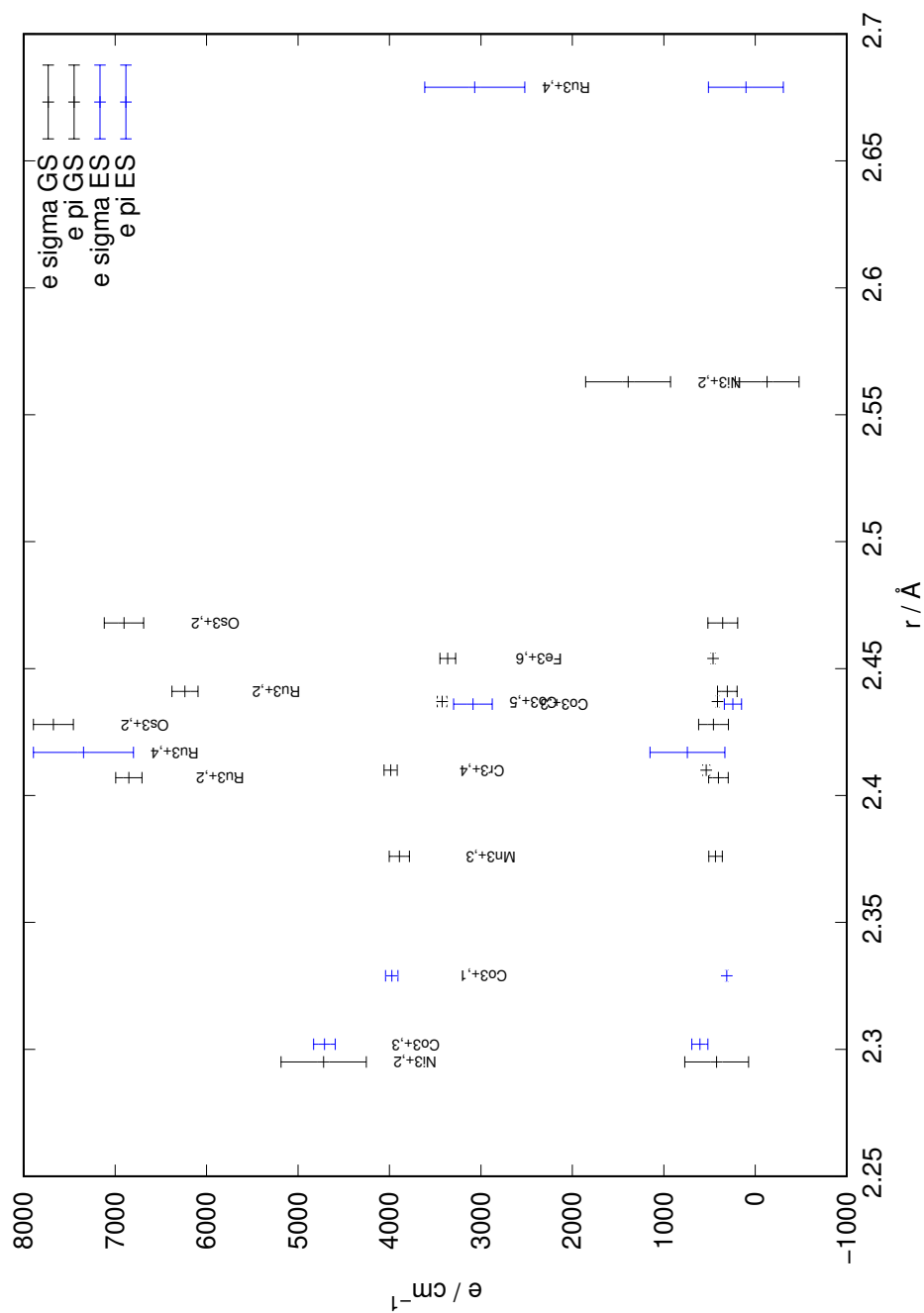


Figure 7: AOM parameters of M^{III} hexachloride complexes plotted versus the corresponding bond length. The upper set of points represents σ parameters, the lower set of points π parameters. Data points of the ground spin state structures (GS) and of structures with less stabilised multiplicities (ES) are colored black and blue, respectively. The error bars show the standard deviations resulting from sampled calculations. Labels indicate the metal with formal charge and multiplicity.

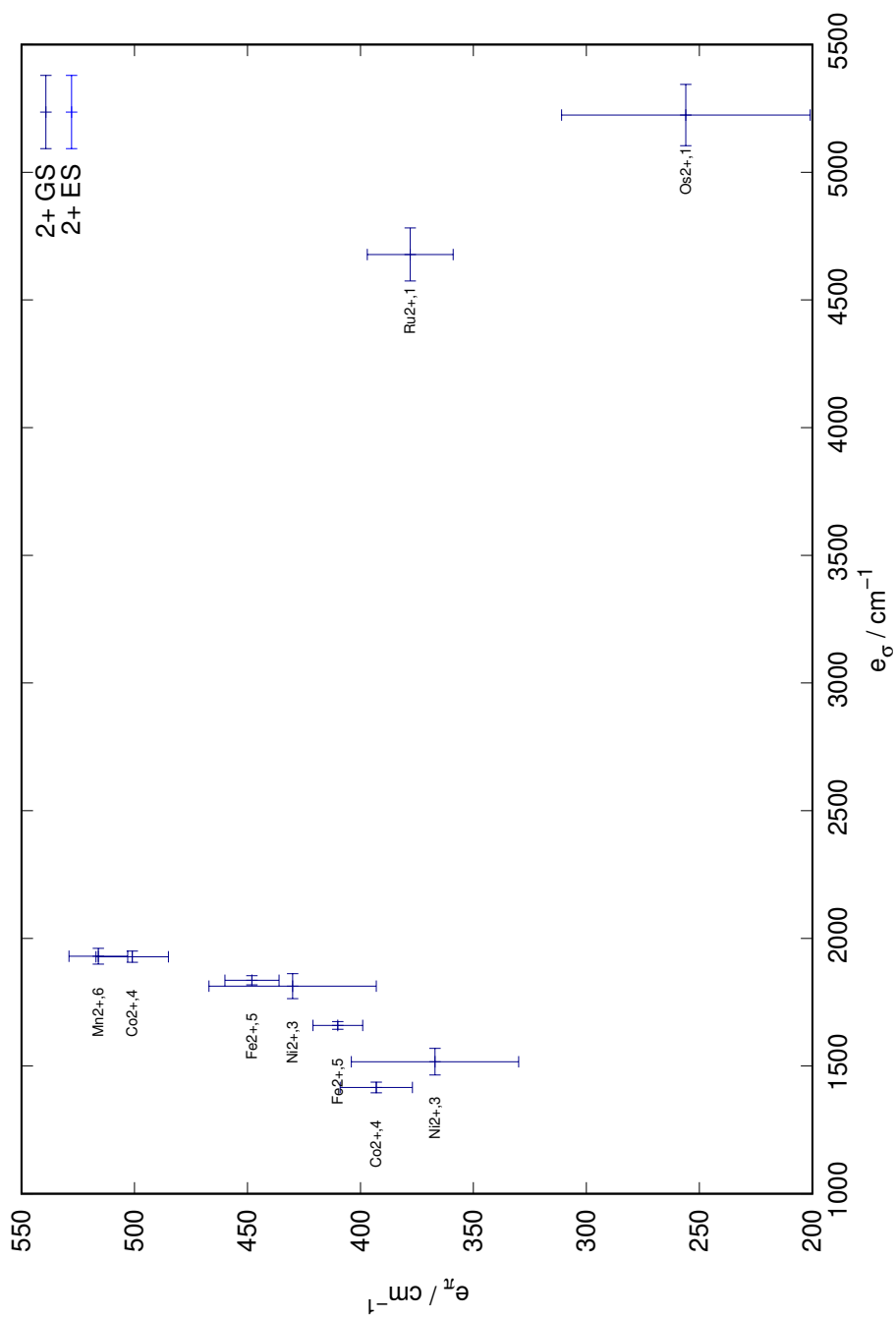


Figure 8: e_σ vs. e_π for M^{II} hexachloride complexes.

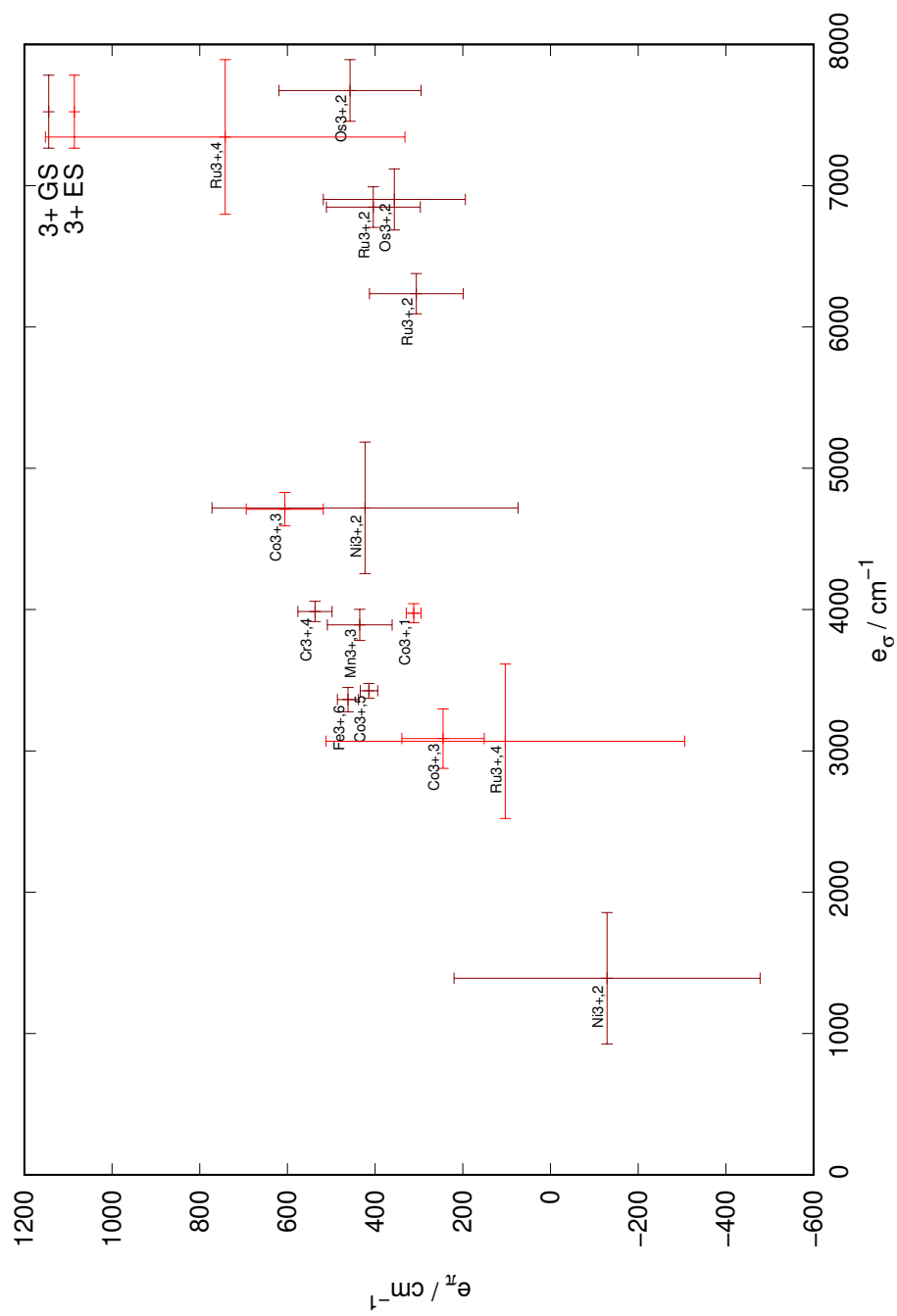


Figure 9: e_σ vs. e_π for M^{III} hexachloride complexes.

7 Table data for tetrammines

Table 8: AOM parameters for fictitious $[M(\text{NH}_3)_4]^{n+}$. Multiplicity refers to the multiplicity of the optimized ground state, ΔE (kJ mol^{-1}) is the energy difference of the given multiplicity to the ground state. If e_{ds} is not shown it was set to 0 in the fit. For shown e_{ds} , the molecule was oriented in the global axis frame for the CAS calculations.

Complex	$2S + 1$	$\Delta E/\text{kJ mol}^{-1}$	bond length / \AA	e_σ/cm^{-1}	e_π/cm^{-1}	e_{ds}/cm^{-1}
$[\text{Cr}(\text{NH}_3)_4]^{2+}$	1	0	2.060(0.000)	6893(37)	1704(32)	
$[\text{Mn}(\text{NH}_3)_4]^{2+}$	6	0	2.191(0.000)	4723(113)	1343(85)	
$[\text{Co}(\text{NH}_3)_4]^{3+}$	5	43	2.073(0.001)	8800(111)	2620(106)	
$[\text{Co}(\text{NH}_3)_4]^{3+}$	3	0	2.000(0.000)	10166(29)	2449(18)	894(17)
$[\text{Fe}(\text{NH}_3)_4]^{3+}$	4	32	2.036(0.000)	9775(40)	2374(27)	966(13)
$[\text{Fe}(\text{NH}_3)_4]^{3+}$	6	0	2.103(0.001)	7101(474)	1614(361)	
$[\text{Ni}(\text{NH}_3)_4]^{3+}$	4	0	2.041(0.000)	8238(555)	1933(429)	

8 Table data for en and dien complexes

Table 9: AOM parameters for $[M(en)_3]^{n+}$.

Complex	$2S + 1$	$\Delta E/\text{kJ mol}^{-1}$		bond length / Å	e_σ/cm^{-1}	e_π/cm^{-1}
$[\text{Cr}(en)_3]^{2+}$	5	0	1	2.583(0.003)	1662(67)	270(45)
$[\text{Cr}(en)_3]^{2+}$	5	0	2	2.184(0.004)	5737(63)	822(48)
$[\text{Cr}(en)_3]^{2+}$	3	37	1	2.166(0.007)	4724(49)	-120(37)
$[\text{Cr}(en)_3]^{3+}$	4	0	1	2.141(0.000)	6010(48)	227(37)
$[\text{Mn}(en)_3]^{2+}$	6	0	1	2.344(0.000)	2517(11)	-106(8)
$[\text{Mn}(en)_3]^{3+}$	5	5	1	2.366(0.001)	2897(59)	71(43)
$[\text{Mn}(en)_3]^{3+}$	5	5	2	2.131(0.003)	6329(56)	588(43)
$[\text{Mn}(en)_3]^{3+}$	3	0	1	2.094(0.003)	5925(90)	106(66)
$[\text{Fe}(en)_3]^{2+}$	1	0	1	2.053(0.001)	3350(139)	-1097(105)
$[\text{Fe}(en)_3]^{2+}$	5	23	1	2.273(0.006)	2513(73)	-135(51)
$[\text{Fe}(en)_3]^{2+}$	3	53	1	2.253(0.000)	3430(58)	263(33)
$[\text{Fe}(en)_3]^{2+}$	3	53	2	2.225(0.001)	2099(62)	-514(26)
$[\text{Fe}(en)_3]^{2+}$	3	53	3	2.040(0.000)	4975(29)	145(22)
$[\text{Fe}(en)_3]^{3+}$	2	0	1	2.057(0.001)	6498(29)	450(21)
$[\text{Fe}(en)_3]^{3+}$	4	62	1	2.312(0.001)	2910(59)	-44(44)
$[\text{Fe}(en)_3]^{3+}$	4	62	2	2.087(0.010)	6331(58)	448(44)
$[\text{Co}(en)_3]^{2+}$	2	0	1	2.359(0.001)	1080(80)	-203(61)
$[\text{Co}(en)_3]^{2+}$	2	0	2	2.023(0.001)	5003(80)	267(60)
$[\text{Co}(en)_3]^{2+}$	4	6	1	2.224(0.001)	2946(14)	219(10)
$[\text{Co}(en)_3]^{3+}$	1	0	1	2.020(0.001)	5959(83)	-149(63)
$[\text{Ni}(en)_3]^{2+}$	3	0	1	2.177(0.000)	2556(52)	-75(39)
$[\text{Ni}(en)_3]^{3+}$	2	0	1	2.255(0.000)	3023(72)	-54(52)
$[\text{Ni}(en)_3]^{3+}$	2	0	2	2.018(0.002)	6968(71)	460(53)
$[\text{Ru}(en)_3]^{2+}$	1	0	1	2.161(0.001)	8489(83)	-542(62)
$[\text{Ru}(en)_3]^{3+}$	2	0	1	2.166(0.001)	11266(34)	587(29)
$[\text{Os}(en)_3]^{2+}$	1	0	1	2.180(0.001)	10466(76)	-487(57)
$[\text{Os}(en)_3]^{3+}$	2	0	1	2.184(0.002)	12880(48)	558(40)

Table 10: AOM parameters for $[M(\text{dien})_2]^{n+}$.

Complex	$2S + 1$	$\Delta E/\text{kJ mol}^{-1}$		bond length / \AA	e_σ/cm^{-1}	e_π/cm^{-1}
$[\text{Cr}(\text{dien})_2]^{2+}$	5	0	1	2.389(0.026)	5446(151)	2012(114)
$[\text{Cr}(\text{dien})_2]^{2+}$	5	0	2	2.149(0.000)	7772(132)	1968(96)
$[\text{Cr}(\text{dien})_2]^{2+}$	3	42	1	2.177(0.010)	8206(687)	2588(519)
$[\text{Cr}(\text{dien})_2]^{2+}$	3	42	2	2.122(0.003)	9018(642)	2387(475)
$[\text{Cr}(\text{dien})_2]^{3+}$	4	0	1	2.140(0.020)	15264(291)	7054(230)
$[\text{Mn}(\text{dien})_2]^{2+}$	6	0	1	2.346(0.020)	5280(98)	1896(143)
$[\text{Mn}(\text{dien})_2]^{3+}$	5	0	1	2.276(0.010)	4515(292)	577(219)
$[\text{Mn}(\text{dien})_2]^{3+}$	5	0	2	2.096(0.000)	7759(264)	968(192)
$[\text{Mn}(\text{dien})_2]^{3+}$	3	11	1	2.095(0.020)	17034(1648)	8328(1233)
$[\text{Fe}(\text{dien})_2]^{2+}$	5	20	1	2.302(0.008)	4660(230)	1646(174)
$[\text{Fe}(\text{dien})_2]^{2+}$	5	20	2	2.237(0.000)	5251(200)	1455(146)
$[\text{Fe}(\text{dien})_2]^{2+}$	3	46	1	2.251(0.025)	4838(90)	1515(67)
$[\text{Fe}(\text{dien})_2]^{2+}$	3	46	2	2.027(0.000)	7412(79)	1668(66)
$[\text{Fe}(\text{dien})_2]^{2+}$	1	0	1	2.049(0.019)	11295(1523)	4753(1135)
$[\text{Fe}(\text{dien})_2]^{3+}$	2	0	1	2.056(0.017)	13350(866)	5482(618)
$[\text{Fe}(\text{dien})_2]^{3+}$	4	47	1	2.091(0.035)	15444(355)	7041(266)
$[\text{Fe}(\text{dien})_2]^{3+}$	4	47	2	2.315(0.019)	11931(371)	7053(274)
$[\text{Fe}(\text{dien})_2]^{3+}$	6	62	1	2.240(0.002)	8525(77)	3239(60)
$[\text{Fe}(\text{dien})_2]^{3+}$	6	62	2	2.304(0.001)	8014(65)	2586(46)
$[\text{Co}(\text{dien})_2]^{2+}$	2	0	1	2.019(0.024)	10387(712)	4115(536)
$[\text{Co}(\text{dien})_2]^{2+}$	2	0	2	2.395(0.070)	5965(747)	3819(554)
$[\text{Co}(\text{dien})_2]^{2+}$	4	17	1	2.253(0.005)	5314(403)	2150(303)
$[\text{Co}(\text{dien})_2]^{2+}$	4	17	2	2.183(0.010)	5901(359)	1985(270)
$[\text{Co}(\text{dien})_2]^{3+}$	1	0	1	2.018(0.014)	17493(3624)	8398(2713)
$[\text{Ni}(\text{dien})_2]^{2+}$	3	0	1	2.204(0.013)	5676(693)	2436(519)
$[\text{Ni}(\text{dien})_2]^{2+}$	3	0	2	2.124(0.000)	6414(641)	2319(482)
$[\text{Ni}(\text{dien})_2]^{3+}$	2	0	1	2.157(0.008)	3314(416)	-757(312)
$[\text{Ni}(\text{dien})_2]^{3+}$	2	0	2	1.986(0.000)	6856(393)	-274(296)
$[\text{Ru}(\text{dien})_2]^{2+}$	1	0	1	2.165(0.004)	17850(675)	6640(505)
$[\text{Ru}(\text{dien})_2]^{2+}$	1	0	2	2.123(0.001)	18865(631)	6100(478)
$[\text{Ru}(\text{dien})_2]^{3+}$	2	0	1	2.159(0.019)	21304(1207)	7859(899)
$[\text{Os}(\text{dien})_2]^{2+}$	1	0	1	2.179(0.002)	21548(2241)	7998(1684)
$[\text{Os}(\text{dien})_2]^{2+}$	1	0	2	2.144(0.000)	22417(2097)	7197(1570)
$[\text{Os}(\text{dien})_2]^{3+}$	2	0	1	2.175(0.017)	23996(603)	8631(489)

5.3 AOMadillo: A program for fitting angular overlap model parameters

M. Buchhorn, V. Krewald, *Journal of Computational Chemistry* **2024**, *45*, 122–134, 10.1002/jcc.27224

With the proof of concept and the application to ammines, we decided to unify the developed software in a single package that is usable in conjunction with the ORCA quantum chemistry package. The package is called *AOMadillo* and available online: <https://git.rwth-aachen.de/ak-krewald/aomadillo>. In the publication, we present the features of the software and also explain some details like the definitions that employed for angles, parameters and the LFT matrix elements. AOMadillo supports common parameterizations in terms of σ , π and d–s mixing parameters, grouping options and the distinction of π_x and π_y interactions with regard to the molecular geometry. Although the parameterization itself is performed by the software by employing a least-squares fit, the complex must be assessed by the user: Information about the desired parameterization and the complex geometry must be given. It might seem inconvenient that these decisions are not made based on an automated analysis, but it is in fact a design choice. There are several use cases discussed in the publication that show that such an automated assessment could very well hide important information from the user. Just as inorganic chemists often needed to try parameter sets based on different assumptions, this is still often necessary with AOMadillo. The obvious advantage of our software is that these different parameterizations are applied much faster, produce machine-readable output and the inclusion of the asymmetry approach presented in section 5.1.

Additional to the publication, we provide a manual with information on the installation and usage of the software. All possible configurations are listed and explained and a detailed walkthrough for a simple octahedral $[\text{VCl}_6]^{3-}$ complex is provided. The manual contains everything that is needed to use the software and therefore complements the journal article that discusses the parameterizations on a more formal level.

AOMadillo: A program for fitting angular overlap model parameters

Moritz Buchhorn  | Vera Krewald 

Theoretische Chemie, Technische Universität Darmstadt, Darmstadt, Germany

Correspondence
 Vera Krewald, Theoretische Chemie,
 Technische Universität Darmstadt, Peter-
 Grünberg-Straße 4, 64287, Darmstadt,
 Germany.
 Email: vera.krewald@tu-darmstadt.de

Funding information
 Deutsche Forschungsgemeinschaft,
 Grant/Award Number: 443703006

Abstract

The angular overlap model (AOM) is an established parameterization scheme within ligand field theory (LFT). In principle, its application is fairly straightforward, but can be tedious and involve a trial-and-error approach to identify and judge the best set of parameters. With the availability of quantum chemical methods to predict d-d transitions in transition metal complexes, a rich source of computational spectroscopic data with unambiguous assignments to electronic states is available. Herein, we present AOMadillo, a software package that is designed to interface the output of *ab initio* LFT calculations from the ORCA suite of programs and performs a least-squares fit for a chosen AOM parameterization. Many steps of the AOM parameterization are automated, so that scans of geometric parameters and evaluations of sets of similar complexes are convenient. The fitting routine is highly configurable, allowing the efficient evaluation of different parameter sets.

KEYWORDS

angular overlap model, ligand field theory, quantum chemistry, transition metals

1 | INTRODUCTION

The angular overlap model (AOM) is a flavor of ligand field theory (LFT), which means it is concerned with the parameterization of d-d transitions in coordination complexes.^{1,2} In contrast to other ligand field parameterizations, AOM parameters are local, that is, each ligand has its own set of parameters that describe the properties of this particular ligand in the complex. The promise of the AOM is thus to transfer the concept of functional groups to coordination chemistry.³ AOM parameters are interpreted in terms of their sign and magnitude: positive parameters are considered to reflect a ligand to metal electron donating interaction, negative parameters an electron accepting interaction.^{2,4} One property that comes with the concept of functional groups is the transferability of their parameters into different coordination complexes, a feature of the AOM that was sometimes assumed,^{5,6} but also opposed on occasion.⁷⁻⁹

Every application of the AOM to a coordination compound requires the parameterization of the one-electron ligand field Hamiltonian V_{LF} , while the two-electron part is generally parameterized in terms of Racah or Condon-Shortley parameters.² A direct way for parameterizing V_{LF} is to express the energy of the electronic d states in terms of the chosen parameterization and to search for a best-fitting set of parameters that reproduce these states. An alternative, indirect approach is the treatment of each element in V_{LF} as an independent parameter, resulting in a maximum of 15 independent elements in a symmetric 5×5 matrix.¹⁰ This corresponds to the Wybourne parameterization of a C_1 complex.¹¹ The two-electron part is again fitted with Racah or Condon-Shortley parameters. The application of the AOM takes place in a second step, where solely V_{LF} is fitted with a chosen set of AOM parameters. AOMadillo employs the second, indirect way by fitting the ligand field Hamiltonian.

Each matrix element is expressed in terms of the general AOM equation.^{1,11,12}

This is an open access article under the terms of the [Creative Commons Attribution-NonCommercial](https://creativecommons.org/licenses/by-nc/4.0/) License, which permits use, distribution and reproduction in any medium, provided the original work is properly cited and is not used for commercial purposes.
 © 2023 The Authors. *Journal of Computational Chemistry* published by Wiley Periodicals LLC.

$$v_{ij} = \delta_{ij}E + \sum_{\lambda} \sum_{L} F_{L,\lambda,i} F_{L,\lambda,j} e_{L,\lambda} + \sum_{L} F_{ds,i} \sqrt{e_{L,ds}} \cdot \sum_{L} F_{ds,j} \sqrt{e_{L,ds}}. \quad (1)$$

E is the spherical contribution to the field, $F_{L,\lambda,i}$ are the angular overlap factors where L specifies the ligand, λ indicates the interaction type which can be σ , π_x or π_y , and i, j are the matrix element indices. F is a function of the angular coordinates of the ligands θ, ϕ, ψ and tabulated.² The parameters e capture the bond length dependent part and are subject to the ligand field fitting procedure. e_{ds} is a parameter that accounts for the d-s orbital mixing in complexes of certain symmetries.^{12,13} Considering e_{ds} , each ligand can thus be parameterized by two to four parameters (see also Section 4.1), which leaves 13 parameters for an average octahedral ($E + 6 \cdot e_{\sigma} + 6 \cdot e_{\pi}$) or square planar complex ($E + 4 \cdot e_{\sigma} + 4 \cdot e_{\pi} + 4 \cdot e_{ds}$). Given that V_{LF} has a maximum of 15 independent elements, it is apparent that the AOM equation system is very likely to be underdetermined.

An interesting dilemma arises at this step: in order to solve the equation system resulting from the AOM parameterization, it is advisable to reduce its complexity. If there are symmetry features in the molecule, these can be used to lower the number of unique elements in the ligand field matrix which makes it easier to calculate the overlap factors and reduces the load of equations. The downside is that almost inevitably an underdetermined equation system results, so that dependencies arise and an infinite number of solutions can be found. It is therefore necessary to reduce the number of AOM parameters and thereby make the equation system determined. Reducing the parameters can be achieved for instance by fixing the ratios of certain parameters or by setting some parameters to zero. However, these choices are driven by the experience and biases of the researcher. The resulting simplifications may underestimate or neglect parameters or overlook the uniqueness of ligands.

The researcher is thus faced with a difficult choice between two options: the introduction of perhaps biased experience into the AOM parameterization, or a much more complicated but often enough analytically unsolvable equation system with a more impartial and complete parameter fit. In the rest of this work, we present how the AOMadillo package mitigates this dilemma by making the evaluation of ligand field Hamiltonians for asymmetric molecules feasible. In many cases, more insightful parameter sets are obtained than with simplifications that may result in underdetermined equation systems.

Starting with version 4, the ORCA quantum chemistry package offers an *ab initio* LFT (aiLFT) module.^{14,15} With the electronic states from a CASSCF calculation, the aiLFT module fits the one-electron ligand field matrix and the two-electron Racah and Slater-Condon parameters. The corresponding CASSCF (CASSCF/NEVPT2) states together with the aiLFT module were shown to reproduce experimental data very well on several occasions.¹⁶⁻²⁰ The most important feature of this theoretical approach to AOM parameters is that, in contrast to the experiment, the investigated structures are rigid. The resulting states are sensitive to the exact input structure instead of an average one. It is thus possible to intentionally make structures that are asymmetric and because the AOM F-factors are angle-dependent, they can account for the changes in the electronic state energies.

With this, it is possible to reliably increase the number of independent elements in V_{LF} , so that more parameters can be fitted. More details on the asymmetric structures are provided in Section 3. All our results are based on ORCA CASSCF calculations which AOMadillo interfaces to perform the AOM parameter fit.

2 | FUNCTIONALITIES OF AOMADILLO

AOMadillo offers a fast and easy application of the AOM to a ligand field Hamiltonian. The quality of the parameterization can be evaluated via the cost of the fit, a semi-objective quantity further elaborated below. This allows a straightforward comparison of different parameterization choices. The input and output work in a stand-alone way, and are designed such that they can be embedded in a shell pipeline. This allows the user to write simple shell scripts to test different parameterizations, scan the parameter space, and process output parameters for further analyses or visualizations. With ORCA as the quantum chemistry software that generates the ligand field Hamiltonian, the user has access to many other means of scanning and automation. The scheme in Figure 1 shows the steps that are necessary to generate an AOM parameterization with AOMadillo.

AOMadillo interfaces the output of the ORCA aiLFT module. Both ORCA 4 and ORCA 5 are supported. It reads the one-electron ligand field Hamiltonian V_{LF} and applies a fitting procedure developed by us to obtain the AOM parameters.²¹ In the rest of this section, we provide a more detailed description of the procedure.

Each Hamiltonian matrix element is expressed as in Equation (1). Each value v_{ij} is calculated by ORCA and thus a known quantity in our problem. It is brought to the right side of the equation, which should then equal 0.

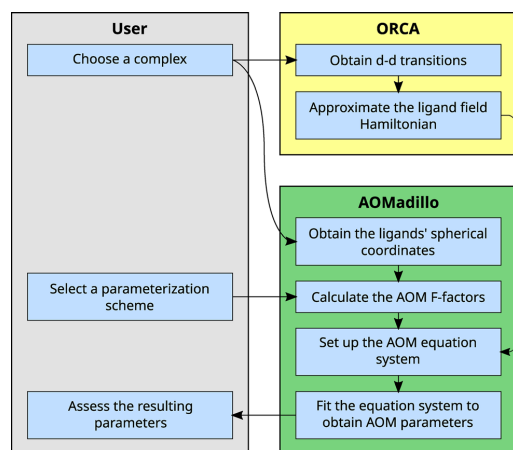


FIGURE 1 Schematic representation of the steps necessary to take full advantage of the AOMadillo package.

$$0 = -V_{ij} + \delta_{ij}E + \sum_L \sum_{\lambda} F_{L,\lambda,i} F_{L,\lambda,j} e_{L,\lambda} + \sum_L F_{ds,i} \sqrt{e_{L,ds}} \cdot \sum_L F_{ds,j} \sqrt{e_{L,ds}} \quad (2)$$

Since the total equation system is in general overdetermined (see Section 3) and inconsistent, no set of parameters can be found that satisfies all equations. Instead, an approximate solution is found by employing a nonlinear least-squares solver and in the above equation 0 is replaced by the so-called residual s_{ij} .^{22–24}

$$s_{ij} = -V_{ij} + \delta_{ij}E + \sum_L \sum_{\lambda} F_{L,\lambda,i} F_{L,\lambda,j} e_{L,\lambda} + \sum_L F_{ds,i} \sqrt{e_{L,ds}} \cdot \sum_L F_{ds,j} \sqrt{e_{L,ds}} \quad (3)$$

The least-squares solver minimizes the equation system with regard to the sum of all equations squared residues s . We refer to this quantity as the “cost” of a fit and omit its dimension or unit, respectively, in the rest of this text.

$$\text{cost} = \sum_j \sum_{i \leq j} s_{ij}^2 \quad (4)$$

V_{LF} is symmetric, so the cost is calculated from the elements s with $i \leq j$ to prevent double counting. The cost can serve as a probe for the quality of a chosen parameterization. When choosing a parameter set that can reproduce the given ligand field Hamiltonian well, the cost is small. Otherwise the cost increases if we chose a set that poorly recovers the Hamiltonian. This assessment can only be applied in a relative manner, that is, if the parameterization is changed and the cost changes at the same time. The specific value of the cost of a single fit does not tell anything about its quality, although a high remaining cost in a detailed parameter set can be seen as a hint that the AOM in the given parameterization might be unsuitable.

Summarized briefly, the AOMadillo software offers the direct application of the AOM to aiLFT results. An obvious advantage over manually or semi-manually solving the AOM equations is that the computer delivers the result. Provided with only the molecular geometry, the program outputs the corresponding equation system, including the on-axis angle ψ which can be tedious to determine manually. A second advantage of AOMadillo lies in the configuration options for the parameterization and the ease with which restraints can be introduced. This allows a fast application of different parameter sets for comparison and batch processing of calculated transitions. In the next sections, the features of AOMadillo are presented in a qualitative overview. For detailed guidance on the actual utilization of the package, the reader is referred to the manual, which is provided with the software package.

2.1 | Possible parameterizations

The AOMadillo package offers various options for parameterization of the ligand field. The default is a parameterization with $e_{\sigma}, e_{\pi}, e_{ds}$ for each ligand, where d-s mixing is considered and the two π -interactions are subsumed.

The d-s mixing parameter can be removed with a flag. This is advisable when the molecule is sufficiently close to a cubic symmetry (O_h or T_d), where d-s mixing plays no role.^{4,10,12}

Similarly, the π -interaction can be removed, although we do not recommend this at all. Even for ligands that had been considered σ -only so far, we expect a significant π -interaction.²⁵

The two π -interactions e_{π_x} and e_{π_y} can be discerned, which increases the parameter space. The additional angle that needs to be defined can be either provided by the user or calculated from the structure of the molecule. In the latter case, a third atom number is specified that defines a plane containing M-L-R which is perpendicular to the π_y -interaction. Vice versa, the π_x -interaction is then defined to lie in the M-L-R plane. Some publications denote the e_{π_x} and e_{π_y} parameters with $e_{\pi_{\parallel}}$ and $e_{\pi_{\perp}}$ to clarify their alignment relative to the respective ligand.^{4,26}

2.2 | Parameter restraints

In addition to global changes of the parameterization scheme, restraints can be introduced. In AOMadillo, hard and soft restraints are distinguished depending on how they are implemented. Hard restraints are those that cannot be violated, no matter how it may increase the cost of the fit. Examples of hard restraints are removing parameters as mentioned above, or setting fixed values for individual parameters. These values cannot be changed during the fitting routine, but are taken into account when calculating the cost.

Soft restraints are introduced as additional equations to the fitting procedure. If the fit deviates from the value specified in the additional equations, the overall cost increases. This permits the parameters to take values that differ from the given restraint. It is of course possible to set soft requirements that cause high costs when they are slightly violated, making them effectively hard.

Natively supported soft restraints are equal e_x parameters for different ligands and equal π_x, π_y interactions for selected ligands. Setting AOM parameters to be equal via a soft restraint is termed “grouping” in AOMadillo. Additional arbitrary restraints can be introduced by providing equations directly, for example to set a value, a ratio or a difference for selected parameters.

An important role of soft restraints is the introduction of independent equations to the system. Given that common complexes with six ligands and three parameters per ligand already exceed the maximum possible number of independent elements in V_{LF} , it is common to group ligands. We intentionally chose the addition of equations over the reduction of the number of parameters to account for small inequalities in the ligands positions and chemical environments.

3 | LIFTING THE UNDERDETERMINATION PROBLEM

Even when the number of AOM parameters is cleverly reduced, the equation system for many complexes remains underdetermined.

Sample	Cl1-Cr-Cl2	Cl3-Cr-Cl4	Cl5-Cr-Cl6	Cl1-Cr-Cl3	Cl1-Cr-Cl5
0	180.000	180.000	180.000	90.000	90.027
1	179.059	179.317	179.243	90.752	89.502
2	179.916	179.262	178.913	89.315	89.368
3	179.403	178.897	179.111	89.969	90.164
4	179.044	179.287	179.226	90.158	89.401
5	179.834	179.363	179.029	89.330	89.804

Note: The atoms 1, 2 and 3, 4 and 5, 6 are situated *trans* to each other. Sample 0 is the reference structure.

The higher the symmetry of the complex, the fewer unique elements V_{LF} has.¹¹ In an experiment, the observed transitions always belong to an ensemble of distorted structures, yielding broadened peaks. The underlying transitions cannot be completely resolved and thus it is necessary to assign the peaks to an assumed average geometry with generally high symmetry. Furthermore, many d-d transitions are hard to detect since they are generally weak and sometimes hidden under other, overlapping transitions. While computational spectroscopy has its own shortcomings, employing computational methods to calculate electronic transitions allows to overcome a few of these problems. Some of these advantages are that there is no ambiguity in the computed spectrum regarding the resolution and the assignment of a transition.

The key to lifting the underdetermination problem lies in intentionally creating asymmetric structures. Here, we make use of the transferability promise of the AOM that works in very limited cases, that is, the same ligand will have comparable AOM parameters in similar bonding situations. If AOMadillo is used with a high-symmetry structure, the ligands are moved slightly in random directions.* Asymmetric structures that yield ligand field potentials with a sufficient number of unique elements are obtained by starting from an optimized geometry. The bond angles are slightly changed while keeping the metal-ligand distance constant. In general, this leads to C_1 symmetry, in which 15 unique matrix elements are available for fitting. The result should be as asymmetric as possible while still being sufficiently similar to the reference structure to justify the AOM parameters to be equal. An example with distorted bond angles is shown in Table 1. We have shown previously that this approach works and allows to fit AOM parameters to formerly underdetermined problems such as tetrahedral²¹ and octahedral²⁵ complexes.

Since the structural distortion uses small random angles of $\leq 0.5^\circ$, two issues can arise. First, the distortion can be too small so that the resulting equation system is still (partly) underdetermined. Second, the resulting structure might be biased: bond angles differ from the average, the ligands might be shifted to one side and so forth. While this does not necessarily pose a problem for the CASSCF calculation and the subsequent fit, we noticed that some structures yield parameter sets that clearly differ from others. We cannot find a common explanation for these observed outliers, and suspect from our broad experience with different transition metals, coordination environments and ligand types that this effect is highly dependent on

the chemistry of the system. Outliers should be identifiable among a sufficiently large number of samples. We recommend performing the structural distortion several times and separately fitting parameters for each distorted structure. In this way, outliers can be identified more easily and the danger of having a non-representative parameter set is reduced.

4 | THE USER'S TASKS

4.1 | Choosing a parameter set

Choosing the parameter set is crucial and may require several attempts in order to recognize bad fitting results, underdetermination problems and specific ligand behaviors. This is an important task that must be conducted carefully by the user. The following points may serve as a guide to evaluate which parameters are sensible to use.

Check for equal ligands: The first step is to check the ligand symmetries and similarities. It is useful to group equal ligands together, although differences in bond length are very important to consider here. Since the AOM parameters are bond length dependent, grouping different bond lengths can lead to conflicting equations that prevent a reasonable solution of the AOM equation system. Nonetheless, grouping bonds of up to approximately 0.1 Å difference can work occasionally. When deciding on the acceptable bond length difference for grouping, the user needs to consider the slope of the distance dependence; while for transition metals the distance dependence of Δ is expected to be r^{-5} ,^{27,28} for lanthanides and actinides it is much steeper, ca. r^{-7} .²⁷

Assess bond symmetry: The next step is to check whether the individual metal-ligand bonds are cylindrical, that is, have $C_{\infty v}$ symmetry. This is not an automated process but rather a step where the users can take important decisions on the parameterization themselves. For symmetric bonds, e_{π_x} and e_{π_y} can be subsumed. If the bond is asymmetric, they must be distinguished. Examples for ligands with cylindrical bonds are halides, NH_3 , CO, CN^- , metallocenes and others. Asymmetric bonds are found for example with water, pyridine and other heterocyclic ligands.

Assess global symmetry: The global symmetry of the coordination site should be evaluated. This is not done automatically by AOMadillo, but programs that can determine the closest global

TABLE 1 Exemplary bond angles in degrees from a set of samples of $[CrCl_6]^{3-}$.

symmetry automatically are available if assistance is required. If at least one d orbital transforms in the totally symmetric irreducible representation of the point group of the coordination site, one must consider d-s mixing.

Based on the parameterization chosen by the user, AOMadillo can be configured to perform the fit accordingly. Note that a chemically plausible set of parameters does not necessarily lead to a good fitting result. A good result is considered to be (over-)determined, low-cost and with parameters of a reasonable magnitude.

4.2 | Assessing the result

The equation systems generally converge well. We never encountered a system where convergence was not achievable, although convergence of a mathematical solution to the equation system is not to be confused with obtaining reasonable parameter values. It is still possible that the system is underdetermined, in which case convergence will be signaled but the resulting fit is not unique. Note that the equation system can be partly underdetermined (see, for example, Section 7.3). In these cases, some of the parameters are reliable to a certain extent, while others depend on each other and are not unique. Because of this, a cost larger than zero does not guarantee an overdetermined system. We recommend to scan the parameter space around the solution in order to recognize partial underdetermination situations.

The cost of a fit is an important quantity to check. High cost values ($>1000 \text{ cm}^{-2}$) are most often caused by an incomplete parameterization, inappropriate ligand grouping or other hard to meet soft restraints. If tweaking groupings and parameter sets does not improve the cost, a suitable parameterization might not be attainable, see Section 5.1.

The resulting parameters should be of reasonable magnitude, that is, within the expectations set by the literature or previous parameterizations of similar systems. An obvious case of an unreliable result is for example a negative e_{σ} parameter. Parameters with significant differences for almost equal ligands or parameters that deviate strongly from reported data are also signs of error.

5 | LIMITATIONS

LFT, ORCA aiLFT and AOMadillo have important limitations that the user needs to be aware of. Some problems rooted in the general theory are carried over to the AOM parameterization. In the following, we will discuss how apparently nonsensical results can be interpreted, what to check before the fit is done and when LFT as such may fail.

Ligand field theory and ORCA aiLFT

LFT assumes pure valence d orbitals, which is a good assumption if there is essentially no mixing or covalency between metals and

ligands. This can be the case if the ligand orbitals are much lower in energy than the metal orbitals. The observed “pure” d orbitals are then in fact the antibonding metal-ligand molecular orbitals. In electronic structure calculations, it is readily seen that the valence molecular orbitals are composed of metal and ligand contributions of different magnitude. LFT is essentially an effective Hamiltonian theory,^{4,29} and as such it is more successful if the configurational space described by the effective Hamiltonian (here the complete ligand field Hamiltonian) is well separated from the rest of the basis.^{10,30} With a decrease of the d orbital contribution to the MOs, that is, more covalent bonds, LFT increasingly loses its justification and obtained parameterizations should be interpreted with caution.

ORCA purifies the metal d orbitals when the aiLFT subroutine is called in order to obtain an active space that fits to the assumptions of LFT.^{31,32} Nonetheless, the resulting orbitals can still have significant ligand character. Especially for more covalently bound ligands like CN^- or PMe_3 , d orbital contributions of about 80% and less to an active orbital are common. For ligands like halides, we generally find orbitals with more than 90% d character. Note that this can make it difficult to describe some common ligands with π -backbonding capabilities, since they arise from metal and ligand AOs that are close in energy and thus strongly mix.

Lastly, if LFT can be applied to a complex and a reasonable parameterization can be made, the calculation itself can have systematic errors. The states predicted by CASSCF or CASSCF/NEVPT2 calculations are associated with errors arising, for example, from the active space size, the basis set size, or the treatment of the environment. These errors translate into the ligand field Hamiltonian. In consequence, the user needs to set up the ORCA calculation according to the desired accuracy and inclusion of environment effects.

AOMadillo

AOMadillo applies the AOM equations to the aiLFT output of ORCA and returns a fitted set of parameters; however it does not provide any further comment on the set. Depending on the complex at hand, the least-squares fitting procedure can have multiple results with the same cost for different parameterizations. While it is possible to scan the parameter space around the solution obtained to find out how deep or well-defined the minimum is, this information does not tell the user how chemically reasonable the solution is. Judging the parameter set is thus a task obliged to the user.

It can be helpful to have a closer look at the AOM parameters of different structure samples. With sample set sizes of five as commonly employed in our initial studies, it has been observed that some samples yield unreasonable results. A unique reason for the outliers has not been identified, but the user is encouraged to investigate the structures further if fits with diverging results are obtained. Additional aiLFT calculations with more samples, possibly including a slight variation of bond lengths in addition to different angles, can be useful to deduce which results are actual outliers.

5.1 | Advanced aspects of the AOM

There are extensions of the AOM that are not yet supported by AOMadillo. One example is d-p mixing,³³ where in principle the same sequence of arguments as for d-s mixing applies. Very often, d-p mixing is subsumed with other parameters and cannot be separated. There are special cases where it becomes relevant and needs parameterization on its own, as for example encountered in Section 7.2. Since the chemical significance of the AOM may suffer by introducing more global parameters, we decided not to implement it.

Another extension is the Orgel effect or phase-coupled ligation.^{34–38} Different treatments and discussions exist in the literature. At the moment no variant is implemented in AOMadillo, which precludes fitting systems with chelating ligands that have conjugated π -systems properly.

Similarly, misdirected valency or off-axis bonding is currently not implemented. Misdirected valency occurs when no symmetry axis of the ligand coincides with the metal-ligand bond. More pictorially speaking, in cases where misdirected valency is important, the ligand does not point exactly at the metal which leads to an orbital energy splitting that cannot be accounted for in terms of distinct σ or π parameters. It is possible to parameterize the resulting splitting with additional AOM parameters which are placed in the off-diagonals of the ligands' local ligand-field matrices.^{30,38–42} These additional parameters may have less obvious chemical significance and rather represent a means to describe a geometric peculiarity within the AOM framework.

5.2 | Metals with f shells

The AOM is generally suitable to parameterize elements with partially filled f orbitals.^{43,44} Urland and coworkers have worked on this topic extensively, including the derivation of the corresponding overlap factors for these elements.^{11,45} The aiLFT module of ORCA provides an f orbital analysis, yielding a 7×7 ligand field matrix V_{LF} . In AOMadillo, the analysis of these aiLFT calculations is not yet implemented.

5.3 | Inclusion of δ interactions

It is common practise in the application of the AOM to omit e_δ entirely.⁷ It is considered small and often leads to overparameterization without additional chemical insight. We therefore decided not to implement it into the fitting routine.

6 | DETAILS

This section provides background information on how certain functions are derived and implemented. For more details on the practical application of the AOMadillo program, we refer the reader to the manual, where a detailed walkthrough is provided.

6.1 | Structure sampling

Structural sampling is crucial to lift the underdetermination problem of the AOM parameterization. It is also important to calculate parameters for several samples, since there might be outliers that can only be recognized in comparison to other parameter sets. In the AOMadillo package, the structural distortions are performed by a dedicated script; the manual provides details on its application. The sampling procedure takes Cartesian coordinates and a definition of ligands as input. Each ligand is then independently rotated by three random Euler angles in a given interval. The interval we use is [0,2,0.5], which has proven sufficient to yield completely asymmetric structures with sufficiently large energy differences in the ORCA aiLFT Hamiltonian. It is possible to apply the procedure to chelating and $\eta^{(\nu)}$ ligands, too. Depending on the ligand structure, a dummy atom in the center of the ligand may need to be defined which is then used as an anchor. For example, cyclopentadienyl (Cp^-) needs a dummy atom in the center of the ring, and ethylenediamine (en) can be moved with a dummy atom between the nitrogen or the carbon atoms.

When the samples are created, it is possible to read in orbitals from another CASSCF calculation performed on the original structure. ORCA has an orbital projection feature that can translate these orbitals onto the sample structures, hence one converged CASSCF calculation can be used as input for the subsequent samples, speeding up the process significantly.

Another feature embedded in the sampling procedure is the option to perform bond length scans. An interval with minimum and maximum bond length as well as the number of steps can be defined. The ligands are then moved accordingly. Note that although possible with the help of dummy atoms, this is not useful for chelating ligands, since their L-M-L bond angles are changed by this as well.

6.2 | AOM equation system

The one electron ligand field matrix is a 5×5 symmetric matrix, so it has up to 15 unique elements. Each element is expressed in terms of Equation (3), with v_{ij} being calculated by ORCA and the AOM overlap factors calculated from the structure of the complex. In general, this equation system is inconsistent and overdetermined. That means there is no set of parameters that satisfies all equations and there are more equations than parameters. Since there is no exact solution, an approximate one is found with the least-squares approximation mentioned in Section 2.

The parameters have hard coded boundaries: all local AOM parameters can have values in the interval $e_s/cm^{-1} \in [-2 \times 10^5, 2 \times 10^5]$, $e_{ds}/cm^{-1} \in [0, 10^4]$ and $E/cm^{-1} \in [-10^7, 0]$.

Soft restraints add equations to the base system. Grouping ligands adds equations of the following structure:

$$s_i = (e_{\lambda L1} - e_{\lambda L2}) \cdot w, \quad (5)$$

with L1 and L2 being arbitrary ligands and λ being the interaction type. The weighting factor w can be adjusted to increase or decrease the

effect of the restraint on the solution. s_i is the residue of the equation, its index i is a running number. In the same manner the equality of π_x and π_y -interactions can be set:

$$s_i = (e_{\pi_x,L} - e_{\pi_y,L}) \cdot W. \quad (6)$$

The least-squares solver will minimize the total cost and thus the absolute residues, so the requirements are met if the parameters are equal and their difference is zero.

With these additional equations, it is possible to have enough linearly independent equations to fit a large set of parameters. As stated, it has proven to be more effective if equations are added compared to the reduction of parameters. The possibility that a restraint can be violated adds valuable flexibility to the fit.

It is possible to add arbitrary equations to the system by giving expressions that should evaluate to zero. Only the right-hand side of the following equations must be given. This can be used to set parameter values without actually enforcing them or introduce ratios and differences. Here are some examples:

$$s_i = e_{\sigma,L} - 6000, \quad (7)$$

$$s_i = 4e_{\pi_x,L} - e_{\sigma,L}, \quad (8)$$

$$s_i = e_{\pi_y} - e_{\pi_x} - 1000. \quad (9)$$

It is up to the user to employ supplemental equations. They are provided to AOMadillo in an optional file; the standard configuration is not to expect such a file. We also note that introducing restraints removes impartiality from the result and should be well justified.

6.3 | Definition of π_x and π_y

It is chemically intuitive that planar ligands like water or pyridine have different π interactions in- and out-of-plane. To distinguish π_x and π_y , we have to resort to the definition of the parameters in the local parameter frame, where the ligand atom resides on the z-axis. The ligand field matrix expressed in the local d orbital basis for each ligand is:

$$V_{LF,local} = \begin{matrix} xy & yz & z^2 & xz & x^2 - y^2 \\ \begin{pmatrix} e_{\delta} & & & & 0 \\ & e_{\pi_y} & & & \\ & & e_{\sigma} & & \\ & & & e_{\pi_x} & \\ 0 & & & & e_{\delta} \end{pmatrix} \end{matrix}, \quad (10)$$

where e_{δ} is generally assumed to be 0. The superposition principle of the AOM requires to set up this matrix for each ligand, rotate it from its local to the global axis frame and then add it to the total ligand field

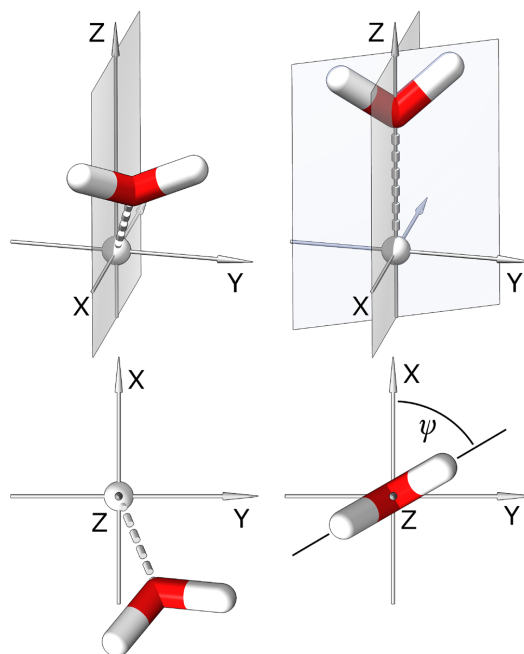


FIGURE 2 Illustration of the rotation of a ligand from an arbitrary position (left, top and bottom) onto the z-axis (right, top and bottom). The remaining angle between the ligand plane and the xz-plane is the angle ψ . The left and right frames each show the same situation from different perspectives in the top and bottom panels.

matrix.^{4,45} This rotation of the local basis can be expressed in terms of Wigner rotation matrices, which represent rotations of spherical harmonics along the three Euler angles θ, ϕ, ψ .^{11,13} The Euler angles are equivalent to the global angular coordinates of the respective ligand, since it is the ligands' global position from which the d orbital basis must be rotated. The sequence of the rotations is fixed such that the ones along θ and ϕ have to be applied in that sequence, while the rotation along ψ can be applied any time.^{11,46}

Employing that rule, we determine ψ for each ligand by rotating it back into its local frame. The ligand is thus rotated by $-\phi$ along the global z-axis and $-\theta$ along the global y-axis. An illustration of this rotation is shown in Figure 2. Additional to the metal position and the ligating atom, an orientation atom is specified that defines the ligand plane, for example, a hydrogen atom in water. The angle between the xz plane and the ligand plane is then ψ , as shown in the bottom right frame in Figure 2. If it is 0, the ligand plane coincides with the xz plane. By this definition, the parameter e_{π_x} lies in the ligand plane, while e_{π_y} is perpendicular, as stated in Section 2.1.

When applying the AOMadillo fitting routine with distinct π_x and π_y interactions, it is possible to specify ψ manually for each ligand, or to specify an orientation atom that, together with the metal and the ligating atom, defines the ligand plane.

7 | CASE STUDIES

7.1 | Methodology

All quantum chemical calculations were performed using the ORCA 4.2.1 software package.^{14,15} The geometries of the $[\text{Mn}(\text{NH}_3)_n]^{2+}$ series were constructed from scratch. The structure of $\text{Cu}(\text{NH}_3)_4(\text{SCN})_2$ was extracted from the crystal structure⁴⁷ with a subsequent optimization of the hydrogen atom positions. The structures of the platinum complexes and the ferric thiocyanates were fully optimized. Optimizations employed the unrestricted Kohn-Sham formalism with the BP86 functional,^{48,49} the def2-SVP basis set⁵⁰ with the def2/J auxiliary basis.⁵¹ The resolution of identity approximation for the Coulomb term was used.^{52,53} Convergence criteria were NormalSCF for all self-consistent field calculations and TightOpt for geometry optimizations. The geometry optimizations employed the default integration grid (Accuracy 2: Lebedev 110 points) for optimization steps and the final SCF at the optimized geometry (Accuracy 4: Lebedev 302 points).

The electronic states corresponding to the d orbitals were calculated using CASSCF^{54,55} with the def2-TZVP basis set.⁵⁰ For the platinum complexes, relativistic effects were captured with the zeroth order regular approximation (ZORA)⁵⁶ with the SARC-ZORA-def2-TZVP basis set for Pt and ZORA-def2-TZVP for other elements.⁵⁷ A CAS($n,5$) active space was chosen, containing n d electrons in the five valence d orbitals. The subsequent *ab initio* LFT analysis was used to construct the effective ligand field Hamiltonian.^{10,18,44} AOM parameters were fitted with the software presented herein, AOMadillo. For each (optimized) complex, five distorted samples were generated.

7.2 | Ligand addition

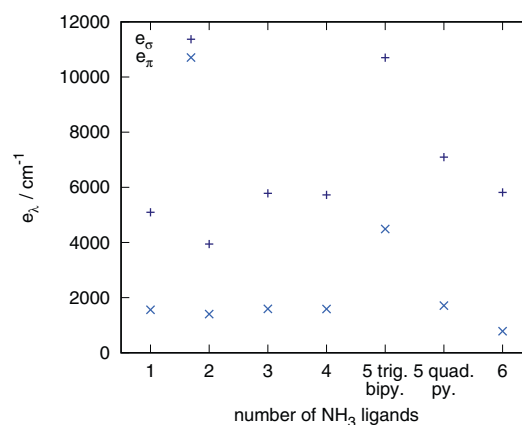
The AOM promises at least a limited transferability of ligand parameters between different complexes. While it is well known that this is rarely reliable, AOMadillo allows the user to systematically check in which cases a transfer might be justified and in which not. In the next section, we discuss the mixing of ligand types in a heteroleptic complex. Here, a simpler case is investigated, where we focus on a series of complexes of the type $[\text{Mn}(\text{NH}_3)_n]^{2+}$, with $n = 1 - 6$. Each complex has the highest possible symmetry, which should be reasonable for manganese in the oxidation state +II due to its preferred high-spin d^5 electronic structure. In the case of $n = 5$, we investigated the trigonal bipyramidal case as well as the quadratic pyramidal one. All bond lengths were arbitrarily set to 2.1 Å and do not differ between coordination numbers to preserve comparability.

Table 2 and Figure 3 show the AOM parameters of the complexes. It is apparent that the magnitude of the parameters is the same for all complexes except the trigonal bipyramidal $n = 5$ case. The linear $n = 2$ complex also has a slightly deviating σ parameter, although this is due to a d-s mixing effect. Introducing d-s mixing here leads to a linear dependency of e_σ and e_{ds} ; this effect is discussed in more detail in the next section on PtA_2B_2 complexes. Omitting a d-

TABLE 2 AOM parameters of ammonia in $[\text{Mn}(\text{NH}_3)_n]^{2+}$.

n	Symmetry	e_σ/cm^{-1}	e_z/cm^{-1}	e_{ds}/cm^{-1}
1	lin.	5094 (0)	1557 (0)	
2	lin.	3945 (0)	1401 (0)	<i>a</i>
3	trig.	5780 (1)	1594 (151)	715 (101)
4	tet.	5726 (168)	1588 (125)	
5	trig. bipy.	10700 (229)	4486 (179)	<i>b</i>
5	quad. py.	7097 (39)	1713 (42)	2524 (92)
6	oct.	5813 (56)	781 (42)	

Note: *a* not included, but relevant; see main text for details. *b* subject to d-p mixing; see main text for details.

FIGURE 3 AOM parameters of ammonia in $[\text{Mn}(\text{NH}_3)_n]^{2+}$. The two $n = 5$ geometries are labeled.

s mixing parameter leads the e_σ of the ligands to absorb its effect and decrease accordingly. If a fixed d-s mixing parameter of 715 cm^{-1} is introduced, we obtain $e_\sigma = 5375 \text{ cm}^{-1}$ which would fit perfectly to the other parameters in the series.

The mutual dependence of e_σ and e_{ds} was noted recently by Deeth, who stated “[...] the extent of σ bonding is no longer directly linked to the size of e_σ , but rather it is masked by the d-s mixing.”⁵⁸ One might also say that without the d-s mixing parameter, the σ parameter of the ligand is artificially lowered since it then absorbs the effect of the admixture of the s orbital. In this case, the “true” σ interaction would be higher than reflected in the parameter value. Both interpretations work within the framework of the AOM, so it is difficult to decide on that basis which one is more appropriate.

The trigonal bipyramidal structure is an example where the parameterization with AOMadillo does not suffice to capture all effects. Its parameters have very high magnitudes, which are essentially unaffected by different grouping options and inclusion of d-s mixing. This complex appears to be an example where d-p mixing effects should not be omitted, as pointed out by Smith.¹² In the given

TABLE 3 AOM expressions for d orbital energies in a trigonal bipyramidal complex in different parameterizations.

Orbital	AOMadillo parameter set	Manually adapted parameter set
d_{z^2}	$2.75e_\sigma - 0.25e_{ds}$	$2.75e_\sigma$
d_{xz}	$3.5e_\pi$	$3.5e_\pi$
d_{yz}	$3.5e_\pi$	$3.5e_\pi$
d_{xy}	$1.125e_\sigma + 1.5e_\pi$	$1.125e_\sigma + 1.5e_\pi - C_{dp}$
$d_{x^2-y^2}$	$1.125e_\sigma + 1.5e_\pi$	$1.125e_\sigma + 1.5e_\pi - C_{dp}$

D_{3h} symmetry, the d_{xy} and $d_{x^2-y^2}$ orbitals are allowed to mix with the p_x and p_y orbitals. Additionally, d-s mixing is expected for the d_{z^2} orbital. The MO coefficients of the active space show that there is almost no d-s mixing with the d_{z^2} orbital (90.9% d_{z^2} , 0.1% s), but indeed a considerable p character in the $d_{xy}/d_{x^2-y^2}$ orbitals (94.4% $d_{xy}/d_{x^2-y^2}$, 1.7% p_x/p_y).[†] We tested a parameterization with slight changes: e_{ds} is set to 0, but we introduced a correction term C_{dp} that decreases the energy of the $d_{xy}/d_{x^2-y^2}$ orbitals. The equations we used are presented in Table 3. With this set of parameters in an ideal D_{3h} geometry, the equation system is underdetermined and at least one parameter needs to be fixed. Setting $e_\sigma = 5800 \text{ cm}^{-1}$ as an example, we obtain $e_\pi = 631 \text{ cm}^{-1}$ and $C_{dp} = 2319 \text{ cm}^{-1}$. We emphasize that C_{dp} is a correction term which subsumes angular factors F_{dp} that would be present in a systematic way of treating d-p mixing. Thus it cannot be compared to other parameters.

Other structures show similar fractions of p orbital admixture, but d-p mixing is absorbed in other parameters. In the trigonal bipyramid, no other parameter can subsume the d-p mixing effect and it must be accounted for explicitly to achieve a reasonable fit. A similar effect explains the extraordinarily large d-s mixing parameter of the quadratic pyramid. Here, a significant d-p mixing contribution is subsumed in e_{ds} , rendering it surprisingly large.

We can conclude that the parameters of ammonia in the given geometries are relatively consistent amongst each other. However, the series shows that the overall symmetry of a complex must be kept in mind (as for $n=2$ and $n=5$) and that it is always possible to encounter geometries for which no reasonable fit can be obtained. Lastly, it is important to emphasize that AOM parameters are bond length dependent, a variable that substantially changes among different heteroleptic complexes. We caution to transfer parameters; this is conceivable only for similar bond lengths, or when using a scan of the respective metal-ligand distance to evaluate the effect on the respective e_i parameters.

7.3 | [PtA₂B₂]

Cisplatin *cis*-[PtCl₂(NH₃)₂] and its homoleptic analogues are well known complexes with planar geometries.^{59,60} We investigated the homoleptic complexes of Pt²⁺ with chloride, ammonia and water as

ligands as well as their heteroleptic [PtA₂B₂]ⁿ⁺ counterparts. The results are shown in Table 4. It is apparent that the homoleptic complexes yield consistent and plausible parameters with d-s mixing included. The values for the ammonia ligands fit well to experimental values, while the chloride parameters seem to be underestimated.⁵⁹ Excluding d-s mixing leads to a very high cost, since the position of the d_{z^2} orbital cannot be accounted for. The heteroleptic complexes are much more complicated: While the π parameters of the *trans* complexes are stable with a small standard deviation, the parameters for the *cis* complexes appear random. The full results over all samples suggest that there is a dependency between e_σ and e_{ds} , whereas e_π is well defined with the given orbital splitting.

To visualize the dependency between e_σ and e_{ds} , we performed a scan along e_{ds} of the water ligands for a single sample of [PtCl₂(H₂O)₂]. The resulting parameters are shown in Figure 4. We can see that there is a cost minimum around $e_{ds} = 2300 \text{ cm}^{-1}$, but it is very shallow. The second panel of Figure 4 illustrates the dependency of e_{ds} and e_σ , with an apparently linear relationship to e_σ of the water ligand. Not depicted but also part of the dependency is e_{ds} of the chloride ligands. In contrast, e_{ds} and e_π are essentially unrelated, as shown in the third panel. Performing the same scan for different samples yields slightly shifted, but qualitatively equal curves. The *trans* complexes are a good example of a partial underdetermination, where some of the orbital energies are well defined, while others are overparameterized.

As apparent in Table 4, the *cis* complexes do not yield a stable or plausible result. The reason is a splitting in the d_{xz} and d_{yz} orbitals that should be degenerate in the AOM parameterization with ligands A and B. Both orbital energies are expressed as

$$e_{d_{xz}} = e_{d_{yz}} = e_{\pi,A} + e_{\pi,B}, \quad (11)$$

but are found with a difference $e_{d_{xz}} - e_{d_{yz}} = 512 \text{ cm}^{-1}$ in the aiLFT analysis.

Such an unexpected orbital energy splitting has been observed for other planar *cis* complexes. Hitchman noticed this type of splitting for Co(salen),⁶¹ which was later attributed to the phase-coupling in the salen ligand.³⁵ Since the Pt complexes studied here do not have phase-coupled ligands, the cause of the d orbital splitting is unclear. Deeth attributed it to an asymmetric π -interaction of coordination voids on the z-axis.²⁶

Without a specific parameter that accounts for the observed energy splitting, the fit cannot work well, making e_π indeterminate. Additionally, the dependency of e_σ and e_{ds} remains a problem as for the *trans* complexes, making it impossible to obtain a reasonable AOM parameterization.

7.4 | [Cu(NH₃)₄(SCN)₂]

[Cu(NH₃)₄(SCN)₂] is a good example of a complex where different parameterizations work well. The geometry is taken from the crystal structure; the coordination units are separate and no other ions are

TABLE 4 AOM parameters of different planar $[\text{PtA}_4]^{n+}$ and $[\text{PtA}_2\text{B}_2]^{n+}$ complexes with the ligands chloride, ammonia and water.

Complex	Cl			NH_3		
	e_σ/cm^{-1}	e_π/cm^{-1}	e_{ds}/cm^{-1}	e_σ/cm^{-1}	e_π/cm^{-1}	e_{ds}/cm^{-1}
$[\text{PtCl}_4]^{2-}$	8739 (1)	1710 (1)	2297 (1)			
$[\text{Pt}(\text{NH}_3)_4]^{2+}$				14109 (5)	1670 (4)	2842 (2)
<i>trans</i> - $[\text{PtCl}_2(\text{NH}_3)_2]$	8770 (1873)	3097 (1)	1298 (933)	23939 (5896)	497 (5)	8525 (2950)
<i>cis</i> - $[\text{PtCl}_2(\text{NH}_3)_2]$	14380 (6382)	4364 (451)	5842 (3748)	9498 (6488)	-1244 (472)	2493 (3281)
Complex	Cl			H_2O		
	e_σ/cm^{-1}	e_π/cm^{-1}	e_{ds}/cm^{-1}	e_σ/cm^{-1}	e_π/cm^{-1}	e_{ds}/cm^{-1}
$[\text{PtCl}_4]^{2-}$	8739 (1)	1710 (1)	2297 (1)			
$[\text{Pt}(\text{H}_2\text{O})_4]^{2+}$				13335 (71)	3946 (102)	1421 (15)
<i>trans</i> - $[\text{PtCl}_2(\text{H}_2\text{O})_2]$	10496 (6684)	1811 (6)	3574 (3309)	13938 (6384)	652 (55)	3957 (3219)
<i>cis</i> - $[\text{PtCl}_2(\text{H}_2\text{O})_2]$	10267 (1899)	1379 (1123)	160 (319)	9568 (1844)	1688 (1093)	9012 (1932)
Complex	NH_3			H_2O		
	e_σ/cm^{-1}	e_π/cm^{-1}	e_{ds}/cm^{-1}	e_σ/cm^{-1}	e_π/cm^{-1}	e_{ds}/cm^{-1}
$[\text{Pt}(\text{NH}_3)_4]^{2+}$	14109 (5)	1670 (4)	2842 (2)			
$[\text{Pt}(\text{H}_2\text{O})_4]^{2+}$				13335 (71)	3946 (102)	1421 (15)
<i>trans</i> - $[\text{Pt}(\text{NH}_3)_2(\text{H}_2\text{O})_2]^{2+}$	20168 (9369)	2525 (20)	6173 (4686)	18607 (9373)	2683 (18)	4259 (4684)
<i>cis</i> - $[\text{Pt}(\text{NH}_3)_2(\text{H}_2\text{O})_2]^{2+}$	34348 (16,547)	21746 (12246)	3891 (3518)	-6821 (16588)	-16587 (12246)	3242 (3540)

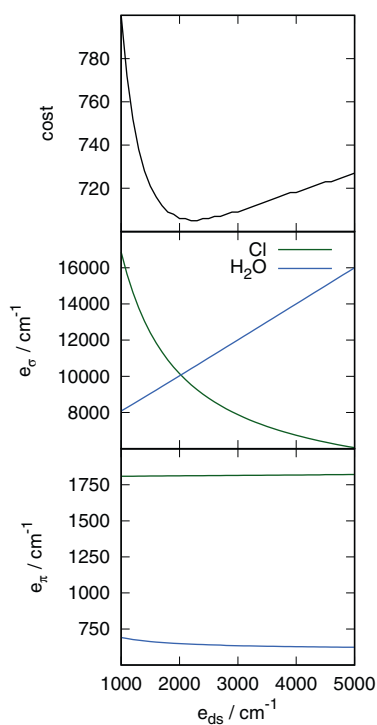


FIGURE 4 AOM parameters and cost of the fits for a single sample of *trans*- $[\text{PtCl}_2(\text{H}_2\text{O})_2]$ while scanning along e_{ds} of the water ligands. Fits are obtained with each chloride and water in a group. Steps in the cost plot are caused by the integer resolution of the fit output.

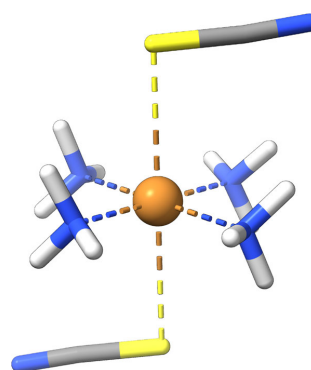


FIGURE 5 Coordination unit of $\text{Cu}(\text{NH}_3)_4(\text{SCN})_2$. Notice the bent Cu-S-CN bond that suggests a distinction between π_x and π_y interactions and explains the pronounced misdirected valency.

present in the crystal.⁴⁷ Hydrogen atoms were added to complete the ammine ligands and a H-only geometry optimization was performed,[†] see Figure 5 for the optimized structure. The sampling procedure was applied and different parameterizations were tested, shown in Table 5. It is interesting to note that the three parameterizations shown yield reasonable parameters, although at different costs. The remaining, relatively high costs in each fit can be explained by a significant misdirected valency because of the bent Cu-S-CN bond, which we cannot capture.

With a D_{4h} coordination sphere, one must in principle consider d-s mixing. However, Gerloch, Woolley, and Deeth showed that placing imaginary ligands at the z-axis can account for the low energy of

TABLE 5 Parameters for $\text{Cu}(\text{NH}_3)_4(\text{SCN})_2$ with different parameterizations.

Ligand	Parameter/cm ⁻¹	no d-s, one e_π	d-s, one e_π	d-s, two e_π
NH ₃	e_σ	3604 (141)	3686 (79)	3769 (76)
	e_{π_x}	114 (108)	170 (59)	232 (59)
	e_{π_y}			232 (58)
	e_{ds}		567 (15)	564 (15)
SCN	e_σ	-779 (133)	356 (61)	438 (62)
	e_{π_x}	-495 (97)	-429 (54)	-400 (51)
	e_{π_y}			-330 (57)
	e_{ds}		1 (1)	0 (1)
Cost		71065 (7441)	6227 (1281)	4507 (1067)

Note: All AOM parameters in /cm⁻¹.

TABLE 6 AOM parameters for a series of $[\text{Fe}(\text{H}_2\text{O})_{6-n}(\text{NCS})_n]^{(3-n)+}$ complexes with different configurations.

Complex	H ₂ O		H ₂ O'		NCS ⁻	
	e_σ/cm^{-1}	e_π/cm^{-1}	e_σ/cm^{-1}	e_π/cm^{-1}	e_σ/cm^{-1}	e_π/cm^{-1}
m6 $[\text{Fe}(\text{H}_2\text{O})_6]^{3+}$	4527 (205)	1055 (154)				
m6 $[\text{Fe}(\text{H}_2\text{O})_5(\text{NCS})]^{2+}$	3321 (150)	694 (81)			9997 (99)	4823 (63)
m4 $[\text{Fe}(\text{H}_2\text{O})_5(\text{NCS})_2]^{2+}$	6500 (24)	974 (21)	1397 (11)	412 (7)	11236 (10)	6493 (11)
m6 <i>trans</i> - $[\text{Fe}(\text{H}_2\text{O})_4(\text{NCS})_2]^{2+}$ ^a	2553 (284)	311 (215)			7715 (282)	2405 (212)
m4 <i>trans</i> - $[\text{Fe}(\text{H}_2\text{O})_4(\text{NCS})_2]^{2+}$ ^b	6309 (14)	1255 (8)	1225 (14)	598 (5)	10,488 (8)	4130 (12)
m6 <i>cis</i> - $[\text{Fe}(\text{H}_2\text{O})_4(\text{NCS})_2]^{2+}$	1877 (150)	-49 (77)			8172 (51)	2544 (34)
m4 <i>cis</i> - $[\text{Fe}(\text{H}_2\text{O})_4(\text{NCS})_2]^{2+}$ ^b	4573 (929)	3511 (686)	15300 (1753)	7962 (1397)	6360 (642)	331 (531)
m2 <i>cis</i> - $[\text{Fe}(\text{H}_2\text{O})_4(\text{NCS})_2]^{2+}$ ^b	2479 (225)	-1342 (154)	1412 (244)	-586 (176)	8316 (265)	415 (195)
m2 <i>cis</i> - $[\text{Fe}(\text{H}_2\text{O})_4(\text{NCS})_2]^{2+}$ ^b	2274 (356)	-1099 (384)			7770 (194)	762 (182)
m6 trig.-bipy. $[\text{Fe}(\text{H}_2\text{O})_2(\text{NCS})_3]^{3+}$ ^c	388 (106)	-256 (127)			6269 (232)	-1160 (81)
m4 <i>mer</i> - $[\text{Fe}(\text{H}_2\text{O})_3(\text{NCS})_3]^{3+}$ ^b	8067 (1434)	5109 (958)			15583 (1366)	6855 (903)
m6 $[\text{Fe}(\text{H}_2\text{O})_2(\text{NCS})_3]^{3+}$ ^c	1386 (153)	90 (102)			6312 (663)	1179 (347)
m4 <i>fac</i> - $[\text{Fe}(\text{H}_2\text{O})_3(\text{NCS})_3]^{3+}$ ^b	4505 (906)	1839 (352)			9778 (804)	3032 (265)

Note: For water sometimes two parameter sets are given in case of different M-O bond lengths.

^aInterestingly, the inclusion of d-s mixing does not change the fit substantially.

^bNot the ground state multiplicity.

^cFive-coordinate.

the d_{z^2} orbital as well. These coordination voids then have a negative e_σ and an e_π of 0.^{4,13,62,63} Indeed, the fits show that the SCN^- ligands, lying on the z-axis, subsume the effect of d-s mixing in their σ parameter. When fitting without d-s mixing parameter, SCN^- seems to be a σ acceptor. With d-s mixing considered, it changes from an acceptor to a weak donor. Of course it is not the chemistry that changes, but rather its projection onto the model. Assuming that SCN^- being a σ acceptor is unlikely, this example shows that the concept of the coordination void (besides other disadvantages that have been noted in the literature³³) might not adequately reproduce the ligand field splitting of these MA_4B_2 quasi D_{4h} complexes. Including a separation of π_x and π_y interactions to account for the bent Cu-S-CN bond does not generally alter the picture. The splitting of the π parameters is small and does not justify an interpretation.

In this example, three different parameterizations yield plausible results and one has to check carefully which one is the most useful, that is, which one can be interpreted chemically. In this case, the first parameterization without e_{ds} leads to a negative e_σ , which seems improbable. The second and third one yield similar results with a much lower cost than the first fit. Since overparameterization is an omnipresent danger when dealing with the AOM, we would prefer the second set with subsumed e_π parameters.

7.5 | Ferric thiocyanates

The heteroleptic $[\text{Fe}(\text{H}_2\text{O})_{6-n}(\text{NCS})_n]^{(3-n)+}$ complexes are known for their intense red color and serve as a qualitative tool for the detection

of Fe^{3+} ions.⁶⁴ Although the characteristic color emerges from a charge-transfer instead of a d-d transition, the stability and variety of this family of complexes makes it a good example for the same ligand having strongly varying parameters in different bonding situations. The thiocyanate ion can coordinate via the sulfur or nitrogen atom. Based on the HSAB principle,⁶⁵ the hard Fe^{3+} ion is likely to prefer a hard Lewis base, hence the Fe-NCS coordination is to be expected. This is supported by experimental evidence⁶⁶ as well as our calculations, which predict the nitrogen coordinating complexes to be ca. 60 $\text{kJ}\cdot\text{mol}^{-1}$ more stable than the sulfur coordinating ones in the $n=1$ case. We investigated and present complexes with $n=0-3$, which includes the *cis* and *trans* configurations for $n=2$ and the *fac* and *mer* configurations for $n=3$. The high-spin $n=3$ complexes are not stable in our solvent-free calculations, they lose one water ligand and form 5-coordinate complexes.

The obtained data is presented in Table 6. It is apparent that the range of parameter values is very large. They differ among the complexes and depend largely on bond distance, global symmetry and other ligands. Here, these dependencies are intertwined in a way that it is impossible to separate them. Transferability issues are well known⁷ and especially the mutual influence of *trans* ligands was discussed critically.⁸ This again shows that transferability of AOM parameters between complexes is extremely limited, even between stereoisomers.

8 | CONCLUSIONS

With the above examples and the ones in previous publications^{21,25} it is shown that our procedure can be applied to a variety of transition metal complexes. Nonetheless, the user must be careful and aware of problems and ambiguities in the AOM parameterization choices that might not be obvious.

In the example of $[\text{Cu}(\text{NH}_3)_4(\text{SCN})_2]$, we saw that different parameterizations for the same complex may work well and yield equally reasonable parameter sets. It is not obvious at first glance which parameterization is the one that corresponds best to the chemistry of the complex. We suggest to refer to the expected properties of the ligands in order to rule out certain results.

The example of ligand addition from a metal-ligand pair up to an octahedral complex brought up a similar problem and another way of treating it: while knowing that the linear $[\text{Mn}(\text{NH}_3)_2]^{2+}$ should have a d-s mixing contribution, its magnitude cannot be determined from the single complex itself. Comparing the obtained AOM parameters with similar complexes gives us a hint of what the parameter is likely to be.

The last example of the ferric thiocyanates brings us close to the boundaries of both approaches. Due to the effects that different ligands have on each other, especially regarding their varying bond lengths in different complexes, the transfer of AOM parameters from one complex to another is delicate.⁷⁻⁹ With the presented data set, it is difficult to determine with high confidence which set is reliable. Ideally, one would compare the obtained parameterization for such

cases with experimental data from electronic absorption measurements or magnetic data.

In treating the platinum complexes, we showed that even for seemingly simple complexes, one can face difficulties to fit a reasonable set of AOM parameters. We showed an example of partial dependencies in the AOM equation system and cases where the parameterization does not fully work.

While the examples above were chosen to highlight challenges and pitfalls in applying the AOM to transition metal complexes, the utility of having an unbiased fitting tool was also demonstrated herein and in earlier works. The easy applicability of AOMadillo combined with the chemically intuitive AOM parameters make it a tool that might be used in teaching as well. With aiLFT results from ORCA, the transitions themselves can be discussed. When using AOMadillo to obtain AOM parameters, the students would be tasked with important choices regarding ligand grouping and parameter sets, while the mathematics are hidden. It is thus a good tool to test different parameterizations and study LFT and the AOM in a hands-on fashion.

There are many examples for which the combination of LFT, AOM and computational chemistry work in a clear and unambiguous way. As we showed in previous publications,^{21,25} it is possible to perform bond length and angle scans that can be automatically parameterized by AOMadillo. Series over different transition metals or different formal oxidation states are often instructive: they yield results that can be parameterized well by the AOM and generally have clear interpretations. Sometimes trickier, but nevertheless often successful, are series with different ligands, where qualitative comparisons between ligands in similar environments can be made.

ACKNOWLEDGMENT

This work was funded by the Deutsche Forschungsgemeinschaft (DFG, German Research Foundation) – CRC 1487, “Iron, upgraded!” – project number 443703006. Open Access funding enabled and organized by Projekt DEAL.

DATA AVAILABILITY STATEMENT

Data from the case studies is available from the authors upon request. The program presented herein is freely available for academic research under <https://git.rwth-aachen.de/ak-krewald/aomadillo>.

ORCID

Moritz Buchhorn  <https://orcid.org/0000-0002-6800-1785>

Vera Krewald  <https://orcid.org/0000-0002-4749-4357>

ENDNOTES

* We note that distortions along normal modes are successfully employed in other research areas such as theoretical photochemistry or concepts for electron transfer; applying a Wigner-type sampling procedure here did not result in useful sample sets.

† For comparison, we found 1.3% s character in the d_{z^2} orbital of D_{4h} $[\text{Cu}(\text{NH}_3)_4]^{2+}$, which can be considered an archetypal example of d-s mixing.²⁵

‡ If optimized freely, the SCN^- ligands orient themselves to the hydrogen atoms and a Cu-SCN-H-N-Cu pseudo-cycle forms.

REFERENCES

- [1] C. E. Schäffer, C. K. Jørgensen, *Mol. Phys.* **1965**, *9*, 401.
- [2] B. N. Figgis, M. A. Hitchman, *Ligand Field Theory and Its Applications*, 1st ed., Wiley-VCH, New York **2000**.
- [3] M. Gerloch, R. G. Woolley, in *Progress in Inorganic Chemistry* (Ed: S. J. Lippard), John Wiley & Sons, Interscience, New York **1984**, p. 371.
- [4] M. Gerloch, J. H. Harding, R. G. Woolley, *Inorganic Chemistry*, Springer, Berlin **1981**, p. 1.
- [5] I. Bertini, D. Gatteschi, A. Scozzafava, *Inorg. Chem.* **1975**, *14*, 812.
- [6] T. Schönherr, in *Topics in current chemistry* (Ed: H. Yersin), Springer, Berlin **1997**, p. 87.
- [7] M. Gerloch, R. G. Woolley, *J. Chem. Soc., Dalton Trans.* **1981**, 1714.
- [8] D. W. Smith, *Inorg. Chem.* **1978**, *17*, 3153.
- [9] A. J. Bridgeman, M. Gerloch, in *Progress in Inorganic Chemistry* (Ed: K. D. Karlin), Wiley, New York **1996**, p. 179.
- [10] M. Atanasov, D. Ganyushin, K. Sivalingam, F. Neese, in *Molecular Electronic Structures of Transition Metal Complexes II. Structure and Bonding* (Ed: D. M. P. Mingos), Springer, Berlin **2011**, p. 149.
- [11] M. Suta, F. Cimpoesu, W. Urland, *Coord. Chem. Rev.* **2021**, *441*, 213981.
- [12] D. W. Smith, *Inorg. Chim. Acta* **1977**, *22*, 107.
- [13] R. J. Deeth, D. L. Foulis, *Phys. Chem. Chem. Phys.* **2002**, *4*, 4292.
- [14] F. Neese, *Wiley Interdiscip. Rev.: Comput. Mol. Sci.* **2012**, *2*, 73.
- [15] F. Neese, *Wiley Interdiscip. Rev.: Comput. Mol. Sci.* **2018**, *8*, e1327.
- [16] E. A. Suturina, D. Maganas, E. Bill, M. Atanasov, F. Neese, *Inorg. Chem.* **2015**, *54*, 9948.
- [17] D. Schweinfurth, M. G. Sommer, M. Atanasov, S. Demeshko, S. Hohloch, F. Meyer, F. Neese, B. Sarkar, *J. Am. Chem. Soc.* **2015**, *137*, 1993.
- [18] S. K. Singh, J. Eng, M. Atanasov, F. Neese, *Coord. Chem. Rev.* **2017**, *344*, 2.
- [19] V. G. Chilkuri, S. DeBeer, F. Neese, *Inorg. Chem.* **2017**, *56*, 10418.
- [20] V. G. Chilkuri, S. DeBeer, F. Neese, *Inorg. Chem.* **2020**, *59*, 984.
- [21] M. Buchhorn, R. J. Deeth, V. Krewald, *Chem. – Eur. J.* **2022**, *28*, e202103775.
- [22] W. H. Press, *Numerical Recipes: The Art of Scientific Computing/William H. Press ... [et al.]*, 3rd ed., Cambridge University Press, Cambridge **2007**.
- [23] P. Virtanen, R. Gommers, T. E. Oliphant, M. Haberland, T. Reddy, D. Cournapeau, E. Burovski, P. Peterson, W. Weckesser, J. Bright, S. J. van der Walt, M. Brett, J. Wilson, K. J. Millman, N. Mayorov, A. R. J. Nelson, E. Jones, R. Kern, E. Larson, C. J. Carey, Í. Polat, Y. Feng, E. W. Moore, J. VanderPlas, D. Laxalde, J. Perktold, R. Cimrman, I. Henriksen, E. A. Quintero, C. R. Harris, A. M. Archibald, A. H. Ribeiro, F. Pedregosa, P. van Mulbregt, *Nat. Methods* **2020**, *17*, 352.
- [24] P. Virtanen, R. Gommers, T. E. Oliphant, M. Haberland, T. Reddy, D. Cournapeau, E. Burovski, P. Peterson, W. Weckesser, J. Bright, S. J. van der Walt, M. Brett, J. Wilson, K. J. Millman, N. Mayorov, A. R. J. Nelson, E. Jones, R. Kern, E. Larson, C. J. Carey, Í. Polat, Y. Feng, E. W. Moore, J. VanderPlas, D. Laxalde, J. Perktold, R. Cimrman, I. Henriksen, E. A. Quintero, C. R. Harris, A. M. Archibald, A. H. Ribeiro, F. Pedregosa, P. van Mulbregt, *Nat. Methods* **2020**, *17*, 261.
- [25] M. Buchhorn, V. Krewald, *Dalton Trans.* **2023**, *52*, 6685.
- [26] R. J. Deeth, *Eur. J. Inorg. Chem.* **2020**, *2020*, 1960.
- [27] D. W. Clack, C. Mingdan, K. D. Warren, *J. Mol. Struct.: THEOCHEM* **1987**, *153*, 323.
- [28] A. Trueba, P. Garcia-Fernandez, J. M. Garcia-Lastra, J. A. Aramburu, M. T. Barriuso, M. Moreno, *J. Phys. Chem. A* **2011**, *115*, 1423.
- [29] F. Neese, L. Lang, V. G. Chilkuri, in *Topology, Entanglement, and Strong Correlations* (Eds: E. Pavarini, E. Koch), Forschungszentrum Jülich, Jülich **2020**.
- [30] M. Atanasov, P. Comba, C. A. Daul, F. Neese, in *Models, Mysteries, and Magic of Molecules* (Eds: J. C. A. Boeyens, J. F. Ogilvie), Springer, Dordrecht, The Netherlands **2008**, p. 411.
- [31] F. Neese, F. Wennmohs, *ORCA 4.2.1 Manual*, Max-Planck-Institut für Kohleforschung, Mülheim an der Ruhr **2019**.
- [32] F. Neese, F. Wennmohs, *ORCA 5.0.4 Manual*, Max-Planck-Institut für Kohleforschung, Mülheim an der Ruhr **2021**.
- [33] C. E. Schäffer, *Inorg. Chim. Acta* **1995**, *240*, 581.
- [34] A. Ceulemans, M. Dendooven, L. G. Vanquickenborne, *Inorg. Chem.* **1985**, *24*, 1153.
- [35] A. Ceulemans, M. Dendooven, L. G. Vanquickenborne, *Inorg. Chem.* **1985**, *24*, 1159.
- [36] C. E. Schäffer, H. Yamatera, *Inorg. Chem.* **1991**, *30*, 2840.
- [37] M. A. Atanasov, T. Schönherr, H.-H. Schmidtke, *Theor. Chim. Acta* **1987**, *71*, 59.
- [38] T. Schönherr, M. Atanasov, H. Adamsky, in *Comprehensive Coordination Chemistry II* (Eds: J. A. McCleverty, T. J. Meyer), Elsevier Pergamon, London **2004**, p. 443.
- [39] R. J. Deeth, M. J. Duer, M. Gerloch, *Inorg. Chem.* **1987**, *26*, 2573.
- [40] R. J. Deeth, M. J. Duer, M. Gerloch, *Inorg. Chem.* **1987**, *26*, 2578.
- [41] R. J. Deeth, M. Gerloch, *Inorg. Chem.* **1987**, *26*, 2582.
- [42] M. J. Duer, N. D. Fenton, M. Gerloch, *Int. Rev. Phys. Chem.* **1990**, *9*, 227.
- [43] A. Bronova, T. Bredow, R. Glaum, W. Urland, *Inorg. Chem.* **2016**, *55*, 6853.
- [44] J. Jung, M. Atanasov, F. Neese, *Inorg. Chem.* **2017**, *56*, 8802.
- [45] W. Urland, *Chem. Phys.* **1976**, *14*, 393.
- [46] M. A. Morrison, G. A. Parker, *Aust. J. Phys.* **1987**, *40*, 465.
- [47] M. A. Porai-Koshits, *J. Struct. Chem.* **1964**, *4*, 531.
- [48] A. D. Becke, *Phys. Rev. B* **1988**, *38*, 3098.
- [49] J. P. Perdew, *Phys. Rev. B* **1986**, *33*, 8822.
- [50] F. Weigend, R. Ahlrichs, *Phys. Chem. Chem. Phys.* **2005**, *7*, 3297.
- [51] F. Weigend, *Phys. Chem. Chem. Phys.* **2006**, *8*, 1057.
- [52] E. J. Baerends, D. E. Ellis, P. Ros, *Chem. Phys.* **1973**, *2*, 41.
- [53] O. Vahtras, J. Almlöf, M. W. Feyereisen, *Chem. Phys. Lett.* **1993**, *213*, 514.
- [54] P. Siegbahn, A. Heiberg, B. Roos, B. Levy, *Phys. Scr.* **1980**, *21*, 323.
- [55] B. O. Roos, P. R. Taylor, P. E. Siegbahn, *Chem. Phys.* **1980**, *48*, 157.
- [56] C. van Wüllen, *J. Chem. Phys.* **1998**, *109*, 392.
- [57] D. A. Pantazis, F. Neese, *WIREs Comput. Mol. Sci.* **2014**, *4*, 363.
- [58] R. J. Deeth, *Eur. J. Inorg. Chem.* **2022**, *2022*, e202100936.
- [59] L. G. Vanquickenborne, A. Ceulemans, *Inorg. Chem.* **1981**, *20*, 796.
- [60] A. J. Bridgeman, M. Gerloch, *J. Chem. Soc., Dalton Trans.* **1995**, 197.
- [61] M. A. Hitchman, *Inorg. Chem.* **1977**, *16*, 1985.
- [62] R. J. Deeth, M. Gerloch, *Inorg. Chem.* **1984**, *23*, 3846.
- [63] R. G. Woolley, *Int. Rev. Phys. Chem.* **1987**, *6*, 93.
- [64] S. A. Lewin, R. S. Wagner, *J. Chem. Educ.* **1953**, *30*, 445.
- [65] R. G. Pearson, *J. Am. Chem. Soc.* **1963**, *85*, 3533.
- [66] T. J. Conoccioli, N. Sutin, *J. Am. Chem. Soc.* **1967**, *89*, 282.

How to cite this article: M. Buchhorn, V. Krewald, *J. Comput. Chem.* **2023**, *1*, <https://doi.org/10.1002/jcc.27224>

AOMadillo Manual

Moritz Buchhorn, Vera Krewald
TU Darmstadt, Theoretische Chemie
Peter-Grünberg-Straße 4, 64287 Darmstadt

2023

Contents

1	Installation	2
1.1	Prerequisites	2
1.2	Package overview	2
2	Tests and examples	4
2.1	Test 1: octahedral ligand sphere, chemically equal ligands	4
2.2	Test 2: metal-ligand pair with different π interactions	5
2.3	Test 3: square-planar ligand sphere, chemically equal ligands	5
2.4	Test 4: MA ₄ B ₂ complex	6
3	Command reference	7
3.1	aomadillo_solve.py	7
3.2	aomadillo_sampler.py	9
3.3	aomadillo_print_d.py	10
4	Guide through a full set of calculations	10
4.1	Geometry optimization	10
4.2	Finding the d orbitals	11
4.3	First CASSCF iteration	12
4.4	Creating structure samples	13
4.5	Second CASSCF iteration	14
4.6	Fitting AOM parameters	15
5	Non-ORCA input	17
6	Tips and Tricks	19

1 Installation

1.1 Prerequisites

The AOMadillo package is designed to be executed from a shell. It takes text input and produces text output. AOMadillo interfaces ORCA output and relies on the aiLFT routine provided by ORCA. We assume that you are familiar with ORCA calculations and have a system with a running installation available.

To install AOMadillo, download the source code from the git repository. You need a working Python environment of version ≥ 3.6 and the modules `numpy` and `scipy` installed. The current AOMadillo version is tested with Python 3.10.10. We recommend the use of `pyenv` for setting up the proper Python version. If you do not use `pyenv`, it might be necessary to adjust the shebang line of the `.py` files in the `AOMadillo` subfolder to point to the correct python installation.

Once Python is ready, you need to open the README file and confirm that you agree to the GNU General Public License under which this software is published. Set the boolean in `LICENSE = FALSE` to `TRUE`. After that, the software should be ready to run. The files that are meant to be executed are the ones in the `AOMadillo` folder, namely `aomadillo_solve.py`, `aomadillo_sampler.py` and `aomadillo_print_d.py`.

1.2 Package overview

When you extract the AOMadillo package, you will find a folder with the following structure and files:

```
AOMadillo
├── .gitignore.....For repository management
├── .python-version..... Sets the python version for pyenv
├── test_files
│   ├── test1.out
│   │   ⋮
│   └── test4.out.....Example files for testing
├── basis
│   ├── aom_fitting.py..... Provides functions for the main modules
│   └── sampler_example_input.txt.....Example input file for
│       aomadillo_sampler.py
├── aomadillo_print_d.py..... Prints d orbitals from output files
├── aomadillo_sampler.py..... Creates structurally distorted samples
├── aomadillo_solve.py..... AOM parameter fitting script
├── manual.pdf ..... What you are reading right now
├── README..... Readme file with the license chackmark
└── LICENSE..... GNU General Public License
```

You can safely remove `.gitignore`. If you do not use `pyenv`, you can also remove `.python-version`. The subfolder `test_files` contains truncated example output files that can be used for testing and are discussed in more detail in the next section. The file `aom_fitting.py` provides functions that are needed by the AOM parameter fitting script `aomadillo_solve.py` and can generally be used to write other useful AOM scripts. Supplementary to `aomadillo_sampler.py`, the file `sampler_example_input.txt` provides a basic template which can be used to construct an appropriate input file.

For a quick overview over the options each script provides, you can call them with the `-h` or `--help` flag. The flag descriptions provided there are shorter than those in the manual, so we recommend to refer to the manual if you need more details.

2 Tests and examples

We provide four test files that can be used to check whether the software is working and to try out some common options. Checking these parameterizations should give you a first understanding of how the software is intended to be used and which flags are common to set.

2.1 Test 1: octahedral ligand sphere, chemically equal ligands

In an octahedral coordination environment, `d-s` mixing plays no role so we set `--nods`. We group all ligands into the same group with `-g [1,1,1,1,1,1]`. The atom numbers 1 to 6 are the ligating atoms, so they are set in the first positional argument. The second positional argument is the output file.

```
$ aomadillo_solve.py --nods -g [1,1,1,1,1,1] [1,2,3,4,5,6] test1.out
#File      Cost      E      esigma  epi      esigma  epi      esigma  ...
test1.out  50      -569609  6717   1010    6717   1011    6720   1009    6718   1011    6732   ...
```

You can see that the AOM parameters slightly deviate although we grouped them. While this behaviour is intended (they are not perfectly equal), we can enforce equality by setting a weight factor with `-w` (see section 3). This will of course increase the cost of the fit. Below, the results of using two different weight factors are printed.

```
$ aomadillo_solve.py --nods -g [1,1,1,1,1,1] -w 2 [1,2,3,4,5,6] test1.out
#File      Cost      E      esigma  epi      esigma  epi      esigma  ...
test1.out  81      -569390  6645   956     6645   956     6646   956     6646   956     6664   ...
$ aomadillo_solve.py --nods -g [1,1,1,1,1,1] -w 10 [1,2,3,4,5,6] test1.out
#File      Cost      E      esigma  epi      esigma  epi      esigma  ...
test1.out  406     -566815  5791   314     5791   314     5792   314     5792   314     5799   ...
```

As you can see, this way of enforcing equal parameters also shifts their values, so one should be careful when introducing such restraints.

2.2 Test 2: metal-ligand pair with different π interactions

This test focuses on a metal ion with a water ligand, which is expected to have different π_x and π_y interactions. We account for that by specifying an atom that defines the ligand plane together with metal and the directly ligating atom. In this case it could be atom 2 or 3, so we choose `--psirel [2]`.

```
$ aomadillo_solve.py --nods --psirel [2] [1] test2.out
#File      Cost      E  esigma  epix  epiy
test2.out  41 -179444  5901  1535  3174
```

If we do not set any of `--psirel`, `--psideg` or `--psirad`, the fit will subsume the π parameters, leading to a high cost and an average e_π :

```
$ aomadillo_solve.py --nods [1] test2.out
#File      Cost      E  esigma  epi
test2.out  671291 -179444  5901  2354
```

57

Attention! In this case, it is pure luck that the subsumed e_π parameter is the average of e_{π_x} and e_{π_y} . In general, the fit can shift unpredictably and may yield nonsensical results if a single e_π parameter is expected to cover chemically distinct e_{π_x} and e_{π_y} interactions.

In this example, we can also see how the cost of a fit can serve as indication that the chosen parameter set might not fit well to the given ligand field splittings.

2.3 Test 3: square-planar ligand sphere, chemically equal ligands

The classic square planar coordination environment requires us to consider d-s mixing, which is the default behaviour of AOMadillo. We do not need to specify anything other than the ligand atoms and the file.

```
$ aomadillo_solve.py -g [1,1,1,1] [1,2,3,4] test3.out
#File      Cost      E  esigma  epi  eds  esigma  epi  eds  ...
test3.out  0 -1839169  3260  1160  428  3260  1160  428  428  ...
```

A cost of 0 is always suspicious and could be a sign of overparameterization, although the parameters seem plausible. It is thus advisable to check for this with the `--monte` option, which makes semi-random start guesses for every parameter (see below for more details).

```
$ aomadillo_solve.py --monte -g [1,1,1,1] [1,2,3,4] test3.out
#File      Cost      E      esigma      epi      eds      esigma      epi      eds      ...
test3.out  0      -1839169  3260  1160  428  3260  1160  428  3260  1160  428  ...

$ aomadillo_solve.py --monte -g [1,1,1,1] [1,2,3,4] test3.out
#File      Cost      E      esigma      epi      eds      esigma      epi      eds      ...
test3.out  0      -1839169  3260  1160  428  3260  1160  428  3260  1160  428  ...
```

Since the two calls yield exactly the same result, this is probably a true minimum. Of course, it is in any case advisable to check the orbital splitting in the ORCA output and confirm that it meets expectations.

2.4 Test 4: MA₄B₂ complex

In the complex provided for this test, there are two types of ligand that must be distinguished. The first four ligands are equal as are the last two. The grouping is chosen accordingly to yield a plausible fit.

```
$ aomadillo_solve.py --nods -g [1,1,1,1,2,2] [1,2,3,4,5,6] test4.out
#File      Cost      E      esigma      epi      esigma      epi      esigma      epi      ...
test4.out  1224  -863085  4061  1106  4042  1100  4036  1110  4068  1098  2901  ...
```

3 Command reference

3.1 aomadillo_solve.py

This script is used to fit a defined set of AOM parameters to the ligand field Hamiltonian printed from an ORCA aiLFT CASSCF calculation. The transition metal must be the very first atom defined in the structure.

aomadillo_solve.py [options] [atom-spec] [files]
Attention! List-like arguments must be given without any whitespace! Whitespaces are interpreted as the end of an argument. They also must have the same length, i.e. number of elements as the list of ligand atoms (first positional argument).

positional arguments

atom-spec Numbers of the ligating atoms in the given structure, given as a list in python format, e.g. [1,2,5,6]. Atom counting starts at 0, no whitespaces are allowed. Only the directly bound atoms need to be specified, not every atom of the ligand.

files Arbitrary number of ORCA CASSCF output files. The ligand field Hamiltonian must be present.

options

-h, --help Show a help message and exit, ignoring all other arguments.

-v, --verbose Prints more output. Gives insight into the least-squares solver parameters at the solution and prints the complete equation system that was used.

parameterization definitions

--nods Remove e_{ds} from the equation system. Recommended for symmetries close to O_h or T_d .

--noep Remove e_π parameters. Not recommended.

--psirad P Define on-axis angles ψ in radians for every ligand. Format: [psi1,psi2,psi3,...], where psi1 is the angle for the first ligand, psi2 for the second one and so on.

--psideg P Define on-axis angles ψ in degree for every ligand. Format: [psi1,psi2,psi3,...], analogous to that of --psirad

--psirel P Define on-axis angles ψ by specifying another atom that defines the molecular plane together with the metal and ligand atom. Format: [rel1,rel2,rel3,...], with rel n being the in-plane additional atom to ligand atom n . ψ is defined such that e_{π_x} lies in the given plane and e_{π_y} is perpendicular to it.

--monte	Make semi-random start guesses for all parameters. Non-fixed AOM parameters (see --fixmap) have a random value in the interval $[0, 10^4]$, the interval for E is $[-10^6, 0]$. For each file, a new random start guess is made. This may help detecting underdetermined systems.
-m, --mode M	Switch for the ORCA output parser. "NEVPT2" and "CASSCF" are supported. The default is CASSCF.
equation system fine tuning	
-g, --group G	Enables soft grouping, which means that an additional equation is added to the system requiring the members to be equal. Format: [t1,t2,t3,...] in the same sequence as the atoms were specified. E.g. [1,1,2,2] requires the parameters for ligand atoms 1 and 2 and ligand atoms 3 and 4 to be the same. Note that this is a soft requirement, the solver may still find lower costs with nonequal parameters.
--epigroup E	Define whether e_{π_x} and e_{π_y} for a ligand atom should be the same (1) or not (0). Format: [a1,a2,a3,...].
-w, --groupweight W	Scales the grouping functions by W . Higher numbers mean that grouping has a stronger effect, since the costs increase if the equation is not satisfied. Default is 1.
--equations E	Provide a file E with additional equations that are fed to the solver. The equations are read by <code>python eval()</code> , which can be unstable. They must be in the same format as they are given when calling the program with <code>-v</code> , but without the equality sign. Each equation is expected to equal 0. Example: " <code>e[2] - 1000</code> " will require that the second parameter in the list minus 1000 cm^{-1} should equal zero. Note that these are soft requirements, for hard requirements use --fixmap.
-x, --fixmap F	Provide a list of fixed values. Format: [f1,f2,f3,...] with f_n being the value of the parameter n . This list must have as many elements as there are AOM parameters, including E . Write x for elements which should not be fixed. Example: for a complex MX_2 , [x,3000,x,3000,x] would fix both e_σ parameters at 3000 but let E and e_π to optimize freely. This is a hard requirement, the set parameters cannot deviate from the given value, but still add to the total cost of the fit.
output control options	
--noheader	Do not print the default table headline. May be useful for automated data processing.

-p P, --plotfiles P	Generate csv-files with the given name P as prefix. The files are generated per ligand and per interaction type, for all output files combined. They consist of two columns: the first is the M–L bond length in Å, the second is the corresponding AOM parameter in cm ⁻¹ .
--plotgroup P	Create groups for the --plotfiles flag, i.e. ligands in the same group have their parameters printed in the same csv-files. Requires -p/--plotfiles to be set. The specification works similar to a mapping and requires a list with the same length as the atom specification list. Format: [t1,t2,t3,...] in the same sequence as the atoms were specified. E.g. [1,1,2,2] prints the atoms 1,2 and 3,4 together. Any string can be given (e.g. [joe,jim,joe,jeff]), whitespaces are not allowed.

Tips and tricks:

1. In the input list formats, the brackets are not necessary, but subjectively improve readability.
2. The AOM parameters are printed in the sequence of the ligand atom specification. So while giving [1,2,3,4] yields the same parameters as [4,3,2,1], their output sequence is inverted.

3.2 aomadillo_sampler.py

This script is used to create structure samples from a reference geometry. The rules according to which the samples are created are defined in a separate input file. Usage:

```
aomadillo_sampler.py [options] [input] [reference]
```

positional arguments

input	Text file with specifications about the sampling parameters. See specifications below.
reference	Cartesian coordinate file with the reference structure. Samples are modifications of this reference.

options

-h, --help	Show a help message and exit, ignoring all other arguments.
-n N, --number N	Create <i>N</i> samples per bond length step. Default is 5.
-p P, --prefix P	Every output sample gets <i>P</i> as prefix.
-s S, --suffix S	Every output sample gets <i>S</i> as suffix.

3.3 aomadillo_print_d.py

This script is used to extract orbital information from the ORCA output file. It evaluates whether an orbital has significant d character and prints each orbital above a set threshold (default is 20%). The output table is useful to set up an active space, or to assess whether a given CAS calculation has the correct active space. Usage:

```
aomadillo_print_d.py [options] [orca_output]
```

positional arguments

orca_output	ORCA output file(s) from a CASSCF, single point calculation or geometry optimization. SP calculations and optimizations need to have the orbital information printed, e.g. via <i>largeprint</i> .
-------------	--

options

-h, --help	Show a help message and exit, ignoring all other arguments.
-t N, --threshold T	Threshold of d orbital contribution (in percent) for the orbitals to be printed. Default is 20.

4 Guide through a full set of calculations

This section guides you through the complete procedure using the example of VCl_3 . This substance is a solid with octahedral $[\text{VCl}_6]^{3-}$ subunits. We start with the preliminary calculations that are done in ORCA, then employ the structure sampling and the AOM parameter solver to obtain an example set of AOM parameters.

4.1 Geometry optimization

Before starting the CASSCF calculation, the geometry should be optimized. This is an important step, since the geometry has a large impact on the AOM parameters. You can create your structure by different means, i.e. a bare bones optimization in vacuum, increasing levels of complexity including solvent models, dispersion corrections or solid-state optimizations with a subsequent embedded cluster creation. We use a very simple calculation here, since it is only for demonstration purposes.

```
# Kohn-Sham-DFT, Becke-Perdew 86 functional,  
# def2-SVP Karlsruhe basis set, geometry optimization  
! UKS BP86 def2-SVP Opt  
  
* xyzfile -3 3 structure-guess.xyz
```

If you are not absolutely sure about the spin state of the system, it is advisable to do a geometry optimization for all possible multiplicities. The level

of theory will depend on the system of interest. Here, we can be relatively sure that the high spin case is the energetically preferred multiplicity.

It is mandatory for the AOM fitting script that the metal is the first atom in the structure! It can be valuable to align the molecule to the global axis frame, ideally according to the closest point group. It makes identification of d orbitals much easier and can also help with the interpretation of the results.

4.2 Finding the d orbitals

In order to define the active space, we need to define the set of orbitals we want to use. While canonical Kohn-Sham orbitals from an unrestricted calculation can be hard to assign, the orbitals from ROHF calculations can be a good starting point in many cases. This often yields clearly defined d orbitals that can be fed to the subsequent CASSCF calculation. Other options based on different localisation schemes exist, and the best option will again depend on the system of interest.

```
# Restricted open-shell Hartree Fock
# Largeprint needs to be set for subsequent evaluation
! ROHF def2-SVP Largeprint

* xyzfile -3 3 optimized-structure.xyz
```

One way of checking the resulting orbitals for their d-character is the script `aomadillo_print_d.py`. Calling it with the output file as the argument yields a table with all orbitals that have > 20% d-character and the number of the HOMO.

```
HOMO: 64
No   Energy      Occ |  dxy  dyz  dz2  dxz dx2y2 | total
-----|-----
63 -0.17595  1.00000 | 50.1 47.9  0.0  0.0  0.0 | 98.0
64 -0.17114  1.00000 |  0.1  0.0  1.9 89.8  5.6 | 97.4
-----|-----
66  0.51510  0.00000 | 46.6 48.8  0.0  0.1  0.0 | 95.5
67  0.54294  0.00000 |  0.0  0.0 21.4  8.0 54.4 | 83.8
68  0.55635  0.00000 |  0.0  0.0 60.0  0.0 23.4 | 83.4
73  1.15599  0.00000 | 33.9 32.5  0.0  0.0  0.0 | 66.4
74  1.16331  0.00000 |  0.0  0.1  0.5 57.9  1.4 | 59.9
80  1.22862  0.00000 | 31.7 33.0  0.0  0.1  0.0 | 64.8
81  1.31836  0.00000 |  0.0  0.0  9.4  0.8 25.1 | 35.3
82  1.32517  0.00000 |  0.0  0.0 25.5  0.0  9.5 | 35.0
123 1.77276  0.00000 | 15.9 15.5  0.0  0.1  0.0 | 31.5
124 1.77674  0.00000 |  0.2  0.0  0.1 31.4  0.2 | 31.9
125 1.79528  0.00000 | 17.0 17.7  0.0  0.0  0.0 | 34.7
130 2.23245  0.00000 |  0.0  0.0  9.8  0.0 26.5 | 36.3
131 2.23737  0.00000 |  0.0  0.0 26.9  0.0  9.9 | 36.8
```

In this list, we find all orbitals that are needed: 63, 64 and 66–68.

4.3 First CASSCF iteration

The active space is defined by a set of orbitals around the HOMO/LUMO gap. In our example, the active space will have two unpaired electrons in five active orbitals, i.e. (2,5) in the (electrons, orbitals) notation. With the HOMO being orbital number 64, the active space has to encompass two orbitals in the occupied space (63–64) and three in the unoccupied space (65–67). Consequently, we have to rotate only two orbitals from the ROHF calculation: 65 would be in the active space and needs to be removed, while 68 would be excluded so we have to insert it. Exchanging the list positions of these two orbitals is achieved in the %scf block in ORCA. We also need to define the active space as shown in the input file below.

```
# read in the orbitals from the single point calculation
! def2-SVP M0read
%moinp "sp-orbitals.gbw"

# here the orbitals are exchanged (rotated)
%scf rotate
    {65, 68}
end end

# definition of the active space
%casscf
    nel 2 # number of electrons
    norb 5 # number of orbitals
    mult 3,1 # all possible multiplicities
    nroots 10,15 # all possible configurations
    actorbs dorbs # call ORCA aiLFT module
end

* xyzfile -3 3 optimized-structure.xyz
```

After the calculation is complete, the output has to be assessed. Calling `aomadillo_print_d.py` on the output file yields:

```
HOMO: 67
No   Energy      Occ |   dxy   dyz   dz2   dxz dx2y2 | total
-----|-----
63   0.42988   0.40000 |  97.2   0.0   0.0   0.0  0.0 |  97.2
64   0.42988   0.40000 |   0.0  97.2   0.0   0.0  0.0 |  97.2
65   0.45586   0.40000 |   0.0   0.0  87.6   0.0  0.0 |  87.6
66   0.42985   0.40000 |   0.0   0.0   0.0  97.2   0.0 |  97.2
67   0.45593   0.40000 |   0.0   0.0   0.0   0.0  87.6 |  87.6
-----|-----
```

73	1.20011	0.00000		27.2	38.3	0.0	0.0	0.0		65.5
74	1.20017	0.00000		33.4	22.8	0.0	9.4	0.0		65.6
75	1.20031	0.00000		5.0	4.4	0.0	56.2	0.0		65.6
81	1.30083	0.00000		0.0	0.0	9.0	0.0	22.8		31.8
82	1.30094	0.00000		0.0	0.0	22.9	0.0	9.0		31.9
123	1.78932	0.00000		2.7	2.4	0.0	27.2	0.0		32.3
124	1.78983	0.00000		16.1	11.1	0.0	5.1	0.0		32.3
125	1.79007	0.00000		13.5	18.7	0.0	0.0	0.0		32.2
130	2.22836	0.00000		0.0	0.0	24.8	0.0	9.7		34.5
131	2.22947	0.00000		0.0	0.0	9.8	0.0	24.8		34.6

Average d contribution: 93.4

Standard deviation of d contribution: 4.7

We find the active orbitals with a non-integer occupation number, confirming that we composed a good active space. You may have noticed that we used a fairly small basis set for a transition metal complex. We can improve on that with a subsequent CASSCF calculation, where we read in the orbitals from the first. In the second calculation, we choose a larger basis set, say def2-TZVP and ORCA will project the smaller basis onto the larger one.

Since finding the d orbitals for the very first CASSCF calculation is easier when the basis is small, it can be helpful to start with a small basis set and increase the size after the first CASSCF calculation is converged.

4.4 Creating structure samples

Since a single calculation can yield unrepresentative AOM parameters, it is strongly advised to create structural samples and run additional CAS calculations on these. The additional workload is in general limited, since it is not necessary to converge the active space from scratch for every sample.

To create the structure samples, `aomadillo_sampler.py` is used. As input, the optimized geometry and a separate input file are needed. This is an input we can use to create a few samples:

```
bond 0,1
atoms 1
bondrel 0,0,1
angrel 0.2,0.5
groupend
```

```
bond 0,2
atoms 2
bondrel 0,0,1
angrel 0.2,0.5
groupend
```

```
bond 0,3
atoms 3
bondrel 0,0,1
angrel 0.2,0.5
groupend
```

```
bond 0,4
atoms 4
bondrel 0,0,1
angrel 0.2,0.5
groupend
```

```
bond 0,5
atoms 5
bondrel 0,0,1
angrel 0.2,0.5
groupend
```

```
bond 0,6
atoms 6
bondrel 0,0,1
angrel 0.2,0.5
groupend
```

This specifies six metal-ligand bonds, defined via the atoms involved in the bond, and the respective intervals for bond lengths and angles. Note that `bondrel 0,0,1` sets no bond length changes at all.

Calling `aomadillo_sampler.py ex-input.inp optimized-structure.xyz` will create five coordinate files called `sample-00-00.xyz` to `sample-00-04.xyz`. The first running number counts the bond length step (0 here because we did not set any), the second identifies a structure with a specific angle value from the randomly generated set of coordinates.

4.5 Second CASSCF iteration

With the structure samples and the first successful CASSCF calculation ready, the sample CASSCF calculations can be run. You will need a separate ORCA input file for each sample. Remember to read in the orbital file from the first CASSCF calculation on the reference structure to accelerate convergence.

```
! def2-SVP M0read
%moinp "casscf-orbitals.gbwn"

%casscf
  nel 2
  norb 5
```

```
    mult 3,1
    nroots 10,15
    actorbs dorbs
end

* xyzfile -3 3 sample-00-00.xyz # one for each sample
```

The calculations should run significantly faster than the first one, since the input orbitals are already converged at a very similar geometry. The composition of the active space of the samples should not have changed significantly from the reference geometry (less than 1% in each orbital).

4.6 Fitting AOM parameters

Before calling `aomadillo.solve.py` to perform the fit, we should have a good idea of what we expect. The given geometry is almost octahedral, so we can safely omit d-s mixing. The M-L bonds are to a very good approximation cylindrical, so it is justified to subsume e_{π_x} and e_{π_y} . We now need to check how similar the different bonds are. While all ligands coordinate via the same element, the bond lengths can be different, which would require different AOM parameters. Checking the bond lengths for this example yields:

bond	V0-Cl1	V0-Cl2	V0-Cl3	V0-Cl4	V0-Cl5	V0-Cl6
bond length / Å	2.509	2.509	2.506	2.506	2.509	2.509

It is safe to assume that these are sufficiently equal to be grouped into one set, but we could also group the ligands 1,2,5,6 and 3,4 separately.

Here is the input and the corresponding output. Because the table is too broad we had to cut the last four columns in this depiction.

```
$ aomadillo_solve.py --nods -g [1,1,1,1,1,1] [1,2,3,4,5,6] sample*.out
#File      Cost      E      esigma      epi      esigma      epi      esigma      epi      ...
sample-00-00-cas.out  135  -182639  3867  747  3865  750  3893  753  3893  754  ...
sample-00-01-cas.out   42  -182600  3852  737  3852  738  3878  744  3878  743  ...
sample-00-02-cas.out   32  -182659  3872  754  3873  752  3899  759  3899  759  ...
sample-00-03-cas.out   34  -182677  3877  757  3877  757  3904  763  3904  762  ...
sample-00-04-cas.out   53  -182658  3871  752  3871  753  3898  757  3898  758  ...
```

Calling the script with the alternative grouping mentioned above does not really change the result.

```
$ aomadillo_solve.py --nods -g [1,1,2,2,1,1] [1,2,3,4,5,6] sample*.out
#File      Cost      E      esigma      epi      esigma      epi      esigma      epi      ...
sample-00-00-cas.out  123  -182639  3866  748  3865  749  3894  754  3894  754  ...
sample-00-01-cas.out   30  -182600  3852  737  3852  738  3878  743  3878  743  ...
sample-00-02-cas.out   19  -182659  3872  753  3872  753  3899  759  3899  759  ...
sample-00-03-cas.out   22  -182678  3877  757  3877  757  3905  763  3905  763  ...
sample-00-04-cas.out   40  -182659  3871  752  3871  752  3899  758  3899  758  ...
```

Let us explain the input we gave. We decided to omit d-s mixing, hence we added the flag `--nods`. The default parameterization already subsumes e_{π_x} and e_{π_y} , so no further action is required here. The `-g` flag is required to group ligands, i.e. introduce restraints that set their parameters to be equal. This works like a map: we provide a list of the same length as the list of ligand atoms and assign a label to each one, in this case the labels we chose were 1 or 2. Ligand atoms with the same label will be grouped. The last two arguments are mandatory: The list of ligating atoms, and a list of files where the fit is performed. Each file is processed separately with a result that is not affected by the other files.

The output is read as follows. The first column is the name of the respective CASSCF output file. The column `Cost` shows the cost of the fit as defined in the least-squares method. `E` is the spherical energy contribution to the ligand field, and the following columns list the AOM parameters. Their order is the same as given in the input list, in this example from 1 to 6.

5 Non-ORCA input

We emphasized that AOMadillo is written to interface ORCA output files. Since the ORCA output files that are read in are in plain text format, it is also possible to provide any file that contains the necessary information. The two blocks that must appear in the text file fed to AOMadillo are the geometry information and the ligand field matrix.

The geometry is read in Cartesian coordinates in Å, starting with the line `CARTESIAN COORDINATES (ANGSTROEM)` and ending at `CARTESIAN COORDINATES (A.U.)`. It then removes the top and bottom two lines. The remainder is interpreted as xyz data separated by whitespace with the first column being the element. This is an example of the text from an ORCA output file that is read in the geometry block; everything that is cut away during processing by AOMadillo is coloured red.

CARTESIAN COORDINATES (ANGSTROEM)

```
-----  
Cr    -0.000000    -0.000000    -0.000000  
N     -2.144339    -0.057192     0.032625  
N      2.146088    -0.031935    -0.028289  
N     -0.023993    -2.145026     0.022996  
N     -0.064076     2.145255    -0.025746  
N      0.010953     0.016644    -2.144513  
N      0.071850     0.067358     2.142185  
H     -2.612167     0.869343     0.038785  
H     -2.550904    -0.545161     0.854201  
H     -2.575132    -0.546367    -0.775666  
H      2.608195     0.897358    -0.033383  
H      2.558402    -0.513438    -0.850767
```

```

H      2.578130   -0.514441    0.783371
H      0.908760   -2.599719   -0.003294
H     -0.532841   -2.578058   -0.771842
H     -0.479416   -2.563140    0.857235
H      0.858490    2.619709   -0.054389
H     -0.531793    2.571377    0.797640
H     -0.571609    2.550693   -0.836000
H      0.678603    0.697604   -2.555600
H     -0.894719    0.260854   -2.589463
H      0.270505   -0.883518   -2.591955
H      0.753651    0.753805    2.519761
H      0.339068   -0.823802    2.602862
H     -0.820626    0.326325    2.605025

```

CARTESIAN COORDINATES (A.U.)

The ligand field matrix is read by searching for the line AILFT MATRIX ELEMENTS (CASSCF). It reads the following nine lines and truncates the head of the list and the first column such that only the five lines with the ligand field matrix remain. This is an example of the text from an ORCA output file that is read from the aiLFT block; everything that is cut away during processing by AOMadillo is coloured red.

AILFT MATRIX ELEMENTS (CASSCF)

Ligand field one-electron matrix VLFT (a.u.) :

	0	1	2	3	4
0	-2.576764	0.000021	0.000221	-0.000005	0.001112
1	0.000021	-2.576725	0.001479	0.000052	0.000814
2	0.000221	0.001479	-2.503497	0.001837	0.000013
3	-0.000005	0.000052	0.001837	-2.576706	-0.001042
4	0.001112	0.000814	0.000013	-0.001042	-2.503660

You can use this parsing behaviour to alter output files that are read by AOMadillo. An example could be the addition of dummy ligands in the structure section of an output file, in order to test arbitrary ligand positions (e.g. coordination voids). It is also possible to compose a text file that has the necessary information so it can be fed into `aomadillo_solve.py`. See the example below:

CARTESIAN COORDINATES (ANGSTROEM)

lines

```

Cr    -0.000000   -0.000000   -0.000000
N     -2.144339   -0.057192    0.032625
N      2.146088   -0.031935   -0.028289

```

```

N      -0.023993   -2.145026    0.022996
N      -0.064076    2.145255   -0.025746
N       0.010953    0.016644   -2.144513
N       0.071850    0.067358    2.142185
are
important
CARTESIAN COORDINATES (A.U.)

AILFT MATRIX ELEMENTS (CASSCF)
lines
must
be
here
just  -2.576764   0.000021   0.000221  -0.000005   0.001112
a      0.000021  -2.576725   0.001479   0.000052   0.000814
column 0.000221   0.001479  -2.503497   0.001837   0.000013
to     -0.000005   0.000052   0.001837  -2.576706  -0.001042
skip   0.001112   0.000814   0.000013  -0.001042  -2.503660

```

The above lines are read by AOMadillo without problems. The line count is important and the file name should end with `.out`.

6 Tips and Tricks

- It is advisable to orient the molecule in the global axis frame to simplify the orbital assignments, as also recommended in the ORCA manual. We had good experience with setting the metal coordinates fixed in the geometry optimization using

```

%geom constraints
  {C 0 C}
end end

```

in the input file.

- A common recommendation when setting up active spaces is to use localized orbitals. We have had good experiences with the ROHF approach mentioned above and needed to localize orbitals only when other ways of obtaining a good d orbital space failed. It can be worthwhile to try different formalisms (HF/KS) and basis set sizes first.

6 Conclusion and Perspective

6.1 Perspective

As it is always the case with scientific work: the more we learn, the more questions we can ask. Some observations that were made in chapter 5 did not allow for drawing clear conclusions, so more research is needed. In this section, I want to point out which topics could be investigated further. Some preliminary results are shown here that can be taken as incentives to investigate the topic in more detail.

6.1.1 Phase-coupling in non-coupled ligators

It was briefly mentioned in chapter 4 and section 5.3 that Deeth observed an orbital splitting for *cis*-[NiF₂(CO)₂] and *cis*-[PtCl₂(NH₃)₂] that resembles the orbital splitting of phase-coupled ligators, although in this complex no coupling should exist.^[84] While I think that the attribution of this effect to coordination void π interactions is wrong, it is certainly an observation that needs to be investigated. During the work on the AOMadillo package, similar results have been obtained for other planar *cis* complexes, although we were not able to explain them. We generally noticed difficulties in finding good parameter sets for complexes with a strong dipole that does not coincide with one of the metal-ligand bonds. Planar *cis* complexes usually have this feature, so there might be a connection between the dipole and the apparent phase-coupling.

Experimental evidence of the observed orbital splitting is needed to confirm that it is not an artefact of the CASSCF calculation. The data obtained must be compared with complexes with truly phase-coupled ligators. This could be supported by the extension of the AOMadillo package by allowing for a parameterization of the Orgel effect. Other complexes with strong dipoles might be investigated to confirm or rule out a possible connection to the phase-coupling.

6.1.2 The divide

In chapter 4, it was stated that neither the d-s mixing approach nor the coordination void was disproven and a few indicators that are in favour of the d-s mixing interpretation were presented. In Table 6.1, the orbital compositions of the active space in the series of [Mn(NH₃)_n]²⁺ are shown, which was also discussed in section 5.3. In addition to this discussion, I want to point out a few things that might help disprove the coordination void concept at some time. In section 5.3, we pointed out that the admixture of s and p orbitals coincides very well with the necessity and even magnitude of d-s mixing parameters. The

connection of the s orbital coefficients and the magnitude of mixing could be investigated further, although it is probably strongly basis set dependent.

In Table 6.1, the orbital composition of the active space of some complexes in the series are shown. It is apparent that there are orbitals with considerable admixtures of p orbitals that can be parameterized without any d–p mixing parameter. These cases are very common, but their parameterization rather works by accident than because it is complete. Other parameters subsume the d–p mixing contribution, as can be well seen for example for the tetrahedral $n = 4$ and square pyramidal $n = 5$ cases in Table 6.1. In other cases, e.g. the linear $n = 2$ one, the orbital composition shows a substantial s contribution, but it cannot be captured due to overparameterization.

We showed that the $n = 5$ case in fact has a significant d–p mixing that cannot be covered by other parameters. From the perspective of coordination void placement, there is no suitable void space in the trigonal bipyramid. In consequence, it is apparently not possible to account for the low d_{xy} and $d_{x^2-y^2}$ orbital energies in the Gerloch–Woolley version of the AOM. Another interesting feature of d–s mixing is that in any symmetry, the complex can be arranged such that the only affected orbital is the d_{z^2} orbital.^[35] The coordination void does not have this feature, it affects orbitals according to its position like a ligand would. That means that although d–s mixing and coordination voids were successfully used especially for D_{4h} complexes, there must be cases where the coordination void affects other orbitals than the d_{z^2} orbital and it might be possible to distinguish both effects. Linear complexes come to mind, where voids would be placed in some shape in the xy-plane, affecting especially the d_{xy} and $d_{x^2-y^2}$ orbitals. Deeth discussed such examples recently, although his arguments are difficult to verify since linear complexes are underdetermined for three or more parameters. His approach to make the parameter sets determined is the negligence of ammonia π interactions, which might be an oversimplification as discussed in section 5.2.^[85]

These approaches could provide a handle to differentiate SJ and GW pictures of the AOM to an extent where the parameterizations are so different, that they cannot be successfully applied to the same problem anymore. A further investigation of linear and trigonal bipyramidal complexes might therefore be worthwhile and could shed new light onto the subject.

6.1.3 Differential covalency

When presenting the derivation of the Condon–Shortley or Racah parameters, respectively, in chapter 3, I stated that I have objections against using LFT with ligands like CO or CN^- . This is because the two-electron parameterization is derived for spherical ions: it assumes all the d orbitals to share the same radial part. This assumption still works well for more covalently bound ligands, as long as the resulting size of the d orbitals is still similar. Problems arise when a strong differential covalency is found. In this case, some d orbitals are spatially more expanded than others, and in consequence the two-electron integrals must differ depending on the integrated orbital. The standard Condon–Shortley parameterization cannot reliably capture this, as the parameter R^k in Equation 3.17

Table 6.1: Active space orbital compositions of complexes of the type $[\text{Mn}(\text{NH}_3)_n]^{2+}$, point groups are given regarding the ligating atoms only. Orbital compositions are given in percent. If an orbital compositions' sum is not 100 %, the rest is composed of ligand orbitals. Orbitals are ordered by their relative energy ε given in cm^{-1} , as obtained by the CASSCF calculation described in section 5.3.

	m_l	$\varepsilon/\text{cm}^{-1}$	d	s	p	AOM representation
$n = 2, C_{\infty v}$	xy	0	100.0			0
	$x^2 - y^2$	0	100.0			0
	xz	2806	98.9			$2e_\pi$
	yz	2806	98.9			$2e_\pi$
	z^2	7895	89.9	6.6	0.8	$2e_\sigma - 4e_{ds}$
$n = 4, T_d$	$x^2 - y^2$	0	98.4			$(24/9)e_\pi$
	z^2	4	98.4			$(24/9)e_\pi$
	yz	4770	93.8		1.9	$(4/3)e_\sigma + (8/9)e_\pi$
	xz	4813	93.8		1.9	$(4/3)e_\sigma + (8/9)e_\pi$
	xy	4856	93.8		1.9	$(4/3)e_\sigma + (8/9)e_\pi$
$n = 5, D_{3h}$	xz	0	98.0			$3.5e_\pi$
	yz	0	98.0			$3.5e_\pi$
	xy	2945	94.4		1.7	$1.5e_\pi + 1.125e_\sigma - C_{dp}$
	$x^2 - y^2$	2945	94.4		1.7	$1.5e_\pi + 1.125e_\sigma - C_{dp}$
	z^2	13744	90.9	0.1		$2.75e_\sigma$
$n = 5, C_{4v}$	yz	0	98.3			$3e_\pi$
	xz	41	98.3			$3e_\pi$
	xy	1674	97.8			$4e_\pi$
	z^2	6512	91.2	1.1	2.6	$2e_\sigma - e_{ds}$
	$x^2 - y^2$	16225	90.7			$3e_\sigma$

does not account for any asymmetry. It is possible that in a fit to electronic states, this asymmetry of the two-electron integrals leaks into the one-electron operator, which is the only one that can account for complex asymmetry.

Investigating this topic might be more complicated, and even more so is finding a better two-electron approximation. The first step that is needed is a rewrite of AOMadillo such that it performs a fit to the electronic states instead of the one-electron ligand field matrix. This enables direct access to the two-electron integrals and their parameterization. While it is a considerable amount of work, it is still straightforward. The second step is the improvement of the Condon–Shortley parameterization which might be less complicated to implement at this point, but there is no established recipe that can be used. An extensive discussion of this problem can be found in ref. [36]. I want to present a rather simple, yet promising idea that might be worth testing.

Hoggard proposed the use of relational parameters that depend on the orbitals in the integrals for octahedral complexes.^[132]

$$\langle d_i d_j | \hat{G} | d_k d_l \rangle = \epsilon^n \langle d_i d_j | \hat{G} | d_k d_l \rangle_0 \quad (6.1)$$

Here, n is the number of e_g orbitals in the integral, automatically accounting for integrals different from an assumed standard integral. The original integral is still parameterized as usual, and thus the above equation does not change the overall structure of electronic state energy expressions. The approach might be especially useful as the differential covalency can be directly derived from MO coefficients in CASSCF calculations, so the rather arbitrary factor ϵ^n could be replaced by one that is derived from *ab initio* results.

6.1.4 Solids and highly charged complexes

Ligand field theory originally emerged from the investigation of crystals, where the first coordination shell of the investigated transition metal was viewed as isolated unit. While it is common practice to extract such coordination subunits from crystal structures for quantum chemical calculations, this approach can pose problems when this unit is highly charged. Many very common solids like simple oxides would result in charges that are so high that an isolated molecule would be unrealistic (e.g. subunits of Fe_2O_3 would be octahedral $[\text{FeO}_6]^{9-}$). In a crystal, the high charges are compensated by the surrounding lattice, something that is not automatically accounted for in a molecular quantum chemical calculation.

A common way to deal with this problem without resorting to solid state calculations with periodical cells and wave functions is to surround the coordination subunit with a simplified model of the crystal lattice. It is separated into three zones: a quantum region that consists of the metal and the first ligand sphere, a frozen orbital or effective core potential¹ region where the electrons of the atoms are represented by orbitals or potentials without optimization, and a point charge region that is designed such that the charges decrease with the distance to the central metal, until they reach zero charge.^[60,134–136] While this *embedded cluster* approach is widespread, the setup of a calculation is more

¹Effective core potentials are designed to substitute orbitals/electrons to reduce computational cost.^[133]

complicated and the structural distortion employed by AOMadillo might need restructuring. At the moment, atoms are grouped and then moved by the same angle per group. In a lattice with different regions, only moving the quantum region could lead to an asymmetric charge compensation, since the next layer would not move accordingly, as schematically depicted in Figure 6.1a. Moving atoms that are grouped to a ligand atom would lead to clashes in the part further away from the metal centre, see Figure 6.1b and 6.1c. A good distortion should be scaled with the distance to the metal, where the closest atoms are moved as usual, the next layer follows that distortion but less pronounced, successively until the end of the lattice, where the distortion should be zero. Such a situation is shown in Figure 6.1d. From the schemes shown in Figure 6.1, it is apparent that the scaled distortion probably yields the best results, as it does not produce steps and preserves local geometries well. However, it also becomes apparent that disregarding the lattice distortion might be a small error and therefore still permissible. The scheme shows a rotation by 5° , much larger than the one usually employed 0.5° in the developed procedure. A static lattice might pose no problem here, but as usual, thorough testing is needed before a definitive statement can be made.

Expanding the scope of the distortion scheme to the embedded cluster approach would enable the investigation of a larger selection of complexes, most notably oxides and sulfides. Since the embedding method is an established scheme, it is very likely that the extension works well.

6.1.5 AOM-enhanced force fields

In chapter 4, the application of the AOM for the generalization of force fields in molecular mechanics calculations is pointed out. The AOM seemed suitable to include effects of ligand field stabilization energies into transition metal force fields, able to account for example for the complex bond angles that are often not explainable by simple repulsion models. Despite the work of Deeth in that field, this approach was not generalized yet, and a major problem was the availability of reliable data. The use of aiLFT is promising, since it provides insight that is almost unobtainable by experiment, as shown in section 5.1 and 5.2. It seems that if the accuracy of the calculated data is reliable enough, Deeth's approach could be enhanced by the calculated data. The true issue with AOM enhanced force fields is the limited transferability of the parameters, and their pseudo-local character. Although they represent a single metal-ligand interaction, they inevitably also include ligand-ligand effects and heavily depend on the rest of the complex. A force field built on a set of AOM parameters thus suffers from the same problems that transition metal force fields have in general: it is specifically designed for a given complex. The transfer of such a force field to other complexes is then limited, at best.

Some features still seem favourable and there might be hope. Several results presented in chapter 5 indicate that AOM parameters for metals in the same period mainly depend on their charge, so some transferability between metals can be assumed. While it was mainly observed for the first transition metal row in the +2 and +3 oxidation states, it seems promising enough to extend the investigation to other transition metals. There is also a

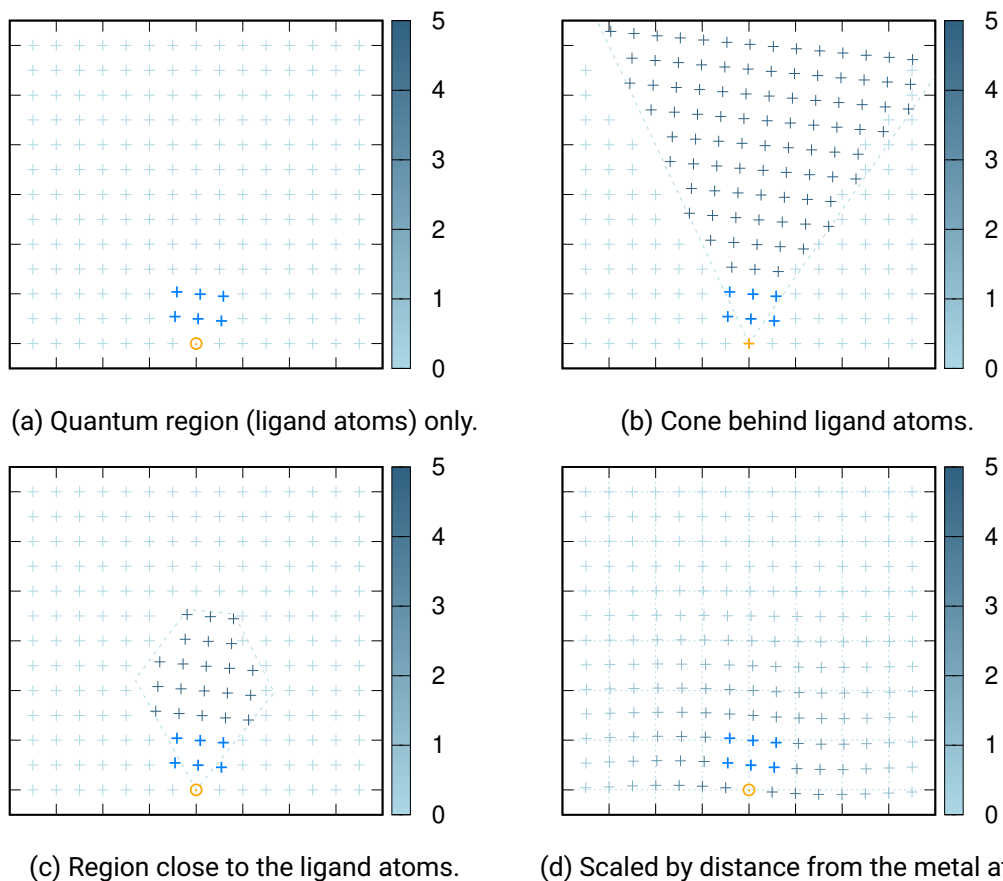


Figure 6.1: Different schemes of applying a 5° rotation to a ligand (web blue). The rest of the lattice is coloured depending on its rotation angle (see colour bar). Pale blue dots are not affected by the rotation at all, the steel-blue ones are rotated by the same angle as the ligand. The metal atom (orange) is placed in the origin. The scaled rotation (d) produces the smoothest lattice, although the simplest rotation (a) might be small enough to be permissible, too.

chance that the influence of ligands on each other can be predicted in some empirical way. From section 5.1, we know for example that hard halide ligands will make softer ligands have longer bond lengths compared to homoleptic complexes. This ligand-ligand interaction might be put into empirical relationships to correct errors that arise from parameter transfer. With the advent of machine-learning techniques, such relationships might be more easily obtained by screening a large set of complexes.

6.2 Conclusion

We saw how aiLFT can be used as a tool to obtain qualitatively correct results. Trends are reproduced correctly, which in principle allows interpolation of unknown AOM parameters for other systems. Although it is known for more than 50 years by now, we also saw how the AOM can yield parameters that represent ligand characteristics in a chemically intuitive way. The presented scheme of using asymmetric distortions was proven to be reliable enough to correctly predict AOM parameters for otherwise underdetermined systems. It is sensitive enough that the ammonia π interactions discussed in section 5.2 were first observed with reference complexes of high symmetry, and the presented proof was found later for cases that do not depend on the asymmetric distortions at all.

On a personal note, I am afraid that the AOM and maybe LFT in general is reaching its limits, as chemistry is becoming more complicated and many transition metal complexes are not easy to describe with this simple model any more. Ligand non-innocence is a popular example, where the formal oxidation state of the metals is not clear and simple d–d transitions often do not exist.^[137] Other cases involve ligands like bipyridine, where metal d orbitals become part of a conjugated system. It is of course still worth trying to parameterize apparently unsuitable complexes in terms of LFT, and there are enough examples of effects that seemed to be impossible to cover but were managed to be included eventually. Moreover, even parameter fits that do not yield reliable data could be of qualitative use. The π backbonding ligands are a good example, since they are probably out of scope for LFT, but still a parameterization can yield valuable insight. The essence of these observations is that we must expect less of LFT in terms of being able to reproduce electronic state energies for complicated molecules, but qualitative fits remain a valuable tool to conceptualize metal-ligand interactions.

Bibliography

- [1] E. I. Solomon, R. K. Szilagyi, S. DeBeer George, L. Basumallick, *Chemical Reviews* **2004**, *104*, 419–458.
- [2] S. K. Kaiser, Z. Chen, D. Faust Akl, S. Mitchell, J. Pérez-Ramírez, *Chemical Reviews* **2020**, *120*, 11703–11809.
- [3] J. Lee, O. K. Farha, J. Roberts, K. A. Scheidt, S. T. Nguyen, J. T. Hupp, *Chemical Society Reviews* **2009**, *38*, 1450–1459.
- [4] S. Royer, D. Duprez, *ChemCatChem* **2011**, *3*, 24–65.
- [5] H. Furukawa, K. E. Cordova, M. O’Keeffe, O. M. Yaghi, *Science* **2013**, *341*, 1230444.
- [6] L. H. Gade, *Koordinationschemie*, Wiley-VCH, **1998**.
- [7] H. Bethe, *Annalen der Physik* **1929**, *395*, 133–208.
- [8] H. A. Kramers in Proceedings of the Royal Academy of Sciences at Amsterdam, Vol. 33, **1930**, p. 959.
- [9] J. H. van Vleck, *Physical Review* **1932**, *41*, 208–215.
- [10] C. J. Ballhausen, *Introduction to Ligand Field Theory*, McGraw-Hill, New York, **1962**.
- [11] M. Gerloch, *Chemometrics and Intelligent Laboratory Systems* **1991**, *10*, 229–237.
- [12] C. J. Ballhausen, *Molecular electronic structures of transition metal complexes*, McGraw-Hill International Book Co, New York and London, **1979**.
- [13] B. N. Figgis, M. A. Hitchman, *Ligand Field Theory and Its Applications*, 1st ed., Wiley-VCH, New York, **2000**.
- [14] C. E. Schäffer, C. K. Jørgensen, *Molecular Physics* **1965**, *9*, 401–412.
- [15] C. J. Cramer, *Essentials of computational chemistry: Theories and models*, 2nd ed., Wiley, Chichester West Sussex England and Hoboken NJ, **2004**.
- [16] M. Atanasov, D. Ganyushin, K. Sivalingam, F. Neese in *Molecular Electronic Structures of Transition Metal Complexes II*, (Ed.: D. M. P. Mingos), Structure and Bonding, Springer Berlin / Heidelberg, Berlin, Heidelberg, **2011 // 2012**, pp. 149–220.
- [17] D. B. Cook, *Handbook of Computational Quantum Chemistry*, Dover ed., Dover Publications, Mineola, New York, **2005**.
- [18] D. A. McQuarrie, *Quantum Chemistry*, 2nd ed., University Science Books, Mill Valley, California, **2008**.

-
- [19] A. Szabó, N. S. Ostlund, *Modern quantum chemistry*, 1st ed., rev, Dover Publications, Mineola, New York, **1996**.
- [20] F. Jensen, *Introduction to Computational Chemistry*, Wiley, Chichester, UK, **2017**.
- [21] M. Bartelmann, B. Feuerbacher, T. Krüger, D. Lüst, A. Rebhan, A. Wipf, *Theoretische Physik 3 | Quantenmechanik*, 1. Aufl. 2018, Springer Spektrum, Berlin, Heidelberg, **2018**.
- [22] H. L. Schläfer, G. Gliemann, *Einführung in die Ligandenfeldtheorie*, Akademische Verlagsgesellschaft, Wiesbaden, **1980**.
- [23] J. Reinhold, *Quantentheorie der Moleküle*, 5., überarb. Aufl. 2015, Springer Spektrum, Wiesbaden, **2015**.
- [24] D. Casanova, *WIREs Computational Molecular Science* **2022**, *12*, e1561.
- [25] E. U. Condon, G. H. Shortley, *The Theory of Atomic Spectra*, Cambridge University Press, **1959**.
- [26] C. E. Schäffer, *Pure and Applied Chemistry* **1970**, *24*, 361–392.
- [27] R. J. Deeth, D. L. Foulis, *Physical Chemistry Chemical Physics* **2002**, *4*, 4292–4297.
- [28] C. E. Schäffer in *Structure and bonding*, Vol. 5, (Eds.: C. K. Jørgensen, J. B. Neilands, R. Nyholm, D. Reinen, R. J. P. Williams), Springer-Verlag, New York, **1968**, pp. 68–95.
- [29] T. Schönher in *Electronic and vibronic spectra of transition metal complexes*, (Ed.: H. Yersin), Topics in current chemistry, Springer, Berlin, **1997**, pp. 87–152.
- [30] M. Suta, F. Cimpoesu, W. Urland, *Coordination Chemistry Reviews* **2021**, *441*, 213981.
- [31] M. A. Morrison, G. A. Parker, *Australian Journal of Physics* **1987**, *40*, 465–497.
- [32] A. R. Edmonds, *Angular Momentum in Quantum Mechanics*, Princeton University Press, Princeton, **1957**.
- [33] D. W. Smith, *Inorganica Chimica Acta* **1977**, *22*, 107–110.
- [34] A. Ceulemans, D. Beyens, L. G. Vanquickenborne, *Inorganica Chimica Acta* **1982**, *61*, 199–206.
- [35] M. J. Riley, *Inorganica Chimica Acta* **1998**, *268*, 55–62.
- [36] A. J. Bridgeman, M. Gerloch in *Progress in Inorganic Chemistry*, (Ed.: K. D. Karlin), Wiley, **1996**, pp. 179–281.
- [37] H. Yamatera, *Naturwissenschaften* **1957**, *44*, 375.
- [38] H. Yamatera, *Bulletin of the Chemical Society of Japan* **1958**, *31*, 95–108.
- [39] D. S. McClure in *Advances in the chemistry of the coordination compounds*, (Ed.: S. Kirschner), Macmillan, New York, **1961**, pp. 498–508.
- [40] C. K. Jørgensen, R. Pappalardo, H.-H. Schmidtke, *The Journal of Chemical Physics* **1963**, *39*, 1422–1430.

-
- [41] C. K. Jørgensen, H.-H. Schmidtke, *Zeitschrift für Physikalische Chemie* **1963**, *38*, 118–120.
- [42] H.-H. Schmidtke, *Zeitschrift für Naturforschung A* **1964**, *19*, 1502–1510.
- [43] D. W. Smith in *New Theoretical Aspects*, Vol. 35, (Eds.: J. D. Dunitz, J. B. Goodenough, P. Hemmerich, J. A. Ibers, C. K. Jørgensen, J. B. Neilands, D. Reinen, R. J. P. Williams), Springer, Berlin, Heidelberg, **1978**, pp. 87–118.
- [44] D. W. Smith, *Journal of the Chemical Society A: Inorganic Physical Theoretical* **1969**, *0*, 1708–1712.
- [45] M. Wolfsberg, L. Helmholz, *The Journal of Chemical Physics* **1952**, *20*, 837–843.
- [46] D. W. Smith in *Encyclopedia of Inorganic Chemistry*, (Eds.: R. B. King, R. H. Crabtree, C. M. Lukehart, D. A. Atwood, R. A. Scott), Wiley, **2005**.
- [47] A. Bencini, C. Benelli, D. Gatteschi, *Coordination Chemistry Reviews* **1984**, *60*, 131–169.
- [48] Y. Nishida, S. Kida, *Coordination Chemistry Reviews* **1979**, *27*, 275–298.
- [49] W. Urland, *Chemical Physics* **1976**, *14*, 393–401.
- [50] K. D. Warren, *Inorganic Chemistry* **1977**, *16*, 2008–2011.
- [51] W. Smith, D. W. Clack, *Revue Roumaine De Chimie* **1975**, *20*, 1243–1252.
- [52] W. Urland, *Chemical Physics Letters* **1977**, *50*, 445–450.
- [53] W. Urland, *Chemical Physics Letters* **1977**, *46*, 457–460.
- [54] W. Urland, *Chemical Physics Letters* **1981**, *83*, 116–119.
- [55] W. Urland, S. R. Niketić, *Chemical Physics Letters* **1986**, *129*, 592–594.
- [56] K. D. Warren, *Inorganic Chemistry* **1980**, *19*, 653–658.
- [57] K. D. Warren, *Inorganic Chemistry* **1981**, *20*, 4223–4228.
- [58] H. Ramanantoanina, W. Urland, F. Cimpoesu, C. Daul, *Physical Chemistry Chemical Physics* **2014**, *16*, 12282–12290.
- [59] A. Bronova, T. Bredow, R. Glaum, W. Urland, *Inorganic Chemistry* **2016**, *55*, 6853–6860.
- [60] D. Aravena, M. Atanasov, F. Neese, *Inorganic Chemistry* **2016**, *55*, 4457–4469.
- [61] J. Jung, M. Atanasov, F. Neese, *Inorganic Chemistry* **2017**, *56*, 8802–8816.
- [62] M. Suta, C. Wickleder, *Journal of Luminescence* **2019**, *210*, 210–238.
- [63] B. J. P. Connolly, J. Y. J. Lian, P. V. Bernhardt, M. J. Riley, *Inorganic Chemistry* **2023**, *62*, 1328–1340.
- [64] AIM Group International, Ed., 44th International Conference on Coordination Chemistry, Rimini, Italy, August 28th - September 2nd 2022 : abstract book, Rome, **2022**.
- [65] C. E. Schäffer, *International Journal of Quantum Chemistry* **1971**, *5*, 379–390.

-
- [66] D. A. Cruse, M. Gerloch, *Journal of the Chemical Society Dalton Transactions* **1977**, 1617.
- [67] J. A. McGinnety, *Journal of the American Chemical Society* **1972**, *94*, 8406–8413.
- [68] J. Ferguson, *The Journal of Chemical Physics* **1964**, *40*, 3406–3410.
- [69] R. G. Woolley, *International Reviews in Physical Chemistry* **1987**, *6*, 93–141.
- [70] M. Gerloch, J. H. Harding, R. G. Woolley in *Inorganic Chemistry*, Springer Berlin Heidelberg, Berlin, Heidelberg, **1981**, pp. 1–46.
- [71] R. G. Woolley, *Molecular Physics* **1981**, *42*, 703–720.
- [72] M. Gerloch, R. G. Woolley in *Progress in inorganic chemistry*, (Ed.: S. J. Lippard), John Wiley & Sons, Interscience, New York, **1984**, pp. 371–446.
- [73] M. Gerloch in *Understanding Molecular Properties*, (Eds.: J. S. Avery, J. P. Dahl, P. R. Hansen), D. Reidel Publishing Company, Dordrecht, **1987**, pp. 111–142.
- [74] R. J. Deeth, M. Gerloch, *Inorganic Chemistry* **1984**, *23*, 3846–3853.
- [75] R. J. Deeth, M. Gerloch, *Journal of the Chemical Society Dalton Transactions* **1986**, 1531–1534.
- [76] R. J. Deeth, M. J. Duer, M. Gerloch, *Inorganic Chemistry* **1987**, *26*, 2578–2582.
- [77] R. J. Deeth, M. J. Duer, M. Gerloch, *Inorganic Chemistry* **1987**, *26*, 2573–2578.
- [78] A. J. Bridgeman, M. Gerloch, *Journal of the Chemical Society Dalton Transactions* **1995**, 197.
- [79] M. A. Hitchman, J. B. Bremner, *Inorganica Chimica Acta* **1978**, *27*, L61–L63.
- [80] M. A. Hitchman, P. J. Cassidy, *Inorganic Chemistry* **1979**, *18*, 1745–1754.
- [81] L. G. Vanquickenborne, A. Ceulemans, *Inorganic Chemistry* **1981**, *20*, 796–800.
- [82] C. E. Schäffer, *Inorganica Chimica Acta* **1995**, *240*, 581–592.
- [83] E. I. Solomon, B. Hedman, K. O. Hodgson, A. Dey, R. K. Szilagy, *Coordination Chemistry Reviews* **2005**, *249*, 97–129.
- [84] R. J. Deeth, *European Journal of Inorganic Chemistry* **2020**, *2020*, 1960–1963.
- [85] R. J. Deeth, *European Journal of Inorganic Chemistry* **2022**, *2022*, DOI 10.1002/ejic.202100936.
- [86] L. E. Orgel, *Journal of the Chemical Society* **1961**, 3683.
- [87] P. Day, N. Sanders, *Journal of the Chemical Society A: Inorganic Physical Theoretical* **1967**, 1536.
- [88] F. Felix, J. Ferguson, H. U. Güdel, A. Ludi, *Chemical Physics Letters* **1979**, *62*, 153–157.
- [89] A. Ceulemans, L. G. Vanquickenborne, *Journal of the American Chemical Society* **1981**, *103*, 2238–2241.

-
- [90] A. Ceulemans, M. Dendooven, L. G. Vanquickenborne, *Inorganic Chemistry* **1985**, *24*, 1159–1165.
- [91] A. Ceulemans, M. Dendooven, L. G. Vanquickenborne, *Inorganic Chemistry* **1985**, *24*, 1153–1158.
- [92] M. A. Atanasov, T. Schönherr, H.-H. Schmidtke, *Theoretica Chimica Acta* **1987**, *71*, 59–73.
- [93] M. A. Atanasov, M. A. Hitchman, *Inorganic Chemistry* **1993**, *32*, 3973–3975.
- [94] C. E. Schäffer, H. Yamatera, *Inorganic Chemistry* **1991**, *30*, 2840–2853.
- [95] R. J. Deeth, *Journal of the Chemical Society Dalton Transactions* **1991**, 1467–1477.
- [96] J. C. Slater in *Advances in Quantum Chemistry*, Vol. 6, (Ed.: P.-O. Löwdin), Academic Press, **1972**, pp. 1–92.
- [97] D. A. Liberman, *Physical Review B* **2000**, *62*, 6851–6853.
- [98] T. Ziegler, A. Rauk, E. J. Baerends, *Theoretica Chimica Acta* **1977**, *43*, 261–271.
- [99] M. Atanasov, C. A. Daul, C. Rauzy, *Chemical Physics Letters* **2003**, *367*, 737–746.
- [100] M. Atanasov, C. Daul, H. U. Güdel, T. A. Wesolowski, M. Zbiri, *Inorganic Chemistry* **2005**, *44*, 2954–2963.
- [101] M. Atanasov, C. A. Daul, *Comptes Rendus Chimie* **2005**, *8*, 1421–1433.
- [102] A. Borel, C. A. Daul, *Journal of Molecular Structure: THEOCHEM* **2006**, *762*, 93–107.
- [103] C. Anthon, C. E. Schäffer, *Coordination Chemistry Reviews* **2002**, *226*, 17–38.
- [104] C. Anthon, J. Bendix, C. E. Schäffer in *Optical spectra and chemical bonding in transition metal complexes*, (Ed.: T. Schönherr), Structure and bonding, 0081-5993, Springer, Berlin and London, **2004**, pp. 207–301.
- [105] C. Anthon, J. Bendix, C. E. Schäffer, *Inorganic Chemistry* **2004**, *43*, 7882–7886.
- [106] C. E. Schäffer, C. Anthon, J. Bendix, *Coordination Chemistry Reviews* **2009**, *253*, 575–593.
- [107] F. Neese, *Wiley Interdisciplinary Reviews: Computational Molecular Science* **2018**, *8*, e1327.
- [108] F. Neese, F. Wennmohs, U. Becker, C. Riplinger, *The Journal of Chemical Physics* **2020**, *152*, 224108.
- [109] F. Neese, *WIREs Computational Molecular Science* **2022**, *12*, DOI 10.1002/wcms.1606.
- [110] M. Atanasov, D. Aravena, E. Suturina, E. Bill, D. Maganas, F. Neese, *Coordination Chemistry Reviews* **2015**, *289-290*, 177–214.
- [111] E. A. Suturina, D. Maganas, E. Bill, M. Atanasov, F. Neese, *Inorganic Chemistry* **2015**, *54*, 9948–9961.

-
- [112] S. K. Singh, J. Eng, M. Atanasov, F. Neese, *Coordination Chemistry Reviews* **2017**, *344*, 2–25.
- [113] G. R. Brubaker, D. W. Johnson, *Coordination Chemistry Reviews* **1984**, *53*, 1–36.
- [114] R. D. Hancock in *Progress in Inorganic Chemistry*, Vol. 37, (Ed.: S. J. Lippard), Wiley, **1989**, pp. 187–291.
- [115] P. Comba, *Coordination Chemistry Reviews* **1993**, *123*, 1–48.
- [116] P. V. Bernhardt, P. Comba, *Inorganic Chemistry* **1992**, *31*, 2638–2644.
- [117] P. V. Bernhardt, P. Comba, *Inorganic Chemistry* **1993**, *32*, 2798–2803.
- [118] P. Comba, *Inorganic Chemistry* **1994**, *33*, 4577–4583.
- [119] P. Comba, T. W. Hambley, M. A. Hitchman, H. Stratemeier, *Inorganic Chemistry* **1995**, *34*, 3903–3911.
- [120] P. Comba, *Coordination Chemistry Reviews* **2003**, *238-239*, 9–20.
- [121] V. J. Burton, R. J. Deeth, C. M. Kemp, P. J. Gilbert, *Journal of the American Chemical Society* **1995**, *117*, 8407–8415.
- [122] V. J. Burton, R. J. Deeth, *Journal of the Chemical Society Chemical Communications* **1995**, DOI 10.1039/c39950000573.
- [123] R. Deeth, *Coordination Chemistry Reviews* **2001**, *212*, 11–34.
- [124] R. J. Deeth, N. Fey, B. Williams-Hubbard, *Journal of Computational Chemistry* **2005**, *26*, 123–130.
- [125] C. M. Handley, R. J. Deeth, *Journal of Chemical Theory and Computation* **2012**, *8*, 194–202.
- [126] J. Y. Xiang, J. W. Ponder, *Journal of Chemical Theory and Computation* **2014**, *10*, 298–311.
- [127] M. Foscatto, R. J. Deeth, V. R. Jensen, *Journal of Chemical Information and Modeling* **2015**, *55*, 1282–1290.
- [128] M. Buchhorn, R. J. Deeth, V. Krewald, *Chemistry - A European Journal* **2022**, *28*, e202103775.
- [129] V. G. Chilkuri, S. DeBeer, F. Neese, *Inorganic Chemistry* **2017**, *56*, 10418–10436.
- [130] M. Buchhorn, V. Krewald, *Dalton Transactions* **2023**, *52*, 6685–6692.
- [131] M. Buchhorn, V. Krewald, *Journal of Computational Chemistry* **2024**, *45*, 122–134.
- [132] P. E. Hoggard, *Zeitschrift für Naturforschung A* **1982**, *37*, 1096–1098.
- [133] M. Krauss, W. J. Stevens, *Annual Review of Physical Chemistry* **1984**, *35*, 357–385.
- [134] A. Shukla, M. Dolg, H. Stoll, P. Fulde, *Chemical Physics Letters* **1996**, *262*, 213–218.
- [135] A. Gellé, M.-B. Lepetit, *The Journal of Chemical Physics* **2008**, *128*, 244716.
- [136] E.-L. Andreici Etimie, N. M. Avram, M. G. Brik, *Optical Materials: X* **2022**, *16*, 100188.

[137] B. Mondal, S. Ye, *Coordination Chemistry Reviews* **2020**, *405*, 213115.